



Stergiou, Athanasios (2022) *Electrocatalysis for the reduction of organic nitroarenes and inorganic nitrite*. PhD thesis.

<https://theses.gla.ac.uk/83331/>

Copyright and moral rights for this work are retained by the author

A copy can be downloaded for personal non-commercial research or study, without prior permission or charge

This work cannot be reproduced or quoted extensively from without first obtaining permission from the author

The content must not be changed in any way or sold commercially in any format or medium without the formal permission of the author

When referring to this work, full bibliographic details including the author, title, awarding institution and date of the thesis must be given

Enlighten: Theses

<https://theses.gla.ac.uk/>
research-enlighten@glasgow.ac.uk

Electrocatalysis for the reduction of organic nitroarenes and inorganic nitrite.



Athanasios Stergiou

Submitted in fulfilment of the requirements for the
Degree of Doctor of Philosophy

School of Chemistry
College of Science and Engineering
University of Glasgow

August, 2022

Abstract

Electrochemistry is an emerging field in the physical sciences, covering a range of processes in a variety of areas. Whilst electrochemistry has been established in applications such as wastewater treatment and fuel production, there is a lot of room for growth in other fields. With the ever-increasing necessity of developing «green» processes to replace the traditional, non-environmentally friendly methods, electrocatalysis rises as a potential solution in many cases. The purpose of the work carried out in this thesis was to develop and examine electrocatalytic processes for the reduction of organic and inorganic substrates.

In Chapter 1, we discuss the use of redox mediators in the concept of organic electrosynthesis and decoupled electrolysis. More specifically, we comprehensively cover the use of polyoxometalates as redox mediators in organic electrosynthesis as well as providing examples of decoupled processes involving organic substrates. We also discuss the use of Vanadium in decoupled water electrolysis, as it has been identified as a potentially effective redox mediator for organic electrosynthesis due to its redox chemistry. In Chapter 2, we cover the theory behind the techniques that are used throughout this thesis. With the theoretical background and recent advances in the field covered in Chapters 1 & 2, we then start the discussion of our experimental work, covered in Chapters 3-5.

In Chapter 3, the development of a novel electrochemical process for the synthesis of various anilines, through the reduction of their corresponding nitrobenzenes, is discussed. By using phosphotungstic acid as the redox mediator (electro-catalyst) and controlling the applied potential in the electrochemical cell, we were able to provide a highly selective and clean electro-synthetic process. Our electrocatalytic route works in aqueous solution, at room temperature and pressure, where the electrons and protons required to reduce the nitrobenzenes are obtained from water. In Chapter 4, the scope of the process developed in Chapter 3 is massively expanded. Phosphotungstic acid mediated reduction of a variety of substituted nitroarenes, including potentially competing reducible groups and substrates that are difficult to reduce selectively by other means, was successfully performed. The performance of this method in terms of starting material conversion and product selectivity was also compared to the direct reduction at the electrode surface. In Chapter 5, we discuss our preliminary studies for the development of an electrocatalytic process for the selective multi-electron reduction of nitrite using iron porphyrins as electro-catalysts. Finally, we investigate the role of PCET in the catalytic process which we believe is crucial for the catalytic efficiency of the electrochemical process.

Table of Contents

ABSTRACT.....	II
TABLE OF CONTENTS	III
LIST OF CONFERENCES AND COURSES.....	VII
LIST OF PUBLICATIONS AND PATENTS.....	VIII
ACKNOWLEDGEMENTS.....	IX
AUTHOR'S DECLARATION.....	X
LIST OF ABBREVIATIONS.....	XI
MEDIATED ELECTROLYSIS IN ELECTROCHEMICAL SYNTHESIS.....	1
1.1 INTRODUCTION.....	3
1.1.1 <i>The Concept of the Indirect Electrochemical Synthesis</i>	3
1.1.2 <i>Chemical and electrochemical properties of polyoxometalates</i>	6
1.2 EARLY WORK IN POLYOXOMETALATE-MEDIATED ELECTROSYNTHESIS.....	9
1.3 RECENT PROGRESS IN POLYOXOMETALATE-MEDIATED ELECTROSYNTHESIS	11
1.3.1 <i>Oxidation of Aromatic Organic Substrates with Polyoxometalate Redox Mediators</i>	11
1.3.2 <i>Oxidation of Non-Aromatic Organic Substrates with Polyoxometalate Redox Mediators</i>	17
1.3.3 <i>Reduction of Organic Substrates using Polyoxometalate Redox Mediators</i>	20
1.4 THE CONCEPT OF DECOUPLED ELECTROLYSIS	22
1.4.1 <i>Decoupled Electrolysis in Organic Processes</i>	23
1.4.2 <i>Decoupled Electrolysis in Inorganic Synthesis</i>	25
1.5 VANADIUM SALTS.....	28
1.6 CONCLUSION	32
1.7 REFERENCES	34
OVERVIEW OF THE TECHNIQUES USED.....	44
2.1 ELECTROCHEMICAL TECHNIQUES	45
2.1.1 <i>Electrodes</i>	45
2.1.2 <i>Ohmic Drop Compensation</i>	47
2.1.3 <i>Cyclic Voltammetry</i>	48
2.1.4 <i>Reversibility of a Redox Process</i>	49
2.1.5 <i>Electrolysis</i>	51
2.1.6 <i>Two-electrode Configuration</i>	52

2.2 NUCLEAR MAGNETIC RESONANCE (NMR) SPECTROSCOPY	53
2.2.1 <i>Fundamentals of NMR</i>	53
2.2.2 <i>The Chemical Shift</i>	56
2.3 MASS SPECTROMETRY (MS)	58
2.3.1 <i>General Remarks</i>	58
2.3.2 <i>Ionisation Source</i>	59
2.3.3 <i>Mass Analyser</i>	60
2.4 REFERENCES	62
AIMS AND OBJECTIVES	63
HIGH YIELD AND SELECTIVE ELECTROCATALYTIC REDUCTION OF NITROARENES TO ANILINES USING REDOX MEDIATORS	70
3.1 INTRODUCTION.....	72
3.2 MATERIALS AND METHODS.....	75
3.2.1 <i>General Experimental Remarks</i>	75
3.2.2 <i>General Electrochemical Methods</i>	76
3.2.3 <i>Electrocatalytic Studies</i>	77
3.2.4 <i>Ex-cell Studies</i>	79
3.2.5 <i>Ex-cell Reactions Between Phenylhydroxylamine and 1-electron Reduced Phosphotungstic Acid</i>	80
3.2.6 <i>Aerial re-oxidation of the Reduced Mediator</i>	80
3.2.7 <i>¹H NMR Determination of Conversions</i>	81
3.3 RESULTS AND DISCUSSION	81
3.3.1 <i>Electrocatalytic Studies</i>	81
3.3.2 <i>Repeated Use of the Polyoxometalate Mediator</i>	91
3.3.3 <i>Reaction Mechanism</i>	92
3.4 CONCLUSION	100
3.5 NMR DATA OF THE OBTAINED PRODUCTS	101
3.6 REFERENCE	113
HIGHLY SELECTIVE ELECTROCATALYTIC REDUCTION OF SUBSTITUTED AROMATIC NITROARENES TO THEIR ANILINE DERIVATIVES USING A POLYOXOMETALATE REDOX MEDIATOR.....	120
4.1 INTRODUCTION.....	122
4.2 EXPERIMENTAL	123

4.2.1 General Experimental Remarks	123
4.2.2 General Electrochemical Methods.....	124
4.2.3 Cyclic Voltammetry.....	124
4.2.4 Electrocatalytic Studies.....	124
4.2.5 ¹ H NMR Determination of Conversions.....	125
4.3 RESULTS AND DISCUSSION	126
4.3.1 Voltammetry.....	126
4.3.2 Substrate Scope	129
4.3.3 Scaled-up Reactions	132
4.4 CONCLUSIONS	134
4.5 CHARACTERISATION OF COMPOUNDS	135
4.5.1 Cyclic Voltammograms	135
4.5.2 NMR Analysis of Obtained Products	142
4.6 REFERENCES	166

INVESTIGATING THE ELECTROCHEMICAL REDUCTION OF NITRITE

USING IRON-PORPHYRIN COMPLEXES.....168

5.1 INTRODUCTION.....	170
5.1.1 Nitrogen Cycle	170
5.1.2 Role of Nitrite in Nitrogen Cycle	172
5.1.3 Proton Coupled Electron Transfer (PCET).....	173
5.1.4 Iron Porphyrins for the Electrochemical Reduction of Nitrite	175
5.2 AIM OF THE PROJECT.....	177
5.3 EXPERIMENTAL PART.....	178
5.3.1 General Experimental Remarks	178
5.3.2 General Electrochemical Methods.....	178
5.3.3 Cyclic Voltammetry.....	179
5.4 RESULTS AND DISCUSSION	179
5.4.1 Synthesis of Dimethyl Hemin	179
5.4.2 Electrochemical Investigation of the Two Complexes	180
5.4.3 Addition of the Nitrite source.....	182
5.4.4 Addition of Proton source	186
5.4.5 Addition of a Weaker Proton Source	190
5.5 CONCLUSION	192
5.6 FUTURE WORK.....	192

5.7 REFERENCES	194
FINAL CONCLUSIONS AND FUTURE WORK.....	197

List of Conferences and Courses

- **Energy Storage and Conversion Section Colloquia**, School of Chemistry, University of Glasgow, UK.
Oral presentation: “*Catalytic electroreduction of Nitroarenes*”
- **Royal Society of Chemistry Electrochem**, Glasgow, UK, 2019 [26/8 – 28/8/2019].
Poster presentation: “*Using Inorganic/Organic Mediator for the Reduction of Nitrobenzene*”
- **Universities of Scotland Inorganic Chemistry (USIC)**, Glasgow, UK, 2019 [29/8 – 30/8/2019].
Poster Presentation: “*Using Inorganic/Organic Mediator for the Reduction of Nitrobenzene*”
- **Butler regional meeting**, University of Newcastle, UK, 2020 [1/09/2020].
Oral presentation: “*Catalytic Electroreduction of Nitroarenes*”
- **International Network of Polyoxometalate Science (INPOMS)**, University of Newcastle, UK, 2021 [9/12 – 10/12/2021].
Oral presentation: “*Electrocatalytic Hydrogenation of Nitroarenes using Polyoxometalate redox mediator*”
- **International Society of Electrochemistry (ISE) regional meeting**, Prague, Czech Republic, 2022 [15/8 – 19/8/2022].
Oral Presentation: “*High Yield and Selective Electrocatalytic Reduction of Nitroarenes to Anilines using Redox Mediators*”
- **Basics of Nuclear Magnetic Resonance**, 5 weeks online course, University of Lille, France, 2021.

List of Publications and Patents

- “Host–Guest-Induced Electron Transfer Triggers Radical-Cation Catalysis”
R. L. Spicer, A. D. Stergiou, T. A. Young, F. Duarte, M. D. Symes and P. J. Lusby.
J. Am. Chem. Soc. 2020, **142**, 2134–2139.
- “Decoupled Electrochemical Water Splitting: From Fundamentals to Applications”
P. J. McHugh, A. D. Stergiou and M. D. Symes. *Adv. Energy Mater.* 2020, **10**, 2002453.
- “Organic Transformations using Electro-Generated Polyoxometalate Redox Mediators”
A. D. Stergiou and M. D. Symes. *Catal. Today*, 2022, **384-386**, 146-155.
- “Anion- π Catalysis Enabled by the Mechanical Bond”
J. R. J. Maynard, B. Galmés, A. D. Stergiou, M. D. Symes, A. Frontera and S. M. Goldup. *Angew. Chem. Int. Ed.* 2022, **61**, e202115961.
- “High yield and selective electrocatalytic reduction of nitroarenes to anilines using redox mediators”
A. D. Stergiou and M. D. Symes. *Cell Rep. Phys. Sci.*, 2022, **3**, 100914.
- “Highly selective electrocatalytic reduction of substituted nitrobenzenes to their aniline derivatives using a polyoxometalate redox mediator”
A. D. Stergiou, D. H. Broadhurst and M. D. Symes. *ACS Org. Inorg. Au*, 2022, <https://doi.org/10.1021/acsorginorgau.2c00047>
- “Electrochemical reduction of nitrobenzene via redox-mediated chronoamperometry”
A. D. Stergiou, D. H. Broadhurst and M. D. Symes. *STAR Protocols*, 2022, **3**, 101817.
- Patent entitled: Method of reducing nitro compounds, application number: EP22386046.1 and GB2211318.7.

Acknowledgements

First and foremost, I would like to thank Prof. Mark Symes for giving me the opportunity to undertake this PhD in his research group. Through these 4 years, Mark was always there to provide guidance and share his knowledge with me, while his vital scientific contribution helped me to improve myself and overcome many dead ends. At the same time, his optimistic view into any given results and his “never give up” attitude, especially when things did not look promising, kept me motivated during my studies. Mark, it was a great pleasure working with you over my PhD and I wish you all the best in your future career.

Second, I would like to thank the Symes group as a whole, both the past and current members, for making this group a nice place to work. Alex for introducing me to electrochemistry and helping me settle in, while always being a good laugh to go out with. Mike was a great colleague and helped me a lot during my first few times in the lab.

Special mention to Paddy and Calum, we have been together since the very beginning and have shared so many great moments on and off work, I couldn't ask for better colleagues and friends. This journey would have never been the same without you, and I am so grateful for everything we have lived together.

I would also like to thank all my project students, and especially Dan for his contribution to this thesis and for being an excellent student making my last months in the lab very productive and enjoyable.

I cannot forget to mention all the staff in the Chemistry department that provided help and their expertise to make my work possible. And of course, to all the fellow PhD students and PDRA for the daily chat in the lab.

I would also like to thank all my friends in Glasgow for being there for me and making memories together that I will never forget. Thank you to my flatmates Anastasis and Takis for all the good times we have had together.

Ioanna, thank you for your love and for supporting and believing in me at all costs.

Finally, a huge thank you to my family for the love, and unconditional support in every step of my academic journey. Mum, you always have a special place in my life and thank you for everything you have done. To my brother, Marios, living with you this past year was the best thing that I could possibly ask for in the last year of my PhD. This year would have not been the same without you.

Author's declaration

I declare that, except where explicit reference is made to the contribution of others, this thesis is the result of my own work and has not been submitted for any other degree at the University of Glasgow or any other institution

I declare that this thesis has been produced in accordance with the University of Glasgow's Code of Good Practice in Research.

I acknowledge that if any issues are raised regarding good research practice based on review of the thesis, the examination may be postponed pending the outcome of any investigation of the issues.

Printed name: **Athanasios Stergiou**

Signature:

List of Abbreviations

δ	Chemical Shift
ρ	Resistivity
A	Area
Ac	Acetyl group
c	Concentration
calcd.	Calculated
Co-TPP	Cobalt (II) <i>meso</i> -tetraphenylporphyrin
CPET	Concerted Proton-Electron Transfer
CV	Cyclic Voltammetry
DCM	Dichloromethane
DFT	Density Functional Theory
DMSO	Dimethyl sulfoxide
E	Potential
$E_{1/2}$	Half-potential of a redox wave
EI	Electron Ionisation
EPT	Electron-Proton Transfer
EPR	Electron Paramagnetic resonance
eq.	Equivalents
ESI	Electrospray Ionisation
F	Faraday Constant
FID	Free Induction Decay
GC-MS	Gas chromatography – mass spectrometry
h	Hours
H-cell	Two-compartment electrochemical cell
HER	Hydrogen Evolution Reaction
i	Current
IPB	Indophenol Blue
l	Length
LSV	Linear Sweep Voltammetry
m	Number of Moles or Mass
Me	Methyl
MeOD	Deuterated methanol
MeOH	Methanol

MHz	Megahertz
min	Minutes
MS/MS	Tandem mass spectrometry
m/z	Mass-to-charge ratio
n	Number of electrons Transferred per Ion
NHE	Normal Hydrogen Electrode
NMR	Nuclear Magnetic Resonance
OER	Oxygen Evolution Reaction
PCET	Proton Coupled Electron Transfer
PET	Proton-Electron Transfer
ppm	Part(s) per million
Q	Charge
R	Resistance
R _f	Distance on TLC plate
R _u	Uncompensated Resistance
r.t	Room Temperature
SCE	Saturated Calomel Electrode
SHE	Standard Hydrogen Electrode
T	Temperature
TBAPF ₆	Tetrabutyl ammonium hexafluorophosphate
TLC	Thin Layer Chromatography
TMS	Tetramethyl Silane
TOF	Time-of-flight mass analyser

Note: Conventional abbreviations for units and physical quantities are not included

Mediated electrolysis in electrochemical synthesis

Acknowledgements and Declaration

This chapter contains extended and updated sections of the following published papers:

“Organic Transformations using Electro-Generated Polyoxometalate Redox Mediators” A. D. Stergiou and M. D. Symes, *Catal. Today*, **2022**, 384-386, 146-155.

“Decoupled Electrochemical Water Splitting: From Fundamentals to Applications” P. J. McHugh, A. D. Stergiou and M. D. Symes, *Adv. Energy Mater.* **2020**, 10, 2002453.

Both papers were written through the contribution of all cited authors.

Synopsis

The use of electrochemistry in organic synthesis (sometimes termed electro-organic synthesis, or just “electrosynthesis”) is a field that is attracting ever-increasing attention on account of its ability to deliver reaction outcomes that cannot be achieved in any other way and on account of its potential to replace toxic and/or sacrificial reagents with cleanly-generated electricity. In the simplest incarnation of electro-organic synthesis, an organic substrate undergoes direct electron transfer with the electrode in a type of heterogeneous catalysis process. However, such direct electrochemical processes may suffer from slow kinetics, poor product selectivities and/or lack of control over the extent of electron transfer to the substrate, all of which can lead to sub-optimal reaction outcomes. A distinct, but extremely important, sub-section of electro-organic synthesis (so-called “indirect electrolysis”) circumvents these limitations through the use of soluble redox mediator molecules, which act as electron shuttles between the heterogeneous electrode and the organic substrate in bulk solution. The advantages of indirect electrolysis for a number of organic transformations is now becoming increasingly clear, typically using either very simple metal salts or small organic molecules as the mediators. Since polyoxometalate mediators were extensively used in the present thesis, we aim to provide a comprehensive study of the current literature of this class of mediators with a particular focus on the most recent and most exciting results. Polyoxometalates (well-defined, soluble metal oxide clusters), offer an especially wide diversity of structures and properties that could revolutionise indirect electrolysis for electro-organic synthesis. Moreover, we briefly introduce the concept of decoupled electrolysis in organic processes as well as discussing the potential use of vanadium as an effective alternative to polyoxometalate redox mediators.

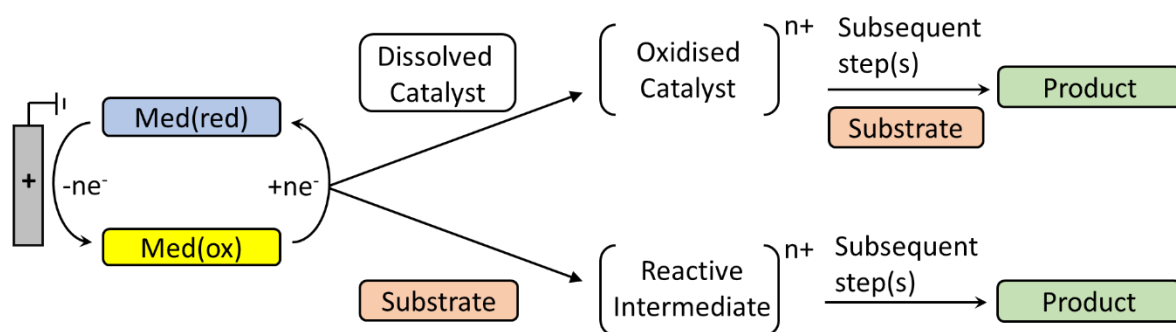
1.1 Introduction

1.1.1 The Concept of the Indirect Electrochemical Synthesis

Electrochemical organic synthesis is a mature field that can trace its origins back to the work of Michael Faraday.¹ It is currently undergoing something of a renaissance on account of its potential as a sustainable alternative to traditional routes for organic synthesis.²⁻⁶ In particular, the ability to drive organic transformations using electricity holds considerable promise for the replacement of dangerous and/or toxic reagents by electric current, reduced use of sacrificial reagents and lower overall energy consumption.^{7,8} All these features are attractive from an environmental point of view, and yet organic electrosynthesis remains rather an under-utilised approach to organic chemistry.⁹ This is at least partly due to the fact that direct electrochemical oxidation or reduction of substrates at the electrode surface can lead to sub-optimal selectivities, specificities and yields.

It is within this context that the sub-field of *indirect electrolysis* continues to attract increasing attention. In an indirect electrochemical process, a carefully selected redox mediator is used as an electron carrier between the electrode and species dissolved in solution. This redox mediator may merely shuttle electrons between the electrode and a catalyst dissolved in solution, or alternatively the mediator itself may react directly with the substrate (in which case, the mediator can also be considered as a soluble electrocatalyst). In both cases, the key point is that it is the redox mediator molecule that undergoes electron transfer at the electrode surface, rather than the substrate itself engaging in electron transfer directly with the electrode. Scheme 1.1 provides some examples of the mode of action of redox mediators in organic oxidation reactions. Hence, the mediator in the reduced form is oxidised at the electrode surface, before diffusing into bulk solution where it reacts either with a dissolved catalyst (top pathway), or directly with an organic substrate (bottom pathway). In the latter case, the mediator can be classified as an electrocatalyst since the electron transfer occurs directly between the mediator and the substrate. Catalytic amounts of the mediator can only be used in the case of the “in-cell” process, as indicated below. This redox electron transfer can proceed either through an outer-sphere mechanism, where no bond formation between the mediator and the substrate takes place or through an inner-sphere mechanism where a chemical reaction involving bond formation/cleavage occurs. The mediator (now reduced again) cycles back to the electrode to be re-oxidised, whilst the oxidised catalyst or substrate undergo any number of subsequent chemical reactions in solution. In this way, and assuming that the mediator is stable to multiple such redox cycles,

a small amount of mediator can be employed to transform a much larger amount of substrate. The mediator can either be used “in-cell” (where the mediator and the organic substrate are both present in the electrochemical cell and thus catalytic amounts of the mediator can be used, as in the examples in Scheme 1.1), or “ex-cell”, whereby the mediator is oxidised or reduced into its active form in an electrochemical cell on its own, and is then subsequently introduced to the substrate in a separate, purely chemical reaction vessel.^{10,11}



Scheme 1.1: A general and simplified illustration of the possible modes of operation of a redox mediator in an indirect “in-cell” electrochemical process, using the example of an organo-oxidation reaction.

Depending on the desired reaction outcome, indirect electrolysis can hold a number of advantages for organic synthesis.¹¹ Firstly, the heterogeneous step (electron transfer from the electrode to species in solution) occurs only between the electrode and the (ideally) robust and recyclable redox mediator, and this heterogeneous step is decoupled from the subsequent solution-phase chemistry. The substrate therefore no longer reacts directly at the electrode, preventing uncontrolled oxidation or reduction of the organic substrate that might lead to polymerisation or degradation. The heterogeneous step can then be optimised for a particular electrode-mediator pairing, whilst the subsequent reactions in the cascade (*e.g.* between the oxidised mediator and the substrate) all occur in solution under more classical (chemical) control. These solution-phase processes can themselves be optimised, possibly even in the absence of any electrode processes. This allows greater scope for otherwise incompatible conditions to be employed. Secondly, the redox mediator will have defined redox levels and a defined level of oxidation/reduction at any given cell potential, which means that its subsequent reaction with the organic substrate will be more controlled, both in the number and reducing power of the electrons added to (or removed from) the substrate.

This adds the prospect of selectivity to what might otherwise be a rather unselective direct reaction at the electrode surface. Well-chosen mediators might also exhibit lower barriers to electron transfer with the electrode than the substrates themselves do in direct electrolysis (improving reaction kinetics) and/or they may allow the use of bias potentials that are lower than that required for the direct electrochemical conversion and hence permit milder reaction conditions to be employed. Therefore, in a well-chosen mediated system, the decrease (or even elimination) of the kinetic inhibition of the heterogeneous electron transfer between the electrode and the substrate (direct process) can lower the overpotential required to drive the reaction. By overpotential, we define the difference in the applied potential during the reaction and the equilibrium potential under specific reaction conditions (thermodynamic potential).^{11,12}

Since the redox mediator is the protagonist in the successful implementation of indirect electrolysis in organic transformations, some of its key elements should be discussed. At first, in a well-found mediator system, only the mediator will undergo oxidation or reduction at the electrode surface and none of the substrates, intermediates or products will interfere with the regeneration of the mediator. Thus, the reduction potential of the mediator should be less than the potential of the substrate in question. Secondly, the mediator should also be stable to multiple redox cycles, reactive in its active form towards the desired substrate and long-lived enough in its active form to travel from the electrode surface to bulk solution to react with the substrate. Therefore, a fast and reversible electron transfer between the electrode and the mediator is a key element. At the same time, fast electron transfer between the mediator and the substrate is crucial for high reaction rates. Finally, both the reduced and oxidised form of the mediator should be soluble in the electrolyte to ensure homogeneity while they should be inert to any side reactions within the electrochemical system. Competing reactions decrease the catalytic activity of the mediator and the overall efficiency of the electrochemical process.^{11,12} Likewise, if the environmental benefits of electrosynthesis are to be fully realised, processes that work well in aqueous solution need to be developed (where water's low toxicity and high abundance make it an ideal solvent medium and proton source).^{13,14}

Indirect electrochemical processes for organic synthesis were first reviewed by Steckhan in the 1980s,¹⁵ and Francke and Little produced a seminal survey of the field in 2014.¹¹ More recently, Stahl and co-workers have reviewed the use of certain specific mediators in indirect electrolysis.¹⁶ However, the main focus of most of these reviews has been on the use of organic species such as quinone and *N*-oxyl mediators; there has been no comprehensive

review of the use of polyoxometalate redox mediators in electro-organic synthesis for at least twenty years.¹⁷ In this section, we seek to address this gap by providing a coherent and readily-accessible collation of examples of the use of polyoxometalate redox mediators for electro-organic synthesis. In doing so, we shall restrict ourselves to the discussion of systems for the controlled interconversion of organic substrates for chemical synthesis, excluding indirect electrochemical approaches to sensing^{18,19} and processes concerning purely inorganic species such as the oxidation and reduction of nitrite, oxygen reduction or water splitting (a field which has been reviewed recently).²⁰

We shall start with an introduction to the chemical and electrochemical properties of polyoxometalates before proceeding with a brief overview of the classical work in this field, before then exploring more recent developments in the use of polyoxometalate redox mediators for electro-organic synthesis in more depth. We will then divide these more recent studies into examples of oxidation of organic substrates and (much less common) examples of reduction of organic substrates. The key results from the works that are discussed herein are summarised in Table 1.1.

1.1.2 Chemical and electrochemical properties of polyoxometalates

Polyoxometalates are a class of molecular metal oxides, with structural diversity, that consist of three or more transition metal oxyanions (MO_x) as their basic structural units, linked by shared oxygen atoms. M , represents the early transition metals, typically from groups 5 and 6 of the periodic table in their highest oxidation (*e.g.* W, Mo and Si).²¹ In today's literature, there is a number of reports where these metals have been partly substituted by other transition metals such as Fe, Co, Cr *etc.*, offering diversity in the polyoxometalate's structure and chemical properties.^{21,22}

Broadly speaking, polyoxometalates can be divided into three main categories, based on their structure. (a) Heteropolyanions: These are clusters that contain, as their name indicates, hetero anions such as SiO_4^{4-} , and PO_4^{3-} . This central heteroatom provides added structural stabilisation compared to isopolyanions. Heteropolyanions, represent the most well-studied class of polyoxometalates with great attention being focused on the Keggin [$\text{XM}_{12}\text{O}_{40}$] and Wells-Dawson [$\text{X}_2\text{M}_{18}\text{O}_{62}$] (where M is W or Mo and X is a tetrahedral template) polyoxometalates. (b) Isopolyanions: These structures do not contain central heteroatoms but only addenda metal and oxygen atoms ($[\text{M}_x\text{O}_y]$, where M is typically a high valence early transition metal); therefore, they are usually less stable than their hetero atom analogues. (c) Mo-blue and Mo-brown reduced polyoxometalate clusters: This sub-category constitutes an

exciting family of clusters in polyoxometalate synthesis.²¹ For the purpose of the present thesis we will be focusing on the chemistry and electrochemical properties of the heteropolyanions and more specifically on the Keggin structure polyoxometalates as these have been used in *Chapters 3&4*.

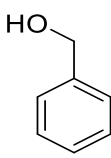
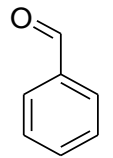
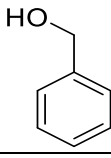
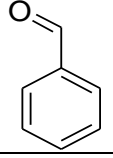
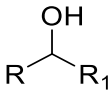
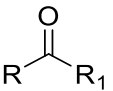
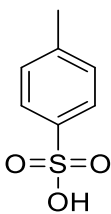
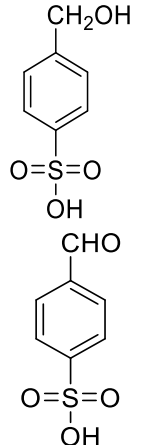
Heteropolyanions usually have a high negative charge while they possess different active sites that make them very attractive catalysts. Protons can act as Brønsted acids to support acid-catalysed reactions. Moreover, terminal oxygen atoms are basic enough to donate electrons to electron acceptors and therefore participate in base-catalysed reactions. On the other hand, the metal ions of the heteropolyanion have unoccupied d or f orbitals that can accept electrons. Therefore, under different conditions, polyoxometalates of this class can act as Lewis bases or Lewis acids.^{23,24} The fact that such clusters display high water solubility and their ability to reversibly receive and donate multiple electrons and protons, normally through outer-sphere mechanisms,^{25,26,27} makes them very promising candidates for the development of sustainable catalytic and electrocatalytic processes, with the latter being the main topic of the present thesis. Polyoxometalates of particular interest, have been used as inorganic molecular redox mediators for organic transformations,²⁸ where the addition/removal of multiple electrons and protons to/from a substrate is often required. Polyoxometalates may also act to prevent electrode fouling by organic species (during the electro-oxidation of phenols, for example).²⁹ However, compared to their use in purely chemical electron transfer and catalysis processes,^{23,30,31} the use of polyoxometalates as electrocatalysts and redox mediators in organic synthesis remains a rather niche area.

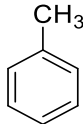
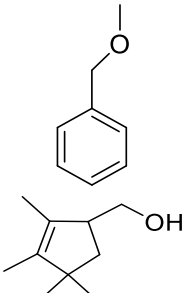
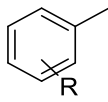
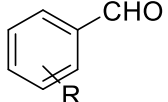
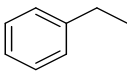
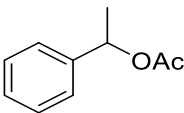
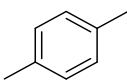
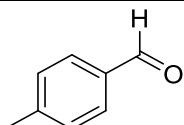
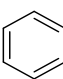
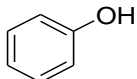
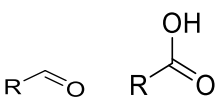
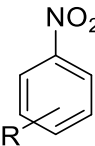
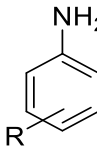
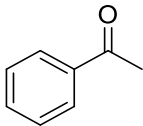
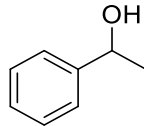
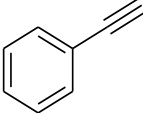
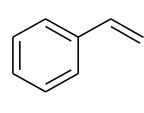
The electrochemistry of Keggin structure polyoxometalates has been vastly exploited in the past years. What we are particularly interested in, is the electrochemical behaviour of these heteropolyacids in aqueous electrolytes, where the pH value of the electrolyte seems to have a key role.^{32,33} Usually, Keggin-type polyoxometalates exhibit at least two successive one-electron reversible redox waves, followed by multielectron redox waves (reversible or irreversible) with concomitant protonation/deprotonation at low pH values.³⁴ In general, molybdenum polyoxometalates exhibit more positive redox potentials than their corresponding tungsten-containing polyoxometalates.³² Worth mentioning is that the polyoxometalate of particular interest for the purpose of this thesis, phosphotungstic acid ($[\text{PW}_{12}\text{O}_{40}]^{3-}$), is only stable at pH values below 1.5,³³ while the addition of a weak base to alter the pH of the solution usually leads to decomposition of the polyoxometalate.¹² Moreover, the known ability of polyoxometalates to act as electron reservoirs, able to store multiple electrons in a reversible manner, in electrochemical systems is a key function for

their use as electrocatalysts in organic transformations.^{33,35} Finally, polyoxometalates have been found to serve the role of both the electron carrier between the electrode and a catalyst (for example Pt/C catalyst in hydrogen production systems)³⁶; and the role of electrocatalyst by reacting directly with the substrate to drive a chemical reaction.^{37,38}

Thus, due to their high electrochemical activity and chemical properties, polyoxometalates can be very promising candidates for the development of electrocatalytic systems that can effectively perform demanding organic electrochemical transformations.

Table 1.1: A summary of the organic transformations mediated by electro-generated polyoxometalate redox mediators discussed.

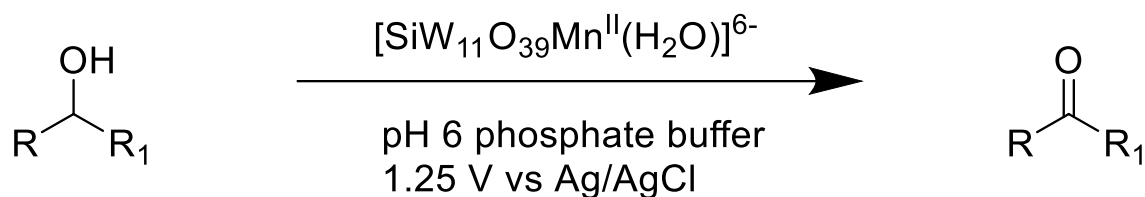
Substrate(s)	Main Product(s)	Mediator(s)	N° of electrons transferred to/from mediator	Relevant mediator redox potential	Ref
		α - [PW ₁₁ O ₃₉ Cr ^{III} (H ₂ O)] ⁴⁻ α_2 - [P ₂ W ₁₇ O ₆₁ Cr ^{III} (H ₂ O)] ⁷⁻	2	1.25-1.60 V vs Ag/AgCl	39
		α - [PW ₁₁ O ₃₉ Ru ^{III} (H ₂ O)] ⁴⁻	3	1.3 V vs SSCE	40
		K ₆ [SiW ₁₁ O ₃₉ Mn ^I (H ₂ O)]	2	1.25 V vs Ag/AgCl	41
		[H ₃ PMo ₁₂ O ₄₀]	2	0.7 V vs Ag/AgCl	42

		$(\text{NH}_4)_3\text{H}_4[\text{P}(\text{Mo}_2\text{O}_7)_6]$	Not reported	30 V cell potential	47
		$\text{H}_5\text{PV}_2\text{Mo}_{10}\text{O}_{40}$	2	1.3 V vs NHE	48
		$[\text{Co}^{\text{IV}}\text{W}_{12}\text{O}_{40}]^{4-}$	1	1.8 V vs Ag/AgN ₃	50
		$[\text{Co}^{\text{IV}}\text{W}_{12}\text{O}_{40}]^{4-}$	1	1.8 V vs Ag/AgN ₃	50
		$[\text{Co}^{\text{IV}}\text{W}_{12}\text{O}_{40}]^{4-}$	1	1.8 V vs Ag/AgN ₃	50
$\text{R}-\text{CH}_2\text{OH}$ R = H or CH ₃		$[\{\text{Ru}_4\text{O}_4(\text{OH})_2(\text{H}_2\text{O})_4\}(\gamma\text{-SiW}_{10}\text{O}_{36})_2]^{10-}$	Up to 4	Varies from 0.66 – 0.93 V vs Fc/Fc ⁺	54
Light hydrocarbons, e.g. ethane, propane, ethene	Corresponding acids and aldehydes	$\{\text{Fe}^{\text{II}}_{10}\text{Fe}^{\text{III}}_{20}\text{W}^{\text{VI}}_{17}_2\}$	10	1.8 V cell potential	57
		$[\text{H}_4\text{SiW}_{12}\text{O}_{40}]$	2	-0.56 V vs Ag/AgCl	60
		$[\text{H}_4\text{SiW}_{12}\text{O}_{40}]$	2	8.3 V cell potential	63
		$[\text{H}_4\text{SiW}_{12}\text{O}_{40}]$	2	8.3 V cell potential	63

1.2 Early Work in Polyoxometalate-mediated Electrosynthesis

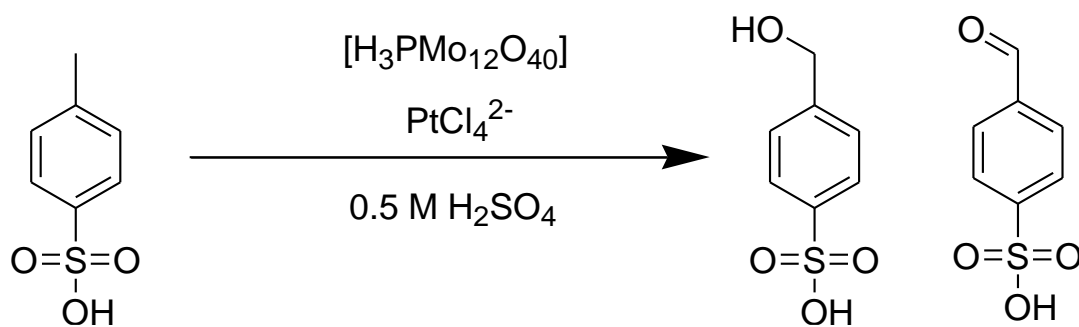
A number of polyoxometalates were examined in the 1990s as electrocatalysts for the oxidation of alcohols to their corresponding ketones and carboxylic acids. Rong and Anson oxidised the chromium-containing polyoxometalates $\alpha\text{-}[\text{PW}_{11}\text{O}_{39}\text{Cr}^{\text{III}}(\text{H}_2\text{O})]^{4-}$ and $\alpha_2\text{-}$

$[\text{P}_2\text{W}_{17}\text{O}_{61}\text{Cr}^{\text{III}}(\text{H}_2\text{O})]^{7-}$ electrochemically to the analogous $\text{Cr}^{\text{V}}=\text{O}$ complexes and used these species as ex-cell mediators to effect the oxidation of ethyl and benzyl alcohols,³⁹ whilst Bart and Anson reported similar activity for the ruthenium-containing polyoxometalate α - $[\text{PW}_{11}\text{O}_{39}\text{Ru}^{\text{III}}(\text{H}_2\text{O})]^{4-}$ after its electrochemical production from α - $[\text{PW}_{11}\text{O}_{39}\text{Ru}^{\text{II}}(\text{H}_2\text{O})]^{5-}$.⁴⁰ In all these cases, however, the reaction rates of the polyoxometalates with the substrates were concluded to be too slow to warrant further investigation of these species as organo-oxidation catalysts. Meanwhile, Sadakane and Steckhan employed α - $[\text{SiW}_{11}\text{O}_{39}\text{Mn}^{\text{II}}(\text{H}_2\text{O})]^{6-}$ as a redox mediator for the indirect electrochemical oxidation of a number of alcohols as shown in Scheme 1.2,⁴¹ although the rate constants for the reactions between this polyoxometalate and the alcohol substrates are on the same order as those reported by Anson and co-workers for their $\{\text{PW}_{11}\text{O}_{39}\}$ -based polyoxometalates, which might also suggest that α - $[\text{SiW}_{11}\text{O}_{39}\text{Mn}^{\text{II}}(\text{H}_2\text{O})]^{6-}$ oxidises alcohols too slowly to be an attractive electrocatalyst.



Scheme 1.2: Indirect electrochemical reduction of alcohols using $\text{K}_6[\text{SiW}_{11}\text{O}_{39}\text{Mn}^{\text{II}}(\text{H}_2\text{O})]$ as the redox mediator as reported by Sadakane and Steckhan.³¹

At around the same time, Freund *et al.* investigated a system for the electrocatalytic hydroxylation of *p*-toluenesulfonic acid (*p*- $\text{HO}_3\text{SC}_6\text{H}_4\text{CH}_3$) to the alcohol *p*-(hydroxymethyl)benzenesulfonic acid (*p*- $\text{HO}_3\text{SC}_6\text{H}_4\text{CH}_2\text{OH}$) and aldehyde *p*-formylbenzenesulfonic acid (*p*- $\text{HO}_3\text{SC}_6\text{H}_4\text{CHO}$) using PtCl_4^{2-} as a C-H activation catalyst and the polyoxometalate phosphomolybdic acid ($[\text{H}_3\text{PMo}_{12}\text{O}_{40}]$) as the redox mediator in 0.5 M H_2SO_4 (see Scheme 1.3).⁴² No conversion was evident in the absence of the phosphomolybdic acid redox mediator, but conversions of >30% were possible using 0.2 M phosphomolybdic acid, with coulombic yields for the hydroxylated products approaching 100%. However, the product selectivity was lost after extended electrolysis times (more than six turnovers), which the authors suggested could be due to the formation of $\text{Pt}(0)$ from PtCl_4^{2-} , citing the known activity of $\text{Pt}(0)$ for alcohol oxidation. Some oxidation of the aromatic ring was also observed, again attributed to oxidation catalysed by $\text{Pt}(0)$.



Scheme 1.3: Indirect electrocatalytic hydroxylation of *p*-toluenesulfonic acid as reported by Freund *et al.*³²

Perhaps because of these relatively modest performances, interest in polyoxometalates as electro-generated redox mediators for organic transformations waned somewhat in the following years. This is understandable when one considers that polyoxometalates are molecules with comparatively high molecular weights, and hence performance has to significantly exceed that which might be produced using smaller (*e.g.* organic) mediators in order to justify the use of such massive species. In the last five years or so, however, interest in polyoxometalates as electro-generated mediators for organic chemistry has been revived and this field now stands poised for considerable growth thanks to the development of new concepts such as decoupled electrolysis,⁴³⁻⁴⁵ where polyoxometalates often display superior stability and electron/proton storage capacity.⁴⁶ This new and exciting chapter in electro-organic synthesis with polyoxometalates will form the bulk of the remainder of this thesis chapter.

1.3 Recent progress in Polyoxometalate-mediated Electrosynthesis

1.3.1 Oxidation of Aromatic Organic Substrates with Polyoxometalate Redox Mediators

Between the mid-1990s and 2015, very little work appears to have been performed on driving organic transformations using electro-generated polyoxometalate redox mediators. One of the very few (possibly the only) example from this time was published in 2007 by Ma and co-workers. These authors employed the polyoxomolybdate (NH₄)₃H₄[P(Mo₂O₇)₆] as a redox mediator for the oxidation of toluene in methanolic solution to give 1-methoxymethylbenzene as the dominant product.⁴⁷ Their set-up (Figure 1.1) consisted of a parallel plate cell with two large (25 cm²) porous graphite electrodes held a distance of 1 cm

apart, and between which a bias of 30 V was applied, delivering initial current densities on the order of 90 mA cm^{-2} . The electrolyte (which appears to have been a somewhat inhomogeneous suspension from the authors' description) consisted of 0.5 M KF in a roughly 1:1 mixture of methanol and toluene, to which was added the polyoxometalate to give a concentration of approximately 20 mM. This mixture was both cooled during electrolysis (to minimise evaporation of the methanol) and stirred in order to maintain some uniformity.

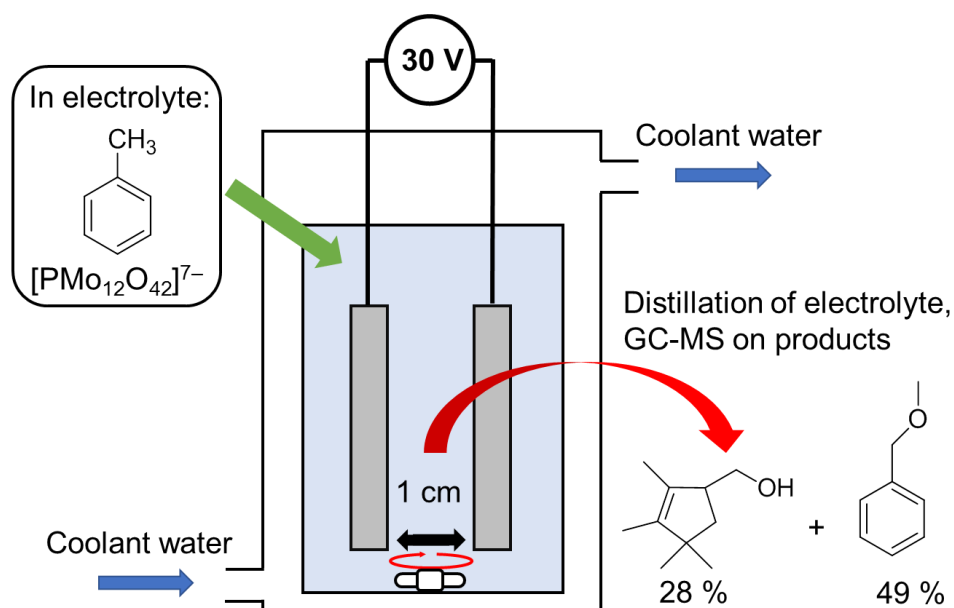
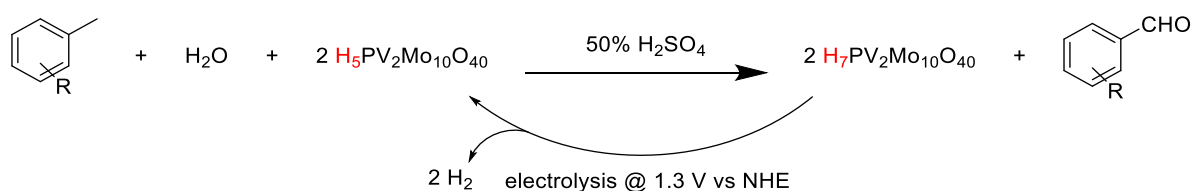


Figure 1.1: The oxidation of toluene in methanolic solution mediated by $(\text{NH}_4)_3\text{H}_4[\text{P}(\text{Mo}_2\text{O}_7)_6]$ as described by Ma and co-workers.³⁷

After electrolysis, the electrolyte mixture was distilled and the volatiles analysed by gas chromatography-mass spectrometry (GC-MS). This allowed the main products of the reaction to be determined as 1-methoxymethylbenzene (49% by mass) and 2,3,4,4-(tetramethylcyclopent-2-ienyl)methanol (28% by mass), with the remainder of the products unidentified. A possible mechanism for the generation of these products was proposed, whereby a toluene radical cation is formed upon oxidation by the polyoxometalate, with this radical then combining with O_2 in solution to give benzaldehyde, which then in turn reacts with methoxy species generated at the cathode to give 1-methoxymethylbenzene. However, very little evidence was presented to support this putative mechanism.

In 2015, Neumann and co-workers reported an electrochemical cycle for the oxidation of methylarenes to their benzaldehyde derivatives using the phosphovanadomolybdate $\text{H}_5\text{PV}_2\text{Mo}_{10}\text{O}_{40}$ as both an ex-cell and in-cell mediator for oxygen transfer catalysis.⁴⁸ Sustainable and low-waste routes from methylarenes to benzaldehydes are highly desirable, as most conventional methods for the synthesis of benzaldehydes do so with low atom economy, accompanied by the formation of significant amounts of waste and frequently employing toxic reagents. To address this issue, the authors selected $\text{H}_5\text{PV}_2\text{Mo}_{10}\text{O}_{40}$ for study on account of its known activity as a chemical oxygenation catalyst of organic substrates in the presence of O_2 .⁴⁹ Their approach is summarised in Scheme 1.4, whereby the polyoxometalate was reacted with the relevant methylarene using 50% aqueous H_2SO_4 as the solvent. For a wide range of substrates, the corresponding aldehydes could be formed with high conversion and excellent selectivity after a few hours, with almost no evidence of over-oxidation to the carboxylic acids.



Scheme 1.4: The oxidation of methylarenes to their aldehyde derivatives mediated by $\text{H}_5\text{PV}_2\text{Mo}_{10}\text{O}_{40}$ as described by Neumann and co-workers.³⁸

After oxidation of the organic substrate, the polyoxometalate mediator exists as the two-electron reduced form, $\text{H}_7\text{PV}_2\text{Mo}_{10}\text{O}_{40}$. Although spontaneous re-oxidation of the polyoxometalate by O_2 to re-generate $\text{H}_5\text{PV}_2\text{Mo}_{10}\text{O}_{40}$ is thermodynamically feasible, this reaction was found to be very slow in the highly acidic solvent environment required to allow the oxygen transfer reaction to proceed. The authors therefore chose to re-generate the active form of the redox mediator by electrolysis in a two compartment cell, re-oxidising green $\text{H}_7\text{PV}_2\text{Mo}_{10}\text{O}_{40}$ to orange $\text{H}_5\text{PV}_2\text{Mo}_{10}\text{O}_{40}$ at a Pt anode with concomitant production of H_2 at a Pt cathode. In this way, the polyoxometalate could be recycled and re-used in oxygen transfer catalysis. Five such cycles were demonstrated for a number of substrates, with substrate conversions and product selectivities found to be within $\pm 3\%$ for each cycle, demonstrating that $\text{H}_5\text{PV}_2\text{Mo}_{10}\text{O}_{40}$ functions very well as an ex-cell mediator for benzaldehyde oxidation under these conditions.

The authors then demonstrated that $\text{H}_5\text{PV}_2\text{Mo}_{10}\text{O}_{40}$ can also work as an in-cell redox mediator for this conversion in catalytic quantities. Hence a solution of toluene (2 M) and $\text{H}_5\text{PV}_2\text{Mo}_{10}\text{O}_{40}$ (50 mM) in 50% H_2SO_4 was subjected to a cell potential of 1.5 V between two Pt electrodes in a single chamber cell at 70 °C, delivering nearly 30 turnovers of the mediator for a 65% yield of benzaldehyde over 10 hours.

A mechanism for the activation of the methylarenes was proposed on the basis of experimental findings and Density Functional Theory (DFT) calculations (see Figure 1.2). Together, these data suggested that the highly acidic solvent protonates the polyoxometalate, producing $[\text{H}_6\text{PV}_2\text{Mo}_{10}\text{O}_{40}]^+$, where both vanadium centres are in the +5 oxidation state. $[\text{H}_6\text{PV}_2\text{Mo}_{10}\text{O}_{40}]^+$ then oxidises the methylarene to give $[\text{H}_6\text{PV}_2\text{Mo}_{10}\text{O}_{40}]$ (where one vanadium has been reduced to V^{4+}) and the radical cation of the methylarene. A further protonation of the polyoxometalate (this time with the proton coming from the methylarene radical cation) generates a neutral methylarene radical species and $[\text{H}_7\text{PV}_2\text{Mo}_{10}\text{O}_{40}]^+$. These two intermediates were calculated to be the highest in energy in the overall process, making the formation of this neutral radical the rate determining step. Moreover, the radical nature of this process was supported by the observation of a large kinetic isotope effect (4.95) for this step. The next step in the proposed mechanism is oxygen transfer from solvent water to the neutral radical to generate benzyl alcohol. Traces of benzyl alcohol were indeed detected in the early stages of the reaction by GC-MS, lending credence to this proposed pathway. The benzyl alcohol is then readily oxidised to benzaldehyde.

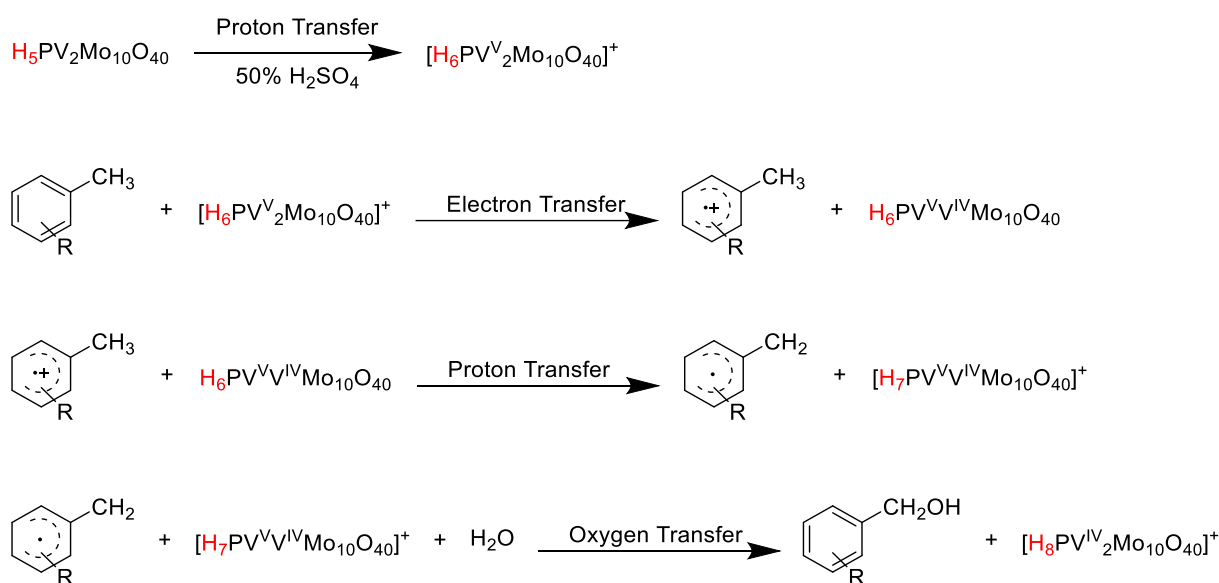
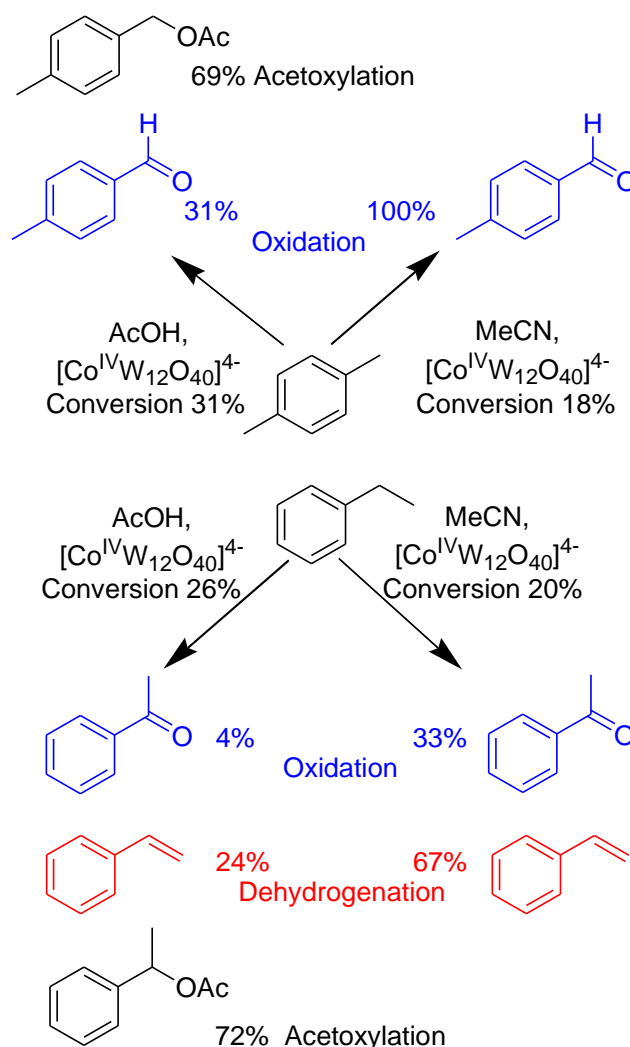


Figure 1.2: The proposed mechanistic steps for the oxidation of methylarenes to their aldehyde derivatives using the polyoxometalate $\text{H}_5\text{PV}_2\text{Mo}_{10}\text{O}_{40}$ as a catalyst.

Overall, this approach has the potential to oxidise methylenes to their aldehyde derivatives with 100% atom economy, in aqueous solvent and with product yields that are typically greater than 95%, and thus has considerable promise for the development of more sustainable routes for this broad class of chemical transformations.

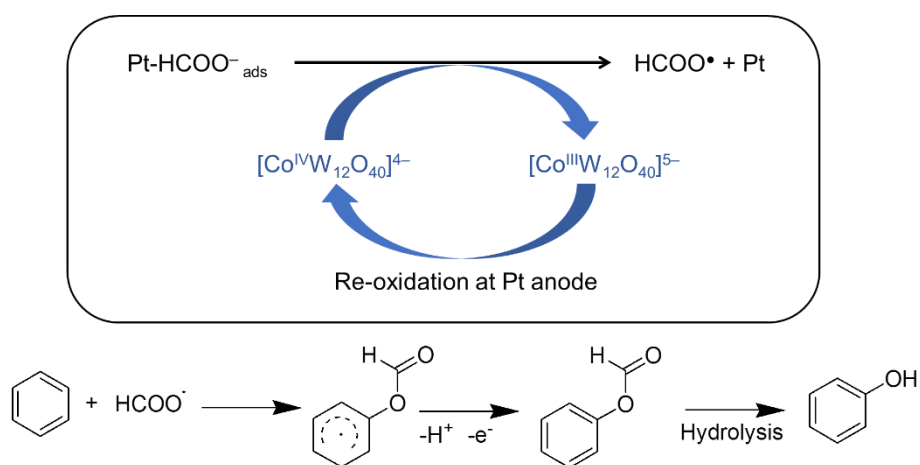
The Neumann group have also investigated the electrochemical dehydrogenation, oxidation, acetoxylation and hydroxylation of arenes using polyoxometalate redox mediators.⁵⁰ In this case, the authors electrochemically oxidised the cobalt-centred polyoxotungstate $[\text{Co}^{\text{III}}\text{W}_{12}\text{O}_{40}]^{5-}$ (originally reported by Ebersson^{51,52}) to give the powerful oxidising agent $[\text{Co}^{\text{IV}}\text{W}_{12}\text{O}_{40}]^{4-}$. This oxidised species proved to show activity for electrochemical dehydrogenation, oxidation and acetoxylation reactions on arene substrates in acetic acid and acetonitrile solvent systems as summarised in Scheme 1.5.



Scheme 1.5: Electrochemical dehydrogenations, oxidations and acetoxylation of arenes mediated by $[\text{Co}^{\text{IV}}\text{W}_{12}\text{O}_{40}]^{4-}$ as described by Khenkin *et al.*⁴⁰ Electrochemical conditions were 1.8 V vs. Ag/AgNO₃.

O₂ was determined to be the source of the oxygen in the ketone and aldehyde products on the basis of ¹⁸O₂ labelling studies, and a mechanism involving the formation of a radical cation and subsequent proton and electron transfers was proposed on the basis of the observation of a kinetic isotope effect. Benzene itself, however, was found not to react under these conditions, which the authors ascribed to the difficulty in forming the required phenyl radical cation.

The situation changed quite considerably when the electrolyte was altered to lithium formate in formic acid. Under these conditions, benzene was oxidised to phenol according to the mechanism given in Scheme 1.6.



Scheme 1.6: Electrochemical hydroxylation of arenes according to Khenkin *et al.*⁴⁰

The first step in this mechanism (shown in the box in Scheme 1.6) occurs at the (Pt) anode, whereby [Co^{III}W₁₂O₄₀]⁵⁻ is electrochemically oxidised to [Co^{IV}W₁₂O₄₀]⁴⁻. Meanwhile, formate adsorbed on the anode is also oxidised at the same time to give the formyloxyl radical, HCOO•. Through various control reactions, the authors established that it is the formation of HCOO• that is catalysed by [Co^{IV}W₁₂O₄₀]⁴⁻. These formyloxyl radicals then react with benzene to produce a cyclohexadienyl formate radical intermediate, which subsequently forms the benzyl formate. In order for this to be a feasible pathway, the formyloxyl radicals must be sufficiently long lived, and in this regard it is interesting to note that HCOO• is known to be more stable than the corresponding acetyloxyl radical,⁵³ perhaps suggesting a reason as to why the formate/formic acid electrolyte facilitates benzene oxidation whereas an acetic acid electrolyte under otherwise similar conditions does not. The radical nature of the process to generate benzyl formate was confirmed by radical trap experiments and the observation of a kinetic isotope effect for benzene oxidation. Aryl

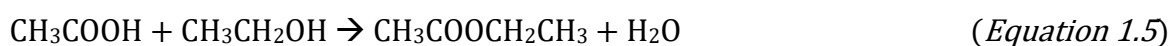
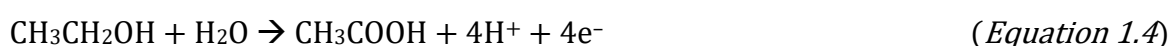
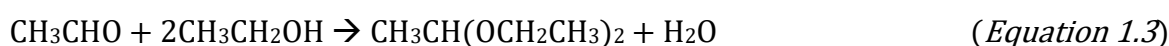
formates are sensitive to hydrolysis, allowing phenol to be obtained from the benzyl formate rapidly by mild acid catalysis. This step also leads to the generation of formic acid, effectively making formic acid a catalyst in this process. The overall process can then be considered as (Equation 1.1):



which the authors showed could proceed with Faradaic yields of up to 75% (with decomposition of formic acid to CO_2 and H_2 being the main side reaction). Meanwhile, selectivity was observed for the formation of the mono-oxidised arene products, with yields of up to 35%, suggesting that further optimisation of the reaction conditions could prove fruitful for more sustainable access to these key chemical feedstocks.

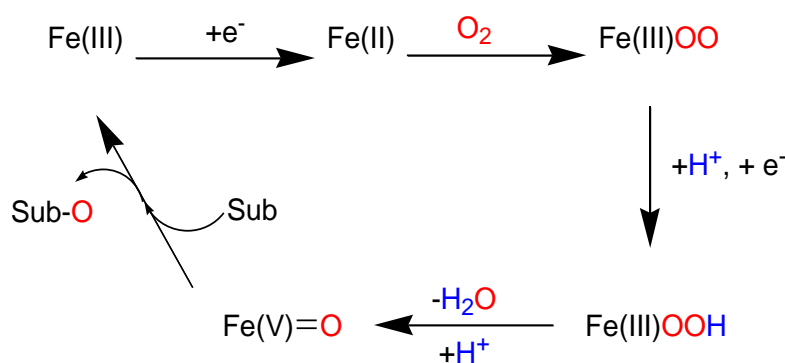
1.3.2 Oxidation of Non-Aromatic Organic Substrates with Polyoxometalate Redox Mediators

In terms of non-aromatic substrates, Bond, Zhang and co-workers reported a study on the electrocatalytic oxidation of light alcohols by $[\{\text{Ru}_4\text{O}_4(\text{OH})_2(\text{H}_2\text{O})_4\}(\gamma\text{-SiW}_{10}\text{O}_{36})_2]^{10-}$ at carbon cloth electrodes.⁵⁴ Over a wide pH range, whether in solution or confined to the electrode, the polyoxometalate was found to be an effective electrocatalyst for the oxidation of methanol and ethanol, producing dimethoxymethane and methyl formate as the ultimate products of methanol oxidation and 1-diethoxyethane and ethyl acetate as the ultimate products of ethanol oxidation. The formation of these species was proposed to occur by the initial production of the acid and aldehyde products of oxidation (formaldehyde and formic acid for methanol, and acetaldehyde and acetic acid for ethanol) followed by the condensation of these species with remaining excess alcohol to give the products observed. These processes (taking the example of ethanol oxidation) are shown in Equations 1.2-1.5:



Such mechanisms would suggest that the electrocatalytic oxidation of the alcohols occurs by two- and four-electron oxidation processes to give the aldehydes and acids respectively. Further oxidation of the substrates (*e.g.* to CO₂) was not observed, and indeed control reactions whereby [$\{\text{Ru}_4\text{O}_4(\text{OH})_2(\text{H}_2\text{O})_4\}(\gamma\text{-SiW}_{10}\text{O}_{36})_2\}^{10-}$] was employed for the attempted oxidation of formate showed that the polyoxometalate does not oxidise formate under the conditions used in the study. The combined Faradaic yields of the aforementioned electrochemical oxidation products was always >94% for both methanol and ethanol. In terms of both electrochemical activity and stability, [$\{\text{Ru}_4\text{O}_4(\text{OH})_2(\text{H}_2\text{O})_4\}(\gamma\text{-SiW}_{10}\text{O}_{36})_2\}^{10-}$] was found to display metrics for alcohol oxidation that compared very favourably to some of the better-performing molecular catalysts for alcohol oxidation then known.^{55,56}

Polyoxometalate redox mediators have also been employed for the selective electrochemical oxidation of light (non-aromatic) hydrocarbons using O₂ as the oxygen source.⁵⁷ To this end, Bugnola *et al.* showed that the porous, spherical iron–tungsten polyoxometalate capsule, $\{\text{Fe}^{\text{III}}_{30}\text{W}^{\text{VI}}_{72}\}$, originally reported by Müller and co-workers,⁵⁸ can be electrochemically reduced by 10 electrons per capsule, yielding the species $\{\text{Fe}^{\text{II}}_{10}\text{Fe}^{\text{III}}_{20}\text{W}^{\text{VI}}_{72}\}$. Armed with this information, the authors used $\{\text{Fe}^{\text{III}}_{30}\text{W}^{\text{VI}}_{72}\}$ as an in-cell redox mediator in aqueous solution (without additional supporting electrolyte) under mixed air/hydrocarbon atmospheres at Pt working/counter electrodes and a cell potential 1.8 V. Under these conditions, various aliphatic hydrocarbons such as ethane, propane and 2-methylpropane can be oxidised with modest Faradaic efficiency (*ca.* 20-35%, with the main competing reaction being the reduction of the oxidised polyoxometalate to give water) and turnover frequencies on the order of 300-400 min⁻¹ as shown in Scheme 1.7.



Scheme 1.8: Proposed mechanism of electrocatalytic oxygen transfer to organic substrates using the polyoxometalate $\{\text{Fe}^{\text{III}}_{30}\text{W}^{\text{VI}}_{72}\}$, showing the suggested pathway for oxygen incorporation into the organic substrates (“Sub”).

Very recently, some of the same authors have expanded on this preliminary report and have shown that benzene and various other more elaborate hydrocarbons can be activated by this mediator.⁵⁹ Of particular note in this regard, cyclopentanone could be converted into cyclopent-2-en-1-one in yields exceeding 98%. For most substrates, however, yields of specific products remained <50%. The mechanism of action of the reduced polyoxometalate was also probed in this study by a number of techniques. Whilst spectral identification of the key intermediates remains elusive, labelling studies using $^{18}\text{O}_2$ showed that ^{18}O is incorporated into the oxidised products, whilst various kinetic isotope effects were observed, supporting the mechanism postulated in Scheme 1.8. The ability to activate light hydrocarbons in this way could be of considerable industrial benefit, although further study of this system is required in order to determine the precise mode of action and hence improve product yields and selectivities.

1.3.3 Reduction of Organic Substrates using Polyoxometalate Redox Mediators

In contrast to reports on the use of electro-generated polyoxometalate redox mediators for the oxidation of organic substrates, the controlled reduction of organic substrates using polyoxometalate redox mediators has been much less-well explored. In 2018, Cronin and co-workers demonstrated an approach for the electrochemical reduction of nitroarenes to their corresponding aniline derivatives using the polyoxometalate silicotungstic acid $[\text{H}_4\text{SiW}_{12}\text{O}_{40}]$ as an ex-cell redox mediator.⁶⁰ The polyoxometalate was first reduced by two electrons at a carbon felt cathode in a two-compartment electrochemical cell (where the

anode reaction was the oxygen evolution reaction), to yield an aqueous solution of the active form of the mediator, $[\text{H}_6\text{SiW}_{12}\text{O}_{40}]$.^{61,62} To this mediator solution were then added aliquots of the various nitroarenes shown in Figure 1.3, allowing direct reduction of these substrates to their corresponding aniline derivatives in generally excellent yields. In the case of 4-aminobenzoic acid, the authors attributed the relatively low isolated yield of this product (45%) to its high water solubility, which may have prevented its full recovery from the aqueous phase during work-up, and similar arguments were used to explain the modest yield of 4-ansidine (65% yield) in the event that the methyl group on this molecule was cleaved. The redox mediator could be recycled using a simple separation process and then re-used without any appreciable drop in performance. In contrast to conventional routes for nitroarene reduction, this indirect electrolysis approach did not require the use of any sacrificial reducing agents, co-catalysts or the handling of hydrogen gas. Another point worth mentioning with regard to this report is the excellent reaction yields that could be obtained even for organic substrates with very low solubility in water (*e.g.* 4-nitroanisole and 4-nitrobenzoic acid). The ability to obtain good conversions from reactions where the substrates are not fully dissolved will be crucial in permitting wider use of aqueous solvent systems (and by extension, most polyoxometalates) in indirect electrochemical methods, and thus helping to facilitate the development of more sustainable chemical processes.

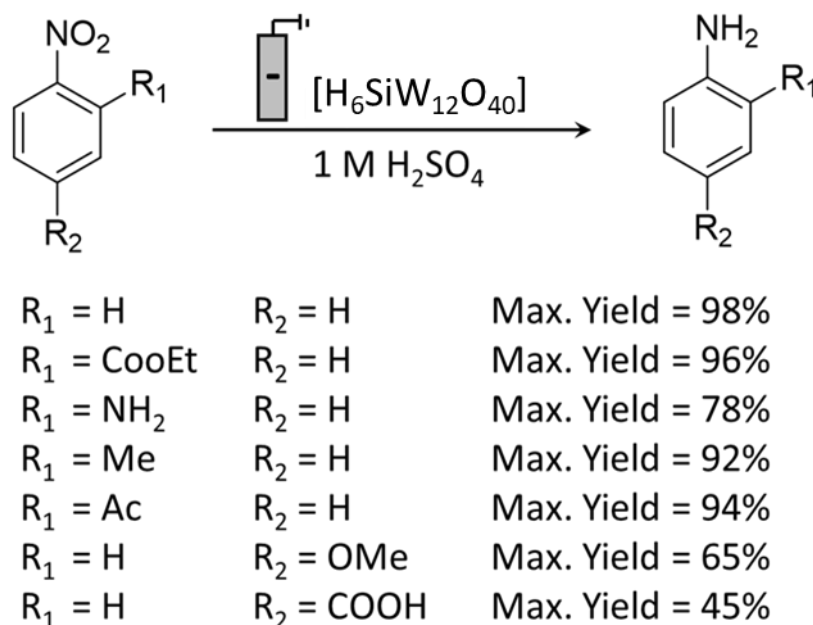


Figure 1.3: Graphic representation of the reduction of nitroarenes to their aniline derivatives mediated by electrochemically-generated $[\text{H}_6\text{SiW}_{12}\text{O}_{40}]$.

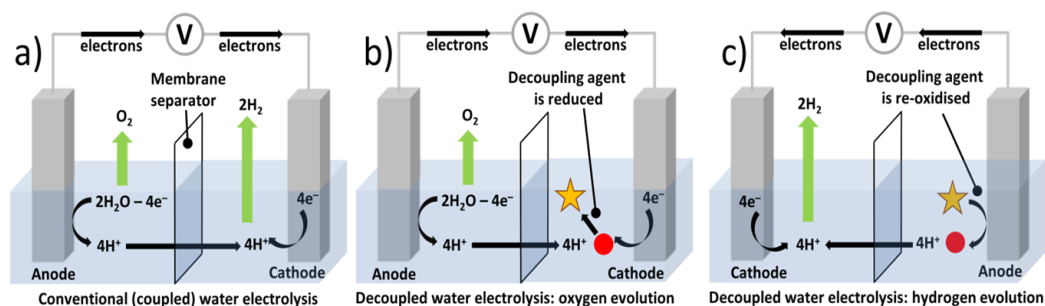


Figure 1.4: A comparison of (panel a) conventional vs. decoupled water electrolysis (panels b and c) under general acidic conditions.

Since electrochemical synthesis is the main topic of interest in this thesis, decoupled electrolysis for water splitting will not be analysed any further, instead we will provide some examples of the utilisation of decoupled electrolysis for processes that go beyond the generation of hydrogen and oxygen from water.

1.4.1 Decoupled Electrolysis in Organic Processes

You and co-workers, inspired by the novel approach introduced by Goodwin and Walsh that spatially decoupled OER and HER (Figure 1.5),⁶⁵ utilised the $\text{Fe}(\text{CN})_6^{3-}/\text{Fe}(\text{CN})_6^{4-}$ decoupling agent and a closed bipolar electrode to decouple hydrogen production from the oxidation of organic pollutants during electrochemical decontamination of wastewater.⁶⁶

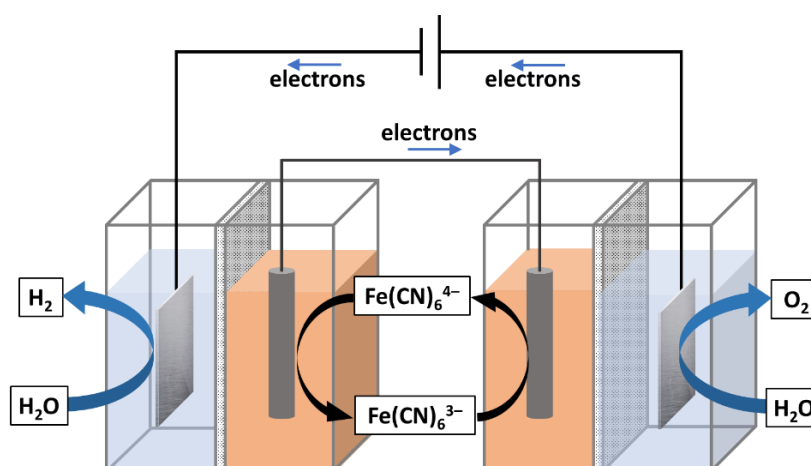


Figure 1.5: The closed bipolar electrode cell system used by Goodwin and Walsh.⁶⁵ Pt electrodes were used for the water splitting half reactions while carbon cloth electrodes were used in the mediator solution.

Bipolar electrodes are conducting components which can promote both anodic and cathodic reactions simultaneously; these electrodes are further denoted as “closed” when their poles are in two separate solutions. In a conventional electrochemical cell for oxidation of organic pollutants, the corresponding cathode reaction is the generation of hydrogen. The authors suggested that this presents a hazard under some conditions and is also wasteful, as the H_2 is rarely harvested. They therefore proposed decoupling as a route by which hydrogen generation could take place outside the pollutant oxidation cell, for safety and ease of hydrogen collection. In a system similar to that used by Goodwin and Walsh, two separate two-compartment cells were bridged by a closed bipolar electrode (Figure 1.6). Inside each two-compartment cell, one end of the closed bipolar electrode was submerged in a solution of $K_3Fe(CN)_6/K_4Fe(CN)_6$ in a 0.1 M phosphate buffer solution ($pH = 7.2 \pm 0.3$). A Nafion membrane separated the two compartments in each cell, thus separating the compartment containing the closed bipolar electrode from the other, containing wastewater in the anode and water on the cathode side. This allowed the generation of hydrogen *via* water splitting at a Pt/C cathode, with concomitant oxidation of $Fe(CN)_6^{4-}$ to occur in one cell. In the other cell, oxidation of the organic pollutant phenol was achieved on a TiSO anode, with accompanying $Fe(CN)_6^{3-}$ reduction.

At current densities of 16 mA cm^{-2} , the phenol removal efficiency at the TiSO anode over 2 h was found to exceed 96%, whilst the Faradaic yield for hydrogen product at the Pt/C cathode in the other cell was quantitative. This hydrogen was generated in a separate cell to the organic oxidation reaction (which generates O_2 as a side product) and so required no further purification.

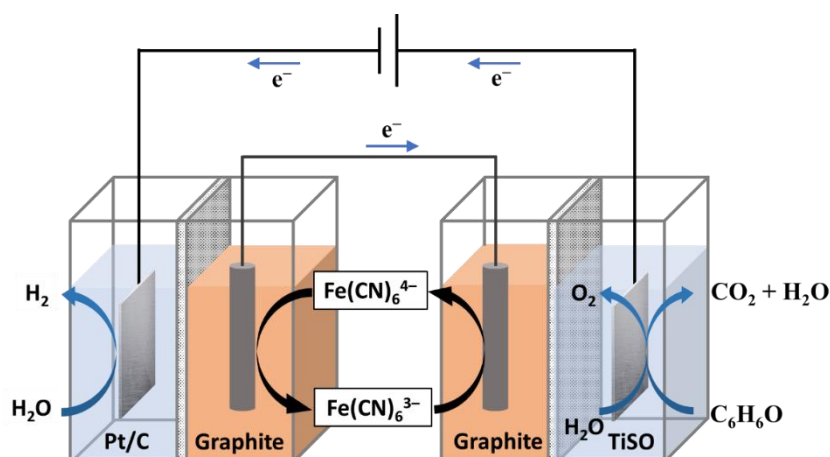


Figure 1.6: Schematic illustration of the electrochemical setup used by You et al.⁶⁶

The authors argued that this would decrease the complexity of any scaled-up version of the process, as well as allowing a portion of the energy spent on anodic oxidation of pollutants (10-20%) to be recovered on account of the value of the hydrogen produced.

Li *et al.* used the decoupling agent $\text{Na}_4[\text{Fe}(\text{CN})_6]$ to decouple the HER from the oxidation of 5-hydroxymethylfurfural to 2,5-furandicarboxylic acid.⁶⁷ 5-Hydroxymethylfurfural is a readily-available product of dehydration of certain sugars, and thus constitutes a sustainable feedstock chemical; the authors proposed that its chemical transformation to 2,5-furandicarboxylic acid represented a higher-value anodic counterpart for hydrogen evolution than the oxidation of water. Accordingly, the authors assembled a two-compartment cell separated by a cation exchange membrane. The HER was first performed at a CoP on carbon electrode, with concomitant oxidation of the decoupling agent at the carbon counter electrode. In the second step, this mediator was re-reduced as 5-hydroxymethylfurfural oxidation occurred at a Ni anode. 100% conversion of 5-hydroxymethylfurfural (giving an 83% yield of 2,5-furandicarboxylic acid) was reported, using mild electrochemical conditions. This approach could offer an effective and environmentally friendly approach for combining the electrolytic production of hydrogen with the generation of useful chemicals in situations where sustainably-sourced organic feedstocks are available.

1.4.2 Decoupled Electrolysis in Inorganic Synthesis

Decoupling the chlor-alkali process is a prime example of the application of the principles of decoupled electrolysis in inorganic chemical synthesis. In the chlor-alkali process, a sodium chloride solution is electrolysed to generate Cl_2 , H_2 and NaOH as the products. Together, these products are themselves used in over 50% of all industrial processes, underlining the fundamental importance of the chlor-alkali process to the chemical industry at large. Historically, Cl_2 , H_2 and NaOH were produced in mercury-containing cells according to the Castner-Kellner process (itself an electrochemical decoupling strategy, whereby Cl_2 and H_2 evolution are decoupled using a mercury amalgam electrode as the decoupling agent).⁶⁸ In recent years, however, mercury cells have fallen out of favour due to concerns over mercury's toxicity. Hence, most chlor-alkali cells now use either asbestos diaphragms or fluorine-containing ion-exchange membranes to separate the chlorine and hydrogen that are produced. However, Hou *et al.* argued that the high cost of these separators and their short lifetimes during operation made the need for improvements vital. Therefore, these authors proposed a membrane-free process whereby the Cl_2 evolution and H_2/NaOH

production steps were decoupled by employing the reversible Na-ion intercalation/de-intercalation reaction of a $\text{Na}_{0.44}\text{MnO}_2$ -based electrode.⁶⁹

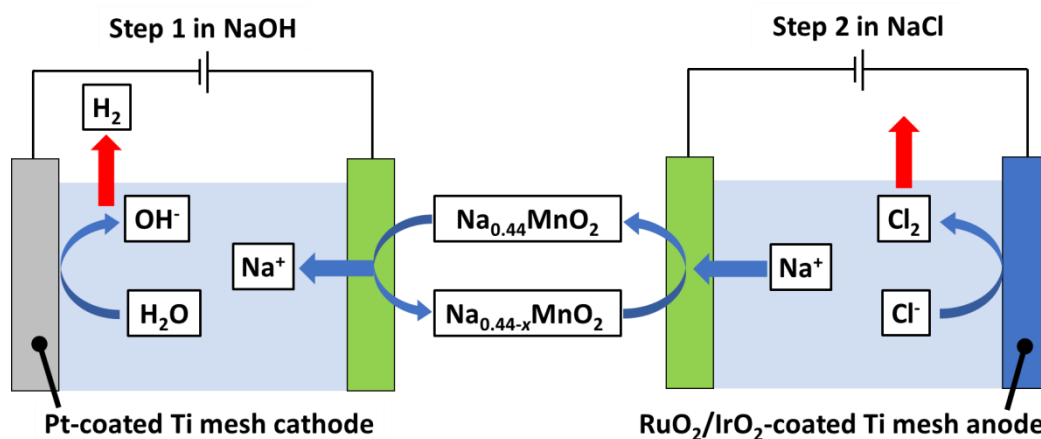


Figure 1.7: The two-step decoupled chlor-alkali process reported by Hou et al.⁵⁹

An illustration of this decoupled process and the reactions involved is provided in Figure 1.7. Hence water reduction to generate H_2 and hydroxide is accompanied by sodium de-intercalation from the decoupling agent electrode. Subsequently, chloride ions are oxidised to Cl_2 with the simultaneous reduction of the decoupling electrode, which occurs together with re-intercalation of sodium ions to restore the original $\text{Na}_{0.44}\text{MnO}_2$ stoichiometry. The $\text{Na}_{0.44}\text{MnO}_2$ -based electrode has previously been employed in sodium ion batteries, and so displays the required sodium ion intercalation/de-intercalation properties; its redox waves are also almost exactly midway between the onset of hydrogen and chlorine evolution.

In the first step, hydrogen evolution on a Pt-coated Ti-mesh electrode was found to proceed at a Faradaic efficiency of 100%, whilst chlorine evolution on a $\text{RuO}_2/\text{IrO}_2$ -coated Ti mesh displayed a Faradaic efficiency of 90%, which the authors attributed to the hydrolysis of Cl_2 to give soluble species such as HClO . The authors also noted that the current density that the system can reach is limited by the kinetics of sodium ion intercalation/de-intercalation into and out of the $\text{Na}_{0.44}\text{MnO}_2$ -based electrode. Technologically-relevant current densities for the HER and chlorine evolution reactions of up to 0.5 A cm^{-2} were achieved, but only if very large $\text{Na}_{0.44}\text{MnO}_2$ electrodes were employed. Attempting to improve the kinetics of this intercalation/de-intercalation process would therefore be one area in which further investigation could prove beneficial, and which might bring about the realisation of some of

the benefits of decoupling for this reaction (including avoiding the need for a membrane separator and preventing mixing of the H₂ and Cl₂ product gases).

Zhao *et al.* have taken this work a step further, by proposing a system for decoupling Cl₂ and NaOH production that uses two decoupling agents and three different electrochemical cell configurations.⁷⁰ An illustration of this concept is provided in Figure 1.8.

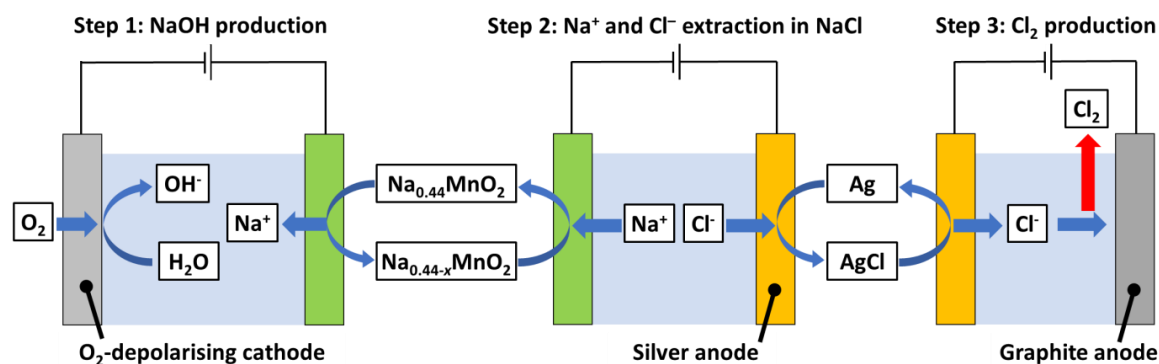
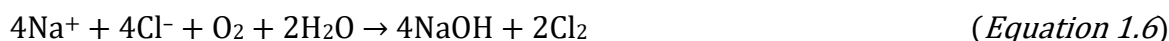


Figure 1.8: The three-step decoupled chlor-alkali process reported by Zhao *et al.*⁶⁰

Hence, in the first cell, oxygen reduction (to hydroxide) is paired with oxidation (and de-sodiation) of a Na_{0.44}MnO₂-based electrode to generate NaOH. The de-sodiated Na_{0.44-x}MnO₂ electrode is then placed in a chloride-containing electrolyte and used as the cathode in a second electrolysis cell, alongside a silver anode. Operating this cell re-reduces (and re-sodiates) the Na_{0.44}MnO₂ electrode, whilst at the anode insoluble AgCl forms. In the final step, the AgCl electrode is used as the cathode in a third electrolytic cell alongside a graphite anode. As the AgCl is reduced (regenerating Ag(0)), chloride ions are released with migrate to the anode and are discharged as Cl₂. The overall reaction thus produces no hydrogen and is:



The authors suggested that such an approach decouples NaOH and chlorine production and so prevents the production of caustic chlorates which could otherwise damage the Na_{0.44}MnO₂ electrode. Using oxygen as the reductive couple in the first cell was also held to reduce the overall voltage requirement for Cl₂ and NaOH production. Excellent stability to multiple redox cycles was demonstrated for each of the three processes, with high Coulombic efficiencies. Moreover, the authors were also able to show that this concept can

be expanded to other salts, *e.g.* to the continuous production of NaOH and HNO₃ from a solution of NaNO₃. This route therefore offers considerable promise, although it may prove non-trivial to design large-scale systems where electrodes are easily switched between cells.

1.5 Vanadium Salts

Vanadium compounds have been extensively used in electrochemistry in various applications such as redox flow batteries and electrochemical catalysis.⁷¹ The chemistry of vanadium and more specifically its variety of easily accessible oxidation states (ranging from +5 to +2) makes it a very promising candidate for electrochemical processes. In terms of electrochemical catalysis applications, vanadium has been involved mainly in oxidation reactions with few examples of electro-reductions including the hydrazine to ammonia process and nitrite reduction.⁷¹ Moreover, the standard potential of the V(III)/V(II) redox couple is -0.255 V vs. SHE under aqueous conditions⁷² which is comparable to the potential used in chapters 3&4 of the present thesis with the polyoxometalate mediators. Preliminary studies have shown us that a vanadium (III) salt can be a promising alternative to the polyoxometalate mediator (phosphotungstic acid) used for the electrochemical reduction of nitrobenzene. A key motivator for the use of vanadium salts as alternative redox mediators is the fact that their molecular weights are a lot lower than that of phosphotungstic acid. In that context, it is to our interest to briefly discuss the application of vanadium in electrochemical processes.

Recently, the electrochemical synthesis of dinitrobenzenes was studied by Mikhalchenko et al.⁷³ In this report, the authors successfully performed the selective electrochemical reduction of *m*-dinitrobenzene to its corresponding aniline using an excess (4 : 1 relative to the starting material) of VCl₃ salt. The catholyte was prepared by dissolving the mediator in 2 M HCl and controlled current electrolysis (-35 mA cm^{-2}) at a lead plate cathode was performed. The process provided an isolated yield of 66% together with a faradaic efficiency of 63%. According to the authors, the isolated yield was not optimal due to the high solubility of the reaction product in the vanadium salt solution. However, in this report, only stoichiometric amounts of the mediator were used with no evidence for a catalytic process.

As we mentioned before, vanadium has been used in different aspects of electrochemistry, with examples of decoupled water electrolysis to be briefly discussed below in an attempt to highlight its potential to be used as an electron carrier in organic electrosynthesis. Decoupled electrolysis systems inspired by redox flow batteries have also been developed using more

conventional flow battery electrolytes. In 2014, Amstutz *et al.* reported a system for the decoupled electrolysis of water using a vanadium-based catholyte and cerium-based anolyte.⁷⁴ To mediate water electrolysis, a solution containing a V(III) salt, in sulfuric acid, was reduced to V(II) solution at a graphite felt electrode. The position of the V(III)/V(II) redox couple (-0.26 V vs. SHE under the conditions used) is negative of the proton reduction couple, and so, exposure of this V(II) solution to hydrogen evolution catalysts should give rise to spontaneous (non-electrochemical) hydrogen generation. Hence, when this V(II) solution was directed into an external catalytic reactor, the HER occurred over a Mo_2C catalyst, with a Faradaic yield of up to 96% (Equation 1.7 and Figure 1.9).

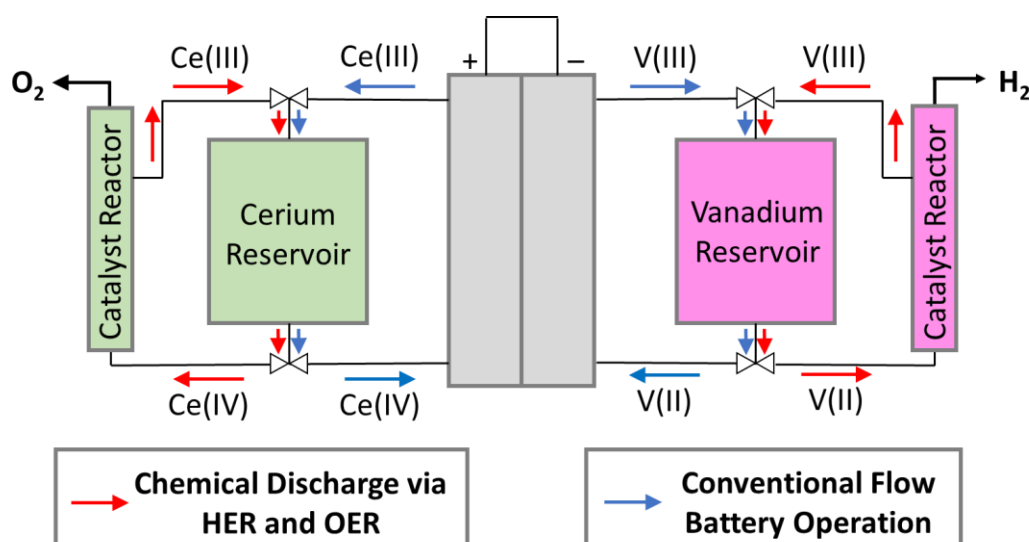


Figure 1.9: Schematic of the Ce-V redox flow battery system employed by Amstutz *et al.*⁶⁴ where valves allow for on-demand H₂ or O₂ production via routing of the electrolytes to external catalytic reactors.

Similarly, at the anode of the flow-battery type system, an acidic solution of Ce(III) was oxidised to Ce(IV). The position of the Ce(III)/ Ce(IV) redox couple under these conditions is more anodic than that for water oxidation, meaning that (in the presence of a suitable catalyst), Ce(IV) should be able to oxidise water to generate oxygen, becoming reduced back

to Ce(III) in the process (Equation 1.8). In practice, Amstutz *et al.* achieved this catalytic water oxidation reaction over RuO₂ nanoparticles. The Faradaic yield for the OER ($78 \pm 8\%$) was somewhat less than optimal, which was attributed to a side reaction (previously reported in literature⁷⁵) whereby Ce(IV) reacts with the RuO₂ catalyst as it is reduced to Ce(III). The authors suggested that this issue could be avoided by adapting the electrolyte to an all-vanadium system (where the OER would then be mediated by the reduction of V(V) to V(IV)).

As with the [P₂W₁₈O₆₂]ⁿ⁻ system,⁷⁶ this device configuration allowed both for conventional operation as a redox flow battery (the electrolyte could be charged and discharged with electrical energy, cycling between V(II) and V(III) at one electrode and between Ce(IV) and Ce(III) at the other), or the conversion of energy to hydrogen, offering considerable flexibility for renewable energy usage to the operator.

Ho *et al.* have also made use of the V(III)/V(II) redox couple in their solar-driven approach to decoupled water electrolysis.⁷⁷ The authors noted that there were numerous examples of earth-abundant OER electrocatalysts, with optimal stability when used at alkaline pH.⁷⁸ However, the V(III)/V(II) couple for HER generation is only soluble at low pH. By employing a bipolar membrane, a large pH differential between the anode and cathode compartments of the electrochemical cell could be maintained, allowing the OER side to be at high pH whilst the HER side was at very low pH (Figure 1.10). This dual electrolyte system consisted of an anodic chamber with a Ni mesh oxygen evolution electrode in concentrated KOH (2.5 M), and a cathodic chamber using a Pt foil electrode in sulfuric acid (2.0 M). At the Ni anode, OH⁻ was oxidised yielding electrons, water and oxygen; these electrons travelled through the external circuit to the cathode, where they reduced V(III) ions to V(II). Once charged, the V(II) solution was then transferred to a separate reactor where, when stirred with an Mo₂C catalyst, hydrogen was produced on-demand. The Faradaic efficiency of the hydrogen production step using this cell was investigated at different depths of charge of the vanadium solution: when this solution was reduced to 27, 55 and 96% of its charging capacity, the amount of hydrogen collected corresponded to Faradaic efficiencies of 87, 87 and 83%, respectively. Hydrogen generation under elevated pressures (important for compression and storage efficiencies) was also demonstrated: at pressures up to 10 atm, hydrogen could be produced at Faradaic efficiencies approaching 60%.

Furthermore, the authors demonstrated that the system could be powered by renewable energy by coupling it to a photovoltaic module: using only the power supplied by this photovoltaic and solar irradiation, hydrogen was produced at a Faradaic efficiency of 80%

and a solar-to-hydrogen energy conversion efficiency of 5.8% was achieved. This represents a significant milestone in demonstrating the practicality of decoupled electrolysis for solar-to-hydrogen conversion.

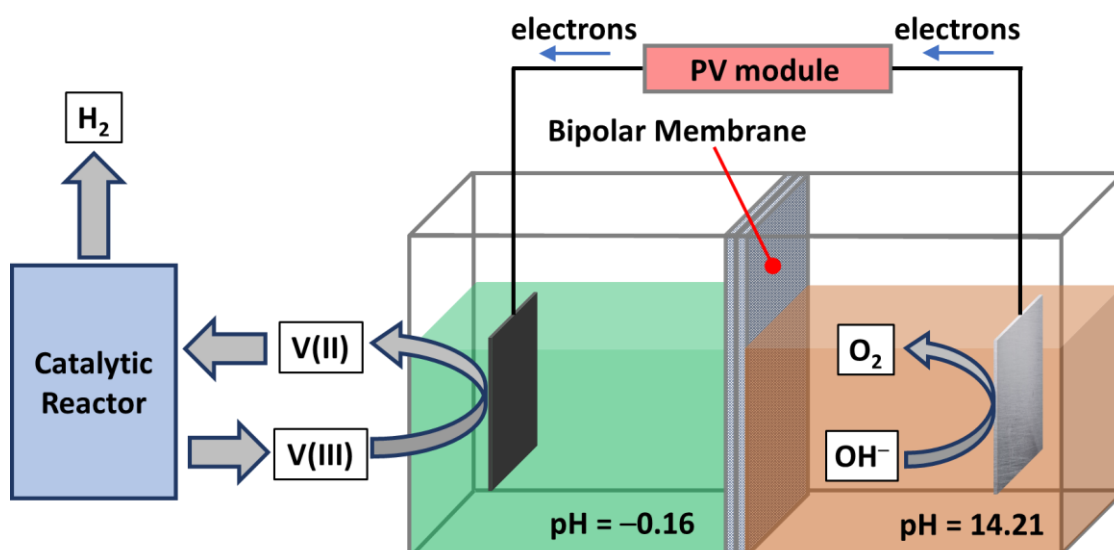


Figure 1.10: Diagram of the setup used by Ho et al.⁷⁷ where alkaline water oxidation is coupled with the reduction of V(III) to V(II) in a dual electrolyte, two-compartment cell separated by a bipolar membrane and powered by a solar-driven photovoltaic. The V(II) species can then be charged into a catalytic reactor, producing hydrogen and regenerating V(III).

1.6 Conclusion

In this chapter, we have attempted to provide an introduction to the concept of indirect electrolysis that is of great scientific interest in the present thesis. We have given an overview of the use of polyoxometalate redox mediators for electro-organic synthesis, which constitutes the main topic of research in this thesis, with a special emphasis on studies conducted in the last seven years. Polyoxometalates are diverse in their structures and properties, and many polyoxometalates possess attributes which make them attractive as mediators in organic electrosynthesis, including (sometimes multiple) reversible redox waves, well-understood electron transfer processes, and solubility in a range of common solvent environments. Polyoxometalates' redox properties can also often be manipulated as a function of the polarity of the medium,⁷⁹ and in this regard the exploration of perfluorinated solvents and ionic liquids as media for electro-organic synthesis with polyoxometalates could act to broaden the field considerably.

To date, polyoxometalate mediators have been utilised mostly in electro-oxidation processes, but recent results have also highlighted their potential as electro-generated reducing equivalents. The sheer number of possible polyoxometalates means that the results that are collated in this chapter represent only a tiny fraction of the possible mediator-substrate pairings, and so there is clearly tremendous scope for further discoveries to be made in this area.

What, then, are the most pressing challenges and most promising future directions for polyoxometalate redox mediators in electro-organic synthesis? Compared to more common organic mediators, polyoxometalates suffer the drawback that they tend to be very large molecules with high molecular weights: their performance in any particular reaction therefore needs to be a significant improvement over that possible with smaller mediators in order to justify the use of polyoxometalates. It is also harder to design systems where the mediator is covalently attached to an electrode for polyoxometalates when compared to organic mediators: polyoxometalates can be functionalised with organic tethers,⁸⁰ but there are only a very few studies where such methodology has been used to covalently attach polyoxometalates to electrodes and then study the effects this has on the electrochemical properties of those polyoxometalates.^{81,82} On the other hand, polyoxometalates make ideal mediators for the concerted movement of both protons and electrons,⁸³ their redox processes are very well understood from a theoretical point of view,^{84,85} and the prospects for combining photoredox chemistry with indirect electrolysis with polyoxometalates look good, as many polyoxometalates display intrinsic photoredox properties.⁸⁶ It seems likely,

therefore, that polyoxometalates will find ever-increasing application in the electro-conversion of organic substrates in complimentary roles to those filled by smaller organic mediator molecules.

We have also introduced the concept of decoupled electrolysis which to date, has been mostly applied to water electrolysis. However, the great advantages that such a system provides including the separation of the anode and cathode reactions in time and space makes it a promising candidate to be used in electrochemical organic synthesis. Early examples have been highlighted in the section 1.4.

Moreover, vanadium salts have been identified as potential suitable alternatives to the polyoxometalate redox mediator for the electrochemical reduction of nitrobenzene to aniline. As such, examples of its use in electrochemical organic synthesis as well as decoupled water electrolysis has been briefly discussed. Vanadium (III) has the potential to be used as an efficient $1 e^-$ carrier in electrochemical reductions, which are more challenging than the oxidation processes as already stated, since the standard potential of the redox couple V(III)/V(II) is -0.255 V vs. SHE in aqueous conditions.

To sum up, in this chapter, we provide a comprehensive study of the current literature in the application of polyoxometalate redox mediators in organic electrosynthesis as well as introducing the concept of decoupled electrolysis in organic processes and inorganic synthesis. We have also identified, and briefly discussed, vanadium (III) as a potential redox mediator alternative, to perform challenging electrochemical reductions.

1.7 References

- 1 M. Faraday, Experimental Researches in Electricity, *Philos. Trans. R. Soc. London* 122 (1832) 125–162, <https://doi.org/10.1098/rstl.1832.0006>
- 2 A. Wiebe, T. Gieshoff, S. Möhle, E. Rodrigo, M. Zirbes, S. R. Waldvogel, Electrifying Organic Synthesis, *Angew. Chem. Int. Ed.* 57 (2018) 5594–5619, <https://doi.org/10.1002/anie.201711060>
- 3 M. C. Leech, A. D. Garcia, A. Petti, A. P. Dobbs, K. Lam, Organic electrosynthesis: from academia to industry, *React. Chem. Eng.* 5 (2020) 977–990, <https://doi.org/10.1039/D0RE00064G>
- 4 A. Shatskiy, H. Lundberg, M. D. Kärkäs, Organic Electrosynthesis: Applications in Complex Molecule Synthesis, *ChemElectroChem* 6 (2019) 4067–4092, <https://doi.org/10.1002/celc.201900435>
- 5 D. S. P. Cardoso, B. Šljukić, D. M. F. Santos, C. A. C. Sequeira, Organic Electrosynthesis: From Laboratorial Practice to Industrial Applications, *Org. Process Res. Dev.* 21 (2017) 1213–1226, <https://doi.org/10.1021/acs.oprd.7b00004>
- 6 F. Marken, J. D. Wadhawan, Multiphase Methods in Organic Electrosynthesis, *Acc. Chem. Res.* 52 (2019) 3325–3338, <https://doi.org/10.1021/acs.accounts.9b00480>
- 7 B. A. Frontana-Urbe, R. D. Little, J. G. Ibanez, A. Palma, R. Vasquez-Medrano, *Green Chem.* 12 (2010) 2099–2119, <https://doi.org/10.1039/C0GC00382D>
- 8 H. J. Schäfer, M. Harenbrock, E. Klocke, M. Plate, A. Weiper-Idelmann, *Pure Appl. Chem.* 79 (2007) 2047–2057, <https://doi.org/10.1351/pac200779112047>
- 9 D. Pletcher, Organic electrosynthesis—A road to greater application. A mini review, *Electrochem. Commun.* 88 (2018) 1–4, <https://doi.org/10.1016/j.elecom.2018.01.006>
- 10 D. Pletcher, F. C. Walsh, *Industrial Electrochemistry* (2nd Ed.), Springer Science+Business Media, LLC: Bangalore, 1993.
- 11 R. Francke, R. D. Little, Redox catalysis in organic electrosynthesis: basic principles and recent developments, *Chem. Soc. Rev.* 43 (2014) 2492–2521, <https://doi.org/10.1039/C3CS60464K>
- 12 F. Wang, S. S. Stahl, Electrochemical Oxidation of Organic Molecules at Lower Overpotential: Accessing Broader Functional Group Compatibility with Electron–Proton Transfer Mediators, *Acc. Chem. Res.* 53 (2020) 561–574,

<https://doi.org/10.1021/acs.accounts.9b00544>

- 13 A. Paul, W. John, *Green Chemistry: Theory and Practice*, Oxford University Press: New York, 1998.
- 14 M.-O. Simon, C.-J. Li, Green chemistry oriented organic synthesis in water, *Chem. Soc. Rev.* 41 (2012) 1415–1427, <https://doi.org/10.1039/C1CS15222J>
- 15 E. Steckhan, Indirect Electroorganic Syntheses - A Modern Chapter of Organic Electrochemistry, *Angew. Chemie Int. Ed.* 25 (1986) 683–701, <https://doi.org/10.1002/anie.198606831>
- 16 J. E. Nutting, M. Rafiee, S. S. Stahl, Tetramethylpiperidine *N*-Oxyl (TEMPO), Phthalimide *N*-Oxyl (PINO), and Related *N*-Oxyl Species: Electrochemical Properties and Their Use in Electrocatalytic Reactions, *Chem. Rev.* 118 (2018) 4834–4885, <https://doi.org/10.1021/acs.chemrev.7b00763>
- 17 M. Sadakane, E. Steckhan, Electrochemical Properties of Polyoxometalates as Electrocatalysts, *Chem. Rev.* 98 (1998) 219-237, <https://doi.org/10.1021/cr960403a>
- 18 Y. Ji, L. Huang, J. Hu, C. Streb, Y.-F. Song, Polyoxometalate-functionalized nanocarbon materials for energy conversion, energy storage and sensor systems, *Energy Environ. Sci.* 8 (2015) 776-789, <https://doi.org/10.1039/C4EE03749A>
- 19 M. Ammam, Polyoxometalates: formation, structures, principal properties, main deposition methods and application in sensing, *J. Mater. Chem. A* 1 (2013) 6291-6312, <https://doi.org/10.1039/C3TA01663C>
- 20 D. Gao, I. Trentin, L. Schwiedrzik, L. González, C. Streb, The Reactivity and Stability of Polyoxometalate Water Oxidation Electrocatalysts, *Molecules* 25 (2020) 157, <https://doi.org/10.3390/molecules25010157>
- 21 D.-L. Long, E. Burkholder, L. Cronin, Polyoxometalate clusters, nanostructures and materials: From self assembly to designer materials and devices, *Chem. Soc. Rev.* 36 (2007) 105–121, <https://doi.org/10.1039/B502666K>
- 22 R. G. Finke, M. W. Droege, P. J. Domaille, Trivalent heteropolytungstate derivatives. 3. Rational syntheses, characterization, two-dimensional tungsten-183 NMR, and properties of tungstometallophosphates P₂W₁₈M₄(H₂O)₂O₆₈10⁻ and P₄W₃₀M₄(H₂O)₂O₁₁₂16⁻ (M = cobalt, copper, zinc), *Inorg. Chem.* 26 (1987) 3886-3896, <https://doi.org/10.1021/ic00270a014>

- 23 S.-S. Wang, G.-Y. Yang, Recent Advances in Polyoxometalate-Catalyzed Reactions, *Chem. Rev.* 115 (2015) 4893-4962, <https://doi.org/10.1021/cr500390v>
- 24 M. M. Heravi, M. Mirzaei, S. Y. S. Beheshtiha, V. Zadsirjan, F. M. Ameli, M. Bazargan, H5BW12O40 as a green and efficient homogeneous but recyclable catalyst in the synthesis of 4*H*-Pyrans via multicomponent reaction, *Appl Organometal Chem.* 32 (2018), <https://doi.org/10.1002/aoc.4479>.
- 25 R. Liu, G. Zhang, H. Cao, S. Zhang, Y. Xie, A. Haider, U. Kortz, B. Chen, N. S. Dalal, Y. Zhao, L. Zhi, C.-X. Wu, L.-K. Yan, Z. Su, B. Keita, Enhanced proton and electron reservoir abilities of polyoxometalate grafted on graphene for high-performance hydrogen evolution, *Energy Environ. Sci.* 9 (2016) 1012-1023, <https://doi.org/10.1039/C5EE03503A>
- 26 N. I. Gumerova, A. Rompel, Synthesis, structures and applications of electron-rich polyoxometalates, *Nat. Rev. Chem.* 2 (2018) 0112, <https://doi.org/10.1038/s41570-018-0112>
- 27 I. A. Weinstock, Homogenous-Phase Electron Transfer reactions of Polyoxometalates, *Chem. Rev.* 98 (1998), 113-170, <https://doi.org/10.1021/cr9703414>
- 28 M. M. Heravi, S. Sadjadi, Recent developments in use of heteropolyacids, their salts and polyoxometalates in organic synthesis, *J. Iran. Chem. Soc.* 6 (2009) 1-54, <https://doi.org/10.1007/BF03246501>
- 29 M. M. Hossain, L. Aldous, Polyoxometalates as solution-phase electrocatalytic mediators for reduced electrode fouling and the improved oxidative response of phenols, *Electrochem. Commun.* 69 (2016) 32-35, <http://dx.doi.org/10.1016/j.elecom.2016.05.020>
- 30 I. A. Weinstock, Homogeneous-Phase Electron-Transfer Reactions of Polyoxometalates, *Chem. Rev.* 98 (1998) 113-170, <https://doi.org/10.1021/cr9703414>
- 31 M. Carraro, G. Fiorani, A. Sartorel, M. Bonchio, Chapter 21: *Polyoxometalates Catalysts for Sustainable Oxidations and Energy Applications*, In: *Handbook of Advanced Methods and Processes in Oxidation Catalysis*, Imperial College Press, London (2014) 586-630, https://doi.org/10.1142/9781848167513_0021

- 32 T. Ueda, Electrochemistry of Polyoxometalates: From Fundamental Aspects to Applications, *Chem. Electro. Chem.* 5 (2018), 823-838, <https://doi.org/10.1002/celc.201701170>
- 33 M. Sadakane, E. Steckhan, Electrochemical Properties of Polyoxometalates as Electrocatalysts, *Chem. Rev.* 98 (1998), 219-237, <https://doi.org/10.1021/cr960403a>
- 34 B. Keita, L. Nadjo, New aspects of the electrochemistry of heteropolyacids: Part II. Coupled electron and proton transfers in the reduction of silicoungstic species, *J. Electroanal. Chem.* 217 (1987), 287-304, [https://doi.org/10.1016/0022-0728\(87\)80225-5](https://doi.org/10.1016/0022-0728(87)80225-5)
- 35 J.-J. Chen, M. D. Symes, L. Cronin, Highly reduced and protonated aqueous solutions of [P₂W₁₈O₆₂]⁶⁻ for on-demand hydrogen generation and energy storage, *Nature Chem.* 10 (2018), 1042-1047, <https://doi.org/10.1038/s41557-018-0109-5>
- 36 B. Rausch, M. D. Symes, G. Chisholm, L. Cronin, Decoupled catalytic hydrogen evolution from a molecular metal oxide redox mediator in water splitting, *Science* 345 (2014), 1326-1330, <https://doi.org/10.1126/science.1257443>.
- 37 A. D Stergiou, M. D. Symes, High yield and selective electrocatalytic reduction of nitroarenes to anilines using redox mediators. *Cell Rep. Phys. Sci.* 3 (2022), 100914, <https://doi.org/10.1016/j.xcrp.2022.100914>
- 38 A. D Stergiou, D. H. Broadhurst, M. D. Symes, Highly Selective Electrocatalytic Reduction of Substituted Nitrobenzenes to their Aniline Derivatives using a Polyoxometalate Redox Mediator. *ACS Org. Inorg. Au* (2022), <https://doi.org/10.1021/acsorginorgau.2c00047>
- 39 C. Rong, F. C. Anson, Simplified Preparations and Electrochemical Behavior of Two Chromium-Substituted Heteropolytungstate Anions, *Inorg. Chem.* 33 (1994) 1064-1070, <https://doi.org/10.1021/ic00084a016>
- 40 J. C. Bart, F. C. Anson, Coordination, electron transfer and catalytic chemistry of a ruthenium-substituted heteropolytungstate anion as revealed in its electrochemical behaviour, *J. Electroanal. Chem.* 390 (1995) 11-19, [https://doi.org/10.1016/0022-0728\(95\)03902-S](https://doi.org/10.1016/0022-0728(95)03902-S)
- 41 M. Sadakane, E. Steckhan, Investigation of the manganese-substituted α -Keggin-heteropolyanion K₆SiW₁₁O₃₉Mn(H₂O) by cyclic voltammetry and its application as

- oxidation catalyst, *J. Mol. Catal. A Chem.* 114 (1996) 221-228, [https://doi.org/10.1016/S1381-1169\(96\)00321-4](https://doi.org/10.1016/S1381-1169(96)00321-4)
- 42 M. S. Freund, J. A. Labinger, N. S. Lewis, J. E. Bercaw, Electrocatalytic functionalization of alkanes using aqueous platinum salts, *J. Mol. Catal.* 87 (1994) L11-L15, [https://doi.org/10.1016/0304-5102\(93\)E0230-E](https://doi.org/10.1016/0304-5102(93)E0230-E)
- 43 A. G. Wallace, M. D. Symes, Decoupling Strategies in Electrochemical Water Splitting and Beyond, *Joule* 2 (2018) 1390-1395, <https://doi.org/10.1016/j.joule.2018.06.011>
- 44 X. Liu, J. Chi, B. Dong, Y. Sun, Recent Progress in Decoupled H₂ and O₂ Production from Electrolytic Water Splitting, *ChemElectroChem* 6 (2019) 2157-2166, <https://doi.org/10.1002/celec.201801671>
- 45 P. J. McHugh, A. D. Stergiou, M. D. Symes, Decoupled Electrochemical Water Splitting: From Fundamentals to Applications, *Adv. Energy Mater.* (2020) 2002453, <https://doi.org/10.1002/aenm.202002453>
- 46 J. J. Chen, M. D. Symes, L. Cronin, Highly reduced and protonated aqueous solutions of [P₂W₁₈O₆₂]⁶⁻ for on-demand hydrogen generation and energy storage, *Nature Chem.* 10 (2018) 1042-1047, <https://doi.org/10.1038/s41557-018-0109-5>
- 47 F. Chen, H. Ma, B. Wang, Q. Zhuo, One-step production of methoxymethyl benzene in electrochemical reaction of toluene with methanol assisted by modified (NH₄)₃H₄[P(Mo₂O₇)₆] catalysts, *J. Mol. Catal. A Chem.* 273 (2007) 81-86, <https://doi.org/10.1016/j.molcata.2007.03.070>
- 48 B. B. Sarma, I. Efremenko, R. Neumann, Oxygenation of Methylarenes to Benzaldehyde Derivatives by a Polyoxometalate Mediated Electron Transfer-Oxygen Transfer Reaction in Aqueous Sulfuric Acid, *J. Am. Chem. Soc.* 137 (2015) 5916-5922, <https://doi.org/10.1021/jacs.5b01745>
- 49 R. Neumann, Activation of Molecular Oxygen, Polyoxometalates, and Liquid-Phase Catalytic Oxidation, *Inorg. Chem.* 49 (2010) 3594-3601, <https://doi.org/10.1021/ic9015383>
- 50 A. M. Khenkin, M. Somekh, R. Carmieli, R. Neumann, Electrochemical Hydroxylation of Arenes Catalyzed by a Keggin Polyoxometalate with a Cobalt(IV) Heteroatom, *Angew. Chem. Int. Ed.* 57 (2018) 5403-5407, <https://doi.org/10.1002/anie.201801372>

- 51 L. Ebersson, Electron-transfer reactions in organic chemistry. 4. A mechanistic study of the oxidation of *p*-methoxytoluene by 12-tungstocobalt(III)ate ion. *J. Am. Chem. Soc.* 105 (1983) 3192–3199, <https://doi.org/10.1021/ja00348a039>
- 52 P. Carloni, L. Ebersson, Strong Medium and Counterion Effects upon the Redox Potential of the 12-Tungstocobaltate (III/II) Couple, *Acta Chem. Scand.* 45 (1991) 373–376, <https://doi.org/10.3891/acta.chem.scand.45-0373>
- 53 A. Rauk, D. Yu, D. A. Armstrong, Carboxyl Free Radicals: Formyloxyl (HCOO[•]) and Acetyloxyl (CH₃COO[•]) Revisited, *J. Am. Chem. Soc.* 116 (1994) 8222–8228, <https://doi.org/10.1021/ja00097a031>
- 54 Y. Liu, S.-F. Zhao, S.-X. Guo, A. M. Bond, J. Zhang, G. Zhu, C. L. Hill, Y. V. Geletii, Electrooxidation of Ethanol and Methanol Using the Molecular Catalyst [$\{\text{Ru}_4\text{O}_4(\text{OH})_2(\text{H}_2\text{O})_4\}(\gamma\text{-SiW}_{10}\text{O}_{36})_2\}]^{10-}$, *J. Am. Chem. Soc.* 138 (2016) 2617–2628, <https://doi.org/10.1021/jacs.5b11408>
- 55 K. R. Brownell, C. C. L. McCrory, C. E. D. Chidsey, R. H. Perry, R. N. Zare, R. M. Waymouth, Electrooxidation of Alcohols Catalyzed by Amino Alcohol Ligated Ruthenium Complexes, *J. Am. Chem. Soc.* 135 (2013) 14299–14305, <https://doi.org/10.1021/ja4055564>
- 56 D. Serra, M. C. Correia, L. McElwee-White, Iron and Ruthenium Heterobimetallic Carbonyl Complexes as Electrocatalysts for Alcohol Oxidation: Electrochemical and Mechanistic Studies, *Organometallics* 30 (2011) 5568–5577, <https://doi.org/10.1021/om101070z>
- 57 M. Bugnola, R. Carmieli, R. Neumann, Aerobic Electrochemical Oxygenation of Light Hydrocarbons Catalyzed by an Iron–Tungsten Oxide Molecular Capsule, *ACS Catal.* 8 (2018) 3232–3236, <https://doi.org/10.1021/acscatal.8b00477>
- 58 A. M. Todea, A. Merca, H. Bögge, T. Glaser, J. M. Pigga, M. L. K. Langston, T. Liu, R. Prozorov, M. Luban, C. Schröder, W. H. Casey, A. Müller, Porous Capsules $\{(M)M_5\}_{12}\text{Fe}^{\text{III}}_{30}$ (M=Mo^{VI}, W^{VI}): Sphere Surface Supramolecular Chemistry with 20 Ammonium Ions, Related Solution Properties, and Tuning of Magnetic Exchange Interactions, *Angew. Chem. Int. Ed.* 49 (2010) 514–519, <https://doi.org/10.1002/anie.200905460>
- 59 M. Bugnola, K. Shen, E. Haviv, R. Neumann, Reductive Electrochemical Activation of Molecular Oxygen Catalyzed by an Iron-Tungstate Oxide Capsule: Reactivity

- Studies Consistent with Compound I Type Oxidants, *ACS Catal.* 10 (2020) 4227–4237, <https://doi.org/10.1021/acscatal.0c00897>
- 60 L. MacDonald, B. Rausch, M. D. Symes, L. Cronin, Selective hydrogenation of nitroarenes using an electrogenerated polyoxometalate redox mediator, *Chem. Commun.* 54 (2018) 1093–1096, <https://doi.org/10.1039/C7CC09036F>
- 61 B. Rausch, M. D. Symes, G. Chisholm, L. Cronin, Decoupled catalytic hydrogen evolution from a molecular metal oxide redox mediator in water splitting, *Science* 345 (2014) 1326–1330, <https://doi.org/10.1126/science.1257443>
- 62 G. Chisholm, L. Cronin, M. D. Symes, Decoupled electrolysis using a silicotungstic acid electron-coupled-proton buffer in a proton exchange membrane cell, *Electrochim. Acta* 331 (2020) 135255, <https://doi.org/10.1016/j.electacta.2019.135255>
- 63 W. Wu, X.-Y. Wu, S.-S. Wang, C.-Z. Lu, Catalytic hydrogen evolution and semihydrogenation of organic compounds using silicotungstic acid as an electron-coupled-proton buffer in water-organic solvent mixtures, *J. Catal.* 378 (2019) 376–381, <https://doi.org/10.1016/j.jcat.2019.09.011>
- 64 M.D. Symes, L. Cronin, Decoupling hydrogen and oxygen evolution during electrolytic water splitting using an electron-coupled-proton buffer, *Nat. Chem.* 5 (2013) 403–409. <https://doi.org/10.1038/nchem.1621>.
- 65 S. Goodwin, D.A. Walsh, Closed Bipolar Electrodes for Spatial Separation of H₂ and O₂ Evolution during Water Electrolysis and the Development of High-Voltage Fuel Cells, *ACS Appl. Mater. Interfaces.* 9 (2017) 23654–23661. <https://doi.org/10.1021/acscami.7b04226>.
- 66 C. Ma, S. Pei, S. You, Closed bipolar electrode for decoupled electrochemical water decontamination and hydrogen recovery, *Electrochem. Commun.* 109 (2019) 106611. <https://doi.org/10.1016/j.elecom.2019.106611>.
- 67 W. Li, N. Jiang, B. Hu, X. Liu, F. Song, G. Han, T.J. Jordan, T.B. Hanson, T.L. Liu, Y. Sun, Electrolyzer Design for Flexible Decoupled Water Splitting and Organic Upgrading with Electron Reservoirs, *Chem.* 4 (2018) 637–649. <https://doi.org/10.1016/j.chempr.2017.12.019>.

- 68 S. Lakshmanan, T. Murugesan, The chlor-alkali process: Work in Progress, *Clean Technol. Environ. Policy*. 16 (2014) 225–234. <https://doi.org/10.1007/s10098-013-0630-6>.
- 69 M. Hou, L. Chen, Z. Guo, X. Dong, Y. Wang, Y. Xia, A clean and membrane-free chlor-alkali process with decoupled Cl₂ and H₂/NaOH production, *Nat. Commun.* 9 (2018) 438. <https://doi.org/10.1038/s41467-018-02877-x>.
- 70 A. Zhao, F. Zhong, X. Feng, W. Chen, X. Ai, H. Yang, Y. Cao, A Membrane-Free and Energy-Efficient Three-Step Chlor-Alkali Electrolysis with Higher-Purity NaOH Production, *ACS Appl. Mater. Interfaces*. 11 (2019) 45126–45132. <https://doi.org/10.1021/acsami.9b16754>.
- 71 P. Galloni, V. Conte, B. Floris, A journey into the electrochemistry of vanadium compounds, *Coord. Chem. Rev.* 301-302 (2015) 240-299. <https://doi.org/10.1016/j.ccr.2015.02.022>
- 72 H. Agarwal, J. Florian, B.R. Goldsmith, N. Singh, V²⁺/V³⁺ Redox Kinetics on Glassy Carbon in Acidic Electrolytes for Vanadium Redox Flow Batteries, *ACS Energy Lett.* 4 (2019) 2368-2377. <https://doi.org/10.1021/acseenergylett.9b01423>.
- 73 L.V. Mikhalchenko, M.Y. Leonova, A.P. Zaplavin, M.V. Abakumov, V.T. Novikov, Reduction of dinitrobenzenes by electron-carrying catalysts in the electrosynthesis of diaminobenzenes, *Russ. Chem. Bull.* 70 (2021) 1927-1933. <https://doi.org/10.1007/s11172-021-3298-9>.
- 74 V. Amstutz, K.E. Toghiani, F. Powlesland, H. Vrubel, C. Comninellis, X. Hu, H.H. Girault, Renewable hydrogen generation from a dual-circuit redox flow battery, *Energy Environ. Sci.* 7 (2014) 2350–2358. <https://doi.org/10.1039/c4ee00098f>.
- 75 A. Mills, T. Russell, Comparative study of new and established heterogeneous oxygen catalysts, *J. Chem. Soc. Faraday Trans.* 87 (1991) 1245–1250. <https://doi.org/10.1039/FT9918701245>.
- 76 J.J. Chen, M.D. Symes, L. Cronin, Highly reduced and protonated aqueous solutions of [P₂W₁₈O₆₂]⁶⁻ for on-demand hydrogen generation and energy storage, *Nat. Chem.* 10 (2018) 1042–1047. <https://doi.org/10.1038/s41557-018-0109-5>.
- 77 A. Ho, X. Zhou, L. Han, I. Sullivan, C. Karp, N.S. Lewis, C. Xiang, Decoupling H₂ (g) and O₂ (g) production in water splitting by a solar-driven V^{3+/2+} (aq, H₂SO₄)

-)KOH(aq) cell, *ACS Energy Lett.* 4 (2019) 968–976. <https://doi.org/10.1021/acseenergylett.9b00278>.
- 78 C.C.L. McCrory, S. Jung, J.C. Peters, T.F. Jaramillo, Benchmarking Heterogeneous Electrocatalysts for the Oxygen Evolution Reaction, *J. Am. Chem. Soc.* 135 (2013) 16977–16987. <https://doi.org/10.1021/ja407115p>.
- 79 J. Zhang, A. M. Bond, D. R. MacFarlane, S. A. Forsyth, J. M. Pringle, A. W. A. Mariotti, A. F. Glowinski, A. G. Wedd, Voltammetric Studies on the Reduction of Polyoxometalate Anions in Ionic Liquids, *Inorg. Chem.* 44 (2005) 5123–5132, <https://doi.org/10.1021/ic050032t>
- 80 A. V. Anyushin, A. Kondinski, T. N. Parac-Vogt, Hybrid polyoxometalates as post-functionalization platforms: from fundamentals to emerging applications, *Chem. Soc. Rev.* 49 (2020) 382–432, <https://doi.org/10.1039/C8CS00854J>
- 81 C. Rinfray, G. Izzet, J. Pinson, S. G. Derouich, J.-J. Ganem, C. Combellas, F. Kanoufi, A. Proust, Electrografting of Diazonium-Functionalized Polyoxometalates: Synthesis, Immobilisation and Electron-Transfer Characterisation from Glassy Carbon, *Chem. Eur. J.* 19 (2013) 13838–13846, <https://doi.org/10.1002/chem.201302304>
- 82 M. A. Rahman, S.-X. Guo, M. Laurans, G. Izzet, A. Proust, A. M. Bond, J. Zhang, Thermodynamics, Electrode Kinetics, and Mechanistic Nuances Associated with the Voltammetric Reduction of Dissolved [*n*-Bu₄N]₄[PW₁₁O₃₉{Sn(C₆H₄)C≡C(C₆H₄)(N₃C₄H₁₀)}] and a Surface-Confined Diazonium Derivative, *ACS Appl. Energy Mater.* 3 (2020) 3991–4006, <https://doi.org/10.1021/acsaem.0c00405>
- 83 M. D. Symes, L. Cronin, Decoupling Hydrogen and Oxygen Evolution During Water Splitting Using an Electron-Coupled-Proton Buffer, *Nature Chem.* 5 (2013) 403–409, <https://doi.org/10.1038/nchem.1621>
- 84 X. López, C. Bo, J. M. Poblet, Electronic Properties of Polyoxometalates: Electron and Proton Affinity of Mixed-Addenda Keggin and Wells–Dawson Anions, *J. Am. Chem. Soc.* 124 (2002) 12574–12582, <https://doi.org/10.1021/ja020407z>
- 85 X. López, J. J. Carbó, C. Bo, J. M. Poblet, Structure, properties and reactivity of polyoxometalates: a theoretical perspective, *Chem. Soc. Rev.* 41 (2012) 7537–7571, <https://doi.org/10.1039/C2CS35168D>

- 86 K. Suzuki, N. Mizuno, K. Yamaguchi, Polyoxometalate Photocatalysis for Liquid-Phase Selective Organic Functional Group Transformations, *ACS Catal.* 8 (2018) 10809–10825, <https://doi.org/10.1021/acscatal.8b03498>

Overview of the Techniques Used

Synopsis

In this chapter we will briefly explain the main techniques (electrochemical and analytical) used in Chapters 3 to 5 as well as providing a theoretical background prior to encountering them in the text.

2.1 Electrochemical Techniques

Broadly speaking, it is possible to categorise electrochemical techniques into four main categories, depending on the variable we choose to control:

- 1) Controlled potential
- 2) Controlled current
- 3) Control of total charge passed
- 4) Impedance techniques

In this section, the electrochemical techniques implemented throughout this thesis are briefly explained with particular emphasis on the information that we can obtain from them as well as the experimental setup(s) used and in which cases it is better to use one over the other.

2.1.1 Electrodes

In general, electrochemical reactions are examined using a typical three-electrode setup consisting of a working electrode, a counter electrode and a reference electrode.¹⁻³ A schematic of a three-electrode configuration electrochemical cell is presented below.

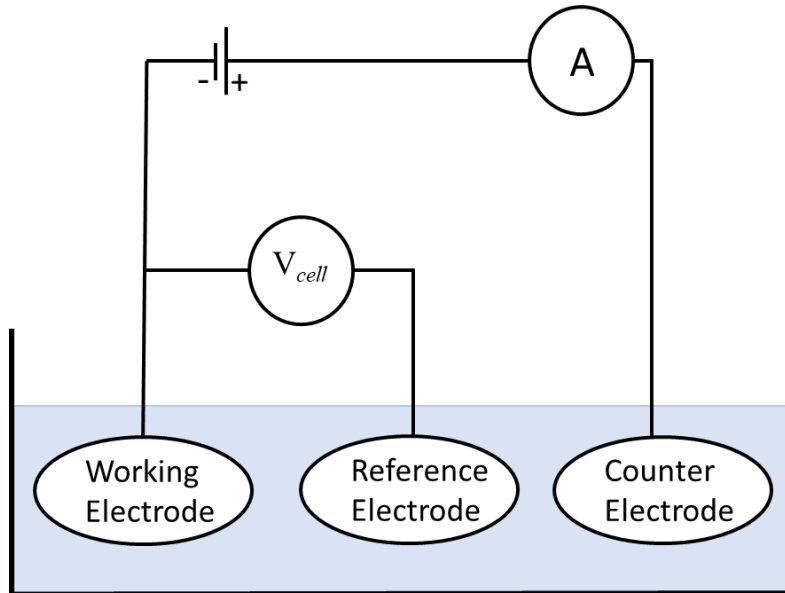


Figure 2.1: Graphical representation of a three-electrode configuration electrochemical cell.

The working electrode is defined as the electrode where the electrochemical reaction of study takes place, and any experiment that examines an electrode reaction must be designed to monitor the changes happening at the working electrode surface or working electrode side

of the cell, in the case of a divided electrochemical cell (Chapters 3&4).^{1,3} There is a very broad range of materials that can be used as working electrodes. The material of choice can either be predetermined by the nature of the experiment (*e.g.*, corrosion of Nickel) or the choice can be free and will be based on factors such as the fabrication cost and/or specific experimental needs. For the purpose of the present thesis, carbon working electrodes in the form of glassy carbon and carbon felt (for larger surface areas) were chosen.

The counter electrode (also called the secondary electrode) constitutes an essential part of an electrochemical cell as it provides a current (and therefore charge) of equal magnitude but opposite sign to that of the working electrode. So, if the reaction at the working electrode is a reduction, the reaction at the counter electrode will be an oxidation and *vice versa*. The process happening at the counter electrode should not interfere in the chemistry (and current response) occurring at the working electrode. Overall, a good counter electrode should provide a ready electron-transfer reaction (to provide the equal and opposite current to the process occurring at the working electrode), while not interfering with the chemistry at the working electrode. Since current flows between the working and counter electrode, the surface area of the counter electrode should be equal or larger than the area of working electrode so that current density at the counter electrode will not be a limiting factor in the kinetics of the electrochemical process under study.^{1,3} The counter electrodes used in this thesis include graphite rod, carbon felt and platinum mesh.

Reference electrodes are galvanic half-cells designed to sustain a constant potential throughout an electrochemical experiment and are designed to have the same value every day. In principle, the half-cell reaction should run independently of the current density. At the same time, potentiostats are designed to ensure that any current flow through the reference electrode is very low.¹⁻³ There is also a sub category of reference electrodes known as pseudo-reference electrodes (used in Chapter 5) that lack a constant thermodynamic equilibrium and therefore cannot maintain a constant potential value every day. These electrodes are used when the nature of the experiment does not allow conventional electrodes to be used, and thus an external reference is required (*e.g.*, non-aqueous electrolytes are used). Such systems are usually reported versus an internal standard which commonly is the well-studied Ferrocene/Ferrocenium couple.²

By convention, the potential of the standard hydrogen electrode (SHE) is zero. This electrode consists of a Pt electrode in a solution containing 1 M protons (H^+) and saturated with hydrogen.¹ Details of commonly used reference electrodes for aqueous electrolytes are presented in the following table (Table 2.1). For the purpose of this thesis, a silver/silver

chloride (Ag/AgCl) aqueous reference electrode was used in Chapters 3&4, while a silver/silver nitrate (Ag/AgNO₃), in 0.1 M AgNO₃ in electrolyte solution, pseudo reference electrode calibrated *vs* the Ferrocene/Ferrocenium couple, was used in Chapter 5.

Table 2.1: Common reference electrodes used in aqueous electrochemical conditions.

Name	Half-cell Reaction	Electrolyte	Potential <i>vs</i> SHE/mV
Standard Hydrogen Electrode	$2\text{H}^+ + 2\text{e}^- \rightleftharpoons \text{H}_2$	1 M H ⁺	0
Saturated Calomel Electrode	$\text{Hg}_2\text{Cl}_2 + 2\text{e}^- \rightleftharpoons 2\text{Hg} + 2\text{Cl}^-$	Saturated KCl	+241
Silver/Silver chloride	$\text{AgCl} + \text{e}^- \rightleftharpoons \text{Ag} + \text{Cl}^-$	Saturated KCl	+197

2.1.2 Ohmic Drop Compensation

As mentioned above, the potential on the working electrode is measured *versus* the reference electrode. Since there will always be some distance (which we always try to minimize in an experimental setup) between the working and reference electrodes, there will be some natural resistance between them, arising from the electrolyte of choice. This can be calculated from equation 2.1.

$$R = \frac{\rho l}{A} \quad (\text{Equation 2.1})$$

Where R is the natural resistance of the electrolyte in Ω , ρ is the resistivity of the electrolyte in Ω m, l is the distance between electrodes in m, and A is the area between the electrodes in m².

This means that by forcing a current through an electrolyte will lead to a voltage drop between the working and reference electrodes. This potential drop is often called Ohmic drop or iR drop^{2,3} and can be calculated using the Ohm's law, equation 2.2.

$$\Delta E_{\text{ohmic}} = iR_u \quad (\text{Equation 2.2})$$

Where ΔE_{ohmic} is the drop in potential in Volts caused by the electrolyte's resistance, i is the current from the working electrode in Amps, and R_u is the resistance between the working and reference electrode in Ω . R_u is often known as uncompensated resistance. Once ΔE_{ohmic} is calculated it can be compensated by subtracting its value from the actual potential reading on the working electrode. Many modern potentiostats are able to do this automatically by

enabling the iR drop function. Uncompensated resistance can also be identified using electrochemical impedance spectroscopy.^{1, 2}

Ohmic drop compensation has been applied in all data presented in Chapters 3-5 of this thesis.

2.1.3 Cyclic Voltammetry

Voltammetry is the most popular amongst the electrochemical techniques due to its ability to produce both qualitative and quantitative data, in a short period of time, by examining the redox activity of the species in study over a range of applied potential. In a typical voltammetry experiment, we measure the difference in the current response of the species in question as the potential of the working electrode changes at a fixed rate. The fixed rate at which the applied potential at the working electrode surface is varied is known as the scan rate of the voltammogram. The two most common voltammetry techniques are the Linear Sweep Voltammetry (LSV) and the Cyclic Voltammetry (CV). In the present thesis only cyclic voltammetry was implemented, and therefore discussed here.

In a typical cyclic voltammetry experiment, an initial potential is chosen (E_i) and then the potential is swept from E_i to E_1 . Then the direction of the sweep is reversed upon reaching E_2 and then reversed back to reach the initial potential E_i completing a full cycle. In some cases, E_i can be equal to E_1 . Figure 2.2 shows a visual representation of a typical CV, presenting a profile of how the potential varies over time. In an LSV the potential is simply swept in one direction. By introducing a return scan in the same experiment in CV, we are able to examine the reversibility of an electrochemical reaction (see subsection 2.1.4).

In cyclic voltammetry, the electrolyte solution must be kept still until the completion of the experiment, to limit mass transport within the solution. This is crucial to ensure that any changes obtained in the current response are attributed to the electrochemical/chemical processes occurring at the working electrode and not due to mass transport within the solution. For the same reason, cyclic voltammograms are often taken under inert atmosphere so atmospheric gases (mainly oxygen) do not react/interfere with the species in question. Again in this case, it is important that the gas supply does not disturb the solution through increased convection.

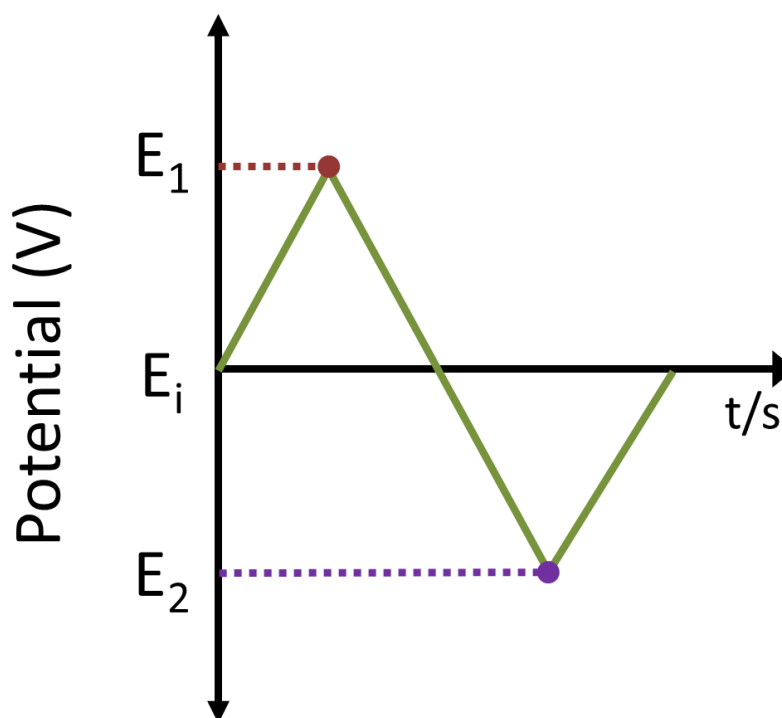
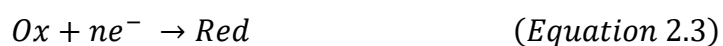


Figure 2.2: Schematic of how the potential is swept over time in a cyclic voltammogram.

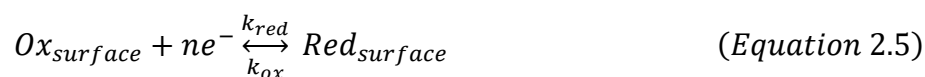
2.1.4 Reversibility of a Redox Process

In electrochemistry, the term reversibility is extensively used, and it usually refers to the electrochemical reversibility of a system as opposed to the chemical reversibility. To address the difference between the chemical and electrochemical reversibility we need to consider the half-equation (equation 2.3):



In a chemically reversible reaction, the oxidised (Ox) species can accept n number of electrons to be reduced to the reduced (Red) species while at the same time Red species can be oxidised back to the Ox species if they lose n number of electrons. If any of the two processes is inhibited, (for instance if the Red species decomposes upon transfer of electrons) then the process is considered as chemically irreversible.⁴

In an electrochemical system we need to take into account both the charge transfer from the electrode to the active species in bulk solution as well as the mass transport from the bulk solution to the electrode surface. To examine this system, we need to divide the equation 2.3 into two concerted processes (Equations 2.4 & 2.5):



If the rates of the oxidation and reduction (k_{ox} and k_{red} , equation 2.5) are large, and larger than the rate of mass transport then the redox process (equation 2.4) remains in equilibrium. Under these conditions, the process can be defined as electrochemically reversible. When k_{ox} and k_{red} are small (and therefore electron transfer is slow compared to mass transfer) the reaction cannot sustain the equilibrium, which shifts towards the reaction with the higher reaction rate. This process is then classified as electrochemically irreversible.^{1, 4, 5}

There is a third classification of an electrochemical process, the so called quasi-reversible regime. In this process, the rate of mass transport is of the same order of magnitude as the rates of reduction and oxidation reaction, but the process is not truly reversible.⁴

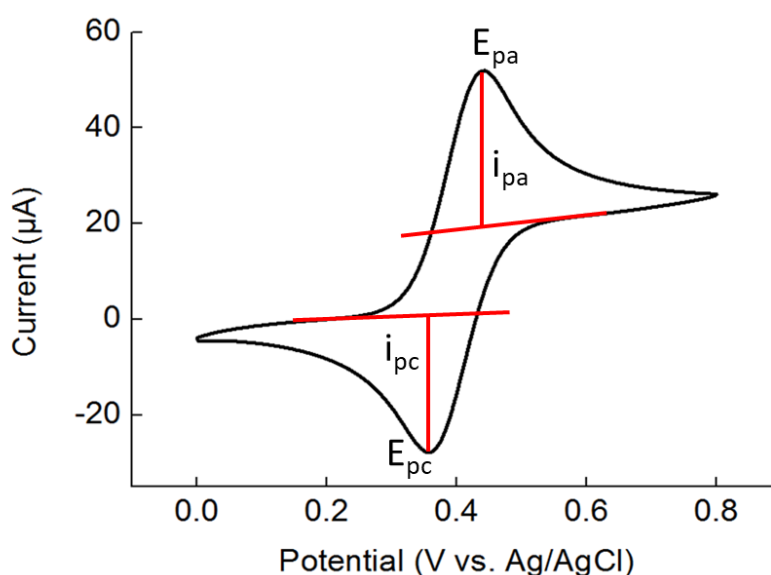


Figure 2.3: A typical cyclic voltammogram of the reversible wave of the ferrocene/ferrocenium redox couple.

A typical cyclic voltammogram of a reversible redox couple (ferrocene/ferricenium) is presented in figure 2.3. Drawn in red lines are the key information that we can extract from such an experiment: the cathodic peak potential (E_{pc}), the anodic peak potential (E_{pa}), the cathodic current (i_{pc}) and the anodic current (i_{pa}). The peak-to-peak separation and the integrated ratio of the oxidation/reduction peaks are important aspects of a CV; as if the ratio is close to 1:1 then the process can be considered reversible. If the ratio is far from this, it indicates that some of the electrogenerated species do not perform the reverse reaction and

so the process is either irreversible or quasi-reversible. At the same time, the current being passed in each process (i_{pc} and i_{pa}) provides a measure of the reaction rate, with larger current responses denoting increased reaction rates.

2.1.5 Electrolysis

Electrolysis is an electrochemical technique where driving force is applied to the system to enable redox reactions that would otherwise not occur spontaneously. Electrolysis reactions can be divided into two different categories, chronoamperometric and chronopotentiometric based on the process variable.^{1,3}

Chronoamperometry is when fixed potential is applied to the working electrode for a certain amount of time and the current response of the system is monitored as a function of time. This technique provides a higher order of control in an electrochemical process as it ensures that specific redox species can be studied based on their redox potential, previously measured by cyclic voltammetry experiments.

Chronopotentiometry (also known as Galvanostatic electrolysis), is when fixed current is demanded from the system and the potential required to achieve this current value is measured *versus* time. In a chronopotentiometry experiment, the potentiostat will increase the applied potential to compensate for low current response and therefore the redox process might alter. Thus, this technique provides less control over the reaction in comparison with chronoamperometry.

Regardless of the type of electrolysis we choose to apply in our system, Faraday's law of electrolysis (equation 2.6) allows the calculation of the total charge passed through the course of the reaction. Calculating or measuring the total charge with a process known as chronocoulometry, a theoretical yield of the reaction product can be calculated, and therefore the Faraday efficiency of the electrochemical process can be determined.¹

$$Q = mnF \quad (\text{Equation 2.6})$$

Where Q is the charge passed in C, m is the number of moles of the electroactive species in question, n is the number of electrons transferred per mole of electroactive species and F is the Faraday constant equal to $96,485 \text{ C mol}^{-1}$.^{1,6}

As chronoamperometry is related to the current response of the electroactive species, we can monitor the state of an electrochemical reaction *in situ*, simply by observing the electrolysis trace. An example of a chronoamperometry trace is depicted in figure 2.4.

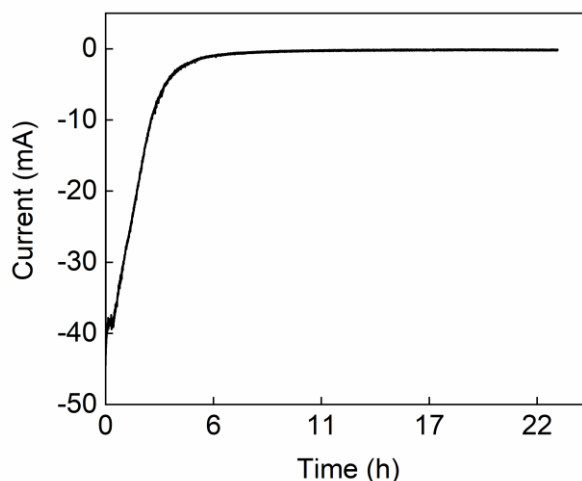


Figure 2.4: Chronoamperometry of the nitroarene ethyl-2-nitrobenzoate, with 10 mol% of the phosphotungstic acid mediator. This electrolysis plot has been taken from Chapter 3.

As we can see, the current constantly decreases over time and we observe that the reaction has run to completion after about 6 h where the current has significantly dropped to around zero (a drop to around $1/100^{\text{th}}$ of the initial current would also be sufficient to consider the process complete) and remains there indefinitely.

2.1.6 Two-electrode Configuration

In the case of a two-electrode configuration (used in Chapters 3&4), the reference electrode is absent and therefore the potential is measured between the working and counter electrodes.¹ As the distance between the working and counter electrodes is usually larger than the distance between the working and reference electrodes, the Ohmic resistance increases in the two-electrode configuration as we expect from equation 2.1. This setup is typically used to measure the performance of an electrochemical cell and it can be more attractive in large-scale/industrial processes over the three-electrode setup, as it is less sophisticated and the use of expensive (and sometimes sensitive) reference electrodes can be avoided. Galvanostatic conditions are typically applied using two-electrode setups, with these processes often suffering from the formation of unwanted side products.^{7,8} However, for potentiostatic experiments, where we can control side reactions better, the use of a reference electrode is necessary to obtain complete control over the applied potential at the working electrode and therefore on the electrochemical process.^{8,9} In such setup, cell

optimisation in terms of current density and cell design (to decrease the resistance) is required to achieve optimal electrochemical conditions.

2.2 Nuclear Magnetic Resonance (NMR) Spectroscopy

2.2.1 Fundamentals of NMR

Nuclear Magnetic Resonance (NMR) spectroscopy is an analytical technique that allows the molecular structure of a material to be analysed by measuring the interaction of nuclear spins in the presence of a magnetic field.¹⁰

NMR is only applicable at nuclei that possesses what is known as a magnetic moment. The magnetic moment (μ) is given by the equation 2.7.

$$\mu = I\gamma \frac{h}{2\pi} \quad (\text{Equation 2.7})$$

Where I is the quantum number for the nuclear spin (determined by the number of protons and neutrons in the nucleus), γ is the gyromagnetic ratio (the ratio of its magnetic moment to its angular momentum), and h is the Planck's constant.

There are three cases that describe the coupling between the protons and neutrons in a nucleus, all related to the value of I . Nucleons of opposite spin can pair (like electrons) but only with nucleons of the same kind. Thus, in atoms where neutrons and protons are in odd numbers, I gives half-integral numbers (such as 1/2, 3/2 etc.) with these atoms to be easily analysed *via* NMR. At the same time, in atoms where neutrons and protons are present in even numbers, all the spins are paired and $I = 0$. In such case (for example the ¹²C isotope) the atoms are magnetically inactive and there is no interaction with the spectrometer. Finally, when both neutrons and protons are present in odd numbers, I is an integer number ($I > 1/2$) and the nucleus additionally possesses an electric quadrupole moment, Q . In such case, the distribution of charge is not spherical, and the NMR spectra can be affected, however, study of such molecules is still technically possible.¹¹

Magnetic moments within atoms can be described as analogous to the needle of a compass (that aligns with Earth's magnetic field), as they are aligned along specific directions but at the same time, they can re-orientated in the presence of an external magnetic field. When a nucleus is placed in an external magnetic field (B_0), the nuclear spin of the atom is re-orientated to align with the external field. The possible orientations are dictated by the quantum number m , that can take $2I + 1$ values. This magnetic moment does not remain in

one place, but precesses around the direction of B_0 .^{10, 11} For example, in the ^1H isotope (where $I = 1/2$), there are two possible orientations: one for nuclei with $m = +1/2$ (also referred to as α spin state) which is aligned in parallel with the external field and is of lower energy than the one for nuclei with $m = -1/2$ (also referred to as β spin state) which is aligned against the magnetic field. The energy of the interaction therefore depends on the angle between the magnetic moment and the applied field.¹¹ These different energy states afford the necessary conditions for spectroscopy. Since the energy difference between the two states is very small (on the order of $10^{-5}/10^{-6}$), electromagnetic radiation of radiowave frequency is enough to cause transition between the energy states. The frequency is obtained from the Bohr relation (equation 2.8) and it can also be expressed in terms of the gyromagnetic ratio for the NMR (equation 2.9).^{10, 11}

$$h\nu = \Delta E \quad (\text{Equation 2.8})$$

$$\nu = B_0 \frac{\gamma}{2\pi} \quad (\text{Equation 2.9})$$

In the literature, this frequency can be found as the Larmor frequency. This frequency is proportional to the strength of the magnetic field (B_0), which therefore makes ΔE larger at higher frequencies and this is the reason why NMR instruments of higher frequency are more sensitive. A graphical representation is depicted in Figure 2.5.

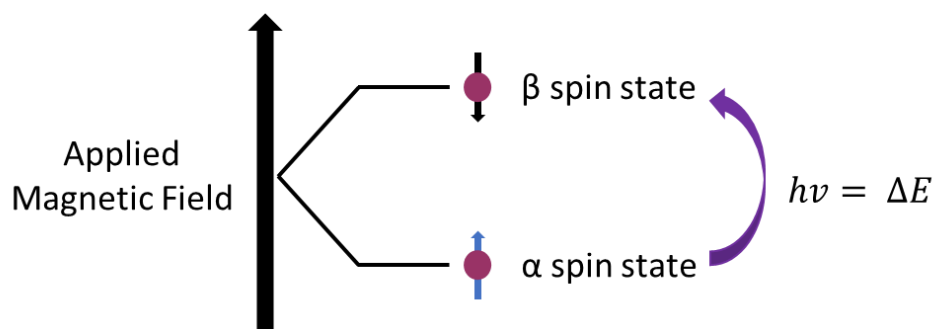


Figure 2.5: Graphical illustration of the spin states and the required energy to cause transition from the α spin-state to the β spin-state.

When the sample is irradiated with the right frequency, energy equal to ΔE is absorbed and a lower state nucleus (α proton) can ‘spin-flip’ to the higher energy state (β proton). In this case, nuclei are in resonance with the applied radiation, hence the terminology ‘nuclear magnetic resonance’. After the excitation, the nucleus returns to its original lower state, releasing the absorbed energy. This process is called relaxation. At this stage, a tiny pulse of

radiofrequency electromagnetic radiation is emitted, which is detected by the NMR machine.¹⁰ At this stage, it will be useful to introduce the vector model to provide a better understanding of the interaction between the radiofrequencies and the nuclei.

A magnetization vector (M_0), is the result of the combination of all the magnetic moments. This is not zero since the magnetic moments do not cancel each other out; as in equilibrium slightly more than half of nuclei within the magnetic field adopt the α state. If we assign M_0 to a z -axis, in a *right-handed* axis system, the radio pulse is introduced to the system along the x -axis, with the absorption of energy leading to re-orientation of M_0 from the z -axis to the xy -plane (Figure 2.6 B). Due to the angular momentum of the magnetic moment, M_0 precesses around the z -axis and therefore if a detector is aligned with the y -axis the signal can be visualised as an oscillating wave (Figure 2.6).

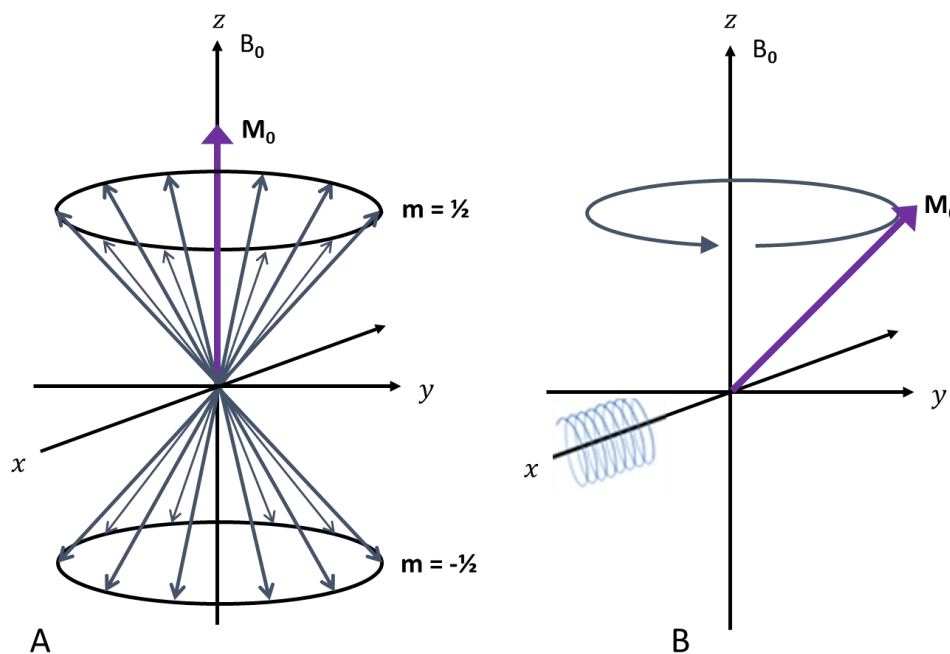


Figure 2.6: On the left (A) is the magnetization vector (M_0) aligned with the applied magnetic field (B_0) along the z -axis. On the right side (B) is the re-orientation of M_0 in a xy -plane under irradiation.

As we mentioned earlier, after the radiofrequency is no longer applied, we observe the relaxation phenomenon, where a signal in the radiofrequency range is emitted. This is a complex signal that decays over time as the absorbed energy is slowly released (leading the M_0 -vector back to its original position in a spiralling motion). There are two ways that the absorbed energy can be released, the spin-spin relaxation (interaction of spin with

surrounding protons) and spin-lattice relaxation (interaction of spin with surrounding molecules). This signal is called Free Induction Decay (FID) that is mathematically processed and converted from intensity *versus* time to intensity *versus* frequency through a Fourier transformation. The frequency is obtained from the equation 2.10, where T represents the period between two successive crests (Figure 2.7).¹¹

$$\nu = \frac{1}{T} \quad (\text{Equation 2.10})$$

In modern NMR machines the magnetic field is held constant, and a radiofrequency pulse of short duration excites all protons simultaneously. This pulse covers a range of frequency, and each individual nucleus absorbs the required frequency to flip its spin and so different nuclei will resonate at different frequencies.

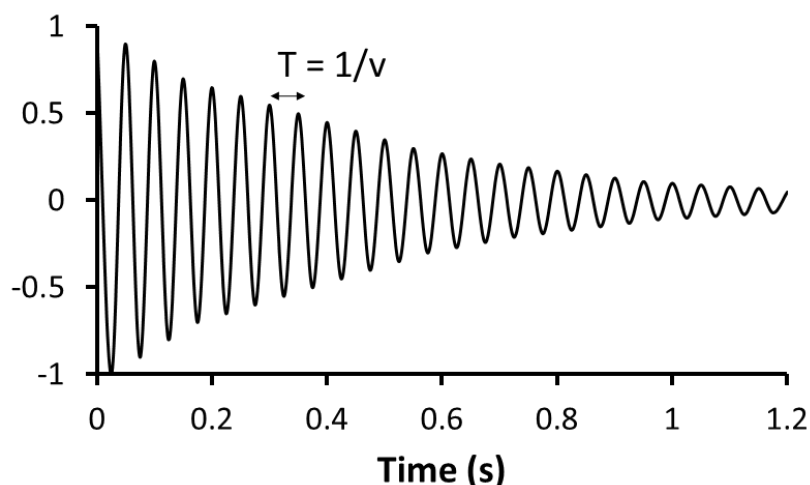


Figure 2.7: An example of a typical free induction decay (FID) signal.

2.2.2 The Chemical Shift

When we study NMR, the chemical environment of the atom affects the frequency of the resonating nuclei. In a chemical structure, nuclei are bonded to other atoms and surrounded by electrons. Since the electrons are charged particles, under the influence of an external field they move in such way that a local magnetic field (B_i) is generated, opposing B_0 . This local magnetic field is much smaller than the external field, however, the effective magnetic field of the nucleus is reduced ($B_{\text{effective}} = B_0 - B_i$). Upon the generation of B_i , the nucleus is said to be shielded by the electron cloud. If a nucleus is bound to an electronegative atom such as oxygen, it experiences a decrease in electron density resulting in smaller B_i ($B_{\text{effective}}$ is larger) and therefore an increase in resonance frequency. These so-called de-shielded nuclei can be seen on the left-hand side of the spectrum, usually called downfield. The exact

opposite effect is observed when less electronegative atoms such as carbon, are bound to the nuclei, shifting the absorption peak upfield. The variation of the absorption frequency is known as the chemical shift.¹⁰

For ease of interpretation of the obtained signals, the frequencies of NMR absorptions of a compound are compared to the internal standard $\text{Si}(\text{CH}_3)_4$ (tetramethyl silane or TMS). The signals arising from TMS in ^1H and ^{13}C NMR are slightly more shielded than those of most organic molecules because of the lesser electronegativity of silicon compared to carbon. Since the carbons and protons in TMS are all in the same environment, a single high-intensity signal is produced that is conveniently removed from the spectrum. Its resonance frequency arbitrarily defined as 0 Hz.¹⁰

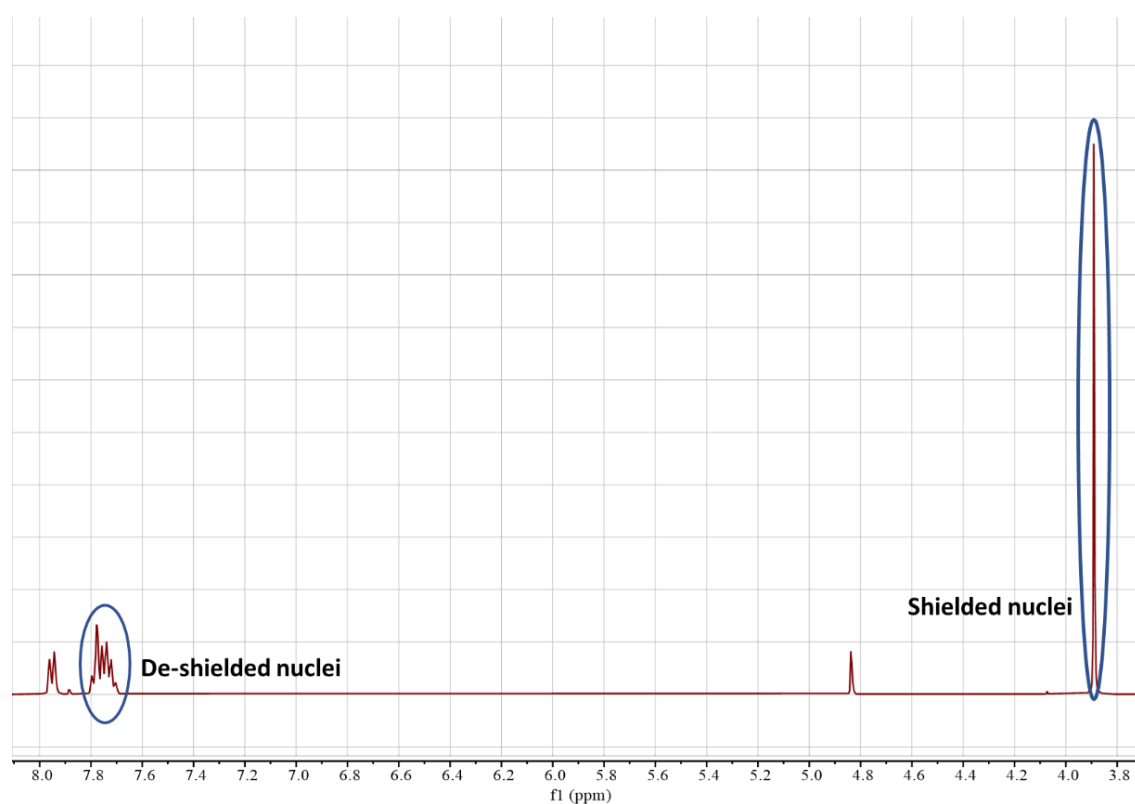


Figure 2.8: ^1H NMR spectra of methyl-2-nitrobenzoate, showing both de-shielded and shielded proton signals. This NMR spectrum has been extracted from Chapter 4.

Moreover, the resonance frequencies are proportional to the strength of the applied magnetic field (B_0) and therefore they are not comparable between machines of different frequencies. To counteract this issue, the relative chemical shift (δ) is introduced (equation 2.11).

$$\delta = \frac{v_H - v_{reference} \text{ (Hz)}}{\text{frequency of the spectrometer (MHz)}} \quad (\text{Equation 2.11})$$

This field-independent value is expressed in parts per million (ppm) and enables the comparison of chemical signals obtained from different NMR machines.¹⁰

The common scale for the chemical shift of ^1H NMR is 0-12 ppm and 0-220 ppm for ^{13}C NMR. In modern systems, the addition of TMS as internal standard is no longer needed as the residual signals of the deuterated solvents have a standard chemical shift vs TMS and therefore can be used as reference ($\nu_{\text{reference}}$).

2.3 Mass Spectrometry (MS)

2.3.1 General Remarks

Mass spectrometry is an analytical technique that provides structural information for a given molecule, thus finds wide application in chemistry laboratories. A mass spectrometer consists of three major components: the ionisation source, the mass analyser and the ion detector (Figure 2.9).¹²

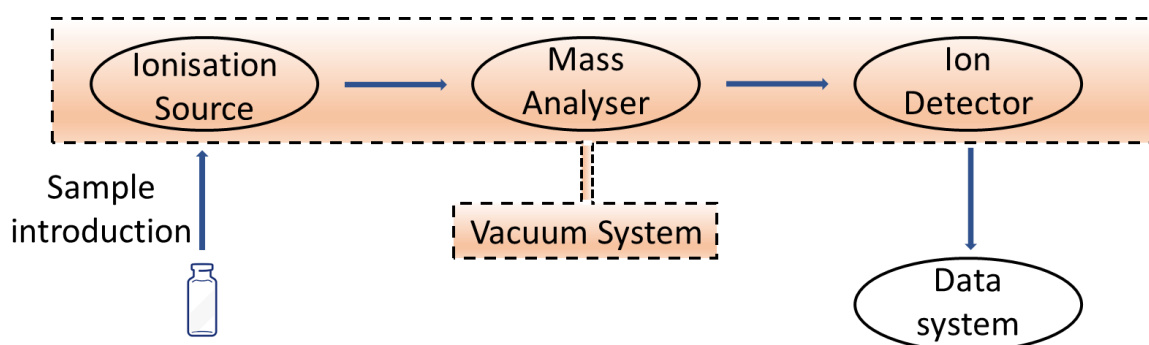


Figure 2.9: Graphical representation of the major components of a Mass Spectrometer.

Mass spectrometry relies on the ionisation and fragmentation of the sample molecules in the gas phase, while the resulting fragmentation pattern is unique for each molecule; providing structural information of the compound in question.¹² However, for the purpose of the present thesis, mass spectrometry is used as a supplementary technique to the NMR to identify specific compounds and not to obtain any specific structural information. Nowadays, mass spectrometry is often coupled with either liquid or gas chromatography. In such systems, samples containing a mixture of compounds, are able to be analysed through the separation of the individual compounds *via* chromatography and then analysed in the mass spectrometer.¹³ Worth mentioning, is the fact that in mass spectrometry, mass is not what is measured (as the name of the technique indicates) but instead, the graph that is

produced determines the mass-to-charge ratio (m/z) or a property related to m/z .¹³ For the current thesis, we will briefly discuss the ionisation sources and mass analysers used to obtain data in Chapters 3, 4 and 5.

2.3.2 Ionisation Source

In the ionisation source, the molecules in question are ionised by one of the many available techniques including electron ionisation (EI), chemical ionisation (CI), electron spray ionisation (ESI), atmospheric pressure chemical ionisation (APCI) and matrix-assisted laser desorption/ionisation (MALDI) amongst others. Some of these techniques require operation under reduced pressure while others (more modern) operate under atmospheric pressure.¹²⁻¹⁴ In this thesis only EI and ESI were implemented.

Electron ionisation is only suitable for gas-phase ionisation and thus its use is limited to compounds sufficiently volatile and thermally stable, while it operates under reduced pressure.^{13, 14} EI consists of a heated filament that emits high-energy electrons. These electrons are attracted from an anode placed opposite to the filament, interacting with the sample molecules. Magnetic field can also be used to increase the probability of interaction with the molecules. During their journey, electrons transfer energy to the sample molecules that is usually enough to overcome the first ionisation potential of most organic compounds. This first positively charged ion is known as the molecular ion and its nominal mass is equal to the molecular mass of the molecule in question. However, the excess energy that has been transferred leads to extended fragmentation of the molecule. This extensive fragmentation often leads to little, or no detection of the molecular ion and thus precise identification of a sample molecule might be difficult in some cases with this method. EI also contains an extractor plate as well as an ion focusing plate both kept under negative potential to attract the positively charged fragments and accelerate them to the mass analyser.¹²

Electron spray ionisation is a more modern technique, that operates under atmospheric pressure and consists of two compartments: a capillary tube and a counter electrode. A solution-based sample is pumped through the capillary tube and a potential difference of about +500 to +6,000 V is applied between the tip of the capillary tube and the counter electrode, depending on the surface tension of the solvent.¹²⁻¹⁴ The electric field that is created generates an aerosol of charged droplets, usually with the introduction of a nebulising gas (such as N₂) to assist the droplet formation. The droplets consist of both solvent and sample molecules and thus drying gas is usually implemented to enhance solvent

evaporation. These droplets have a net positive or negative charge, depending on the polarity of the applied voltage. Repulsion between same charged molecules eventually leads to solvent-free ions that make their way into the mass analyser.^{12, 13} ESI is considered as a 'soft' ionisation method; however, it commonly yields multiple fragments. These characteristics make ESI very attractive for analysing large, non-volatile molecules.¹²

2.3.3 Mass Analyser

Upon ionisation, fragmented ions are accelerated into the mass analyser where they are separated according to their m/z . As with the ionisation sources, numerous different mass analysers have been developed including the ion trap mass analyser, time-of-flight mass analyser (TOF) and quadrupole mass analyser amongst others.¹²⁻¹⁴ Tandem mass spectrometry (MS/MS) has also been developed and as its name indicates, it involves two stages of mass analysis. In the first stage, ions of a selected m/z are isolated and then undergo a chemical reaction that changes either their mass (m) or charge (z). In the second stage, these ions are analysed. MS/MS can be divided into two categories known as tandem in space and tandem in time. Tandem in space is achieved by coupling two different mass analysers while tandem in time is achieved by performing a sequence of analysis in an ion trap mass analyser.¹²⁻¹⁴ Herein, tandem in space MS/MS was implemented, coupling a quadrupole and a TOF mass analyser (Q-TOF).

In a TOF mass analyser the ions are separated based on their velocity. In theory, all the ions are generated at the same time in the ionisation source and subsequently accelerated into the drift tube of the TOF through a fixed potential. Therefore, all the ions with the same charge obtain the same kinetic energy with the low m/z ions obtaining higher velocities and therefore they travel faster and reach the detector before the high m/z ions, yielding separation.^{12, 13} An advantage of the TOF analyser over the other alternatives is that the mass range of the ions that can be analysed is in theory unlimited.¹³

A quadrupole mass analyser (Figure 2.10) consists of four parallel conducting rods and the separation of the ions occurs through their motion in a dynamic electric field (in the radiofrequency range), depending on their m/z . The rods are directly connected to radiofrequency and direct current generators, with adjacent rods being of opposite radiofrequency phase. Under a specific set of applied radiofrequency and direct current only ions with a very narrow m/z range will have a stable trajectory that leads to the detector whereas the other ions will be attracted by the rods of the opposite charge and neutralise.

The mass spectrum is scanned by varying the radiofrequency amplitude and direct current in a way that their ratio remains constant and in a way that ions with increasing m/z reach the detector.^{12, 13} Based on the physical parameters of a quadrupole analyser the maximum detected m/z ions vary from 300 to 4000.¹³

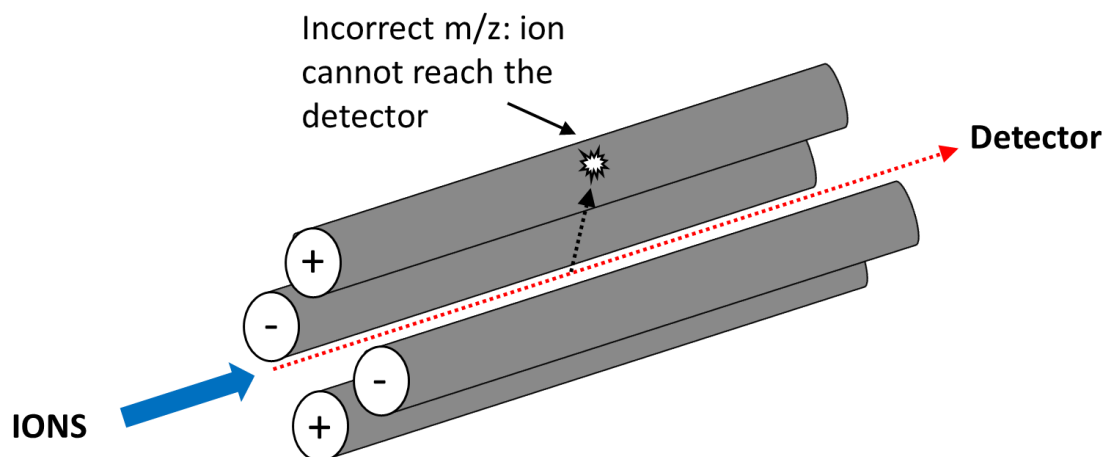


Figure 2.10: Schematic of a quadrupole mass analyser, with the red arrow representing the trajectory of the ions with the correct m/z while the black arrow represents the ions with incorrect m/z that do not reach the detector.

2.4 References

1. D. Pletcher, *A First Course in Electrode Processes*, RSC Publishing, Cambridge, 2nd edn., 2009.
2. G. Inzelt, A. Lewenstam and F. Scholz, *Handbook of Reference Electrodes*, Springer Berlin, Heidelberg, 2013.
3. A. J. Bard and L. R. Faulkner, *Electrochemical Methods: Fundamentals and Applications*, John Wiley & Sons, New York., 2nd edn., 2001.
4. P. Zanello, *Inorganic Electrochemistry: Theory, Practice and Application*, The Royal Society of Chemistry, Cambridge, 2003.
5. N. Elgrishi, K. J. Rountree, B. D. McCarthy, E. S. Rountree, T. T. Eisenhart and J. L. Dempsey, *J. Chem. Educ.*, 2018, **95**, 197-206.
6. M. Faraday, *Philosophical Transactions, The Royal Society* 1834, **124**, 77-122.
7. M. C. Leech, A. D. Garcia, A. Petti, A. P. Dobbs and K. Lam, *React. Chem. Eng.*, 2020, **5**, 977-990.
8. C. Gütz, B. Klöckner and S. R. Waldvogel, *Org. Process Res. Dev.*, 2016, **20**, 26-32.
9. C. Schotten, T. P. Nicholls, R. A. Bourne, N. Kapur, B. N. Nguyen and C. E. Willans, *Green Chem.*, 2020, **22**, 3358-3375.
10. J. Keeler, *Understanding NMR Spectroscopy* John Wiley & Sons, Ltd, 2005.
11. J.W.Akitt and B. E. Mann, *NMR and Chemistry: An introduction to modern NMR spectroscopy*, Cheltenham : Stanley Thornes, c2000, 4th edn., 2000.
12. R. W. Smith, *Encyclopedia of Forensic Sciences*, Academic Press, Waltham, 2nd edn., 2013, pp. 603-608.
13. G. L. Glish and R. W. Vachet, *Nat. Rev. Drug Discov.*, 2003, **2**, 140-150.
14. E. de Hoffmann and V. Stroobant, *Mass Spectrometry : Principles and Applications*, John Wiley & Sons, Incorporated, New York, 3rd edn., 2007.

Aims and Objectives

The general purpose of the experimental work detailed in the present thesis is to examine and develop alternative, more sustainable methods for the synthesis of broadly used organic (anilines) and inorganic (nitrogen-containing) compounds. Examining electrochemical systems, an emerging field in the research community, we aim to develop and interrogate environmentally friendly processes and provide solid evidence that these systems demonstrate the potential to be used as the primary method for the production of such compounds in the future.

In **Chapters 3&4**, we examine the development of a mediated electrochemical system for the synthesis of an industrially used class of chemical compounds, the anilines. Anilines are important building blocks in the synthesis of a wide range of nitrogen-containing compounds including dyes, polymers, agrochemicals and pharmaceuticals (such as paracetamol which is a derivative of *p*-aminophenol).^{1,2,3} To this day, the most common way to produce anilines is by the reduction of their corresponding nitroarenes,⁴ typically at high temperatures of around 300 °C and elevated pressure (5 bar). These methods also require the use of hydrogen gas and metal-based catalysts to enhance the selectivity.⁵ Approaches where the use of hydrogen gas has been replaced with soluble hydrogenation agents (formate, hydrazine etc.), in the presence of metal catalysts, have been reported in the past years, in an attempt to tackle the selectivity issues.^{1,6,7,8,9} Although less harsh experimental conditions have been used in these methods, the irreversible consumption of the soluble hydrogenation agents as well as their toxic nature, constitute a major drawback in the development of a more sustainable methodology. Electrochemistry on the other side can provide a sustainable alternative for this hydrogenation reaction, as both the electrons and the protons needed for this process can originate from water. However, to this day and to the best of our knowledge, in the electrochemical methods that have been developed, at least one key facet of the process (conversion of nitrobenzene, process conditions, Faradaic efficiency and/or selectivity for aniline) is sub-optimal.^{10,11,12,13} Therefore, the development of a sustainable and selective process would be of great interest.

In **Chapter 3**, using the knowledge that reduced polyoxometalates can spontaneously generate hydrogen under certain conditions,¹⁴ we hypothesize that they can also act as a soluble source of hydrogen to drive organic transformations. The use of polyoxometalates in organic electrosynthesis is not a new concept and has been discussed in Sections 1.2 & 1.3 of the introduction of this thesis. More specifically, the report of Cronin *et al.* where the polyoxometalate silicotungstic acid (in stoichiometric amounts) mediated the selective

hydrogenation of nitroarenes,¹⁵ proved that such a process can be possible. Therefore, the electrochemical properties of the polyoxometalates (see Section 1.1.2) and their high solubility in aqueous electrolytes, together with their proven activity in the hydrogenation of nitroarenes (in stoichiometric amounts at this point) provide a very promising starting point for the investigation and development of an electrocatalytic system that will promote this transformation selectively. Since a lot of the current methods show sub-optimal selectivity towards the aniline product, we believe that it is key to investigate the reaction mechanism and obtain the full reaction profile. Moreover, the main competing electrochemical reaction reported in the literature is the hydrogen evolution at the electrode surface. Thus, we assume that the applied potential, which is the potential at which the polyoxometalate is reduced, will be key to the Faradaic efficiency of the process. Therefore, investigation of the most suitable polyoxometalate, based on its redox potential, is necessary prior to the development of the catalytic system. Using this information, we would then aim to conduct studies on the reaction of functionalised nitroarenes as well as experiments where systems more applicable to an industrial set-up will be tested.

In *Chapter 4*, utilising the information obtained for the reaction process and the method developed in *Chapter 3*,¹⁶ we make the hypothesis that we can potentially expand the scope to a variety of functionalised nitroarenes. We believe that by examining nitroarenes where the functional group can itself be reduced (for example, ketones or esters) or cleave off the benzene ring (for example, hydrogenolysis of substituted halogens), and therefore form reaction side-products, can significantly expand the versatility and usability of our developed methodology. In this way, we aim to prove that our process can overcome these selectivity barriers that other processes report, even in the most challenging cases such as the halogen-substituted nitrobenzenes.¹⁷ To achieve this, the electrochemical reduction of a selection of nitroarenes with different substituted groups will be examined, with the polyoxometalate phosphotungstic acid acting as an electrocatalyst. Moreover, we believe that studies of galvanostatic electrolysis, which is the method of choice in the industry due to its simplicity, will make our process more approachable for large-scale (industrial) applications.

In *Chapter 5*, the electrochemical multi-electron reduction of nitrite (NO_2^-) will be examined in an attempt to provide insight into the reaction mechanism and develop a selective electrochemical process. The current method for the production of ammonia (which is the product of the $6 e^-$ reduction of nitrite), the Haber-Bosch process, operates under harsh reaction conditions while fossil fuels are the source of the required hydrogen. Therefore,

alternative methodologies where efficient ammonia production will be achieved in a more sustainable fashion are of tremendous importance. In nature, these multi-electron reactions are mediated by enzymes containing a haem-type unit in their active sites.¹⁸ We therefore hypothesise that complexes based on iron-porphyrin assemblies will be a good starting point for the development of an artificial enzyme-mimicking system targeting the selective multi-electron reduction of nitrite. To this date, studies using iron-porphyrins to mediate the reduction of nitrite lead to sub-optimal selectivity of the reaction product.^{19,20} Moreover, the role of PCET (proton-coupled electron transfer) mechanism has been investigated before in the *Symes* group for the selective 1 e⁻ reduction of nitrite to nitric oxide. The reaction mechanism was examined via the comparison of the reactivity of two Cu complexes, one containing a proton relaying unit (carboxylic acid group) in its secondary coordination sphere and one that lacked such functionality. In this case, the presence of this proton-relaying moiety was found to have a key role in tuning the reactivity of the catalyst.²¹ Using the same principles and two iron-porphyrins with different moieties, we aim to develop a selective electrochemical method for the reduction of nitrite by exploring the role of the PCET mechanism in this transformation.

References

- 1 Kadam, H. K. and Tilve, S. G. (2015) Advancement in methodologies for reduction of nitroarenes. *RSC Adv.* 5, 83391-83407. <https://doi.org/10.1039/C5RA10076C>
- 2 Jurado- Sánchez, B., Ballesteros, E. and Gallego M. (2013) Comparison of microwave assisted, ultrasonic assisted and Soxhlet extractions of N-nitrosamines and aromatic amines in sewage sludge, soils and sediments. *Sci. Total Environ.* 463-464, 293-301. <https://doi.org/10.1016/j.scitotenv.2013.06.002>
- 3 Ellis, F. Paracetamol: a curriculum resource. (Royal Society of Chemistry, Cambridge, 2002).
- 4 Travis, A.S. *Manufacture and Uses of the Anilines: A Vast Array of Processes and Products.* (PATAIS Chemistry of Functional Groups. John Wiley & Sons, Chinchester, 2009).
- 5 Formenti, D., Ferretti, F., Scharnagl, F. K. and Beller, M. (2019) Reduction of nitro compounds using 3d-Non-Noble metal catalysts. *Chem. Rev.* 119, 2611-2680. <https://doi.org/10.1021/acs.chemrev.8b00547>
- 6 Gladiali, S. and Alberico, E. (2006) Asymmetric transfer hydrogenation: chiral ligands and applications. *Chem. Soc. Rev.* 35, 226-236. <https://doi.org/10.1039/B513396C>
- 7 Samec, J. S. M., Bäckvall J. E., Andersson P. G. and Brandt, P. (2006) Mechanistic aspects of transition metal-catalyzed hydrogen transfer reactions. *Chem. Soc. Rev.* 35, 237-248. <https://doi.org/10.1039/B515269K>
- 8 Garcia-Verdugo, E., Liu, Z., Ramirez, E., Garcia-Serna, J., Fraga-Dubreuil, J., Hyde, J. R., Hamley, P. A. and Poliakoff, M. (2006) In situ generation of hydrogen for continuous hydrogenation reactions in high temperature water. *Green Chem.* 8, 359-364. <https://doi.org/10.1039/B515470G>
- 9 Joshi, M. V. and Mukesh, D. (1997) Transfer hydrogenation of nitro compounds with heteropolyacid catalysts. *J. Cat.* 168, 273-277. <https://doi.org/10.1006/jcat.1997.1619>
- 10 Marquez, J. and Pletcher, D. (1980) A study of the electrochemical reduction of nitrobenzene to p-aminophenol. *J. Appl. Electrochem.* 10, 567-573. <https://doi.org/10.1007/BF00615477>

- 11 Chong, X., Liu, C., Huang, Y., Huang, C. and Zhang, B. (2020) Potential-tuned selective electrosynthesis of azoxy-, azo- and amino-aromatics over a CoP nanosheet cathode. *Natl. Sci. Rev.* 7, 285-295. <https://doi.org/10.1093/nsr/nwz146>
- 12 Sheng, X., Wouters, B., Breugelmans, T., Hubin, A., Vankelecom, I. F. J. and Pescarmona, P. P. (2014) Cu/Cu_xO and Pt nanoparticles supported on multi-walled carbon nanotubes as electrocatalysts for the reduction of nitrobenzene. *Appl. Cat. B*, 147, 330-339. <https://doi.org/10.1016/j.apcatb.2013.09.006>
- 13 Zhang, Q., Liu, Y., Chen, S., Quan, X. and Yu, H. (2014) Nitrogen-doped diamond electrode shows high performance for electrochemical reduction of nitrobenzene. *J. Hazard. Mater.* 265, 185-190. <https://doi.org/10.1016/j.jhazmat.2013.11.065>
- 14 M.D. Symes, L. Cronin, Decoupling hydrogen and oxygen evolution during electrolytic water splitting using an electron-coupled-proton buffer. *Nat. Chem.* 5 (2013) 403–409. <https://doi.org/10.1038/nchem.1621>.
- 15 MacDonald, L., Rausch, B., Symes, M. D. and Cronin, L. (2018) Selective hydrogenation of nitroarenes using an electrogenerated polyoxometalate redox mediator. *Chem Commun.* 54, 1093-1096. <https://doi.org/10.1039/C7CC09036F>
- 16 Stergiou, A. D. and Symes, M. D. (2022) High yield and selective electrocatalytic reduction of nitroarenes to anilines using redox mediators. *Cell Rep. Phys. Sci.* 3, 100914. <https://doi.org/10.1016/j.xcrp.2022.100914>
- 17 Pietrowski, M. Recent Development in Heterogeneous Selective Hydrogenation of Halogenated Nitroaromatic Compounds to Halogenated Anilines. (Bentham Science Publishers, 2012).
- 18 Maia, L. B. and Moura, J. J. G. (2014) How Biology Handles Nitrite. *Chem. Rev.* 114, 5273-5357. <https://doi.org/10.1021/cr400518y>.
- 19 Heinecke, J. L., Khin, C., Pereira, J. C. M., Suárez, S. A., Iretskii, A. V., Doctorovich F. and Ford, P. C. (2013) Nitrite Reduction Mediated by Heme Models. Routes to NO and HNO?. *J. Am. Chem. Soc.* 135, 4007-4017. <https://doi.org/10.1021/ja312092x>.
- 20 Kudrik, E. V., Makarov, S. V., Zahl, A. and van Eldik, R. (2005) Kinetics and Mechanism of the Iron Phthalocyanine Catalyzed Reduction of Nitrite by Dithionite and Sulfoxylate in Aqueous Solution. *Inorg. Chem.* 44, 6470-6475. <https://doi.org/10.1021/ic0505955>.

- 21 Cioncoloni, G., Roger, I., Wheatley, P. S., Wilson, C., Morris, R. E., Sproules S., and Symes, M. D. (2018) Proton-Coupled Electron Transfer Enhances the Electrocatalytic Reduction of Nitrite to NO in a Bioinspired Copper Complex. *ACS Catal.* 8, 5070-5084. <https://doi.org/10.1021/acscatal.8b00361>.

High Yield and Selective Electrocatalytic Reduction of Nitroarenes to Anilines using Redox Mediators

Published as “*High yield and selective electrocatalytic reduction of nitroarenes to anilines using redox mediators*” A. D. Stergiou and M. D. Symes. *Cell Rep. Phys. Sci.*, 2022, 3, 100914.

Acknowledgments and Declaration

Athanasios Stergiou performed the experimental work, data analysis and co-wrote the paper. Mass spectrometry analysis was conducted by Mr Gangi Ubbara. Mark Symes conceived the idea, assisted with data analysis, and co-wrote the paper.

Synopsis

Anilines are major commodity chemicals used extensively in the production of pharmaceuticals, dyes and polymers. Typically, these anilines are produced from their corresponding nitrobenzene precursors by reaction with hydrogen at high temperatures. However, this route suffers from a number of drawbacks, including the requirement to handle hydrogen gas, rather harsh reaction conditions that lead to a lack of selectivity and/or toleration of certain functional groups, and questionable environmental sustainability. In light of this, routes to the reduction of nitrobenzenes to their aniline derivatives that operate at room temperature, in aqueous solvent and without the requirement to use harsh process conditions, hydrogen gas, or sacrificial reagents could be of tremendous benefit. Herein, we report on an electrocatalytic route to the reduction of nitrobenzenes to their aniline derivatives that works in aqueous solution at room temperature and pressure, where the electrons and protons required to reduce the nitrobenzenes are obtained from water. Excellent selectivity for the aniline derivatives is obtained for a range of nitrobenzenes, including for nitrobenzene substrates such as ortho-iodides that are very challenging to reduce effectively by other methods. Our approach relies on the use of a polyoxometalate redox mediator that shuts off the direct electro-reduction of the nitrobenzene at the electrode surface and thus prevents unproductive side reactions. Given the scale and current environmental impact of global aniline production, this electrochemical route holds promise for the development of more sustainable processes for the production of these vital chemical feedstocks.

3.1 Introduction

Aromatic amines (anilines) are important building blocks in the synthesis of a wide range of nitrogen-containing compounds including dyes, polymers, agrochemicals and pharmaceuticals (for example, one of the most widely produced pharmaceuticals, paracetamol, is a derivative of *p*-aminophenol).¹⁻³ Anilines are also the precursors for various important functional handles such as amides, diazonium salts and imines, and thus access to a range of aniline derivatives is important for both industrial mass production of key commodity chemicals and also for the development of new synthetic methodologies and chemical discovery.^{1,4,5} Currently, the most common way to produce these anilines is by the reduction of their corresponding nitro-compounds,⁶ typically at temperatures of around 300 °C and elevated pressure (5 bar). These methods also require the use of hydrogen gas and metal-based catalysts (Cu, Pd, Ni or Pt) on activated carbon or oxidic supports, usually in combination with other metals (Pb, V, P, Cr, Fe) to enhance the selectivity.⁷ Such catalytic systems are very effective for the reduction of unfunctionalized nitrobenzene to aniline, but for functionalized nitro-compounds, the selectivity of hydrogenation is variable.⁷ For example, halogen-substituted nitroarenes are especially challenging to convert to their aniline derivatives using conventional methods as there is a tendency for hydro-dehalogenation to occur, forming side-products where the halogen has been lost.^{7,8,9} This is particularly true for ortho-substituted iodo-nitroarenes, where selectivity in reduction is often very difficult to achieve.^{8,9}

In recent years, this lack of selectivity in the hydrogenation of functionalized nitro-compounds using traditional methods has spawned a number of studies examining alternative protocols for nitrobenzene reduction.¹⁰⁻¹⁵ A common focus of such research is the substitution of H₂ gas by a different hydrogenation agent and/or avoiding the use of high temperatures and pressures. One such route involves the use of soluble hydrogenation agents in the presence of metal catalysts, allowing the hydrogenation to proceed without the direct use of H₂ gas under less harsh reaction conditions.^{1,16-18} However, a considerable drawback of such approaches is that these reducing agents, such as sodium borohydride, formate and hydrazine,^{1,13-15,19,20} are toxic and are also irreversibly consumed during the hydrogenation reaction. Methods based on such sacrificial reagents are therefore inherently unsustainable.

In contrast, electrochemical reduction offers the prospect of a more sustainable route to aniline production, where the protons and electrons required for nitrobenzene reduction are obtained from water, rather than from expensive and/or toxic reagents. To date, however, electrochemical methods for the hydrogenation of nitrobenzenes have lacked selectivity. In

a seminal study in 1979, Marquez and Pletcher investigated the direct electrochemical reduction of nitrobenzene at a copper electrode in a mixture of aqueous organic solvents, using sulfuric acid as the proton source. Direct electrochemical reduction led to a mixture of products with the main product, *p*-aminophenol, obtained in 75% yield under the optimal conditions, with aniline and azoxybenzene found as only minor constituents of the product mix.²¹ Since then, a number of studies reporting the electrochemical reduction of nitrobenzenes to anilines have been reported, as summarized in Table 3.1. Amongst these existing studies, the highest overall conversion (98%) and selectivity (99%) for nitrobenzene reduction to aniline have been reported by the Zhang group, using either a cobalt phosphide (CoP) nanosheet cathode or a cathode composed of Ti-supported $\text{Co}_3\text{S}_{4-x}$ nanosheets with sulfur vacancies (Table 3.1, entries 1 and 2),^{22,23} although hydrogen evolution competes with nitroarene reduction in both cases. Further inspection of Table 3.1 demonstrates that for all entries at least one key facet of reaction (conversion of nitrobenzene, process conditions, Faradaic efficiency and/or selectivity for aniline) is sub-optimal. A truly selective, efficient and mild-condition electrocatalytic process for the reduction of a wide range of nitrobenzenes to their aniline derivatives has therefore yet to be reported.

Table 3.1: A summary of recent studies on the electrochemical reduction of nitrobenzenes to anilines

Entry	Nitrobenzene Conversion (%)	Aniline Selectivity (%)	Other notable products	Process Conditions	Ref
1	98	99	-	CoP nanosheet cathode (1 cm ²), -1.2 V vs. Ag/AgCl, 1 M KOH	22
2	98	99	-	Ti-supported Co ₃ S ₄ -x nanosheets with sulfur vacancies (1 cm ²), -0.6 to -1.1 V vs. Hg/HgO, 1 M KOH with traces (~4%) of CD ₃ CN.	23
3	61	87	Nitrosobenzene (3.6%) Para-ethoxyaniline (5.4%) Azoxybenzene (3.3%)	N-containing ordered mesoporous carbon, -0.75 V vs. Fc/Fc ⁺ , 52 h, 0.3 M HClO ₄ ethanolic solution.	24
4	44	< 18	Azoxybenzene (82%)	Cu/Cu _x O MWCNT (multi-walled carbon), H ₂ , -0.62 V vs. Fc/Fc ⁺ , 52 h, 0.3 M HClO ₄ .	25
5	95	95	-	Carbon nanotube-modified packed-bed flow reactor, -1.20 V vs. SCE in pH 5 solution, Faradaic efficiency 46%.	26
6	51	8	Azoxybenzene (77%)	Cu/Cu _x O supported on Norit activated carbon, H ₂ , -0.62 V vs. Fc/Fc ⁺ , 52 h, 0.3 M HClO ₄ ethanolic solution.	27
7	Not reported	87	-	Ti/TiO ₂ electrodes, in 10% H ₂ SO ₄ , T = 50-60 °C, cell potential 5-6 V.	28
8	54	82	Para-ethoxyaniline (11%)	Cu-PANI-AC-A (AC: activated carbon, PANI: polyaniline), -0.75 V vs. Fc/Fc ⁺ , 52 h, 0.3 M HClO ₄ ethanolic solution.	29
9	44	1	Azoxybenzene (36%)	Cu/MWCNT (multi-walled carbon nanotubes), H ₂ , -0.62 V vs. Fc/Fc ⁺ , 52 h, 0.3 M HClO ₄ .	30
10	96.5	88.4	-	Nitrogen-doped diamond electrode, -0.9 V vs. Ag/AgCl, 0.14 M Na ₂ SO ₄ , 26% coulombic efficiency.	31
11	5.3 % per pass	>99%	-	Cu/C felt, -1 V cell potential, 5 wt % acetic acid in methanol/H ₂ O (80:20 by weight).	32
12	>99%	>99%	None	Mediated process using as little as 1 mol% H ₃ [PW ₁₂ O ₄₀] mediator. Aniline is obtained in >90% isolated yield with up to 95% Faradaic efficiency.	This work

Herein, we demonstrate for the first time just such a selective and mild electrocatalytic process for the reduction of various nitrobenzenes to their aniline derivatives. Our approach circumvents the direct reduction of the nitrobenzene starting material at the electrode (which we show is the primary cause of the lack of selectivity in previous electrochemical studies), and instead uses a soluble redox mediator as an electron and proton shuttle to allow the clean and selective reduction of the nitro group to an amine in the presence of other functional groups that remain intact (-I, -OH, -COCH₃, -COOCH₂CH₃). Our process is conducted in an aqueous medium which provides both the protons and electrons required for nitrobenzene reduction and the resulting anilines are readily isolated without the need for extensive purification directly from the reaction medium after adjusting the pH and extracting into an organic solvent. The fact that this procedure allows the hydrogenation of functionalized nitrobenzenes to their aniline derivatives without the need to use H₂ gas, high temperatures, elevated pressures, co-catalysts or sacrificial reagents marks it out as a promising potential alternative for the more sustainable production of these key chemical feedstocks.

3.2 Materials and Methods

3.2.1 General Experimental Remarks

Nitrobenzene (99%), ethyl 2-nitrobenzoate (97%), 2-nitroacetophenone (97%) and phosphoric acid (85%) were purchased from Alfa Aesar. 4-nitrophenol (99%), 1-iodo-2-nitrobenzene (97%) and 1-iodo-4-nitrobenzene (98%) were supplied by Sigma Aldrich. Phosphotungstic acid (reagent grade) was supplied by both Sigma Aldrich and Alfa Aesar. Chloroform (99.8%), acetone (99.5%) and sulfuric acid (95%) were purchased from Fisher Scientific. Dichloromethane (99.5%) and magnesium sulfate (99.2%) were purchased from VWR while the diethyl ether (99.5%) was purchased from Scientific Laboratory Supplies Ltd. Deuterated chloroform (99.8%), dimethyl sulfoxide (99.9%) and methanol (99.8%) were supplied by Cambridge Isotope Laboratories. 254 μm -thick Nafion N-1110 membrane, used in H-cell, was purchased from Fuel Cell Stores and soaked in 1 M sulfuric acid solution overnight prior to use. All chemical reagents and solvents were used as purchased. Carbon felt, used as a high surface area electrode, was purchased from Alfa Aesar (3.18 mm thick, 99.0%).

All electrolyte solutions were prepared with ultrapure deionised water (18.2 M Ω -cm resistivity), obtained from a Sartorius Arium Comfort combined water system. All NMR

data were collected using a Bruker AV 400 instrument, at a constant temperature of 300 K. pH determinations were made with a Hanna HI 9025 waterproof pH meter. All other materials were obtained as stated in the text. Experiments performed at “room temperature” were carried out at 25 °C.

3.2.2 General Electrochemical Methods

Electrochemical studies were performed in a three-electrode configuration (unless otherwise stated) using either a CH Instruments CHI600D potentiostat or a BioLogic SP-150 potentiostat. A glassy carbon button electrode or carbon felt were used as the working electrodes, a graphite rod or a piece of carbon felt were used as the counter electrode, and an Ag/AgCl (NaCl, 3 M) reference electrode was used as specified. Glassy carbon working electrodes (area = 0.071 cm²) were polished using polishing powder and then washed with acetone and deionized water prior to use. Carbon felt electrodes were not re-used.

Cyclic voltammograms were collected in single chamber cells using a three-electrode set-up at room temperature at a scan rate of 10 mV/s (unless otherwise stated) in 1 M aqueous H₃PO₄ electrolyte. The solvent (10 mL) was thoroughly degassed with N₂ prior to the experiments and kept under inert atmosphere throughout the process. To this was added 1.9×10^{-4} mol of the relevant nitroarene substrate and subsequently, when needed, 1 equivalent of the phosphotungstic acid mediator relative to the nitroarene. For the cyclic voltammograms of the substituted nitroarenes a higher amount of starting material (9.74×10^{-4} mol) was used, with the rest of the conditions remaining as above. A glassy carbon button electrode was used as the working electrode (area = 0.071 cm²), a graphite rod was used as the counter electrode and an Ag/AgCl reference electrode was used. Measurements were conducted without stirring and with *iR* compensation enabled.

Bulk electrolysis was performed in both three-electrode and two-electrode configurations in a two-compartment electrochemical cell or H-cell (Figure 3.1), unless otherwise stated. Cell resistances were measured by the *iR* test function available on the CH or BioLogic potentiostats, using the general method developed by He and Faulkner.³³ The two compartments of the H-cell were separated by a Nafion N-1110 membrane, with the phosphotungstic acid solution in the working compartment with a carbon felt working electrode and an Ag/AgCl reference electrode. The counter compartment was filled with 1 M aqueous H₃PO₄ of a comparable pH (~0.5) to that of the phosphotungstic acid to prevent

a pH gradient forming. A large area piece of carbon felt was used as the counter electrode for the three-electrode configurations, while a Pt mesh was used for the counter electrode in the two-electrode setup. Solutions were stirred at around 450-500 rpm, keeping the same stirring rate for all experiments and bubbled constantly with nitrogen (unless otherwise stated) to prevent the oxidation of the solution by the air (two-electron reduced phosphotungstic acid is slowly re-oxidized by air, see studies in section 3.2.6).

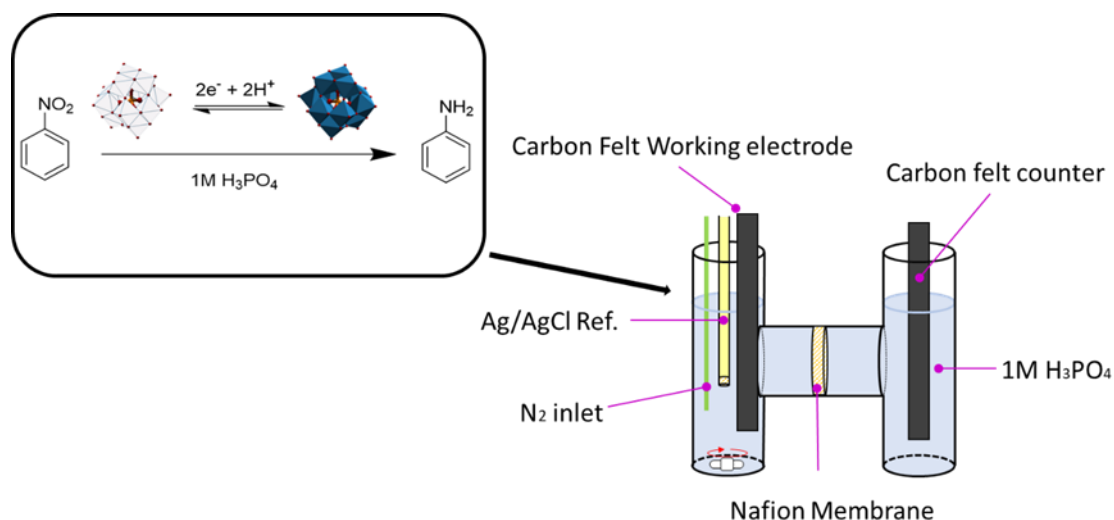


Figure 3.1: Graphic representation of the two-compartment electrochemical cell (or H-cell) that was used during the bulk electrolysis experiments. The left side of the cell is the working side, where the reaction takes place and the right is the counter side where the counter electrode is placed. The two compartments are separated by the Nafion membrane.

3.2.3 Electrocatalytic Studies

Electrocatalytic studies were performed as follows. Unless otherwise stated, 9.74×10^{-4} mol of the relevant nitroarene was added to 30 mL of a 3.3 mM aqueous solution of phosphotungstic acid (i.e. a 10 mol% ratio of phosphotungstic acid relative to the nitroarene). This solution (although typically the nitroarene substrate did not dissolve completely at this stage) was then placed in the working electrode compartment of the H-cell, with a 1.8×2 cm carbon felt electrode. For the less soluble nitroarenes (ethyl-2-nitrobenzoate, 2-nitroacetophenone, 1-iodo-2-nitrobenzene and 1-iodo-4-nitrobenzene) half this amount of starting material was used, *i.e.* 4.87×10^{-4} mol, but still with a 10 mol% ratio of phosphotungstic acid relative to the nitroarene. The counter side of the cell was filled with 1 M aqueous H₃PO₄ electrolyte solution. Typically, bulk electrolysis was then carried out at -0.38 V vs. Ag/AgCl until substrate reduction was complete, as judged by the falling off of the current to background levels (see example in Figure 3.2).

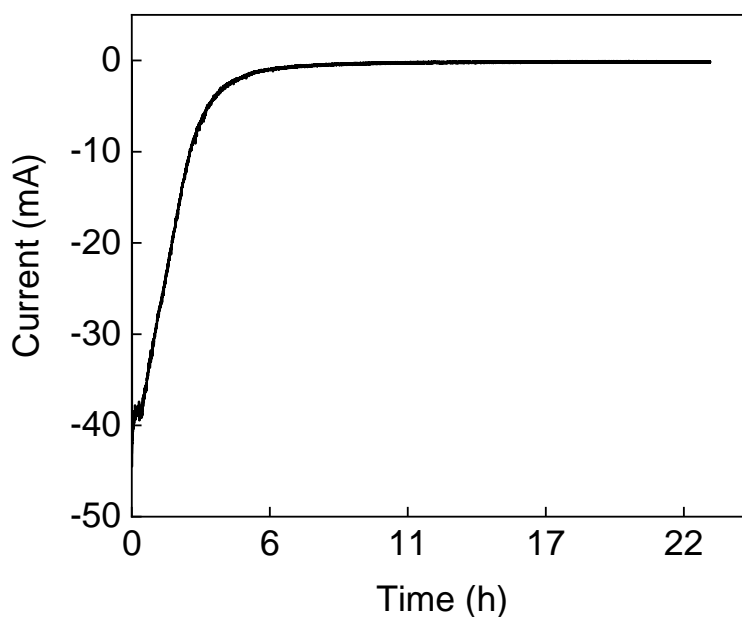


Figure 3.2: Bulk electrolysis of the nitroarene ethyl-2-nitrobenzoate, where 0.095 g (4.87×10^{-4} moles) of the starting material were used together with 4.86×10^{-5} moles (10 mol%) of the polyoxometalate mediator in 30 mL electrolyte.

After electrolysis for a given time, the (now dark blue) solution was removed from the working electrode compartment of the H-cell. The pH of this solution was then raised above the pK_a value of the anticipated product using 1 M NaOH in order to deprotonate the $R-NH_3^+$ salt and form the neutral $R-NH_2$ state. This in turn allowed the reduced organic product to be extracted into organic solvents for isolation. The pH values in question for the various conversions were: nitrobenzene to aniline, pH = 5.6, ethyl 2-nitrobenzoate to ethyl 2-aminobenzoate, pH = 3.2, 4-nitrophenol to 4-aminophenol, pH = 6.0, 2-nitroacetophenone to 2-aminoacetophenone, pH = 9.0, 1-iodo-2-nitrobenzene to *o*-iodoaniline, pH = 2.6 and 1-iodo-4-nitrobenzene to *p*-iodoaniline pH = 2.34.

Aniline, *o*-iodoaniline and *p*-iodoaniline were extracted using chloroform, 4-nitrophenol was extracted using dichloromethane and the other aromatic organics were extracted using diethyl ether. In all cases, after extraction, magnesium sulfate was added to the organic phase in order to remove any remaining water. The organic phase was then filtered and concentrated under reduced pressure using a rotary evaporator to give the isolated reduced aniline derivatives.

In the case of the 4-aminophenol, special treatment of the reaction medium was needed. The very polar nature of the compound made its extraction from the aqueous phase very difficult

and significantly less efficient than for the other aniline derivatives. For this reason, the aqueous phase was first concentrated in the rotary evaporator until it reached a volume of about 5 mL. The pH was then adjusted using a solution of 5 M NaOH to keep the volume lower than 7-8 mL. The NaOH solution was added very slowly to a round-bottom flask which was kept in ice. After the pH adjustment, an acetone/dry ice bath, with a temperature of $-78\text{ }^{\circ}\text{C}$ was prepared. The round-bottom flask containing the aqueous solution was put into the acetone/dry ice bath for a few seconds, and just before freezing, the contents of the flask were transferred to a separating funnel and extracted with dichloromethane. This process was repeated 3-4 times, allowing most of the organic product to be extracted from the aqueous phase. The combined organic extracts were then dried over magnesium sulfate as described above.

For the larger scale experiments, a larger H-cell and larger carbon felt electrodes were used ($3.2 \times 4.5\text{ cm}$). 1.23 g (10 mmol, 1.025 mL) of nitrobenzene was added to 100 mL of a 10 mM aqueous solution of phosphotungstic acid (i.e. a 10 mol% ratio of phosphotungstic acid relative to the nitrobenzene). The isolated amount of aniline was 766 mg (82%).

For the two-electrode setup the regular H-cell and starting material/mediator quantities were used while the carbon felt counter electrode was replaced with a Pt mesh. The applied potential was -2.2 V . The internal resistance of the cell was calculated to be 58-60 Ohm.

3.2.4 Ex-cell Studies

For the *ex-cell* studies, a 0.3 M solution of aqueous phosphotungstic acid was prepared. This solution was then placed in the working compartment of the H-cell and reduced by two-electrons at $-0.4\text{ V vs. Ag/AgCl}$ under a nitrogen atmosphere with constant stirring. A large area piece of carbon felt was again used as the counter electrode. Portions of the relevant substrates for reduction were placed into 50 mL round-bottom flasks, each of which was equipped with a magnetic stirrer bar and a rubber septum to seal the flask. The flasks were all flushed with nitrogen to remove any oxygen. Various aliquots of the two-electron reduced phosphotungstic acid were then injected into these flasks, depending on whether the aim of the experiment was to obtain a series of ratios of mediator to substrate (see Figure 3.15), or simply to ensure that excess two-electron reduced mediator was present. For example, $9.7 \times 10^{-4}\text{ mol}$ of azoxybenzene or azobenzene were placed in round-bottom flasks into which 35 mL of 0.22 M two-electron reduced phosphotungstic acid were added (providing an excess of electrons at the more cathodic position of the second redox wave of the mediator). Each

flask was then stirred overnight (12-18 h) at room temperature and under an N₂ atmosphere in order for the reaction to complete. After this time, the pH of the reaction mixtures was adjusted above the p*K*_a of the expected aniline product and the reaction mixture was then extracted into organic solvent as per the methods described above for the electrocatalytic studies.

3.2.5 Ex-cell Reactions Between Phenylhydroxylamine and 1-electron Reduced Phosphotungstic Acid

One-electron reduced phosphotungstic acid was prepared according to the method described in Section 3.2.4, with the exception that the potential on the working electrode was restricted to -0.16 V *vs.* Ag/AgCl in order to prevent reduction by more than one electron per mediator molecule. This one-electron reduced phosphotungstic acid was then added to aliquots of phenylhydroxylamine in a purely non-electrochemical reaction step as described in Section 3.2.4. After this time, the pH of the reaction mixture was adjusted above 5.6 before extraction into organic solvent and subsequent isolation according to the general methods in Section 3.2.3. The conversion to aniline was then quantified and plotted against the equivalents of reduced phosphotungstic acid (see Figure 3.13).

3.2.6 Aerial re-oxidation of the Reduced Mediator

To gauge the rate of spontaneous aerial re-oxidation of the reduced mediator, 0.280 g of H₃[PW₁₂O₄₀] were dissolved in 35 mL of 1 M aqueous H₃PO₄ and added to the working side of the H-cell, which was equipped with a 1 × 1 cm carbon felt working electrode and a Ag/AgCl reference electrode. Other details of the cell were as described in Section 3.2.2. Then, a potential of -0.4 V *vs.* Ag/AgCl was applied across this cell under a nitrogen atmosphere with constant stirring in order to fully reduce the mediator by two electrons. Once fully reduced, the nitrogen purge line was removed from the H-cell, and the two-electron reduced mediator solution was allowed to stir at room temperature open to air. After a defined period of time, the purge line was re-inserted and the solution was then electrochemically re-oxidised at $+0.2$ V *vs.* Ag/AgCl until completely re-oxidised. Through varying the length of time that the solution was allowed to stir open to air before electrochemical re-oxidation, a curve such as that shown in Figure 3.9 was obtained.

3.2.7 ^1H NMR Determination of Conversions

After extraction into organic solvent and concentration under reduced pressure, the conversion of the starting material was determined *via* the integration of the relevant ^1H NMR peaks. After the ^1H NMR peaks in any given spectrum had been identified and assigned, peaks corresponding to the same number of protons in both the starting material and the various products were compared, allowing the percent of starting material converted to each product (or not converted, and hence still present as starting material) to be determined.

3.3 Results and Discussion

3.3.1 Electrocatalytic Studies

A schematic illustrating the electrochemical redox mediator approach³⁴⁻³⁶ to nitrobenzene reduction is shown in Figure 3.3.

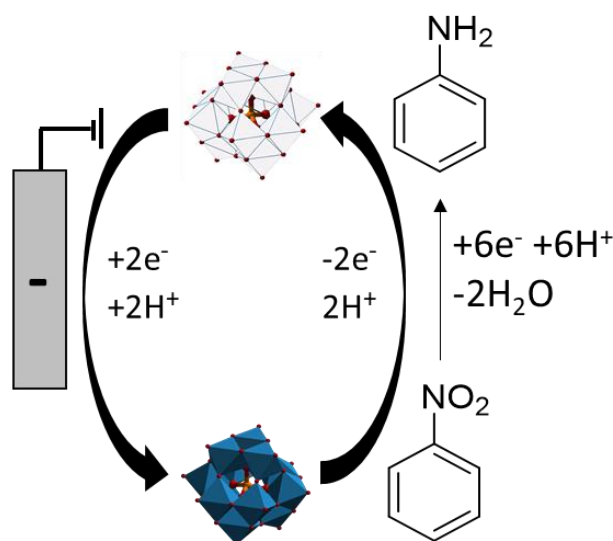


Figure 3.3: Schematic describing the electrochemical hydrogenation of nitrobenzene to aniline using a polyoxometalate redox mediator. Phosphotungstic acid is electrochemically reduced at the surface of the electrode and then reacts with the nitrobenzene in solution to make aniline.

A suitable mediator should therefore be water-soluble and exhibit excellent stability to repeated electrochemical cycling, with the ability to donate electrons to the nitroarene in a rapid and reversible fashion. Figure 3.4 shows the polyoxometalate phosphotungstic acid ($\text{H}_3[\text{PW}_{12}\text{O}_{40}]$),³⁷ fits this specification well. As shown in Figure 3.4 (red line), phosphotungstic acid has two reversible (one-electron) redox waves located at -0.02 V and

-0.30 V vs. Ag/AgCl in 1 M aqueous H_3PO_4 at pH 0.3. Upon addition of 1 equivalent of nitrobenzene to this phosphotungstic acid solution, there is evidence of an electrocatalytic process associated with the second reduction wave of phosphotungstic acid at -0.30 V vs. Ag/AgCl (green line), indicating that the two-electron reduced phosphotungstic acid is reacting with nitrobenzene. Meanwhile, the direct reduction of an equivalent amount of nitrobenzene at the electrode surface in the absence of any mediator is shown by the blue trace in Figure 2: there is little appreciable activity for direct reduction at potentials more positive than -0.35 V vs. Ag/AgCl. These data suggested to us that by careful control of the reaction conditions, it should be possible to reduce phosphotungstic acid by two electrons and have this two-electron reduced species react with nitrobenzene, without significant competing direct reduction of nitrobenzene at the electrode. In turn, we hypothesized that the outcome of this mediated process would be more selective than direct reduction of nitrobenzene at the electrode surface.

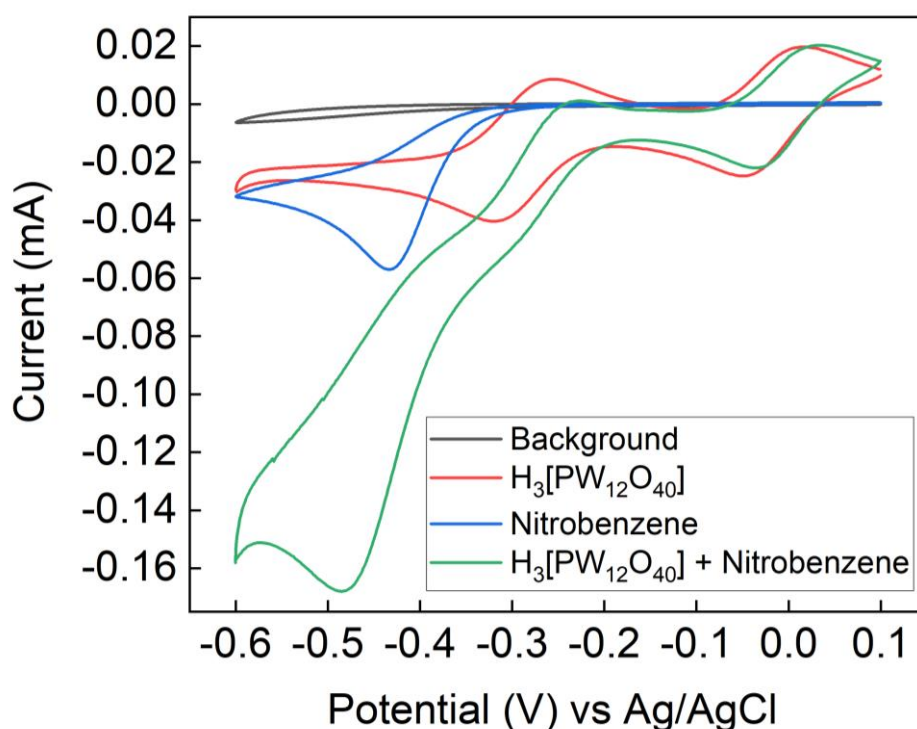


Figure 3.4: Cyclic voltammetry showing the effects of phosphotungstic acid ($\text{H}_3[\text{PW}_{12}\text{O}_{40}]$) on the reduction profile of nitrobenzene. Cyclic voltammetry was performed in a single chamber cell, at a scan rate of 10 mV/s, using 1 M aqueous H_3PO_4 (10 mL) as the electrolyte (pH 0.3) at 25 °C. The working electrode was a glassy carbon button electrode (area = 0.071 cm²), a graphite rod was the counter electrode and Ag/AgCl (3 M NaCl) was used as the reference electrode. The concentration of phosphotungstic acid was 9.75×10^{-3} M and 1 equivalent (10 μL) of nitrobenzene was added to the electrolyte solution under inert atmosphere. The cyclic voltammogram of the 1 M aqueous H_3PO_4 electrolyte on its own is shown as the black trace.

Accordingly, the catalytic electrochemical reduction of nitrobenzene to aniline was attempted. In a typical procedure, 0.1 equivalents (10 mol%) of $\text{H}_3[\text{PW}_{12}\text{O}_{40}]$ (concentration = 2.78×10^{-3} M) relative to the nitrobenzene substrate was dissolved in 1 M aqueous H_3PO_4 and placed into one side (the “working electrode” side) of a two-compartment electrochemical cell (see Figure 3.1). Meanwhile, the counter electrode side was filled with 1 M aqueous H_3PO_4 . The two chambers of the electrochemical cell were separated by a Nafion membrane in order to confine the starting materials and products to the cathode chamber as far as possible, and so to aid our determination of the reaction yields. Two large-area carbon felt electrodes were used as the anode and cathode, and an Ag/AgCl reference electrode was also employed (except in those cases where two-electrode operation was probed – see below). The relevant nitroarene substrate was added to the working electrode side of the cell and this side of the cell was kept under an inert atmosphere of nitrogen. Electrolysis was then initiated (with constant stirring of the working electrode compartment) at -0.38 V vs. Ag/AgCl until substrate reduction was complete, as judged by the falling-off of the current to background levels (see example in Figure 3.2). At the end of the reaction, the pH of the reaction medium was adjusted so that it was above the $\text{p}K_{\text{a}}$ value of the anticipated product, and the reaction mixture was then extracted with an organic solvent. In the case of aniline, the pH value of the reaction mixture was raised to 6, using an aqueous 1 M NaOH solution, and chloroform was used for the extraction. Magnesium sulfate was then added to remove any remaining trace of water from the organic phase before concentration of this organic phase under reduced pressure. Other nitroarenes were isolated by similar methods (see Section 3.2.3).

The identity and purity of the various nitroarenes was then confirmed by ^1H NMR spectroscopy. Table 3.2 lists the yields and selectivity of conversion for a number of nitrobenzenes, showing excellent selectivity for the corresponding aniline derivatives over other possible products (indeed, typically only the aniline product was observed) and good-to-excellent yields. Cyclic Voltammograms of all the substituted nitrobenzenes are presented below in Figures 3.5 – 3.7.

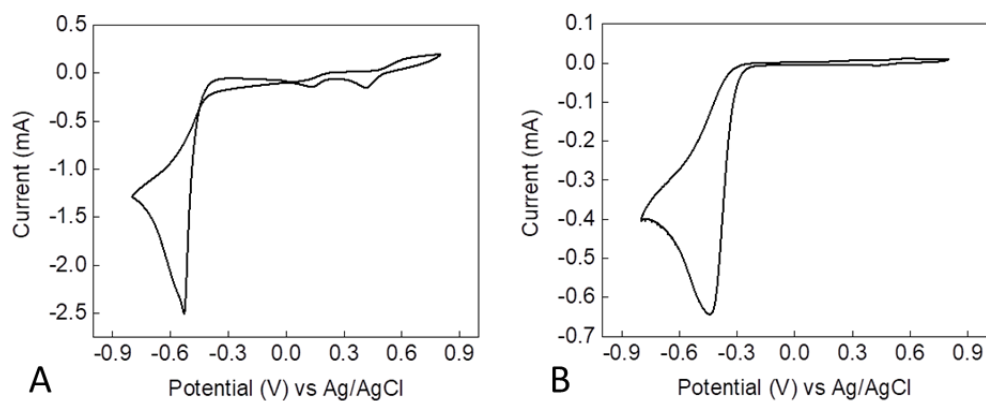


Figure 3.5: **A:** Cyclic voltammogram of the starting material 4-nitrophenol. **B:** Cyclic voltammogram of 2-nitroacetophenone. The scan was started at 0 V, sweeping first to -0.8 V and then sweeping anodically. Scan rate: 100 mV/s.

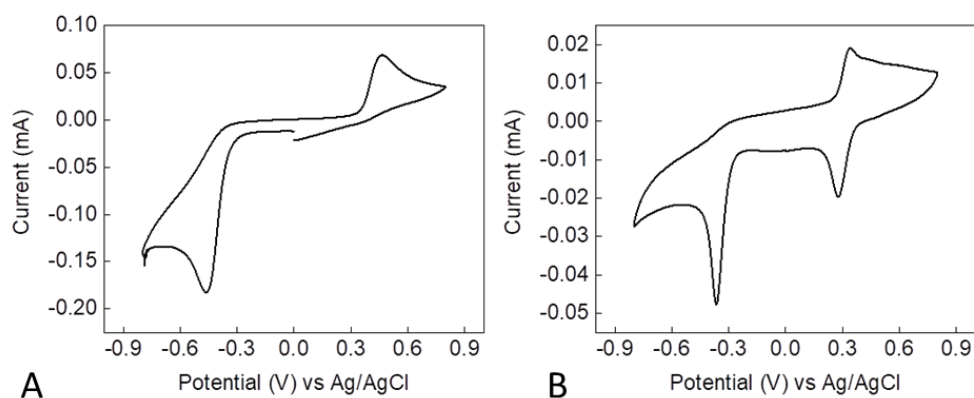


Figure 3.6: **A:** Cyclic voltammogram of the starting material ethyl-2-nitrobenzoate. **B:** Cyclic voltammogram of 1-iodo-2-nitrobenzene. The scan was started at 0 V, sweeping first to -0.8 V and then sweeping anodically. Scan rate: 100 mV/s

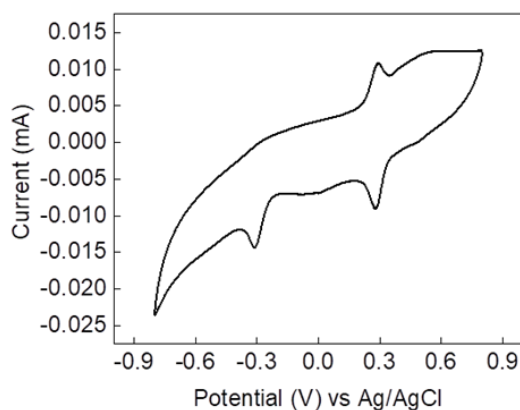


Figure 3.7: Cyclic voltammogram of 1-iodo-4-nitrobenzene. The scan was started at 0 V, sweeping first to -0.8 V and then sweeping anodically. Scan rate: 100 mV/s.

Conversion of the starting material was determined by ^1H NMR analysis of the reaction mixture after extraction into organic solvent (see Sections 3.2.3 and 3.2.7). Figure 3.8 shows a stacked ^1H NMR plot summarizing the reaction outcome of the mediated reduction of nitrobenzene. Stacked ^1H NMR plots of the substrates and products of the other conversions are shown in Section 3.5, Figures 3.15 – 3.32.

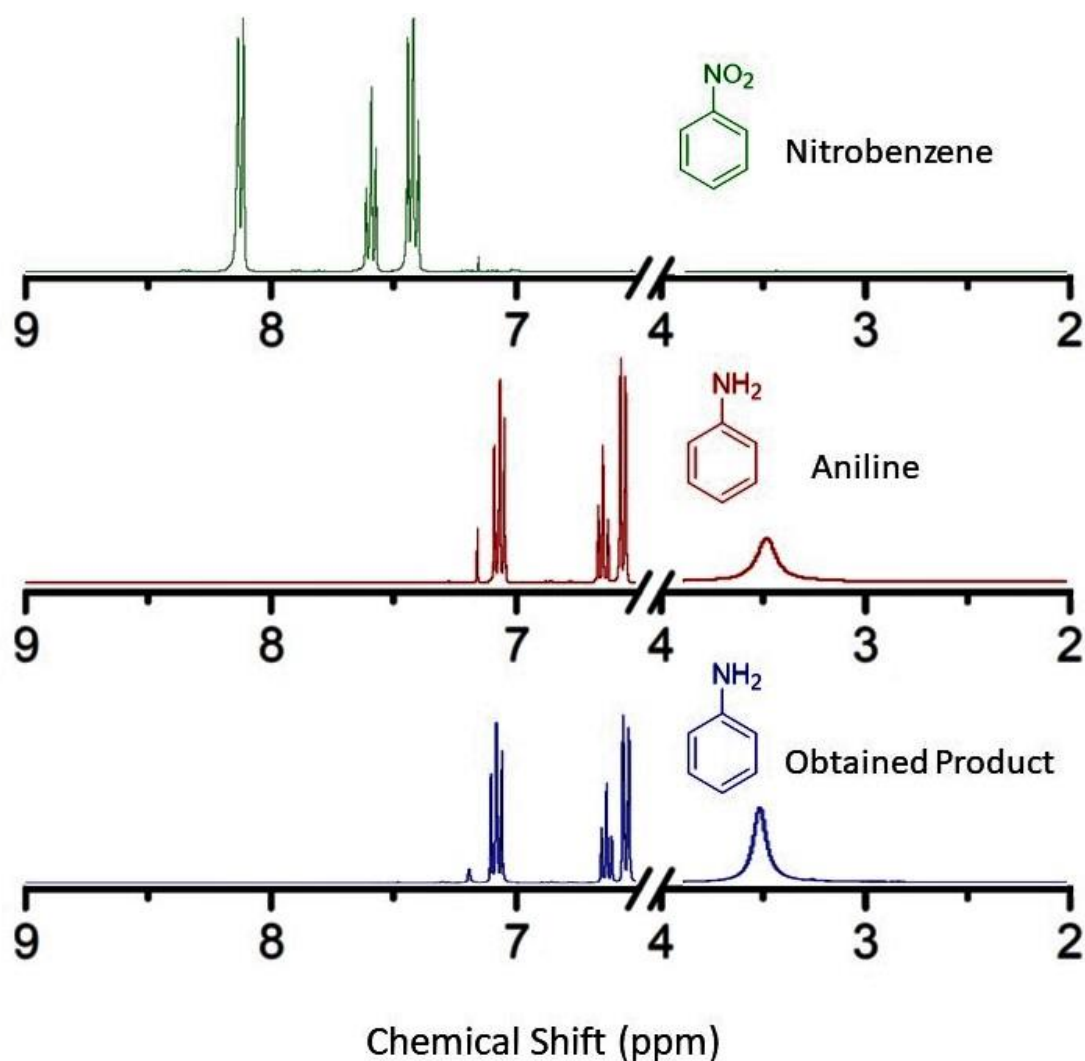
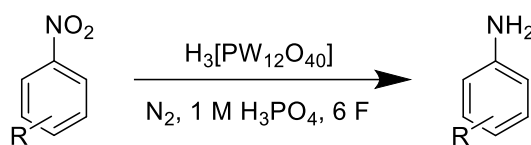


Figure 3.8: Stacked ^1H NMR plot (CDCl_3 , 300 K, 400 MHz) summarizing the outcome of the mediated electroreduction of nitrobenzene. Shown in green at the top is a spectrum of the nitrobenzene starting material. Beneath this (red) is a spectrum of a pure aniline standard sample. The bottom spectrum (blue) is that of the extracted and concentrated reaction medium from a mediated electrochemical reduction of nitrobenzene. The peak at 7.26 ppm originates from residual CHCl_3 .

Table 3.2: Table of obtained products with yields (relative to starting material) using 10 mol% loading of the mediator relative to the substrate. 1 F = one equivalent of electrons. Reaction times for completion were between 5-12 h, as dictated by the relative solubility of the starting material.



Entry	Substrate	Product	Using 10% mediator			Using 0% mediator		
			Conversion of starting material (%)	Selectivity for aniline (%)	Isolated yield of aniline product (%)	Conversion of starting material (%)	Selectivity for aniline (%)	Isolated yield of aniline product (%)
1			>99%	>99%	91 ± 2	95	78	60 ± 1
2			>99%	>99%	80 ± 3	>99%	1.4 ^a	< 1
3			>99%	>99%	81 ± 1	~77	~34	~25
4			>99%	>99%	72 ± 3	2.5	2.5	1
5			82 ± 2% ^b	>99%	61 ± 4	0	0	0
6			97 ± 1	96 ± 2	71 ± 3	0	0	0

^a The main product of this reaction is the hydroxylamine intermediate, 2-hydroxylaminoacetophenone, as identified by ¹H NMR and mass spectrometry (see figure 3.18). ^b After a reaction time of 12 h, approximately 18% starting material was still left unconverted.

Reactions with a mediator can be compared to reactions in the absence of mediator, where the nitrobenzene was therefore undergoing direct reduction at the electrode surface (0% mediator loading entries in Table 3.2). In all cases without a mediator, yields of the aniline derivatives are substantially reduced. Direct reduction of nitrobenzene at the electrode (Table 3.2, entry 1) proceeds with decent selectivity for aniline under these conditions (78%), although this is still significantly lower than for the corresponding mediated process (>99% conversion). Apart from aniline, the main other species isolated from the reaction mixture of the direct reduction of nitrobenzene (in the absence of mediator) was azoxybenzene (13%, see Table 3.3).

In the case of entries 2, 4, 5 and 6 in Table 3.2, there is essentially no direct reduction of the nitrobenzene to the corresponding aniline (*i.e.* in the absence of mediator). For entries 4, 5 and 6 this is because there is only minimal conversion of the nitroarene starting material in the absence of the mediator. In the case of entry 2, conversion of the starting material in the absence of the mediator is quantitative, but the main product is the hydroxylamine intermediate (suggesting incomplete reduction) rather than the desired aniline derivative (see Section 3.5, Figure 3.18). This is in stark contrast to the situation when the polyoxometalate mediator is employed, which gives essentially complete selectivity for nitroarene reduction to the corresponding aniline for all the entries in Table 3.2. Only in the case of *o*-iodonitrobenzene (entry 6) was a small amount (2-6 %) of the intermediate *N*-hydroxy-2-iodonitrobenzene identified. Isolated yields when using the mediator were generally good or excellent. In the case of aminophenol synthesis (entry 4) the comparatively low isolated yield (70-75%) is a function of the very polar nature of this compound which makes it difficult to separate the product from the aqueous reaction medium (see discussion in the Section 3.2.3). Meanwhile, the comparatively low isolated yields obtained for the two iodoaniline substrates (entries 5 and 6) are attributed to the lower solubility of these two compounds in the 1 M aqueous H₃PO₄ electrolyte compared to the other starting materials that were used. In any case, and regardless of the position of the substituent, only the nitro group was reduced under our mediated reaction conditions with the other functional group remain intact, implying excellent chemoselectivity.

The reduction of unfunctionalized nitrobenzene to aniline was selected for in-depth investigations regarding catalyst loading and mechanistic studies. Firstly, the effect of mediator loading on reaction times, average current densities and product distributions was assessed, as shown in Table 3.3. These results show that the selectivity towards aniline remains at >99% when using 1 mol% loading of the mediator (entry 2), with isolated yields

(~90%) and Faradaic efficiency (94%) essentially indistinguishable from that obtained using 10 mol% loading. At 0.1 mol% mediator loading (entry 3), side products are evident, and the yield of aniline is reduced, and this trend is even more pronounced in the absence of mediator (where only direct reduction of the nitrobenzene at the electrode surface is occurring, entry 4). It therefore seems likely that at very low mediator loadings some direct reduction of the nitrobenzene is happening at the electrode surface, leading to side product formation (see mechanistic discussion below). That said, even at 0.1 mol% mediator loading, conversion of nitrobenzene to aniline is significantly cleaner and side-product formation correspondingly lower than for the direct process.

The reduction of nitrobenzene to aniline is also effective under air (Table 3.3, entry 5). In this case, there was still >99% selectivity towards aniline (isolated yield of 91%), but the Faradaic efficiency declined to 73% (compared to 95% under inert atmosphere). One reason for this is surely that the two-electron reduced mediator can be re-oxidized by oxygen in the air and so some charge is lost to this aerial re-oxidation, rather than going towards nitrobenzene reduction. Our studies (see Section 3.2.6 for details), depicted in Figure 3.9, have shown that a “half-life” for aerial re-oxidation of the reduced mediator of just over 30 minutes can be estimated. In Figure 3.9, a charge state of 100% corresponds to a fully two-electron reduced mediator solution, 50% corresponds to a fully one-electron reduced mediator solution and 0% corresponds to a fully oxidised mediator solution. It is striking however that the introduction of oxygen has no more serious effect on the reaction outcome than this moderate loss in efficiency, and aniline is still the only reduction product obtained when the mediator is employed under air.

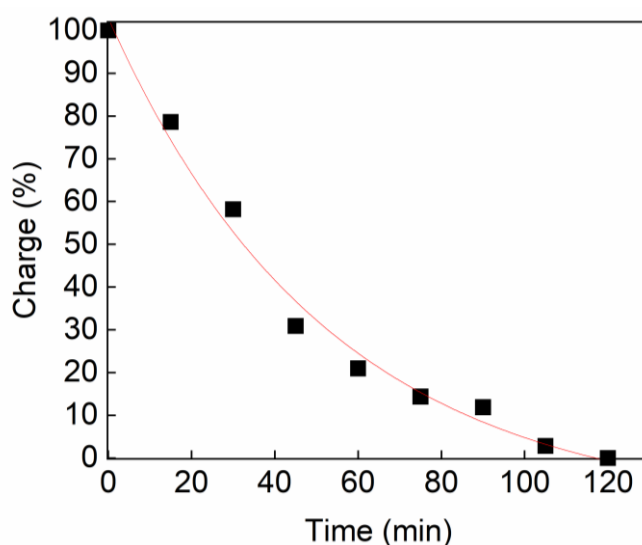


Figure 3.9: Aerial re-oxidation of the reduced mediator over time. The red line is provided as a guide to the eye.

Entries 6 and 7 in Table 3.3 compare the conversion and selectivity for nitrobenzene reduction at an applied potential of -0.2 V vs. Ag/AgCl. As shown by Figure 3.4 and entry 7 in Table 3.3, this potential is clearly not cathodic enough to allow the direct electroreduction of nitrobenzene to aniline at the electrode. However, entry 6 shows that there is a 15% conversion of nitrobenzene to aniline at this potential in the presence of the mediator. This is strong evidence that the mediated pathway occurs at lower potentials than the direct pathway, in turn suggesting a route by which the greater selectivity of the mediated pathway is achieved. As the potential is made more cathodic (-0.3 V, entries 8 and 9), the direct electroreduction reaction becomes possible, but the mediated pathway shows considerably greater current density and also much superior selectivity for aniline.

The final two entries in Table 3.3 suggest that the mediated route from nitrobenzene to aniline shows some promise for applications beyond the laboratory. Firstly, entry 10 shows that the process remains effective on the 10 mmol scale ($>99\%$ selectivity for aniline and 82% isolated yield), suggesting that a large-scale lab procedure can be effected without a significant compromise in efficiency. The slightly reduced isolated yields compared to experiments with lower loadings of starting material are likely due to the longer reaction times necessary to drive complete conversion of the nitrobenzene in this unoptimized cell. These extended reaction times provide more opportunity for the product to diffuse into the anode compartment, thus reducing the aniline harvest from the catholyte (on which the isolated yields are based).

Meanwhile, entry 11 shows that the reference electrode (essential for controlling the cell potential in a proof-of-concept study such as this, but not usually employed in industrial electrochemical contexts) can be dispensed with. Hence in a two-electrode cell, $>99\%$ selectivity for aniline production can be achieved. Whilst these conditions have not been optimised in terms of current density or cell design, the combination of these results (high selectivity at low mediator loadings, ability to tolerate operation under air, potential for scale-up and amenability to two-electrode operation) all suggest that this approach could hold promise for the reduction of nitroarenes at preparative scale.

Table 3.3: Summary of the effects of different mediator loadings on the electrochemical reduction of nitrobenzene, including yields (relative to starting material), the selectivity towards different products (as gauged by ^1H NMR), Faradaic efficiencies and reaction times.

Entry	1	2	3	4	5	6	7	8	9	10	11
Mediator loading	10%	1%	0.1%	0%	10% ^b	10% ^c	0% ^c	10% ^d	0% ^d	10% ^e	10% ^f
Time (h)	5	18	23	24	16	23	20	14	22	40	15
Average current density (mA/cm ²) ^a	-5.31	-2.58	-1.75	-1.97	-5.26	-0.14	-5.93 x 10 ⁻³	-4.11	-0.28	-3.4	-2.21
Nitrobenzene conversion (%)	>99	>99	98	95	>99	15	0	>99	24	>99	>99
Aniline Selectivity (%)	>99	>99	94	78	>99	>99	0	>99	9.9	>99	>99
Azoxybenzene selectivity (%)	0	0	1.4	13	0	0	0	0	9.4	0	0
Phenylhydroxylamine selectivity (%)	0	0	2	2	0	0	0	0	4.7	0	0
Nitrosobenzene selectivity (%)	0	0	0.6	2	0	0	0	0	0	0	0
Isolated yield of aniline (%)	89-93	89-92	83-85	59-61	91	13.8	0	90	7	82	91
Faradaic efficiency	95	94	93	89	73	94	0	94	25	83	90

^a Over the first 2.5 h of the reaction. ^b Reaction performed under air. ^c Reaction performed at a potential of -0.2 V vs. Ag/AgCl. ^d Reaction performed at a potential of -0.3 V vs. Ag/AgCl. ^e 1.23 g of nitrobenzene (10 mmol) was used for scaling up purposes. ^f Two electrode setup with cell voltage of -2.2 V with Pt mesh as the counter electrode.

3.3.2 Repeated Use of the Polyoxometalate Mediator

The results above suggest some versatility for this mediated electrocatalytic system for the selective reduction of different nitroarenes. Hence, we next tested the ability of the catalyst to perform multiple rounds of nitrobenzene reduction. For this purpose, a nitrobenzene reduction experiment was performed over the course of a week, with more nitrobenzene being periodically added into the working compartment of the cell. As shown in Figure 3.10, each of these aliquots of nitrobenzene was fully reduced to aniline without any other alterations to the ongoing reaction, showing that the mediator is able to function as part of a continuous cycle. The reduction profiles become somewhat less steep with successive cycles, which we believe is caused by some precipitation of the polyoxometalate mediator from the solution as the aniline product builds up (a white solid precipitate was noted at the end of the fourth cycle, which mass spectrometry showed to be phosphotungstic acid). Optimization of the reaction process (*e.g.* to a continuous flow system) could help to mitigate this issue. After extraction at the end of the fourth cycle, the ^1H NMR of the resulting product showed >99% selectivity towards aniline with a 92% overall isolated yield for the reaction, within the range found for the single-pass experiments outlined in Table 3.3.

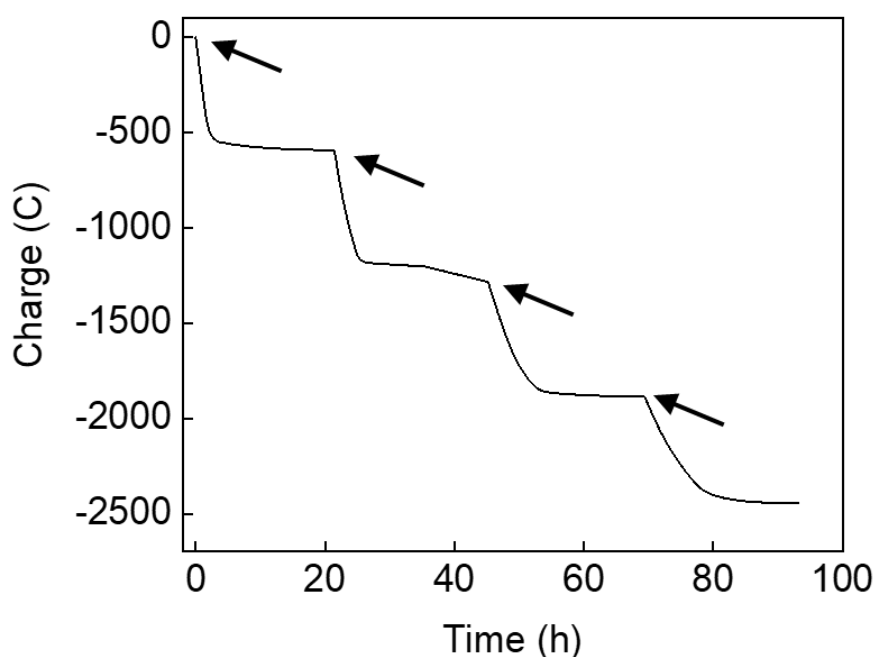


Figure 3.10: Electrocatalytic reduction of nitrobenzene to aniline using the phosphotungstic acid mediator in four consecutive full conversion cycles. 9.74×10^{-5} moles (10 mol%) of phosphotungstic acid were dissolved in 30 mL 1 M aqueous H_3PO_4 using the typical two-compartment cell setup. 100 μL of nitrobenzene were added at $t = 0$ h and then periodically as indicated by the arrows. 100 μL of nitrobenzene (9.74×10^{-4} mol) requires 564 C for the full 6-electron reduction to aniline, so the minimum theoretical charge required to reduce all 400 μL of nitrobenzene is 2256 C.

3.3.3 Reaction Mechanism

In order to gain insight into the mechanism of nitroarene reduction in this mediated system, aliquots from ongoing (*i.e.* not yet complete) electrocatalytic reduction reactions of nitrobenzene were extracted and analysed by ^1H NMR spectroscopy, allowing the identification of three reaction intermediates: phenylhydroxylamine, azoxybenzene and nitrosobenzene. Figure 3.11 shows a plot of the relative amounts of nitrobenzene, aniline, phenylhydroxylamine and azoxybenzene present in the reaction medium at various different time points: phenylhydroxylamine and azoxybenzene were the main intermediate species, while nitrosobenzene was only ever detected in trace amounts (specifically at $t = 4$ h, not shown in the figure).

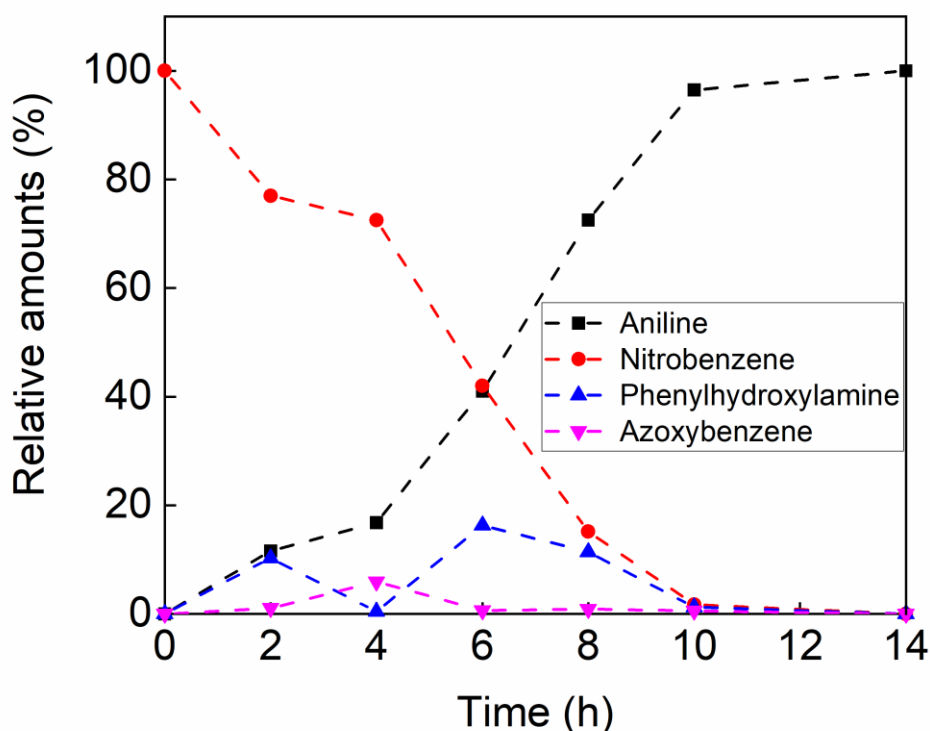


Figure 3.11: The relative amounts of the various nitrobenzene-derived species detected in incomplete reaction mixtures as a function of time. Typical reaction conditions were employed; namely, 1.94×10^{-4} mol of nitrobenzene was added to 30 mL of a 10% mol aqueous solution of phosphotungstic acid and the reaction was subjected to a cathodic potential of -0.38 V vs. Ag/AgCl.

It is interesting to compare these data with the mechanism proposed by Marquez and Pletcher²¹ for the direct electroreduction of nitrobenzene at an electrode surface under acidic conditions (which in Marquez and Pletcher's case gave rise predominantly to *p*-

aminophenol, rather than aniline). The most obvious distinction is that in our process, *p*-aminophenol is never observed. Secondly, Marquez and Pletcher proposed that nitrobenzene was reduced directly to phenylhydroxylamine, whereas the traces of nitrosobenzene that we observe would tend to suggest that this process happens through at least one intermediate step; namely, the two-electron reduction of nitrobenzene to nitrosobenzene, followed by a further two-electron reduction of that nitrosobenzene to phenylhydroxylamine. The fact that nitrosobenzene is only ever observed fleetingly in our studies (and not at all by Marquez and Pletcher) suggests that onward reaction of nitrosobenzene is rapid.²⁹ Azoxybenzene was also observed in our reaction mixture, but only as an intermediate, whereas Marquez and Pletcher found this as one of the end products of their reaction. There is some debate in the literature as to whether azoxybenzene can^{38,39} or cannot^{25,27,40} be converted to aniline electrochemically. In our case, we have been able to show unambiguously that azoxybenzene can be cleanly reduced to aniline by the 2-electron reduced phosphotungstic acid. This was achieved by reducing a solution of phosphotungstic acid of known concentration by two electrons per mediator molecule, and then adding this solution to azoxybenzene under an inert atmosphere in an “ex-cell” (*i.e.* non electrochemical) process (see Section 3.2.4). Under such conditions (with roughly eight equivalents of the two-electron reduced phosphotungstic acid present), azoxybenzene converts to aniline in >99% yield. This suggests that one of the reasons for the excellent selectivity of our mediated process is that the reduced mediator is itself able to reduce azoxybenzene to aniline. Meanwhile, azobenzene was not identified as an intermediate in any of our experiments, although if it does form then it too can be reduced to aniline by adding an excess of the two-electron reduced mediator in an ex-cell fashion (see Section 3.2.4), implying that the reduced mediator in an electrocatalytic process would be able to reduce azobenzene to aniline as well.

The reaction mechanism for the electrochemical reduction of nitrobenzene that we think best explains our results (Scheme 3.1), mostly agrees with the one that has been reported previously for chemical reduction of nitrobenzene using reducing agents and metal catalysts.^{41,42} Hence nitrobenzene is reduced by two electrons to form nitrosobenzene which is then reduced by another two electrons to form phenylhydroxylamine. As Figure 3.12 shows, both nitrosobenzene and phenylhydroxylamine display quasi-reversible redox waves, the reductive parts of which have peaks at +0.2 V vs. Ag/AgCl (for nitrosobenzene) and +0.1 V vs. Ag/AgCl (for phenylhydroxylamine).

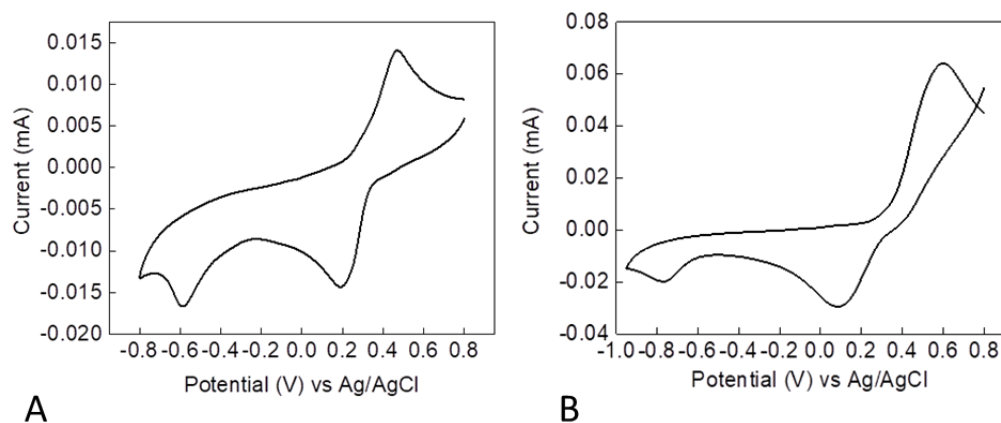


Figure 3.12: **A:** Cyclic voltammogram of nitrosobenzene (the first two-electron reduced intermediate of the reduction of nitrobenzene). **B:** Cyclic voltammogram of *N*-phenylhydroxylamine (the product of four-electron reduction of nitrobenzene). The scan was started at +0.8 V and was then swept cathodically (reducing). Scan rate: 100 mV/s.

This suggests that these two species are both relatively easy to reduce under the prevailing conditions, either at the electrode surface or on contact with reduced phosphotungstic acid. The latter assumption is borne out by “ex-cell” reactions between phenylhydroxylamine and 1-electron reduced phosphotungstic acid (see section 3.2.5 for details), whereby two equivalents of 1-electron reduced phosphotungstic acid can reduce phenylhydroxylamine to aniline with a yield of around 90% (full conversion can be achieved if excess 1-electron reduced phosphotungstic acid is used) as we can see from Figure 3.13.

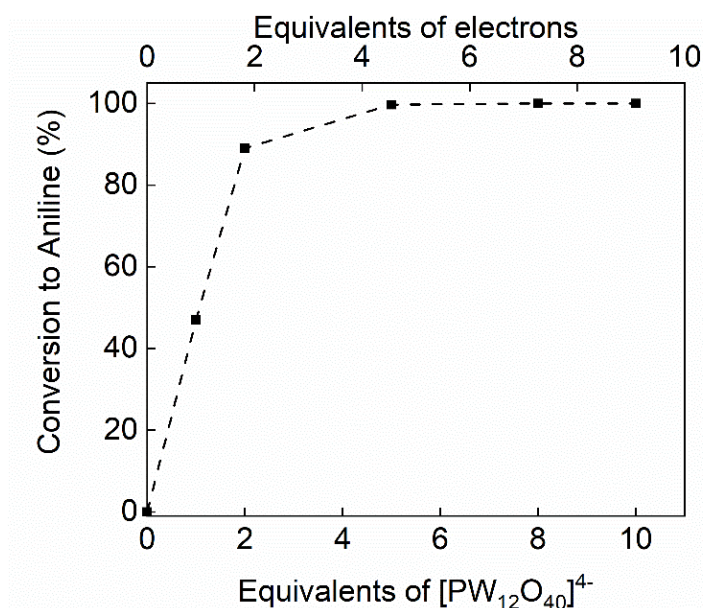


Figure 3.13: Ex-cell reduction of phenylhydroxylamine with one-electron reduced phosphotungstic acid (“ $[PW_{12}O_{40}]^{4-}$ ”).

However, a cyclic voltammogram of nitrobenzene itself (Figure 3.14) presents a rather different picture, displaying a single irreversible reduction wave at approximately -0.5 V vs. Ag/AgCl.

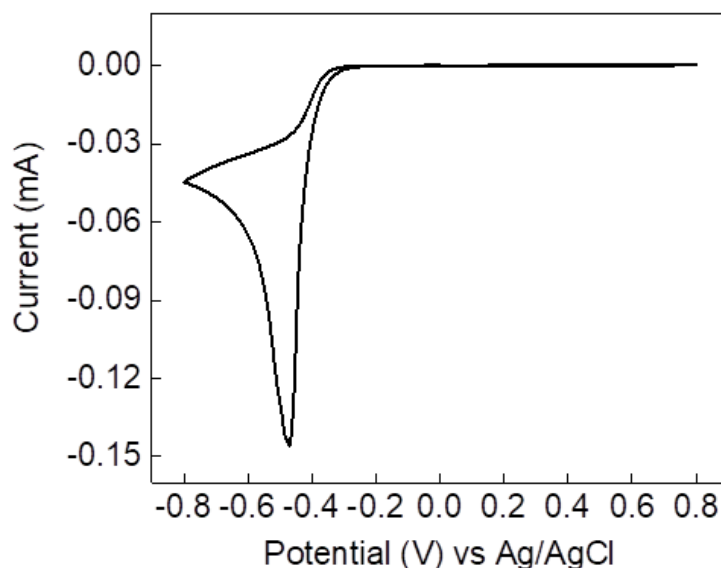


Figure 3.14: Cyclic voltammogram of the starting material nitrobenzene, collected under the general conditions described above. The scan was started at 0 V, sweeping first to +0.8 V and then sweeping cathodically. Scan rate: 100 mV/s.

The presence of nitrosobenzene and phenylhydroxylamine in the reaction mixture, and their apparent ease of reduction, therefore, suggests that it is the initial reduction of nitrobenzene to nitrosobenzene that is especially challenging during direct reduction at the electrode surface, requiring potentials as cathodic as -0.5 V. Once nitrosobenzene has formed, it will be rapidly reduced at those potentials to phenylhydroxylamine. Phenylhydroxylamine can be further reduced at those potentials to aniline, but it also has a tendency to undergo reaction with nitrosobenzene to give azoxybenzene, and/or to dimerize (also giving azoxybenzene). Under direct electrolysis conditions, where large cathodic potentials are applied to drive the initial reduction of nitrobenzene, there is likely to be a high local concentration of both nitrosobenzene and phenylhydroxylamine at the electrode surface and this is likely to lead to considerable loss of selectivity for aniline production by the generation of azoxybenzene. Azoxybenzene is poorly soluble in aqueous solution (only ~ 1 mg is dissolved per litre at 293 K), and its precipitation if it forms in significant amounts may account for some of the conflicting reports in the literature as to whether or not it is an end product of nitrobenzene reduction.

The above discussion explains why the cyclic voltammogram of nitrobenzene has only one large irreversible wave (as after the initial reduction to nitrosobenzene subsequent steps are facile and rapid) and also why direct reduction processes produce azoxybenzene. The redox mediator in our system is therefore acting to increase the selectivity of the reaction in at least three ways. Firstly, the mediator acts to lower the cathodic potential necessary for initial nitrobenzene reduction (Figure 3.4 and Table 3.3), perhaps by presenting both protons and electrons to the nitrobenzene simultaneously and thereby bypassing high energy intermediates. This is also in agreement with the principles of indirect electrolysis (see Section 1.1.1 of the introduction), by which the mediator lowers the overpotential required to drive the reaction, improving the overall kinetics of the electrolysis. Previous models of nitrobenzene reduction to nitrosobenzene have invoked an initial one-electron, one-proton reduction to the anion $\text{ArN}(\text{OH})\text{O}^-$, which then undergoes further (possibly stepwise) protonation and reduction to yield nitrosobenzene.⁴³ Were such a stepwise mechanism to operate at the electrode surface it is likely that this would impede the kinetics of reduction; in contrast, as a soluble source of both protons and electrons, the reduced polyoxometalate mediator may be able to circumvent some of these kinetic barriers through a proton-coupled-electron transfer mechanism.⁴⁴ The findings of cyclic voltammetry can also be supported by our “ex-cell” studies, where sub-stoichiometric and excess equivalents of polyoxometalate redox mediator were used (Figure 3.15).

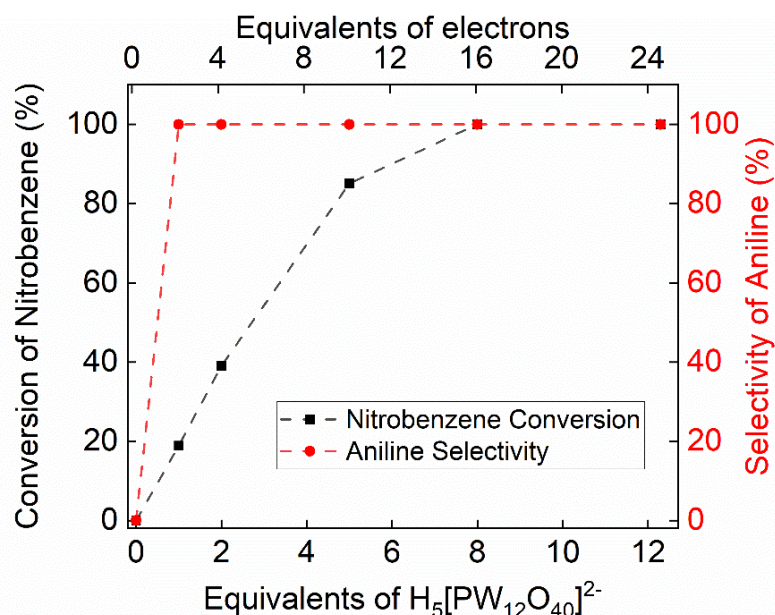
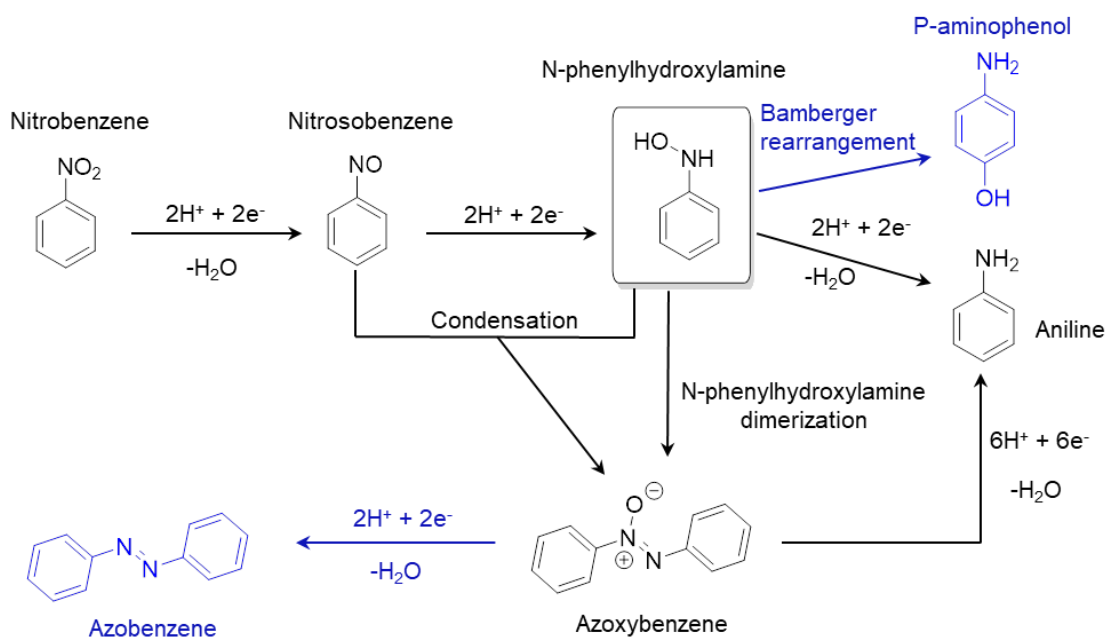
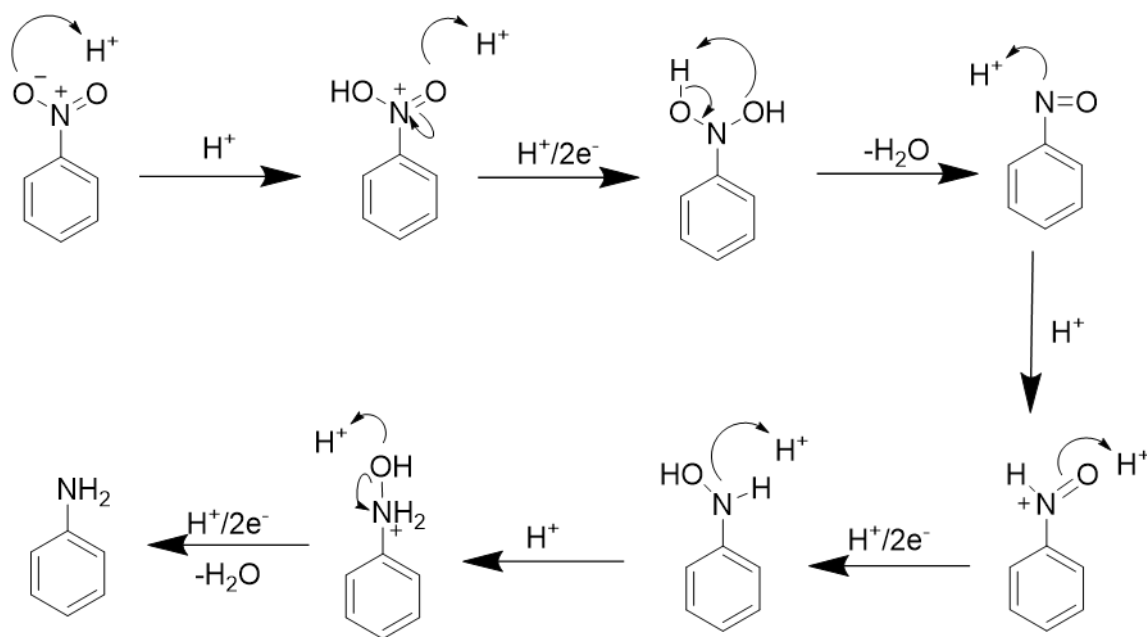


Figure 3.15: Ex-cell studies of the reduction of nitrobenzene with different amounts of the polyoxometalate redox mediator.

The fact that in those studies the selectivity of the mediated process towards aniline was always $\geq 99\%$ (as no intermediate products were obtained in ^1H NMR analysis), even when sub-stoichiometric amounts of the redox mediator were used (and therefore fractional conversion was obtained), indicates that after the initial reduction of nitrobenzene to nitrosobenzene the following steps to form aniline are rapid. Therefore, by overcoming the kinetic barriers of the challenging reduction of nitrobenzene to nitrosobenzene, we triggered a downhill multi-electron process that yields aniline. The method of the electron transfer between the mediator and the substrate can also be discussed. Polyoxometalates are well known outer-sphere reagents as we discussed in Section 1.1.2. In this case, our mediator acts as an electrocatalyst since it directly provides the protons and the electrons to the substrate. Discussion can be made on whether there is inner-sphere electron transfer involved in this process, however it will be difficult to prove if the substrate binds with the polyoxometalate. NMR could be a suitable way to monitor substrate binding in the polyoxometalate, by observing a shift in the peaks of the substrate (^1H spectrum). However, this would only work in the case of the oxidised polyoxometalate since its reduced form might be paramagnetic and also it has been proven by our previous experiments that it reacts with the substrate. The same implications apply in the case of Diffusion-Ordered NMR spectroscopy (DOSY) experiments where substrate binding to the large polyoxometalate molecule could potentially yield in slower diffusion. Moreover, substrate binding to the redox mediator could be tested electrochemically by calculating the diffusion coefficient, with slower diffusion indicating substrate binding to the large polyoxometalate. Again, the fact that the mediator reacts with the substrate makes these experiments very complicated. Therefore, whilst substrate binding may play a role in the catalytic process, we have considered the electron transfer between our electrocatalyst and the substrate proceeds in an outer-sphere mechanism. Secondly, the reduction reactions mediated by the polyoxometalate mediator are occurring in bulk solution, as opposed to direct electrochemical reduction which necessarily occurs at the electrode surface. In bulk solution, the concentrations of nitrosobenzene and phenylhydroxylamine will be much lower than they are at the electrode surface during direct reduction. This means that the mediated system is much less prone to the coupling reactions between nitrosobenzene and phenylhydroxylamine (and/or phenylhydroxylamine dimerization) that form azoxybenzene. Thirdly, even if azoxybenzene does form, the reduced polyoxometalate mediator is capable of cleanly reducing this to aniline.



Scheme 3.1: Proposed reaction pathway for the electrocatalytic reduction of nitrobenzene to aniline mediated by phosphotungstic acid. Processes shown with blue arrows indicate pathways that have previously been identified in other reports, but which were not observed in this study.



Scheme 3.2: Proposed mechanism of the polyoxometalate-mediated (top pathway on Scheme 3.1) reduction of nitrobenzene to aniline, based on the Bechamp reaction.⁴⁵

It is interesting to compare this mechanism with those for direction reduction of nitrobenzene at the electrode surface. With regard to direct reduction at the electrode, different electrolyte

pH and cathode materials can lead to the formation of different products,^{40,46-49} while in general the applied potential is held to alter the ratio of these products.^{50,51} *P*-aminophenol (the main product of Marquez and Pletcher's study²¹) most likely forms from phenylhydroxylamine via the Bamberger rearrangement. *P*-aminophenol was also identified as the major reduction product (with aniline being completely absent) under bulk electrolysis at -0.37 V vs. Ag/AgCl in a comprehensive study on the effect of the applied potential on nitrobenzene reduction in acidic media at a mercury cathode published by Harwood et al.⁵⁰ Only as the potential was made more cathodic (-0.77 V vs. Ag/AgCl) were significant amounts of aniline formed (50% maximum yield), and variable amounts of side products such as *p*-aminophenol, azoxybenzene and *p*-phenetidine were found at all the different applied potentials.⁵⁰ Moreover, simply making the reaction potential more cathodic in the hope of promoting aniline formation has its limits, as increasingly cathodic potentials facilitate competing hydrogen evolution, and the tendency to over-reduction (*e.g.* to cyclohexylamine) also increases. Hence we postulate that the origin of the poor selectivity for aniline in many of the previous reports on electrochemical nitrobenzene reduction arises largely through the difficulty in controlling the reactivity of the phenylhydroxylamine intermediate at the potentials that are required to reduce nitrobenzene directly at an electrode surface.^{50,52,53} In contrast, the mediated approach expounded here avoids a significant build-up of phenylhydroxylamine and hence prevents any significant flux through the Bamberger rearrangement to *p*-aminophenol. Experiments whereby *p*-aminophenol was reacted in an ex-cell fashion with 10 equivalents of 2-electron reduced phosphotungstic acid failed to yield any conversion to aniline after stirring at room temperature for 12 h. This suggests that *p*-aminophenol does not form at all in our mediated route (or else we would observe it in our product mixtures) and instead that its formation is prevented.

3.4 Conclusion

Herein, we have described a highly selective route for the electrochemical reduction of nitroarenes to their corresponding anilines. The procedure is simple and potentially more sustainable than traditional routes, avoiding the use of hydrogen gas, high temperatures, precious metal co-catalysts and sacrificial reagents. Instead, the approach described in this work proceeds in aqueous solution at room temperature and pressure, with the electrons and protons required to reduce the nitrobenzenes originating from water. Faradaic efficiencies are typically greater than 90%, even for catalyst loadings as low as 0.1% relative to the nitroarene starting material, and the selectivity for the aniline product is near-quantitative, even under an atmosphere of air. With the aid of various control reactions and mechanistic studies, we propose a reaction pathway that explains why this electro-mediated approach gives such superior conversion and selectivity compared to direct electrochemical reduction of the substrates at the electrode surface, and we show that our mild electrocatalytic conditions allow the clean and efficient conversion of sensitive nitrobenzene substrates such as ortho-iodides to their aniline derivatives in good yield. Given the scale and environmental impact associated with the production of anilines, this electrochemical route could hold considerable promise for the development of more sustainable processes for the production of these vital chemical feedstocks.

3.5 NMR Data of the Obtained Products

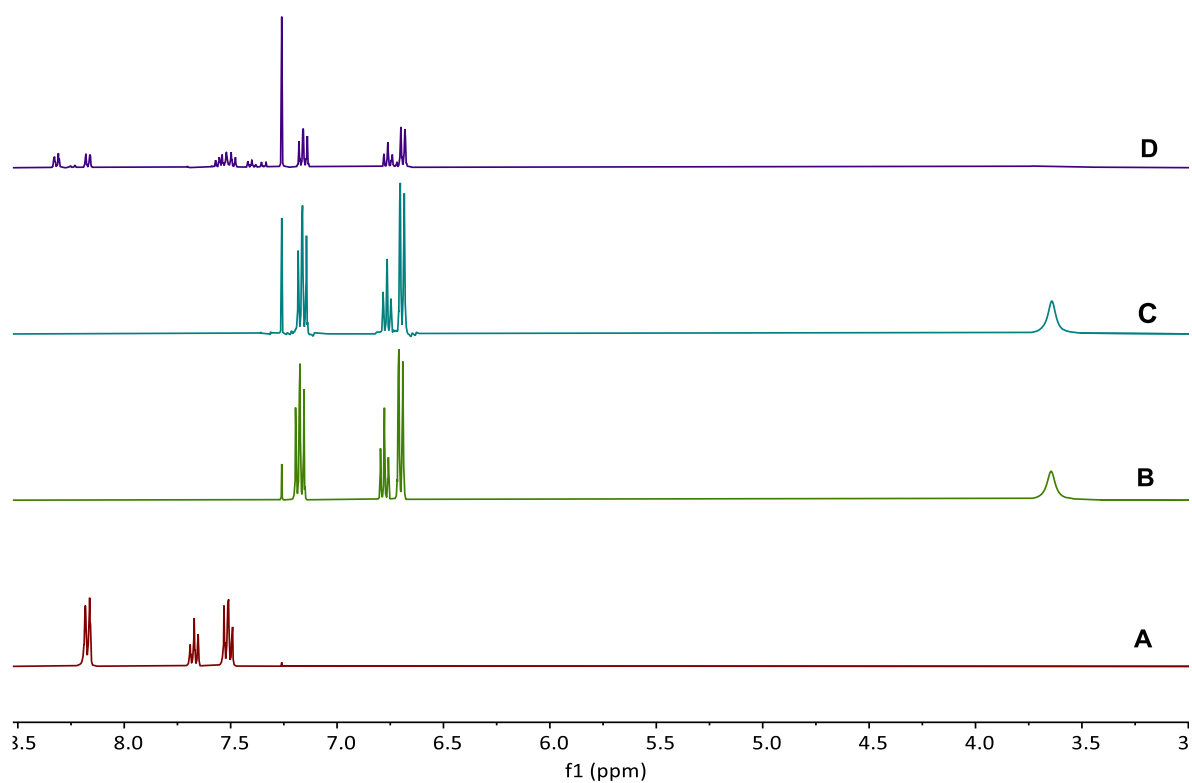


Figure 3.15: Reduction of nitrobenzene. ^1H NMR spectra of the nitrobenzene starting material (A), a sample of pure aniline (B), the spectrum of the electrocatalytic reaction medium after extraction and concentration (C) and the spectrum of the extracted and concentrated reaction medium from a direct (i.e. non-mediated) electrochemical reduction of nitrobenzene (D). All spectra were obtained in CDCl_3 .

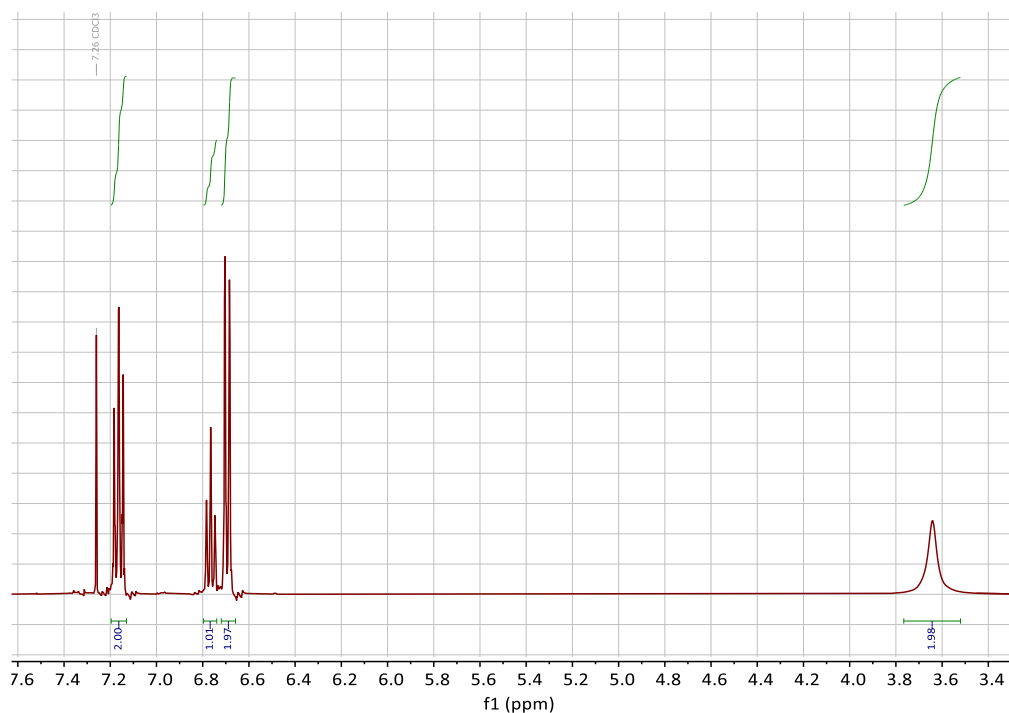


Figure 3.16: ^1H NMR spectrum of the obtained product, aniline, from the mediated process (spectrum C from Figure 3.15) including the integrations. The spectrum was obtained in CDCl_3 . The signal at $\delta = 7.26$ is due to residual CHCl_3 .

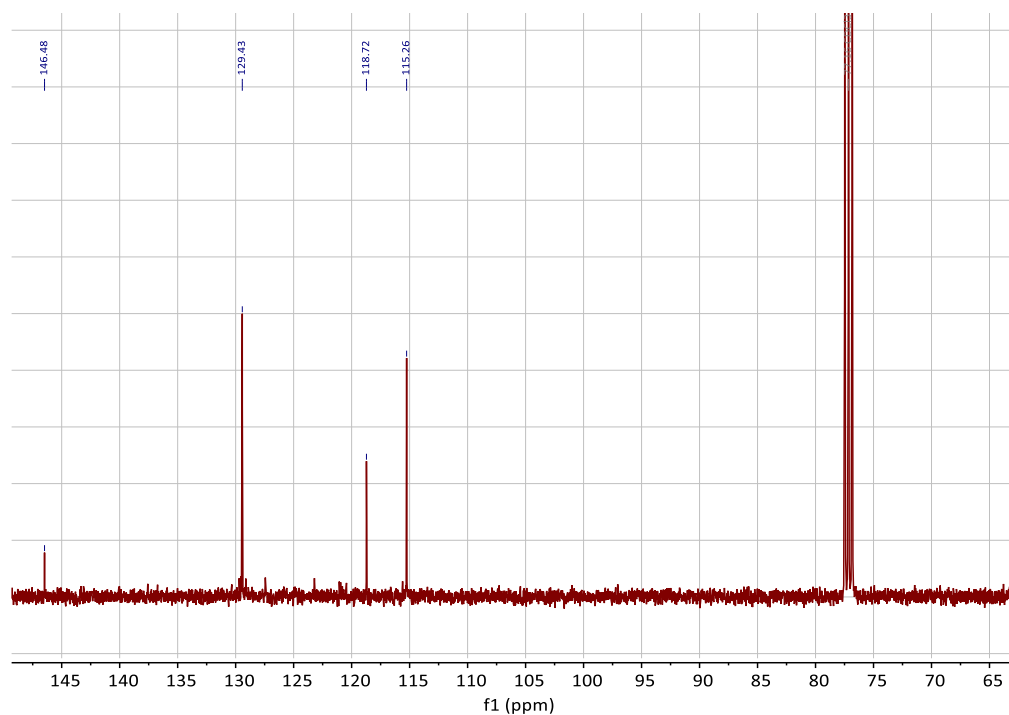


Figure 3.17: ^{13}C NMR spectrum of the obtained product, aniline, from the electrocatalytic reaction medium after extraction and concentration. The spectrum was obtained in CDCl_3 . ^{13}C NMR (100 MHz, CDCl_3) $\delta = 146.5, 129.4, 118.7, 115.3$. The signal at $\delta = 77.2$ is due to CDCl_3 . Data for this compound were in agreement with those reported for aniline.⁵⁴

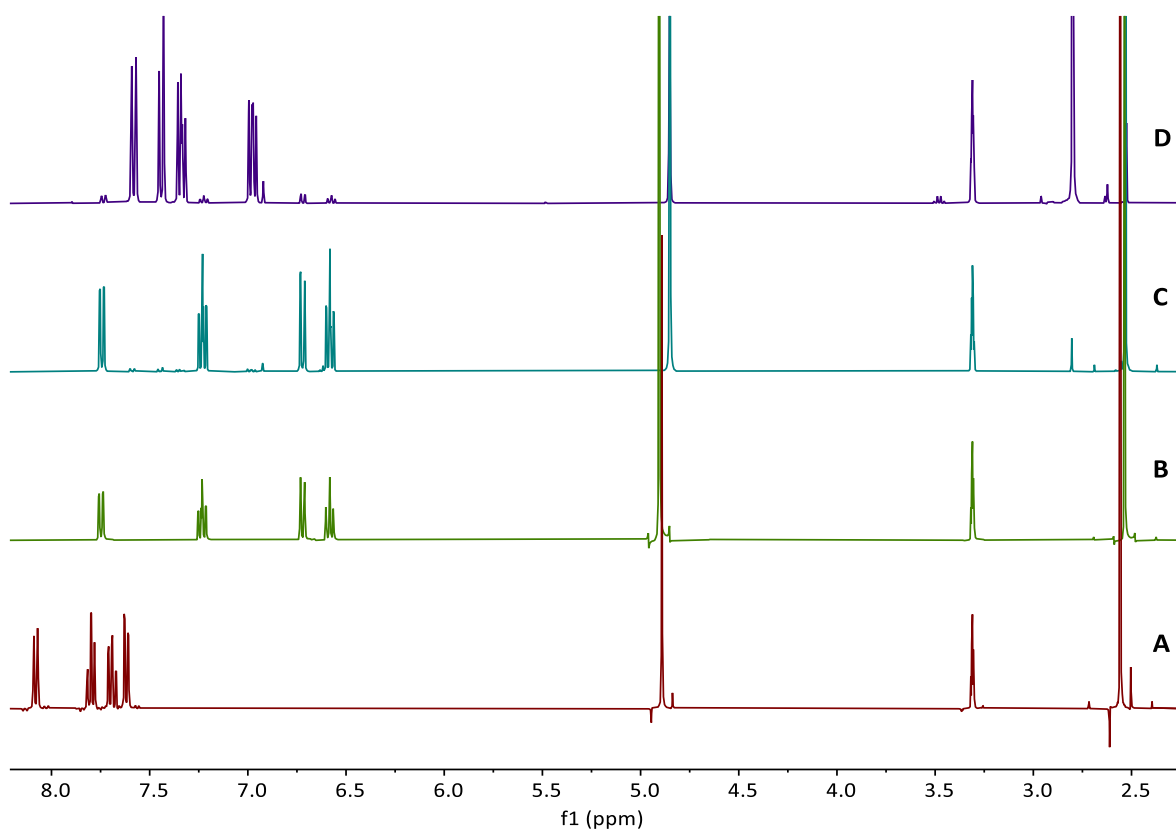
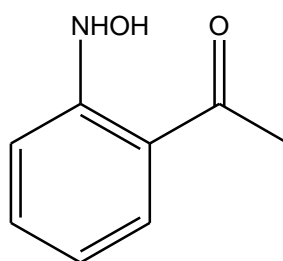


Figure 3.18: Reduction of 2-nitroacetophenone. ^1H NMR spectra of the 2-nitroacetophenone starting material (A), a sample of pure 2-aminoacetophenone (B), the spectrum of the electrocatalytic reaction medium after extraction and concentration (C) and the spectrum of the extracted and concentrated reaction medium from a direct (i.e. non-mediated) electrochemical reduction of 2-nitroacetophenone (D). All spectra were obtained in d_4 -methanol.

The main product of the direct electrochemical reduction (spectrum D) is the hydroxylamine derivative (i.e. incomplete reduction has occurred). As this compound (pictured below) has hitherto not been reported in any detail, we give here the following characterisation:



Mass spectrum: ESI-QTOF (acetonitrile/water 70/30% with 0.1% formic acid): $m/z = 152.0712$ $[\text{M}+\text{H}]^+$ (calcd. for $\text{C}_8\text{H}_{10}\text{NO}_2$; 152.07115).

^1H NMR (400 MHz, MeOD) $\delta = 7.58$ (d, $J = 8.8$ Hz, 1H), 7.44 (d, $J = 9.1$ Hz, 1H), 7.38 – 7.29 (m, 1H), 7.02 – 6.90 (m, 1H), 2.80 (s, 3H).

^{13}C NMR (100 MHz, MeOD), $\delta = 167.9, 158.1, 132.7, 124.0, 121.3, 116.8, 114.9, 11.6$.

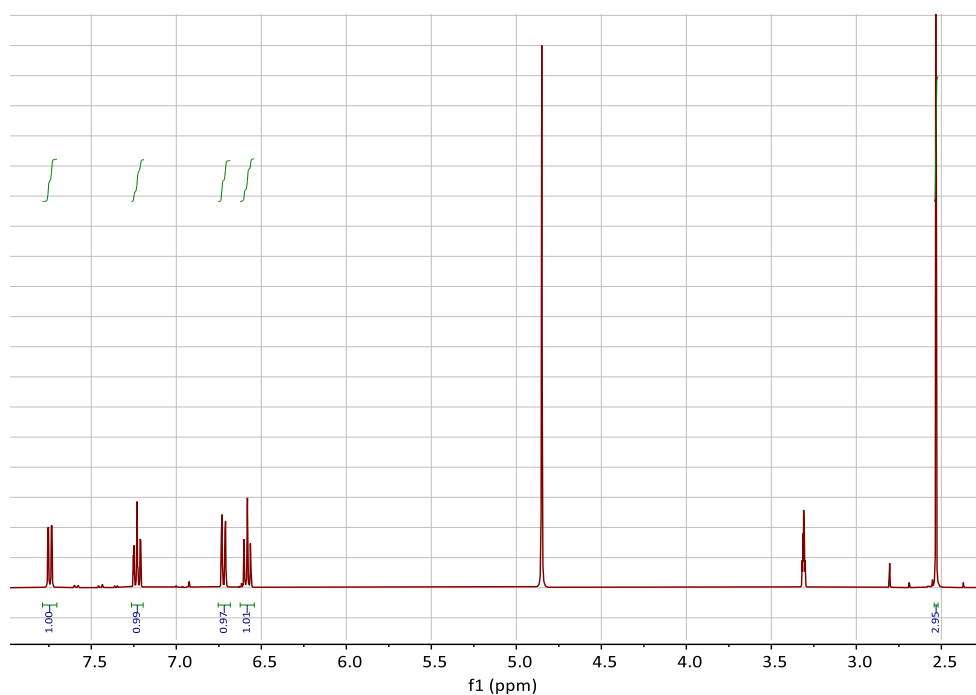


Figure 3.19: ^1H NMR spectrum of the obtained product, 2-aminoacetophenone, from the electrocatalytic reaction medium after extraction and concentration (spectrum C from Figure 3.18) including the integrations. The spectrum was obtained in d_4 -methanol. The signals at $\delta = 3.31$ and 4.78 are due to residual MeOH.

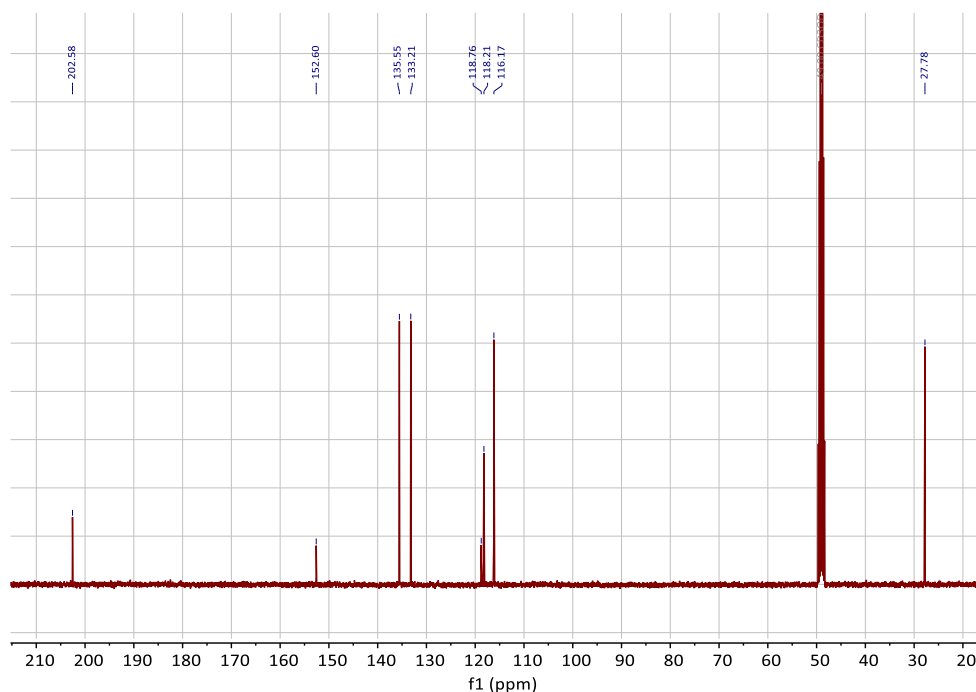


Figure 3.20: ^{13}C NMR spectrum of the obtained product, 2-aminoacetophenone, from the mediated process. The spectrum was obtained in d_4 -methanol. ^{13}C NMR (100 MHz, MeOD) $\delta = 202.6, 152.6, 135.6, 133.2, 118.8, 118.2, 116.2, 27.8$. The signal at $\delta = 49.2$ is due to MeOD. Data for this compound are in agreement with those reported for 2-aminoacetophenone.⁵⁵

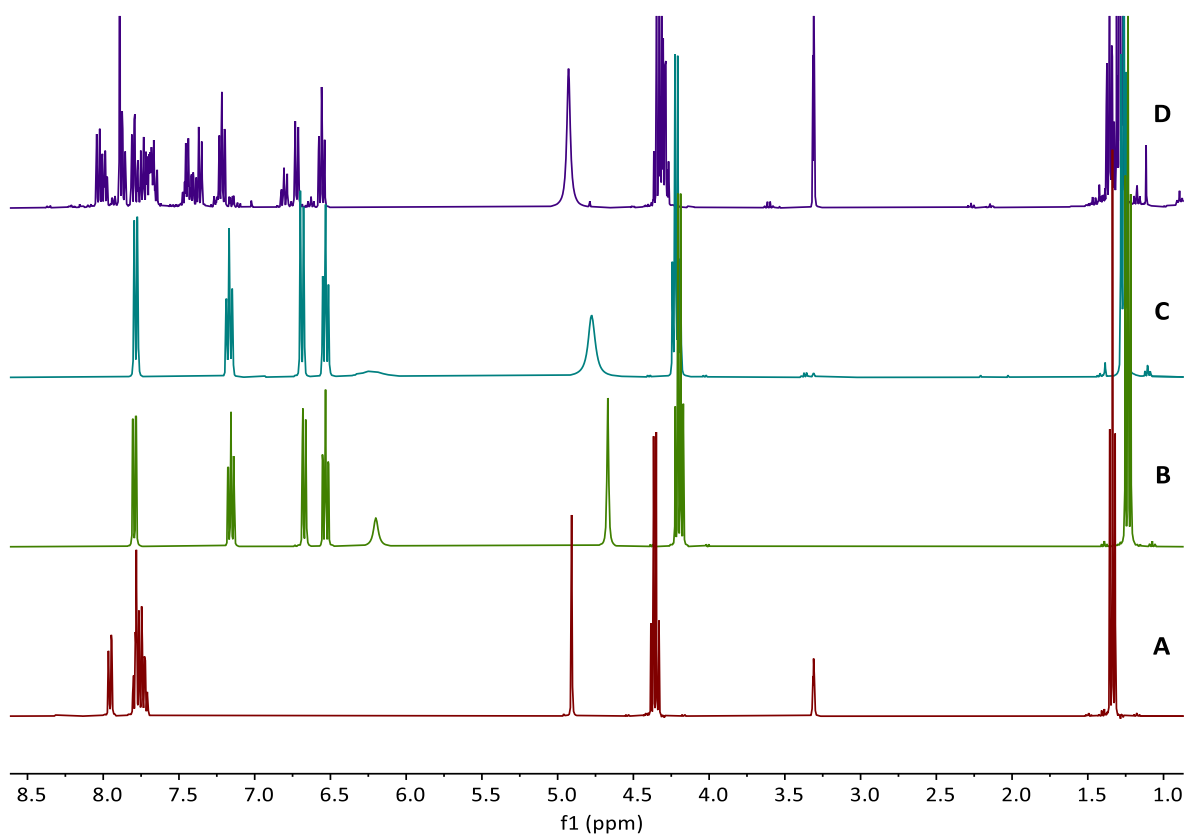


Figure 3.21: Reduction of ethyl-2-nitrobenzoate. ¹H NMR spectra of the ethyl-2-nitrobenzoate starting material (A), a sample of pure ethyl-2-aminobenzoate (B), the spectrum of the electrocatalytic reaction medium after extraction and concentration (C) and the spectrum of the extracted and concentrated reaction medium from a direct (i.e. non-mediated) electrochemical reduction of ethyl-2-nitrobenzoate (D). All spectra were obtained in d₄-methanol.

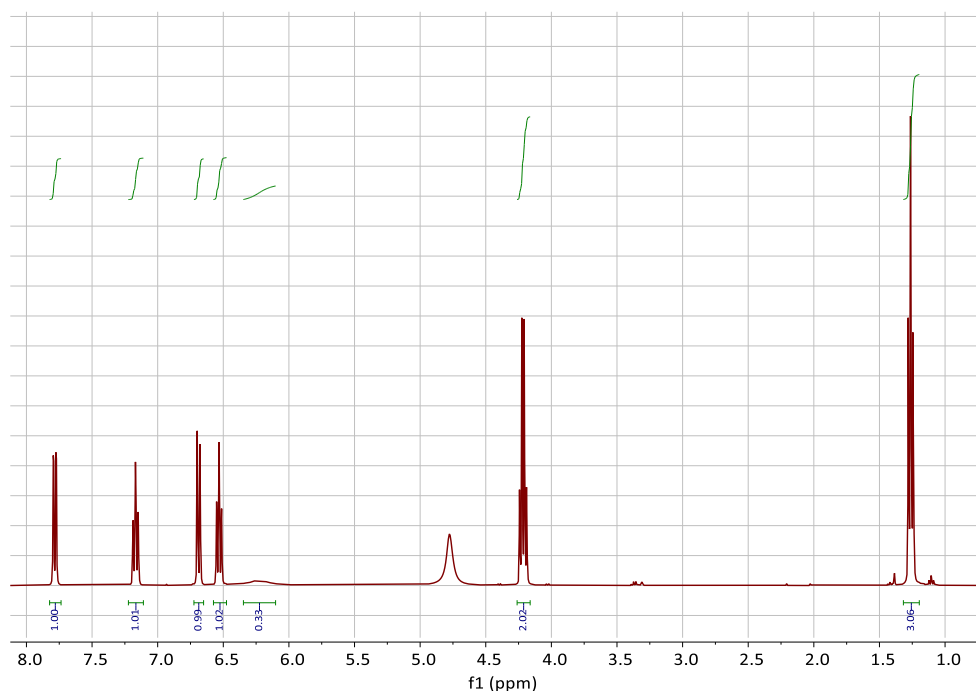


Figure 3.22: ^1H NMR spectrum of the obtained product, ethyl-2-aminobenzoate, from the electrocatalytic reaction medium after extraction and concentration (spectrum C from Figure 3.21) including the integrations. The spectrum was obtained in d_4 -methanol. The signals at $\delta = 3.31$ and 4.78 are due to residual MeOH. The broad signal at around 6.2 ppm is attributed to the NH_2 protons.

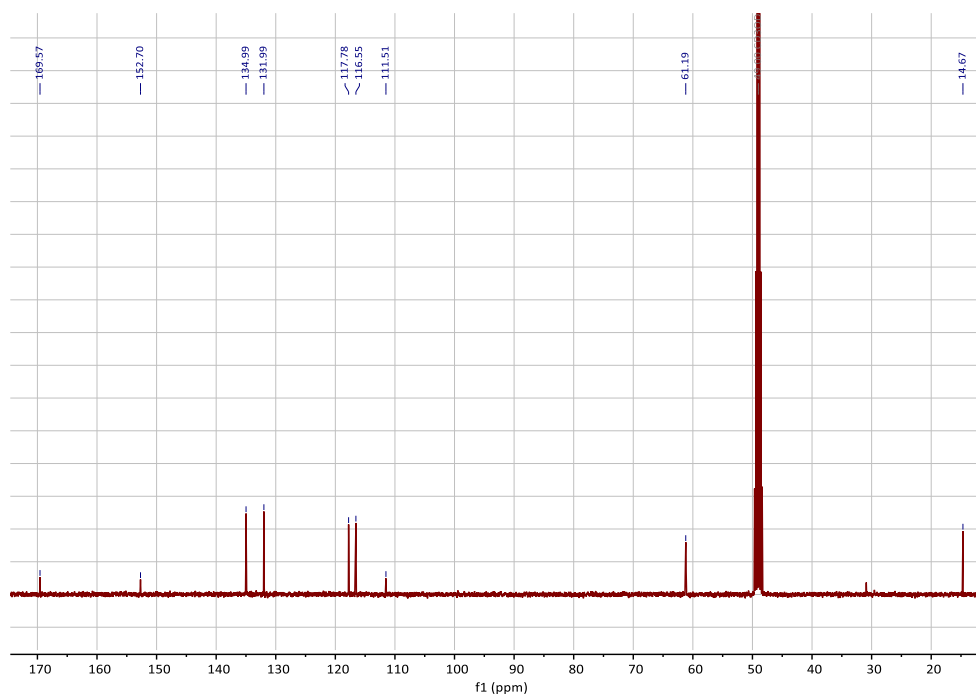


Figure 3.23: ^{13}C NMR spectrum of the obtained product, ethyl-2-aminobenzoate, from the mediated process. The spectrum was obtained in d_4 -methanol. ^{13}C NMR (100 MHz, MeOD) $\delta = 169.6, 152.7, 135.0, 132.0, 117.8, 116.6, 111.5, 61.2, 14.7$. The signal at $\delta = 49.2$ is due to MeOD. Data for this compound were in agreement with those reported for ethyl 2-aminobenzoate.⁵⁶

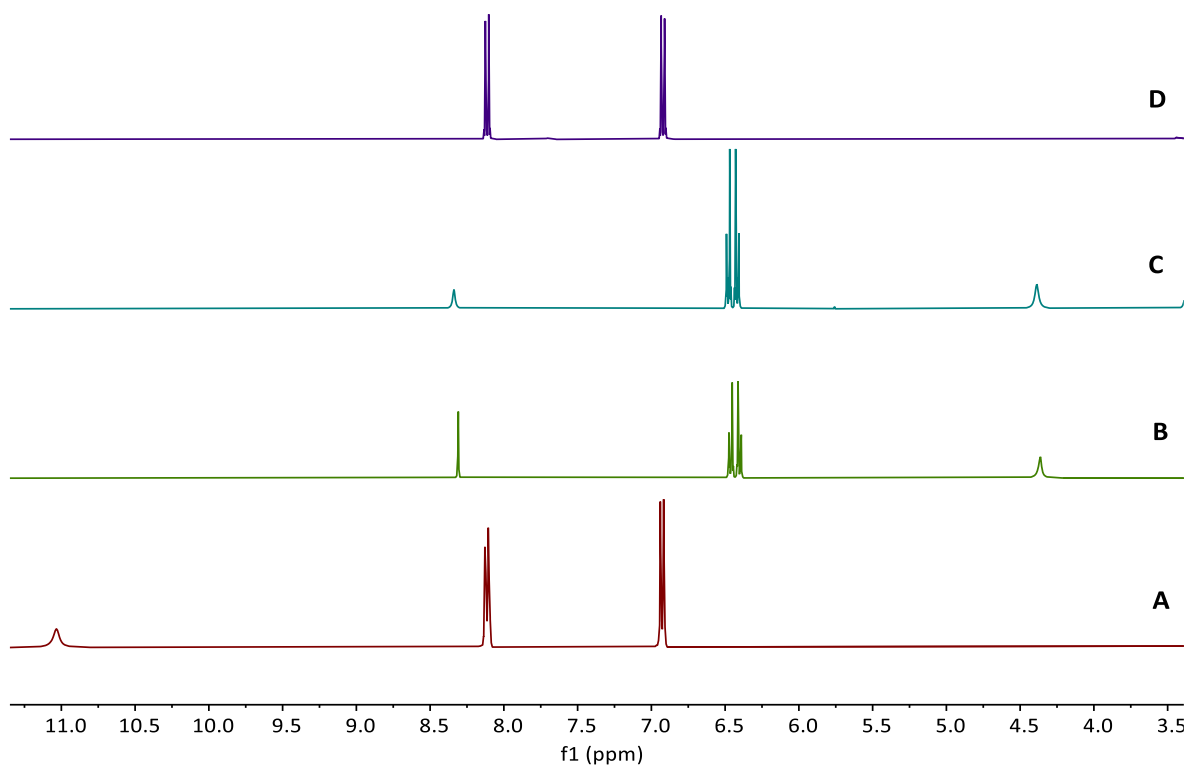


Figure 3.24: Reduction of *p*-nitrophenol. ¹H NMR spectra of the *p*-nitrophenol starting material (A), a sample of pure *p*-aminophenol (B), the spectrum of the electrocatalytic reaction medium after extraction and concentration (C) and the spectrum of the extracted and concentrated reaction medium from a direct (i.e. non-mediated) electrochemical reduction of *p*-nitrophenol (D). All spectra were obtained in d₆-DMSO.

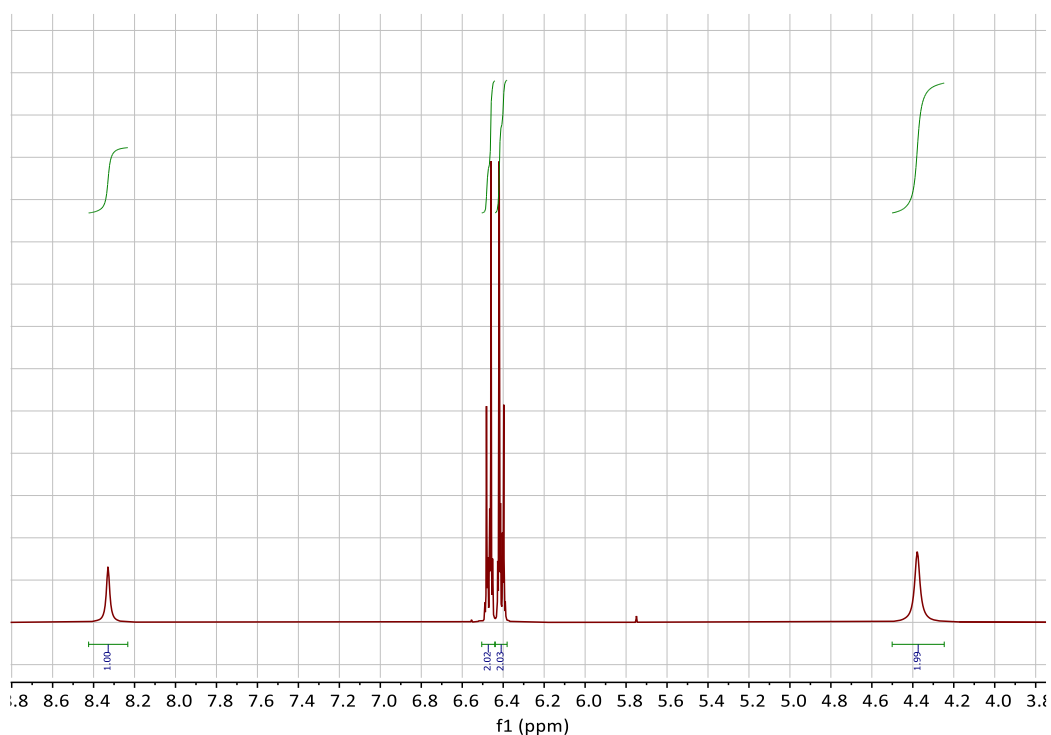


Figure 3.25: ^1H NMR spectrum of the obtained product, *p*-aminophenol, from the electrocatalytic reaction medium after extraction and concentration (spectrum C from Figure 3.24) including the integrations. The spectrum was obtained in d_6 -DMSO.

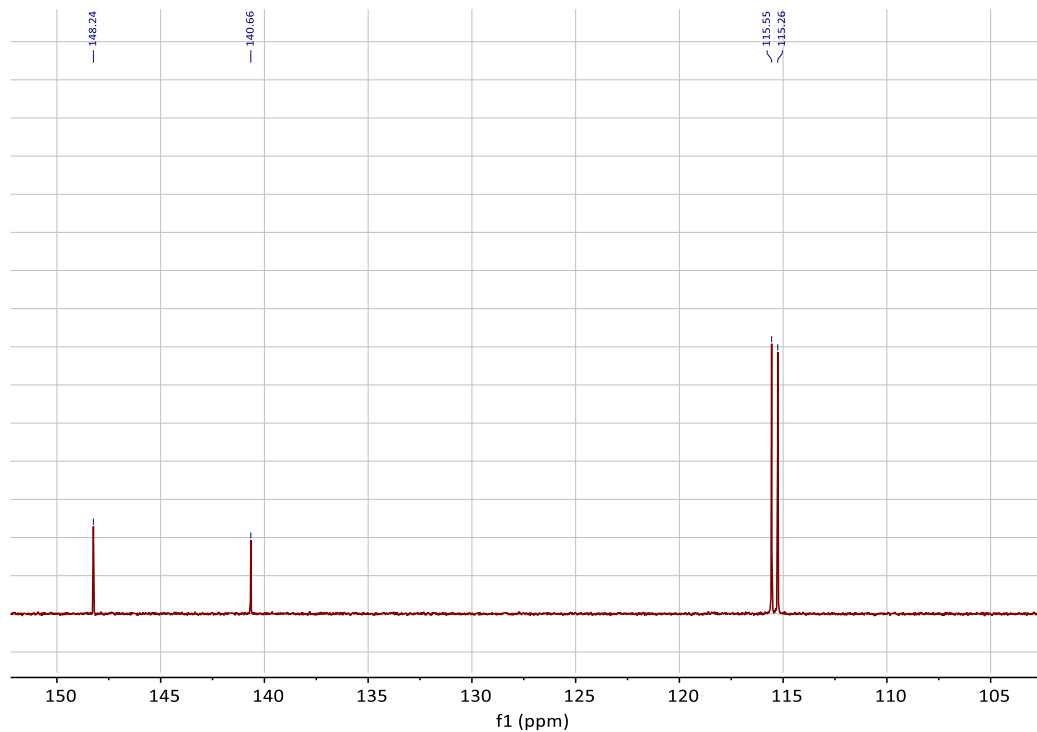


Figure 3.26: ^{13}C NMR spectrum of the obtained product, *p*-aminophenol, from the mediated process. The spectrum was obtained in d_6 -DMSO. ^{13}C NMR (100 MHz, DMSO) $\delta = 148.2, 140.7, 115.6, 115.3$. Data for this compound were in agreement with those reported for 4-aminophenol.⁵⁷

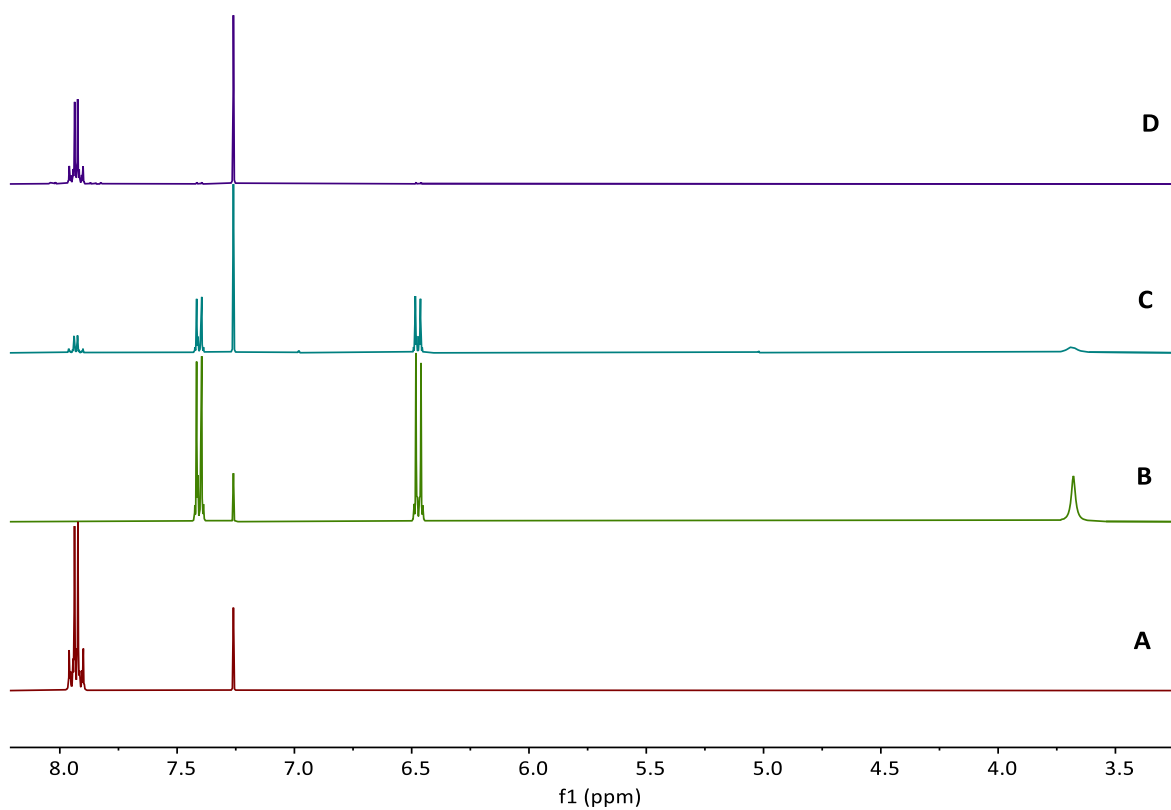


Figure 3.27: Reduction of 1-iodo-4-nitrobenzene. ¹H NMR spectra of the 1-iodo-4-nitrobenzene starting material (A), a sample of pure 1-iodo-4-aminobenzene (B), the spectrum of the electrocatalytic reaction medium after extraction and concentration (C) and the spectrum of the extracted and concentrated reaction medium from a direct (i.e. non-mediated) electrochemical reduction of 1-iodo-4-nitrobenzene (D). All spectra were obtained in CDCl₃.

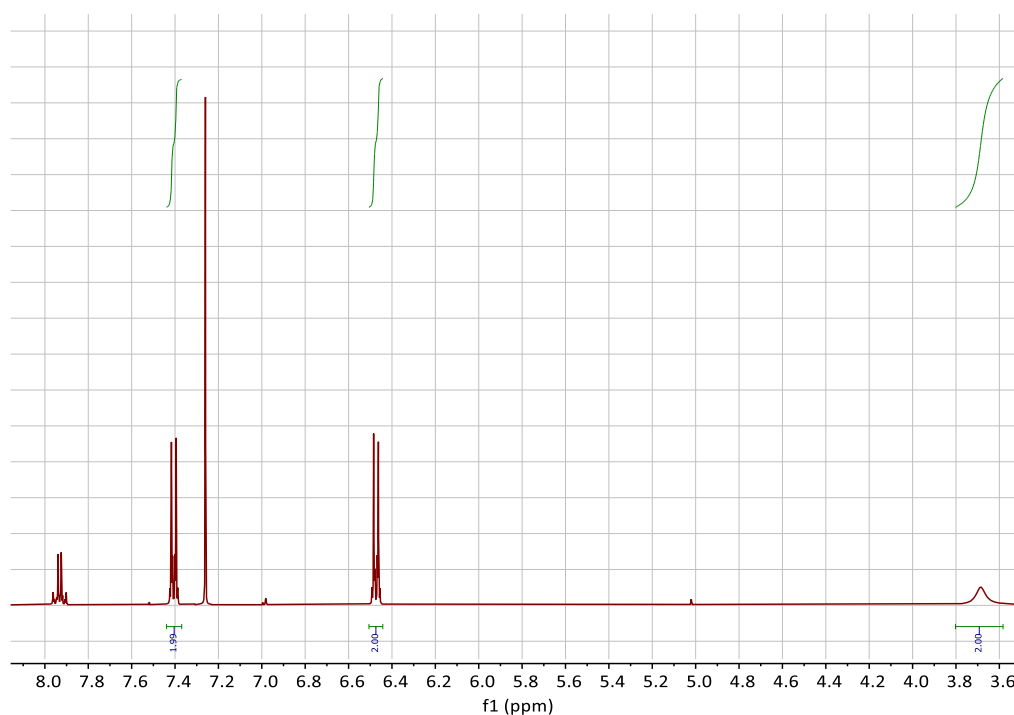


Figure 3.28: ^1H NMR spectrum of the obtained product, 1-iodo-4-aminobenzene, from the electrocatalytic reaction medium after extraction and concentration (spectrum C from Figure 3.27) including the integrations. The spectrum was obtained in CDCl_3 . The signal at 7.9 ppm is due to remaining starting material (see Figure 3.27). The signal at $\delta = 7.26$ is due to residual CHCl_3 .

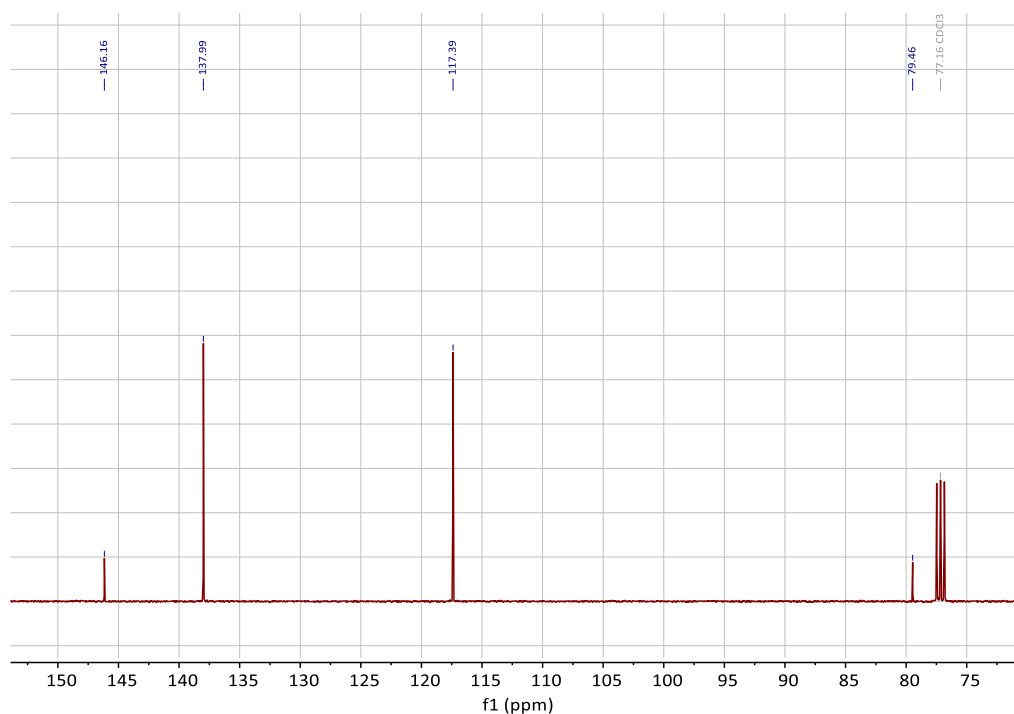


Figure 3.29: ^{13}C NMR spectrum of the obtained product, 1-iodo-4-aminobenzene, from the mediated process. The spectrum was obtained in CDCl_3 . ^{13}C NMR (100 MHz, CDCl_3) $\delta = 146.2, 138.0, 117.4, 79.5$. The signal at $\delta = 77.2$ is due to CDCl_3 . Data for this compound were in agreement with those reported for 4-iodoaniline.⁵⁸

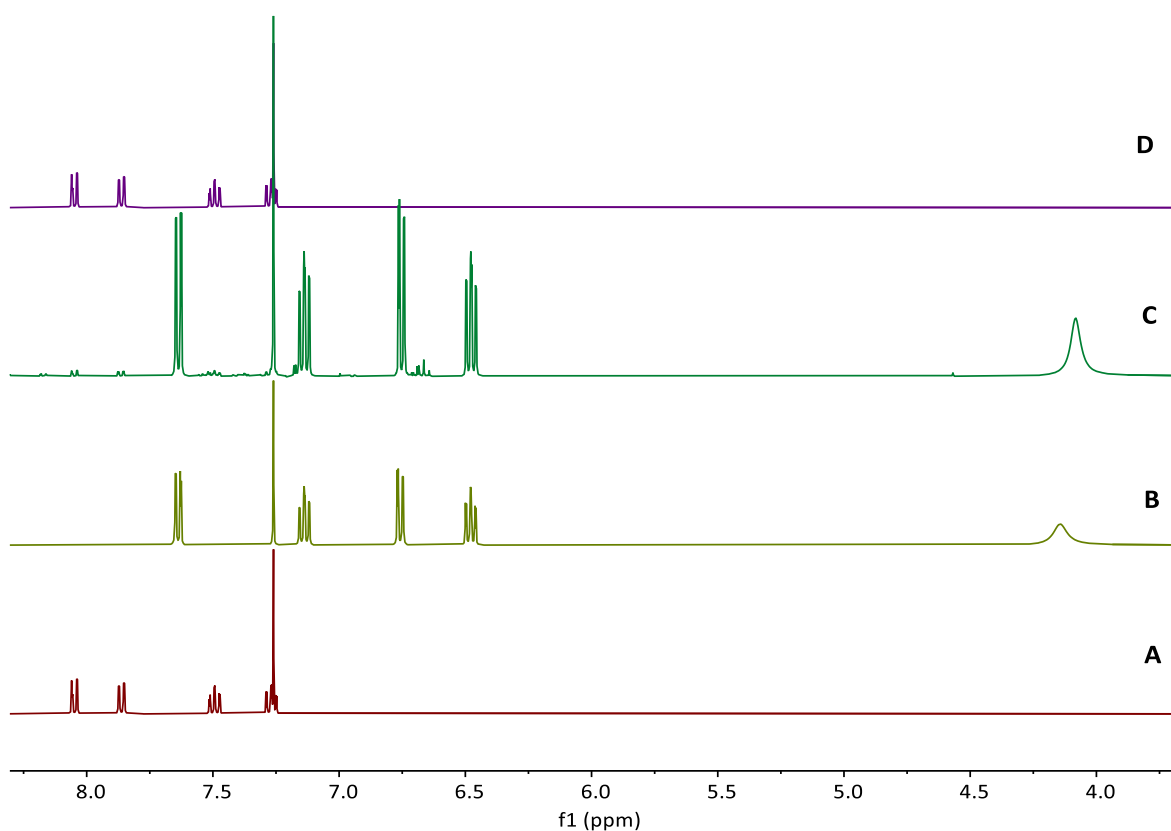


Figure 3.30: Reduction of 1-iodo-2-nitrobenzene. ¹H NMR spectra of the 1-iodo-2-nitrobenzene starting material (A), a sample of pure 1-iodo-2-aminobenzene (B), the spectrum of the electrocatalytic reaction medium after extraction and concentration (C) and the spectrum of the extracted and concentrated reaction medium from a direct (i.e. non-mediated) electrochemical reduction of 1-iodo-2-nitrobenzene (D). All spectra were obtained in CDCl₃.

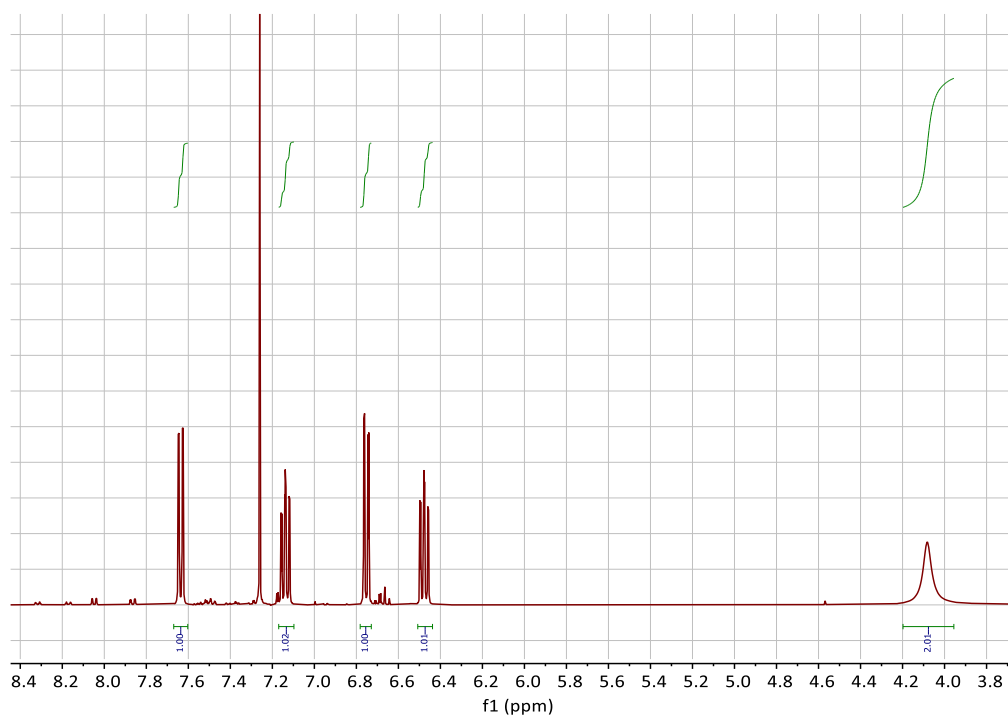


Figure 3.31: ^1H NMR spectrum of the obtained product, 1-iodo-2-aminobenzene, from the electrocatalytic reaction medium after extraction and concentration (spectrum C from Figure 3.30) including the integrations. The spectrum was obtained in CDCl_3 . The signal at $\delta = 7.26$ is due to residual CHCl_3 .

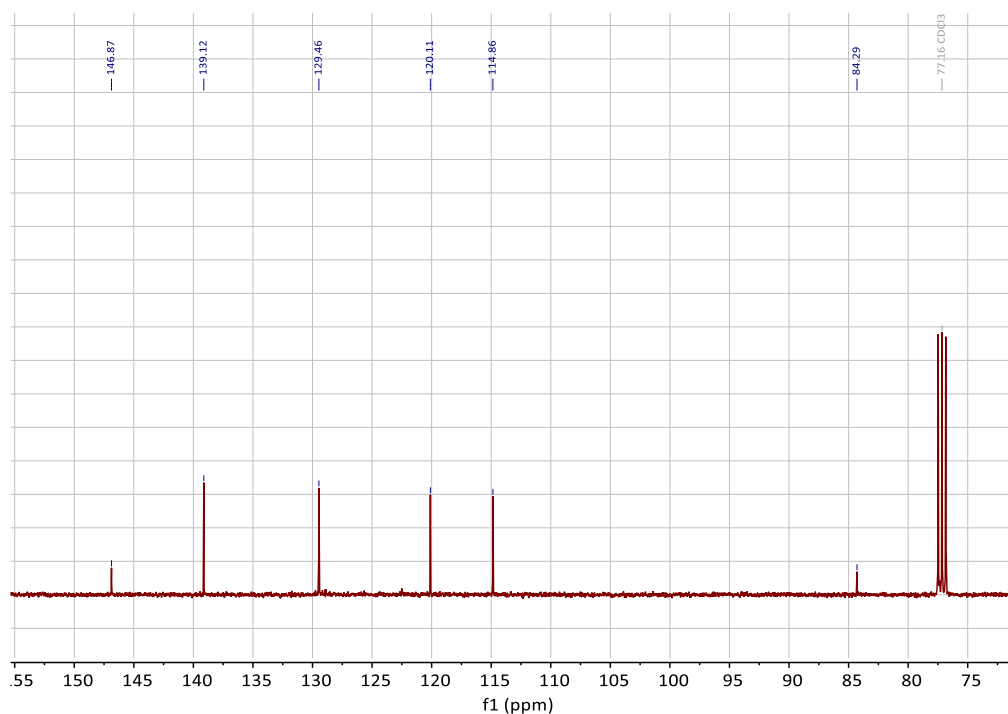


Figure 3.32: ^{13}C NMR spectrum of the obtained product, 1-iodo-2-aminobenzene, from the mediated process. The spectrum was obtained in CDCl_3 . ^{13}C NMR (100 MHz, CDCl_3) $\delta = 146.9, 139.1, 129.5, 120.1, 114.9, 84.3$. The signal at $\delta = 77.2$ is due to CDCl_3 . Data for this compound were in agreement with those reported for 2-iodoaniline.⁵⁹

3.6 Reference

- 1 Kadam, H. K. and Tilve, S. G. (2015) Advancement in methodologies for reduction of nitroarenes. *RSC Advances*, 5, 83391-83407. <https://doi.org/10.1039/C5RA10076C>
- 2 Jurado- Sánchez, B., Ballesteros, E. and Gallego M. (2013) Comparison of microwave assisted, ultrasonic assisted and Soxhlet extractions of N-nitrosamines and aromatic amines in sewage sludge, soils and sediments. *Sci. Total Environ.* 463-464, 293-301. <https://doi.org/10.1016/j.scitotenv.2013.06.002>
- 3 Ellis, F. *Paracetamol: a curriculum resource*. (Royal Society of Chemistry, Cambridge, 2002).
- 4 Sreedhar, B., Devi, D. K. and Yada, D. (2011) Selective hydrogenation of nitroarenes using gum acacia supported Pt colloid an effective reusable catalyst in aqueous medium. *Cat. Commun.* 12, 1009-1014. <https://doi.org/10.1016/j.catcom.2011.02.027>
- 5 Tsukinoki, T. and Tsuzuki, H. (2001) Organic reaction in water. Part 5. Novel synthesis of anilines by zinc metal-mediated chemoselective reduction of nitroarenes. *Green Chem.* 3, 37-38. <https://doi.org/10.1039/B008219H>
- 6 Travis, A.S. *Manufacture and Uses of the Anilines: A Vast Array of Processes and Products*. (PATAI'S Chemistry of Functional Groups. John Wiley & Sons, Chinchester, 2009).
- 7 Formenti, D., Ferretti, F., Scharnagl, F. K. and Beller, M. (2019) Reduction of nitro compounds using 3d-Non-Noble metal catalysts. *Chem. Rev.* 119, 2611-2680. <https://doi.org/10.1021/acs.chemrev.8b00547>
- 8 Pietrowski, M. (2012) Recent developments in heterogeneous selective hydrogenation of halogenated nitroaromatic compounds to halogenated anilines. *Curr. Org. Synth.* 9, 470-487. <https://doi.org/10.2174/157017912802651456>
- 9 Baumeister, P., Blaser, H. U. and Scherrer W. (1991) Chemoselective hydrogenation of aromatic chloronitro compounds with amidine modified nickel catalysts. *Stud. Surf. Sci. Catal.* 59, 321-328. [https://doi.org/10.1016/S0167-2991\(08\)61137-4](https://doi.org/10.1016/S0167-2991(08)61137-4)
- 10 Blaser, H. U., Steiner, H. and Studer, M. (2009) Selective catalytic hydrogenation of functionalized nitroarenes: An update. *ChemCatChem* 1, 210-221. <https://doi.org/10.1002/cctc.200900129>

- 11 Wu, G., Huang, M., Richards, M., Poirier, M., Wen, X. and Draper, R. W. (2003) Novel ZnX₂-Modulated Pd/C and Pt/C Catalysts for Chemoselective Hydrogenation and Hydrogenolysis of Halogen-Substituted Nitroarenes, Alkenes, Benzyl Ethers, and Aromatic Ketones. *Synthesis*, 1657-1660. <https://doi.org/10.1055/s-2003-40878>
- 12 Corma, A. and Serna, P. (2006) Chemoselective hydrogenation of nitro compounds with supported gold catalysts. *Science*, 313, 332-334. <https://doi.org/10.1126/science.1128383>
- 13 Layek, K., Kantam, M. L., Shirai, M., Nishio-Hamane, D., Sasaki, T. and Maheswaran, H. (2012) Gold nanoparticles stabilized on nanocrystalline magnesium oxide as an active catalyst for reduction of nitroarenes in aqueous medium at room temperature. *Green Chem.* 14, 3164-3174. <https://doi.org/10.1039/C2GC35917K>
- 14 Sharma, U., Verma, P. K., Kumar, N., Kumar, V., Bala, M. and Singh, B. (2011) Phosphane-Free green protocol for selective nitro reduction with an iron-based catalyst. *Chem. Eur. J.* 17, 5903-5907. <https://doi.org/10.1002/chem.201003621>
- 15 Doherty, S., Knight, J. G., Backhouse, T., Summers, R. J., Abood, E., Simpson, W., Paget, W., Bourne, R. A., Chamberlain, T. W., Stones, R., Lovelock, K. R. J., Seymour, J. M., Isaacs, M. A., Hardacre, C., Daly, H. and Rees, N. H. (2019) Highly selective and solvent-dependent reduction of nitrobenzene to *N*-phenylhydroxylamine, azoxybenzene, and aniline catalyzed by phosphino-modified polymer immobilized ionic liquid-stabilized AuNPs. *ACS Catal.* 9, 4777-4791. <https://doi.org/10.1021/acscatal.9b00347>
- 16 Gladiali, S. and Alberico, E. (2006) Asymmetric transfer hydrogenation: chiral ligands and applications. *Chem. Soc. Rev.* 35, 226-236. <https://doi.org/10.1039/B513396C>
- 17 Samec, J. S. M., Bäckvall J. E., Andersson P. G. and Brandt, P. (2006) Mechanistic aspects of transition metal-catalyzed hydrogen transfer reactions. *Chem. Soc. Rev.* 35, 237-248. <https://doi.org/10.1039/B515269K>
- 18 Wienhöfer, G., Sorribes, I., Boddien, A., Westerhaus, F., Junge, K., Junge, H., Llusar, R. and Beller, M. (2011) General and selective iron-catalyzed transfer hydrogenation of nitroarenes without base. *J. Am. Chem. Soc.* 133, 12875-12879. <https://doi.org/10.1021/ja2061038>
- 19 Garcia-Verdugo, E., Liu, Z., Ramirez, E., Garcia-Serna, J., Fraga-Dubreuil, J., Hyde, J. R., Hamley, P. A. and Poliakov, M. (2006) In situ generation of hydrogen for

- continuous hydrogenation reactions in high temperature water. *Green Chem.* 8, 359-364. <https://doi.org/10.1039/B515470G>
- 20 Joshi, M. V. and Mukesh, D. (1997) Transfer hydrogenation of nitro compounds with heteropolyacid catalysts. *J. Cat.* 168, 273-277. <https://doi.org/10.1006/jcat.1997.1619>
- 21 Marquez, J. and Pletcher, D. (1980) A study of the electrochemical reduction of nitrobenzene to p-aminophenol. *J. Appl. Electrochem.* 10, 567-573. <https://doi.org/10.1007/BF00615477>
- 22 Chong, X., Liu, C., Huang, Y., Huang, C. and Zhang, B. (2020) Potential-tuned selective electrosynthesis of azoxy-, azo- and amino-aromatics over a CoP nanosheet cathode. *Natl. Sci. Rev.* 7, 285-295. <https://doi.org/10.1093/nsr/nwz146>
- 23 Zhao, Y., Liu, C., Wang, C., Chong, X. and Zhang, B. (2020) Sulfur Vacancy-Promoted Highly Selective Electrosynthesis of Functionalized Aminoarenes via Transfer Hydrogenation of Nitroarenes with H₂O over a Co₃S_{4-x} Nanosheet Cathode. *CCS Chem.* 2, 507-515. <https://doi.org/10.31635/ccschem.020.202000218>
- 24 Daems, N., Risplendi, F., Baert, K., Hubin, A., Vankelecom, I. F. J., Cicero, G. and Pescarmona, P. P. (2018) Doped ordered mesoporous carbons as novel, selective electrocatalysts for the reduction of nitrobenzene to aniline. *J. Mater. Chem. A*, 6, 13397-13441. <https://doi.org/10.1039/C8TA01609G>
- 25 Sheng, X., Wouters, B., Breugelmans, T., Hubin, A., Vankelecom, I. F. J. and Pescarmona, P. P. (2014) Cu/Cu_xO and Pt nanoparticles supported on multi-walled carbon nanotubes as electrocatalysts for the reduction of nitrobenzene. *Appl. Cat. B*, 147, 330-339. <https://doi.org/10.1016/j.apcatb.2013.09.006>
- 26 Li, Y.-P., Cao, H.-B., Liu, C.-M. and Zhang, Y. (2007) Electrochemical reduction of nitrobenzene at carbon nanotube electrode. *J. Hazard. Mater.* 148, 158-163. <https://doi.org/10.1016/j.jhazmat.2007.02.021>
- 27 Sheng, X., Wouters, B., Breugelmans, T., Hubin, A., Vankelecom, I. F. J. and Pescarmona, P. P. (2014) Pure and alloyed copper-based nanoparticles supported on activated carbon: synthesis and electrocatalytic application in the reduction of nitrobenzene. *ChemElectroChem*, 1, 1198-1210. <https://doi.org/10.1002/celc.201402015>

- 28 Ravichandran, C., Noel, M. and Anantharaman, P. N. (1994) Comparative evaluation of electroreduction of nitrobenzene and *m*-dinitrobenzene on Ti/TiO₂ electrodes in H₂SO₄. *J. Appl. Electrochem.* 24, 1256-1261. <https://doi.org/10.1007/BF00249890>
- 29 Daems, N., Wouters, J., Van Goethem, C., Baert, K., Poleunis, C., Delcorte, A., Hubin, A., Vankelecom, I. F. J. and Pescarmona, P. P. (2018) Selective reduction of nitrobenzene to aniline over electrocatalysts based on nitrogen-doped carbons containing non-noble metals. *Appl. Cat. B*, 226, 509-522. <https://doi.org/10.1016/j.apcatb.2017.12.079>
- 30 Wouters, B., Sheng, X., Boschini, A., Breugelmans, T., Ahlberg, E., Vankelecom, I. F. J., Pescarmona, P. P. and Hubin, A. (2013) The electrocatalytic behaviour of Pt and Cu nanoparticles supported on carbon nanotubes for the nitrobenzene reduction in ethanol. *Electrochim. Acta*, 111, 405-410. <https://doi.org/10.1016/j.electacta.2013.07.210>
- 31 Zhang, Q., Liu, Y., Chen, S., Quan, X. and Yu, H. (2014) Nitrogen-doped diamond electrode shows high performance for electrochemical reduction of nitrobenzene. *J. Hazard. Mater.* 265, 185-190. <https://doi.org/10.1016/j.jhazmat.2013.11.065>
- 32 Egbert, J. D., Thomsen, E. C., O'Neill-Slawecki, S. A., Mans, D. M., Leitch, D. C., Edwards, L. J., Wade, C. E., Weber, R. S. (2019) Development and scale-up of continuous electrocatalytic hydrogenation of functionalized nitro arenes, nitriles, and unsaturated aldehydes. *Org. Process Res. Dev.* 23, 1803-1812. <https://doi.org/10.1021/acs.oprd.8b00379>
33. He, P., and Faulkner, L. R. *Anal. Chem.* **1986**, 58, 517.
- 34 Francke, R. and Little, R. D. (2014) Redox catalysis in organic electrosynthesis: basic principles and recent developments. *Chem. Soc. Rev.* 43, 2492-2521. <https://doi.org/10.1039/C3CS60464K>
- 35 Stergiou, A. D. and Symes, M. D. (2022) Organic transformations using electro-generated redox mediators. *Catal. Today*, 384-386, 146-155. <https://doi.org/10.1016/j.cattod.2021.05.003>
- 36 MacDonald, L., Rausch, B., Symes, M. D. and Cronin, L. (2018) Selective hydrogenation of nitroarenes using an electrogenerated polyoxometalate redox mediator. *Chem Commun.* 54, 1093-1096. <https://doi.org/10.1039/C7CC09036F>

- 37 Keggin, J. F. (1933) Structure of the molecule of 12-phosphotungstic acid. *Nature*, 131, 908-909. <https://doi.org/10.1038/131908b0>
- 38 Yu, H.-Z., Wang, Y.-Q., Cheng, J.-Z., Zhao, J.-W., Cai, S.-M., Inokuchi, H., Fujishima, A. and Liu, Z.-F. (1996) Electrochemical behaviour of azobenzene self-assembled monolayers on gold. *Langmuir*, 12, 2843-2848. <https://doi.org/10.1021/la950632c>
- 39 Cyr, A., Huot, P., Belot, G. and Lessard, J. (1990) The efficient electrochemical reduction of nitrobenzene and azoxybenzene to aniline in neutral and basic aqueous methanolic solutions at devarda copper and raney nickel electrodes: electrocatalytic hydrogenolysis of N-O and N-N bonds. *Electrochim. Acta*, 35, 147-152. [https://doi.org/10.1016/0013-4686\(90\)85052-O](https://doi.org/10.1016/0013-4686(90)85052-O)
- 40 Cyr, A., Huot, P., Marcoux, J.-F., Belot, G., Laviron, E. and Lessard, J. (1989) The electrochemical reduction of nitrobenzene and azoxybenzene in neutral and basic aqueous methanolic solutions at polycrystalline copper and nickel electrodes. *Electrochim. Acta*, 34, 439-445. [https://doi.org/10.1016/0013-4686\(89\)87023-9](https://doi.org/10.1016/0013-4686(89)87023-9)
- 41 Wang, J., Yuan, Z., Nie, R., Hou, Z. and Zheng, X. (2010) Hydrogenation of nitrobenzene to aniline over silica gel supported nickel catalysts. *Ind. Eng. Chem. Res.* 49, 4664-4669. <https://doi.org/10.1021/ie1002069>
- 42 Corma, A., Concepción, P. and Serna, P. (2007) A different reaction pathway for the reduction of aromatic nitro compounds on gold catalysts. *Angew. Chem. Int. Ed.* 46, 7266-7269. <https://doi.org/10.1002/anie.200700823>
- 43 El-Hout, S. I., El-Sheikh, S. M., Hassan, H. M. A., Harraz, F. A., Ibrahim, I. A. and El-Sharkawy, E. A. (2015) A green chemical route for synthesis of graphene supported palladium nanoparticles: A highly active and recyclable catalyst for reduction of nitrobenzene. *Appl. Catal. A Gen.* 503, 176-185. <https://doi.org/10.1016/j.apcata.2015.06.036>
- 44 Gao, D., Trentin, I., Schwiedrzik, L., Gonzalez, L. and Streb, C. (2020) The reactivity and stability of polyoxometalate water oxidation electrocatalyst. *Molecules*, 25, 157. <https://doi.org/10.3390/molecules25010157>
- 45 Béchamp, M. A. (1854) De l'action des protosels de fer sur la nitronaphtaline et la nitrobenzine. Nouvelle méthode de formation des bases organiques artificielles de Zinin. *Ann. Chim. Phys.*, 42, 186-195.

- 46 Cyr, A., Laviron, E. and Lessard, J. (1989) Electrochemical behaviour of nitrobenzene and phenylhydroxylamine on copper rotating disk electrodes. *J. Electroanal. Chem. Interf. Electrochem.* 263, 69-78. [https://doi.org/10.1016/0022-0728\(89\)80124-X](https://doi.org/10.1016/0022-0728(89)80124-X)
- 47 Popp, F. D. and Schultz, H. P. (1962) Electrolytic reduction of organic compounds. *Chem. Rev.* 62, 19-40. <https://doi.org/10.1021/cr60215a002>
- 48 Rubistein, I. (1985) Voltammetric study of nitrobenzene and related compounds on solid electrodes in aqueous solution. *J. Electroanal. Chem. Interf. Electrochem.* 183, 379-386. [https://doi.org/10.1016/0368-1874\(85\)85503-9](https://doi.org/10.1016/0368-1874(85)85503-9)
- 49 Nishihara, C. and Shindo, H. (1986) Reduction of nitrobenzene in aqueous alkaline solution at an Ag electrode: observation by SERS, RRDE and UV absorption. *J. Electroanal. Chem. Interf. Electrochem.* 202, 231-239. [https://doi.org/10.1016/0022-0728\(86\)90121-x](https://doi.org/10.1016/0022-0728(86)90121-x)
- 50 Harwood, W. H., Hurd, R. M. and Jordan, W. H. (1963) Electrochemical reduction of nitrobenzene at controlled potentials. *Ind. Eng. Chem. Process Des. Dev.* 2, 72-77. <https://doi.org/10.1021/i260005a015>
- 51 Chen, X., Xiong, L., Wang, W., Zhang, X. and Yu, H. (2015) Efficient and selective electro-reduction of nitrobenzene by the nano-structured Cu catalyst prepared by an electrodeposited method via tuning applied voltage. *Front. Environ. Sci. Eng.* 9, 897-904. <https://doi.org/10.1007/s11783-015-0782-1>
- 52 Mahata, A., Rai, R. K., Choudhuri, I., Singh, S. K. and Pathak, B. (2014) Direct vs. indirect pathway for nitrobenzene reduction reaction on a Ni catalyst surface: a density functional study. *Phys. Chem. Chem. Phys.* 16, 26365-26374. <https://doi.org/10.1039/c4cp04355c>
- 53 Grošková, D., Štolcová, M. and Hronec, M. (2000) Reaction of N-phenylhydroxylamine in the presence of clay catalysts. *Catal. Lett.* 69, 113-116. <https://doi.org/10.1023/A:1019097217875>
- 54 Pouchert, C.J., and Behnke, J.(1993). *The Aldrich library of 13C and 1H FT NMR spectra* (Milwaukee : Aldrich Chemical Co., c1993), vol 2, pp. 451.
- 55 Pouchert, C.J., and Behnke, J.(1993). *The Aldrich library of 13C and 1H FT NMR spectra* (Milwaukee : Aldrich Chemical Co., c1993), vol 2, pp. 868.
- 56 Pouchert, C.J., and Behnke, J.(1993). *The Aldrich library of 13C and 1H FT NMR spectra* (Milwaukee : Aldrich Chemical Co., c1993), vol 2, pp. 1262.

- 57 Pouchert, C.J., and Behnke, J.(1993). *The Aldrich library of ^{13}C and ^1H FT NMR spectra* (Milwaukee : Aldrich Chemical Co., c1993), vol 2, pp. 485.
- 58 Pouchert, C.J., and Behnke, J.(1993). *The Aldrich library of ^{13}C and ^1H FT NMR spectra* (Milwaukee : Aldrich Chemical Co., c1993), vol 2, pp. 482.
- 59 Pouchert, C.J., and Behnke, J.(1993). *The Aldrich library of ^{13}C and ^1H FT NMR spectra* (Milwaukee : Aldrich Chemical Co., c1993), vol 2, pp. 462.

Highly Selective Electrocatalytic Reduction of Substituted Aromatic Nitroarenes to their Aniline Derivatives using a Polyoxometalate Redox Mediator

Published as “*Highly selective electrocatalytic reduction of substituted nitrobenzenes to their aniline derivatives using a polyoxometalate redox mediator*”
A. D. Stergiou, D. H. Broadhurst and M. D. Symes. *ACS Org. Inorg. Au*, 2022,
<https://doi.org/10.1021/acsorginorgau.2c00047>.

Acknowledgments and Declaration

Athanasios Stergiou and Daniel Broadhurst performed the experiments and analysed the data. AS performed all the CV and scale-up reaction experiments as well as repeats of the compounds in Table 4.1. DB, master student supervised by AS, performed the majority of the experiments for Table 4.1. Mark Symes conceived the idea, assisted with data analysis, and supervised the project. The authors co-wrote the manuscript.

Synopsis

Anilines and substituted anilines are used on the multi-ton scale for producing polymers, pharmaceuticals, dyes and other important compounds. Typically, these anilines are produced from their corresponding nitrobenzene precursors by reaction with hydrogen at high temperatures. However, this route suffers from a number of drawbacks, including the requirement to handle hydrogen gas, rather harsh reaction conditions that lead to a lack of selectivity and/or toleration of certain functional groups, and questionable environmental sustainability. In light of this, routes to the reduction of nitrobenzenes to their aniline derivatives that operate at room temperature, in aqueous solvent and without the requirement to use harsh process conditions, hydrogen gas, or sacrificial reagents could be of tremendous benefit.

Herein, we report on a highly selective electrocatalytic route for the reduction of nitrobenzenes to their corresponding anilines that works in aqueous solution at room temperature, and which does not require the use of hydrogen gas or sacrificial reagents. The method uses a polyoxometalate redox mediator which reversibly accepts electrons from the cathode and reacts with the nitrobenzenes in solution to reduce them to the corresponding anilines. A variety of substituted nitroarenes are explored as substrates, including those with potentially competing reducible groups and substrates that are difficult to reduce selectively by other means. In all cases, the selectivity for the redox-mediated route is higher than for the direct reduction of the nitroarene substrates at the electrode, suggesting that redox-mediated electrochemical nitroarene reduction is a promising avenue for the more sustainable synthesis of substituted anilines.

4.1 Introduction

Aromatic amines (anilines) are key nitrogen-containing building blocks for the production of pharmaceuticals, dyes and polymers, with a prime example being the synthesis of paracetamol, a derivative of 4-aminophenol.¹⁻³ Typically, aromatic amines are synthesized through the reduction of the corresponding nitroarene compounds, using heterogeneous catalysts at elevated temperatures and pressures, and employing hydrogen gas as the reductant.^{4,5} Although these conditions give good results for the reduction of unfunctionalized nitrobenzene to aniline, the reduction of more complex (substituted) nitroarenes to their aniline products is much more difficult to achieve with high selectivity.^{5,6} From amongst the substituted nitroarenes with reducible groups (e.g. carbonyls, esters, amines and halide groups), the most challenging substrates are the halogenated aromatics as the hydro-dehalogenation reaction can occur very readily under the standard high temperature and pressure reduction conditions, leading to a marked drop in selectivity.⁵⁻⁹ In recent years, new methods have been developed to tackle the issue of the lack of chemoselectivity for the reduction of substituted nitroarenes. These methods have mostly focused on the replacement of H₂ gas by a different hydrogenation agent (such as sodium borohydride, formate or hydrazine) and/or on avoiding the need for high temperature and pressure.^{2,10} However, the aforementioned alternative reducing agents are generally toxic and are irreversibly consumed during the reduction process,^{11,12} and there is still the need to employ a heterogeneous catalyst.

A far simpler and more sustainable alternative to these current approaches to the synthesis of substituted anilines could be the electrochemical reduction of the corresponding nitrobenzenes; however, studies have shown that the lack of chemoselectivity towards the desired product (even in the case of unsubstituted nitrobenzene itself) remains a drawback when direct electroreduction of nitroarenes at the cathode is attempted.^{13,14} In recent years, numerous electrochemical methods have been developed, often using modified cathodes.¹⁵⁻²⁴ Of these studies, the Zhang group reported the highest conversion and selectivity towards the desired products. However, hydrogen evolution competes with nitroarene reduction, impairing the Faradaic efficiency.^{15,16}

Very recently, we reported a new electrochemical method for the reduction of nitrobenzene and a small number of other functionalized nitrobenzenes to their corresponding anilines, using a polyoxometalate redox mediator (phosphotungstic acid) in aqueous solution under mild conditions (potentials of -0.38 V (vs. Ag/AgCl), room temperature and pressure).²⁵ The mediator acts to shut down the direct electrochemical reduction of the nitroarenes at the

cathode that would otherwise lead to undesirable side-reactions. However, the scope of the reactions reported in this previous study was limited, as our aim was primarily to elucidate the mechanism of reaction for the electrochemical reduction of nitrobenzene to aniline.

Herein, we significantly expand the scope of this approach to a variety of substituted nitroarenes, including potentially competing reducible groups and substrates that are difficult to reduce selectively by other means. In all cases, we compare the electro-mediated approach to the direct reduction of the nitroarene substrates at the electrode surface, and find that the use of the polyoxometalate redox mediator almost always leads to better conversions of the starting material and always gives higher selectivity for the aniline product.

4.2 Experimental

4.2.1 General Experimental Remarks

1-bromo-4-nitrobenzene (98%), ethyl-4-nitrobenzoate (98%), 1-fluoro-2-nitrobenzene (99%), 2-nitrophenol (98%), 1-iodo-2-nitrobenzene (97%), 4-nitroacetophenone (98%), 1-fluoro-4-nitrobenzene (99%), 4-nitrobenzoic acid (99%) and 1-chloro-2-nitrobenzene (99%) were purchased from Alfa Aesar. 4-nitroanisole (97%), methyl-2-nitrobenzoate (>98%) and 2-nitrobenzotrile (>98%) were purchased from Sigma Aldrich, while ethyl-3-nitrobenzoate (99%) was purchased from Fluorochem. Phosphotungstic acid (reagent grade) was supplied by both Sigma Aldrich and Alfa Aesar. Chloroform (99.8%), acetone (99.5%) and phosphoric acid (85%) were purchased from Fisher Scientific. Dichloromethane (99.5%) and magnesium sulfate (99.2%) were purchased from VWR while diethyl ether (99.5%) was purchased from Scientific Laboratory Supplies Ltd. Deuterated chloroform (99.8%), dimethyl sulfoxide (99.9%) and methanol (99.8%) were supplied by Cambridge Isotope Laboratories. 254 μm -thick Nafion N-1110 membrane, used in the H-cells, was purchased from Fuel Cell Store and soaked in 1 M sulfuric acid solution overnight prior to use. Otherwise, all chemical reagents and solvents were used as purchased. Carbon felt, used as a high surface area electrode, was purchased from Alfa Aesar (3.18 mm thick, 99.0%). All electrolyte solutions were prepared with ultrapure deionised water (18.2 M Ω -cm resistivity), obtained from a Sartorius Arium Comfort combined water system. All NMR data were collected using a Bruker AV 400 instrument, at a constant temperature of 300 K. pH determinations were made with a Hanna HI 9025 waterproof pH meter. All other materials were obtained as stated in the text. Experiments performed at “room temperature”, were carried out at 25 °C.

4.2.2 General Electrochemical Methods

Electrochemical studies were performed in a three-electrode configuration (unless otherwise stated) using either a CH Instruments CHI600D potentiostat or a BioLogic SP-150 potentiostat. A glassy carbon button electrode (surface area = 0.071 cm²) or carbon felt were used as the working electrodes (as specified), a Pt wire or a piece of carbon felt were used as the counter electrode (as specified), and an Ag/AgCl (NaCl, 3 M) reference electrode was used when specified. Glassy carbon working electrodes were polished using polishing powder and then washed with acetone and deionized water prior to use. Carbon felt electrodes were not re-used.

4.2.3 Cyclic Voltammetry

Cyclic voltammograms were collected in single chamber cells using a three-electrode set-up at room temperature at a scan rate of 10 mV/s (unless otherwise stated) in 1 M aqueous H₃PO₄ electrolyte. The solvent (10 mL) was thoroughly degassed with N₂ prior to the experiments and kept under inert atmosphere throughout the process. Typically, to this degassed solvent was added 9.75×10^{-5} mol of the relevant nitroarene substrate (unless noted otherwise). To this solution, 1 equivalent mol of H₃[PW₁₂O₄₀] (0.28 g) was then added in the electrochemical cell, followed by degassing and stirring for 5 min. A glassy carbon button electrode was used as the working electrode (area = 0.071 cm²), a Pt wire was used as the counter electrode and an Ag/AgCl (3 M NaCl) reference electrode was used. Measurements were conducted without stirring and with *i*R compensation enabled.

4.2.4 Electrocatalytic Studies

Electrocatalytic studies were performed as follows. Unless otherwise stated, 9.74×10^{-4} mol of the relevant nitroarene was added to 30 mL of a 3.3 mM aqueous solution of phosphotungstic acid (*i.e.* a 10 mol% ratio of phosphotungstic acid relative to the nitroarene). This solution was then placed into the working electrode compartment of an H-cell. For the less soluble nitroarenes (ethyl-2-nitrobenzoate, 4-nitroacetophenone, etc.) half this amount of starting material was used, *i.e.* 4.87×10^{-4} mol, but still with a 10 mol% ratio of phosphotungstic acid (1.65 mM) relative to the nitroarene. The counter electrode side of the cell was filled with 1 M aqueous H₃PO₄ electrolyte solution. The two compartments of the H-cell were separated by a Nafion N-1110 membrane. Typically, bulk electrolysis was then

carried out at -0.38 V vs. Ag/AgCl under an inert atmosphere until substrate reduction was complete, as judged by the falling off of the current to background levels.

After electrolysis for a given time, the (now dark blue) solution was removed from the working electrode compartment of the H-cell. The pH of this solution was then raised above the pK_a value of the anticipated product using 1 M NaOH in order to deprotonate the $R-NH_3^+$ salt and form the neutral $R-NH_2$ state. This in turn allowed the reduced organic product to be extracted into organic solvents for isolation. The pH values in question for the various conversions were: 2-nitrophenol to 2-aminophenol, pH = 6.0, 1-bromo-4-nitrobenzene to 4-bromoaniline, pH = 6.1, 2-nitrotoluene to 2-aminotoluene, pH = 5.7, 2-nitrobenzotrile to 2-aminobenzotrile, pH = 6.1, methyl-2-nitrobenzoate to methyl-2-aminobenzoate, pH = 3.5, 1-chloro-2-nitrobenzene to 2-chloroaniline, pH = 3.7, ethyl-4-nitrobenzoate to ethyl-4-aminobenzoate, pH = 5.0, 4-nitrobenzoic acid to 4-aminobenzoic acid, pH = 3.7, 4-fluoro-1-nitrobenzene to 4-fluoroaniline, pH = 6.3, 4-nitroacetophenone to 4-aminoacetophenone, pH = 4.0, 1-iodo-3-nitrobenzene to 3-iodoaniline, pH = 5.0 and ethyl-3-nitrobenzoate to ethyl-3-aminobenzoate, pH = 4.0.

Ethyl-4-aminobenzoate, ethyl-3-aminobenzoate and 3-iodoaniline were extracted using chloroform, 2-aminophenol was extracted using dichloromethane and 4-bromoaniline, 4-fluoroaniline, 2-aminotoluene, methyl-2-aminobenzoate, 2-aminobenzotrile, 2-chloroaniline, 4-aminobenzoic acid and 4-aminoacetophenone were extracted using diethyl ether. In all cases, after extraction, magnesium sulfate was added to the organic phase in order to remove any remaining water traces. The organic phase was then filtered and concentrated under reduced pressure using a rotary evaporator to give the isolated reduced aniline derivatives.

4.2.5 1H NMR Determination of Conversions

After extraction into organic solvent and concentration under reduced pressure, the conversion of the starting material was determined *via* the integration of the relevant 1H NMR peaks. After the 1H NMR peaks in any given spectrum had been identified and assigned, peaks corresponding to the same number of protons in both the starting material and the various products were compared, allowing the percentage of starting material converted to each product (or not converted, and hence still present as starting material) to be determined.

4.3 Results and Discussion

4.3.1 Voltammetry

A diagrammatic representation of the redox-mediated approach for the reduction of nitroarenes is depicted below (Figure 4.1), where the polyoxometalate mediator is electrochemically reduced at the surface of the cathode and subsequently reacts in solution with the corresponding nitrobenzene to yield the aniline derivative. The mediator becomes re-oxidized in the process, and is thus able to be reduced again at the cathode (leading to turnover). The corresponding direct electrochemical reduction reactions (*i.e.* in the absence of any mediator) were also studied to provide a comprehensive understanding of the mediated reactions.

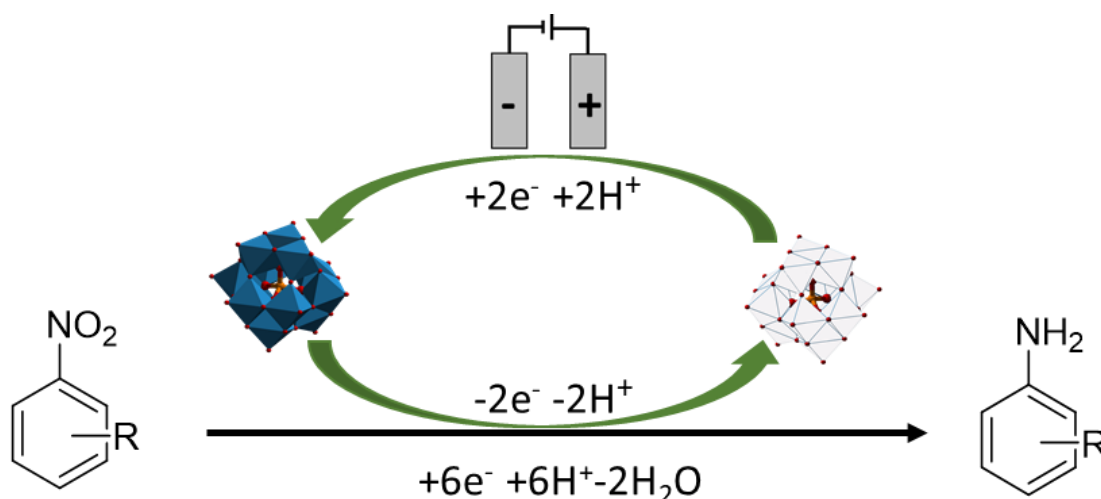


Figure 4.1: Illustration of the electrocatalytic hydrogenation of nitrobenzenes using a phosphotungstic acid redox mediator.

In the following, the mediated experiments were performed using 10 mol% of the redox mediator relative to the starting material. Cyclic voltammograms of all the selected substrates in 1 M H_3PO_4 were recorded (see Section 4.5.1, Figures 4.6-4.17) and the data obtained for the (peak) positions of the redox waves of these substrates relative to the peak position of the second reversible reduction wave of the polyoxometalate mediator (-0.38 V vs. Ag/AgCl) are summarized in Figure 4.2.

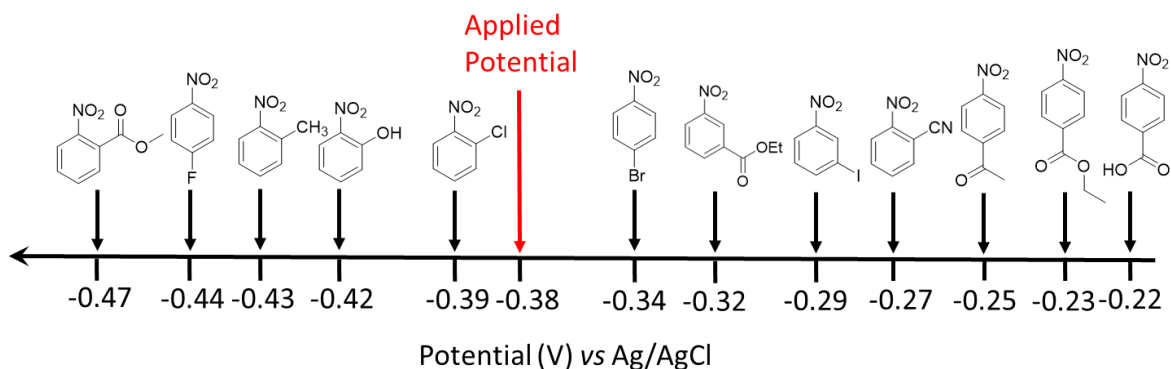


Figure 4.2: Schematic illustration of the reduction potentials of the examined substituted nitrobenzenes. The reduction potentials were extracted from the cyclic voltammograms recorded using a glassy carbon working electrode (surface area = 0.071 cm²), a Pt wire counter electrode and an Ag/AgCl reference electrode. The electrolyte was 1 M aqueous H₃PO₄ and the scan rate was 10 mV/s in all cases. The scale bar is non-linear in order to allow the relative ordering of the various redox processes to be more clearly seen.

An example of the reactivity of the redox mediator is depicted in Figure 4.3 for the starting material ethyl-3-nitrobenzoate. The red trace represents the electro-activity of the phosphotungstic acid redox mediator on its own, exhibiting two reversible one-electron redox waves at -0.04 V and -0.32 V vs. Ag/AgCl. The black trace represents the direct reduction of ethyl-3-nitrobenzoate at the electrode surface in the absence of the polyoxometalate mediator, with the main feature being an irreversible reduction at around -0.3 V vs. Ag/AgCl. When the phosphotungstic acid redox mediator is present together with ethyl-3-nitrobenzoate, the second reduction peak of the redox mediator at -0.32 V vs. Ag/AgCl exhibits enhanced reductive current, indicating that an electrocatalytic process is occurring between the two-electron reduced mediator and the substrate.

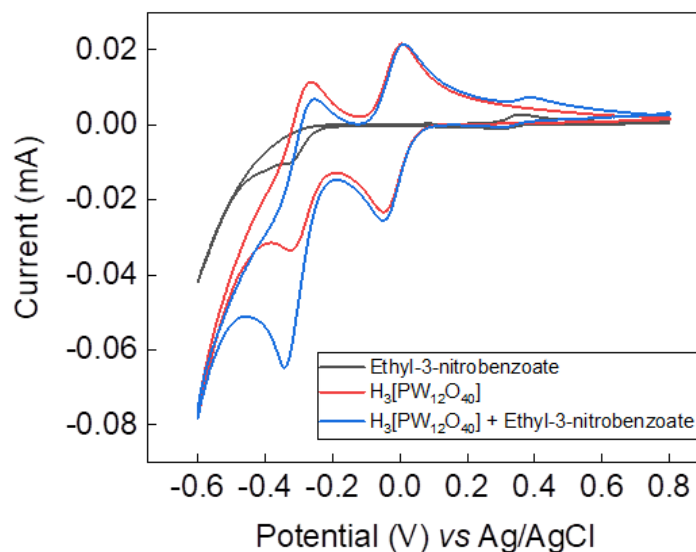


Figure 4.3: Cyclic voltammogram of ethyl-3-nitrobenzoate in 10 mL 1 M aqueous H_3PO_4 , using 9.74×10^{-5} mol of both the nitroarene and the redox mediator. A glassy carbon working electrode (surface area = 0.071 cm^2), a Pt wire counter electrode and an Ag/AgCl reference electrode were used. The scan rate was 10 mV/s.

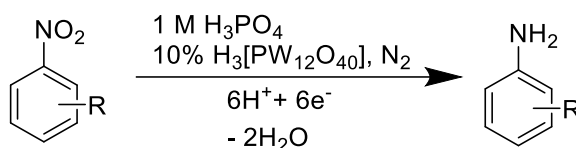
For the rest of the compounds (see Section 4.5.1, Figures 4.6-4.17), the redox mediator has a similar reactivity as its second reduction peak always shows enhanced reductive current in the presence of the different nitrobenzene starting material, indicating electrocatalytic process. However, some differences in the cyclic voltammograms can be observed. First of all, the low solubility of some starting materials in the electrolyte solution lead to smaller cathodic current in some cases. More specifically, 1-bromo-4-nitrobenzene (Figure 4.11), 4-nitrobenzoic acid (Figure 4.14), ethyl-4-nitrobenzoate (Figure 4.15) and ethyl-3-nitrobenzoate (Figure 4.17) show a small reduction peak in the absence of the redox mediator, that yields in smaller reductive current of the second polyoxometalate peak in the presence of starting material, compared with the other nitrobenzenes. Nevertheless, the electrocatalytic activity of the mediator is still evident. Additionally, the cyclic voltammogram of 1-iodo-3-nitrobenzene (Figure 4.10) shows some interesting features. First of all, the current for the first redox wave of the starting material at about + 0.3 V vs Ag/AgCl is significantly increased in the presence of the redox mediator compared to the other nitrobenzene starting materials (similar activity on the first redox wave is only present in the cyclic voltammogram of 4-nitroacetophenone, Figure 4.12). This redox wave is usually attributed to the redox couple of nitrosobenzene/phenylhydroxylamine (see Chapter

3, Section 3.3.3). Moreover, the increase in the reductive current of the second peak of the polyoxometalate in the presence of the starting material is substantial for a compound with low solubility. This is an indication of enhanced electrocatalytic activity, which however needs to be tested with electrolysis experiments. We can also observe a “loop” in the cyclic voltammogram of 1-iodo-3-nitrobenzene in the presence of the redox mediator. Such loops are known from other systems and usually imply that the electrode surface is temporarily activated or deactivated towards the reaction in question in the potential region of the “loop”. A classic example of this is the oxidation of glucose on gold/gold oxide surfaces.²⁶

4.3.2 Substrate Scope

Table 4.1 summarises the conversion of the nitroarene starting materials and the selectivity for the aniline derivatives for the various substrates listed, under both mediated and direct electrochemical reduction (the latter corresponding to “0% mediator”).

Table 4.1: Comparison between the mediated and non-mediated nitroarene reduction reactions.



Entry	Starting material	Product	10 % Mediator		0 % Mediator	
			Conversion (%)	Selectivity (%)	Conversion (%)	Selectivity (%)
1			>99	>99	72	90
2			63	>99	6	5
3			>99	29 ^a	>99	0
4			95	>99	96	0

5			>99	>99	>99	10
6			89	91 ^b	74	0
7			54	89 ^b	45	9
8			73	>99	39	4
9			91	>99	23	0
10			86	>99	41	5
11			49	>99	61	43
12			65	>99	44	25

^aThe main product of this reaction is the hydroxylamine intermediate as identified by ESI-mass spectrometry ($m/z = 124.0760$ for $[M+H]^+$). ^bThe balance of the starting material of this reaction was found to have converted to the hydroxylamine intermediate, as identified by ^1H NMR.

As can be seen from Table 4.1, the use of the polyoxometalate redox mediator usually improves the conversion of the starting material and always improves the selectivity for conversion of the starting material to the aniline derivative when compared to the result found in the corresponding direct electrochemical reduction reaction. In terms of the direct

electrochemical reduction, the sub-optimal selectivity of the process yielded in reaction mixtures that are difficult to fully characterize. In entries 3,6,7 and 10, the dominant side product of the direct process identified as the phenylhydroxylamine derivative. At the same time, in entry 4 two reaction intermediates can be identified, which we believe are the phenylhydroxylamine and the azoxybenzene derivatives, while zero formation of the aniline product was observed. In all cases, the reduction of the substituted nitrobenzene was incomplete, presumably yielding to known reduction intermediates of this process (see Scheme 3.1) and/or no aniline derivative. Only the direct reduction of 2-nitrophenol (entry 1) presents a rather different outcome. In this case, the dominant product is the 2-aminophenol, with little formation of the phenylhydroxylamine intermediate. The significantly high conversion of the starting material can be attributed to its higher solubility in our electrolyte, compared with the other nitrobenzene compounds. Figure 4.4 illustrates stacked ^1H NMR plots for one such example, using methyl-2-nitrobenzoate as the substrate (Table 4.1, entry 5). ^1H NMR stacked plots for the other substrates that were probed can be found in Section 4.5.2 (Figures 4.18-4.41).

Even in the cases of halide-substituted nitrobenzenes (-F, -Cl, -Br, -I; Table 4.1, entries 2, 6, 9 and 11), which often suffer from cleavage of the halide from the aromatic ring under standard hydrogenation conditions, the selectivities for the production of the halide-substituted aniline compounds are very high. This is in contrast to the 0% mediator reaction outcomes under otherwise identical conditions, where both conversions and/or selectivities are generally markedly poorer. In some cases in Table 4.1, conversion of the starting material is less than quantitative (meaning in the case of the mediated reaction in Entry 8 for example that the reaction mixture contains just starting material and aniline product at the end of the reaction in a 27:73 ratio). Such instances of less than complete conversion are due to the low solubility of the relevant substrates in the aqueous electrolyte. However, it is significant that the mediated reaction still proceeds highly selectively despite the poor solubility of some of the substrates, generally producing only the desired aniline derivative as the sole reduction product. The fact that such “on water” reactions are feasible with the mediated system enhances the sustainability aspects of this approach.

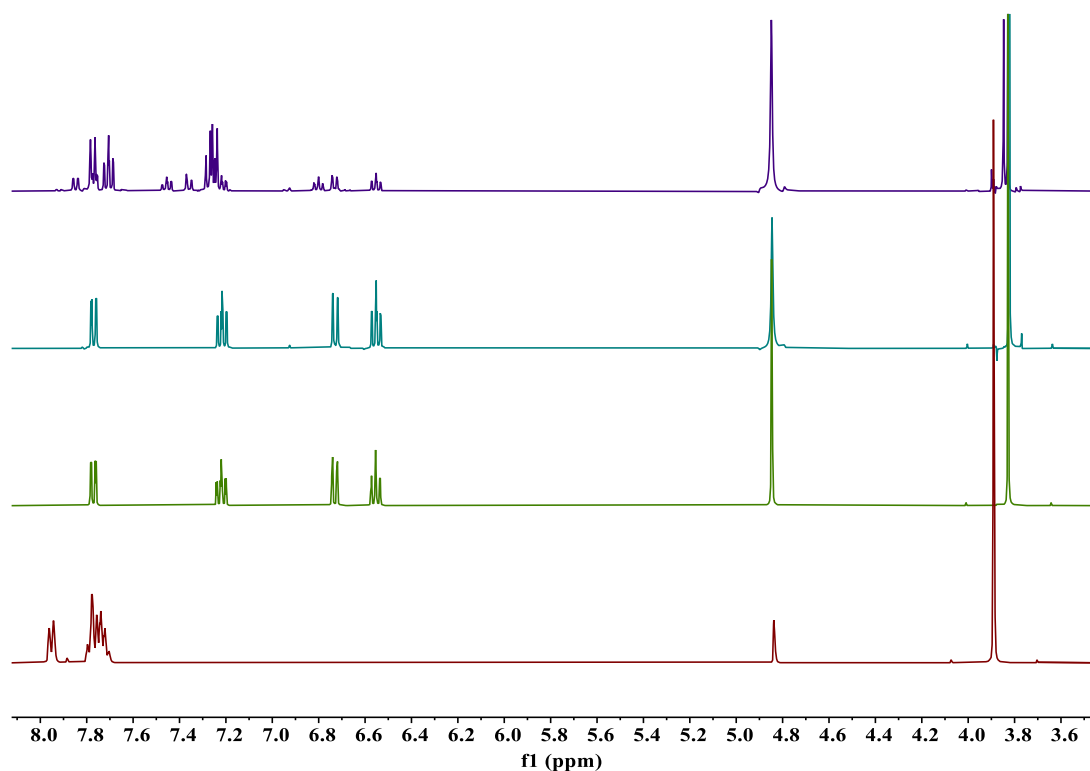


Figure 4.4: Stacked ^1H NMR plot (MeOD, 300 K, 400 MHz) summarizing the outcome of the mediated electroreduction of methyl-2-nitrobenzoate. Shown in purple at the top is a spectrum of the extracted and concentrated reaction medium from a non-mediated reaction (direct substrate reduction at the cathode). Beneath this (turquoise) is a spectrum of the extracted and concentrated reaction medium from a mediated electrochemical reduction of methyl-2-nitrobenzoate. Beneath this (green), is a pure methyl-2-aminobenzoate standard sample. The bottom spectrum (red) is that of the starting material. The peak at 4.78 ppm originates from residual MeOH.

4.3.3 Scaled-up Reactions

In order to show that there is the potential to develop this into a process for nitroarene reduction under preparative conditions (where the ability to operate at larger scale, without the need for a reference electrode, and under controlled current would be useful), a galvanostatic electrolysis on the substrate methyl-2-nitrobenzoate was performed using a two-electrode setup in an H-cell. All the components were as described above, apart from the counter electrode, which was replaced with a large surface area Pt mesh. 90 mg of methyl-2-nitrobenzoate was thus dissolved in 35 mL of 1 M aqueous H_3PO_4 (giving a 14 mM solution) in the presence of 10% mol equivalents of the redox mediator. The chosen applied cathodic current was 20 mA (current density = 2.7 mA/cm^2). After a reaction time of 6 h, 92% of the starting material had been converted to the aniline product (2-aminobenzoic acid methyl ester) with >99% selectivity (*i.e.* no other reduction product was

detected). Figure 4.5 shows a V-t curve for this reaction. A gram-scale reaction was also performed, maintaining the same current density but increasing the size of the electrochemical cell. Therefore, 1 g of starting material was dissolved in 100 mL of 1 M aqueous H_3PO_4 in the presence of 10% mol equivalents of the redox mediator. After 22 h, the conversion of the in-solution substrate was 93%. However, some of the starting material had precipitated, meaning that the conversion was not quantitative and resulting in a total isolated yield of 2-aminobenzoic acid methyl ester of only 60% (0.41 g). The selectivity of the reaction for the material that did convert was still very high (>97%), meaning that essentially only the desired aminobenzoic acid methyl ester product and the starting material were present in the reaction mixture. The Faradaic yield was also impacted by the precipitation of the starting material, but even so it was reasonable at 46%.

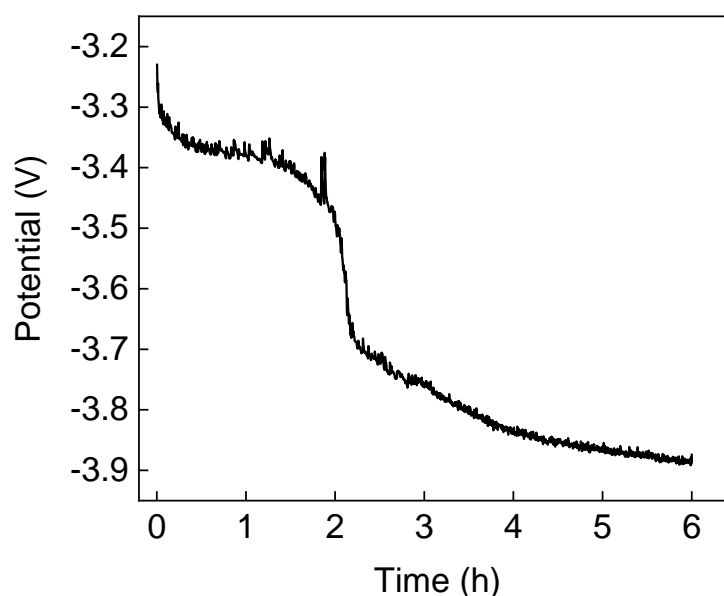


Figure 4.5: Voltage-time plot of the controlled-current reduction of methyl-2-nitrobenzoate in 1 M aqueous H_3PO_4 at -20 mA using a 2-electrode setup. A platinum mesh was used as the counter electrode (anode) and carbon felt was used as the working electrode (cathode).

4.4 Conclusions

Herein, we have shown that the polyoxometalate phosphotungstic acid is an effective redox mediator for the electrocatalytic reduction of halogenated, and alkyl-, carbonyl-, ester-, hydroxyl-, cyano- and acid-substituted nitrobenzenes. In all cases, electrochemical reduction of these substrates in the presence of the redox mediator occurred with higher selectivity than for the direct reduction of the substrates at the electrode surface. Scaled-up reactions were also effective, returning only the desired aniline product and unreacted starting material, with essentially no formation of unwanted side-products. The process is notable not only for its high selectivity, but also for its potential sustainability advantages over conventional methods for nitrobenzene reduction, including mild process conditions (aqueous solution at room temperature), the ability to work without extraneous reducing agents (including hydrogen gas) and the fact that a heterogeneous precious metal catalyst is not required. Further optimization of these procedures is currently underway in our laboratories.

4.5 Characterisation of Compounds

4.5.1 Cyclic Voltammograms

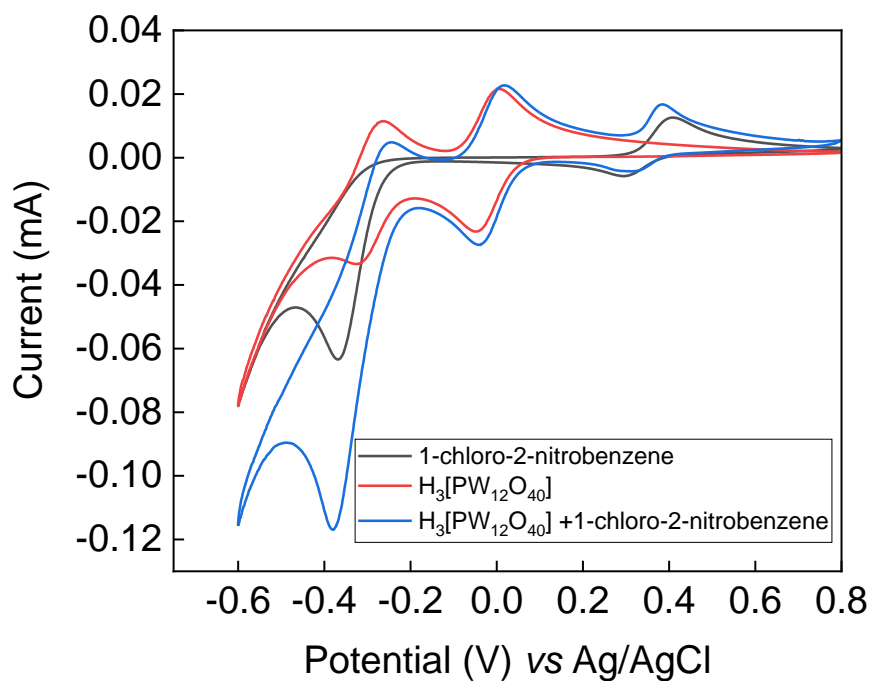


Figure 4.6: Cyclic voltammogram of the starting material 1-chloro-2-nitrobenzene in 1 M aqueous H₃PO₄, using 9.74×10^{-5} mol of both the nitroarene and the redox mediator. A glassy carbon working electrode (surface area = 0.071 cm²), a Pt wire counter electrode and a Ag/AgCl reference electrode were used. Scan rate 10 mV/s.

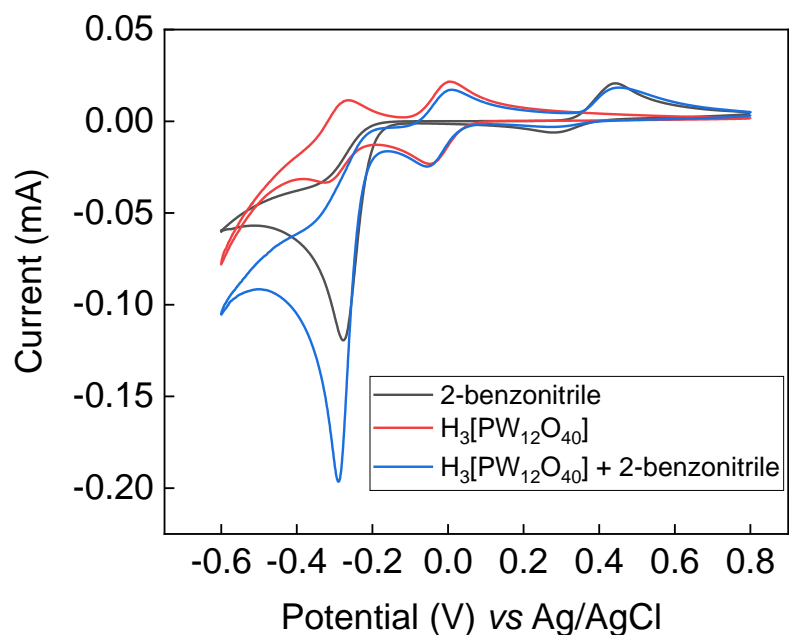


Figure 4.7: Cyclic voltammogram of the starting material 2-benzonitrile in 1 M aqueous H_3PO_4 , using 9.74×10^{-5} mol of both the nitroarene and the redox mediator. A glassy carbon working electrode (surface area = 0.071 cm^2), a Pt wire counter electrode and a Ag/AgCl reference electrode were used. Scan rate 10 mV/s.

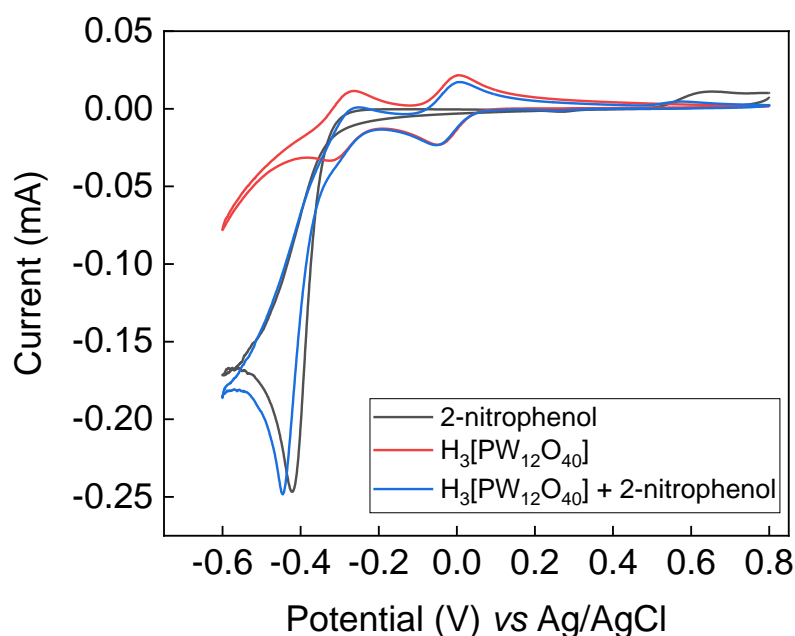


Figure 4.8: Cyclic voltammogram of the starting material 2-nitrophenol in 1 M aqueous H_3PO_4 , using 9.74×10^{-5} mol of both the nitroarene and the redox mediator. A glassy carbon working electrode (surface area = 0.071 cm^2), a Pt wire counter electrode and a Ag/AgCl reference electrode were used. Scan rate 10 mV/s.

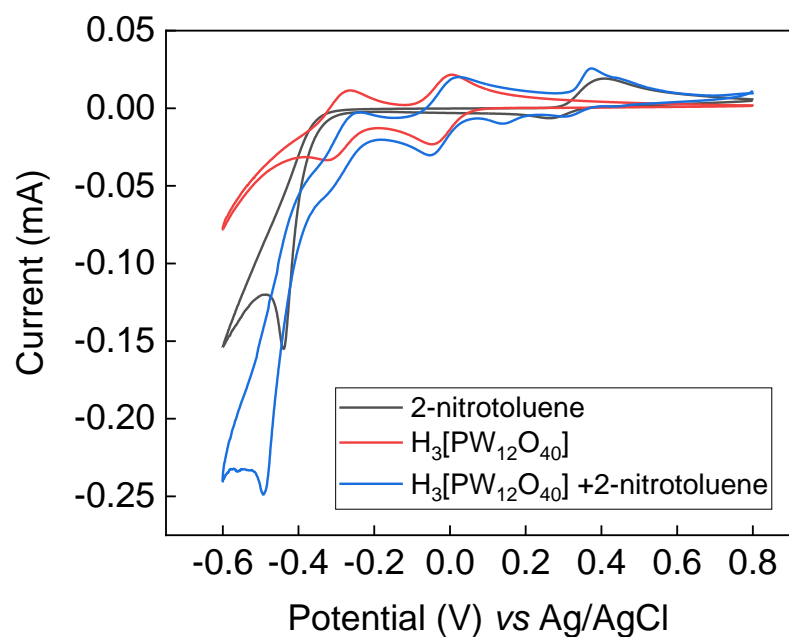


Figure 4.9: Cyclic voltammogram of the starting material 2-nitrotoluene in 1 M aqueous H_3PO_4 , using 9.74×10^{-5} mol of both the nitroarene and the redox mediator. A glassy carbon working electrode (surface area = 0.071 cm^2), a Pt wire counter electrode and a Ag/AgCl reference electrode were used. Scan rate 10 mV/s.

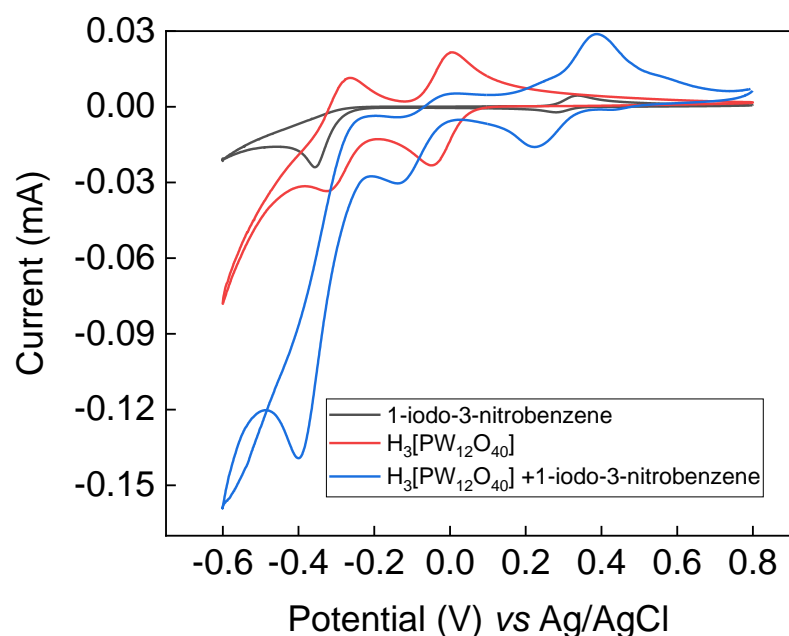


Figure 4.10: Cyclic voltammogram of the starting material 1-iodo-3-nitrobenzene in 1 M aqueous H_3PO_4 , using 1.95×10^{-4} mol of starting material and 9.74×10^{-5} mol of the redox mediator. A glassy carbon working electrode (surface area = 0.071 cm^2), a Pt wire counter electrode and a Ag/AgCl reference electrode were used. Scan rate 10 mV/s.

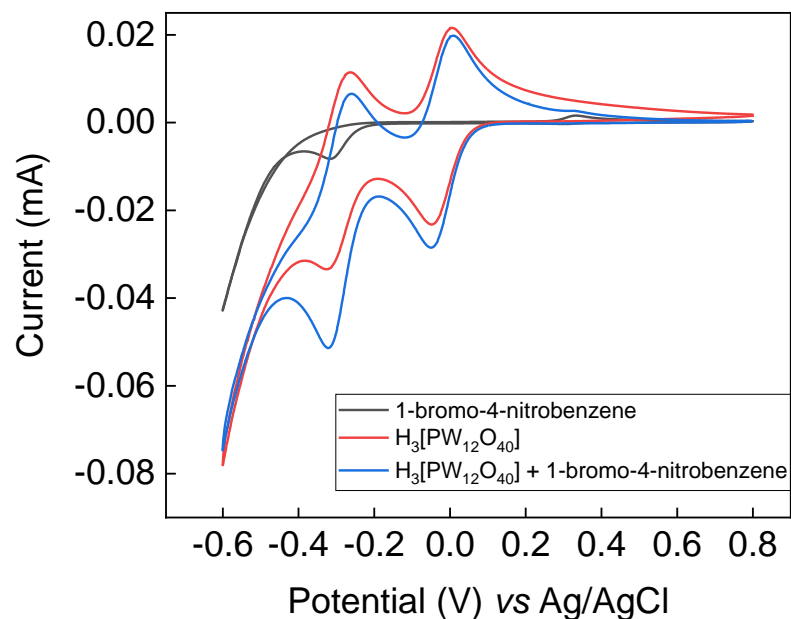


Figure 4.11: Cyclic voltammogram of the starting material 1-bromo-4-nitrobenzene in 1 M aqueous H_3PO_4 , using 1.95×10^{-4} mol of starting material and 9.74×10^{-5} mol of the redox mediator. A glassy carbon working electrode (surface area = 0.071 cm^2), a Pt wire counter electrode and a Ag/AgCl reference electrode were used. Scan rate 10 mV/s.

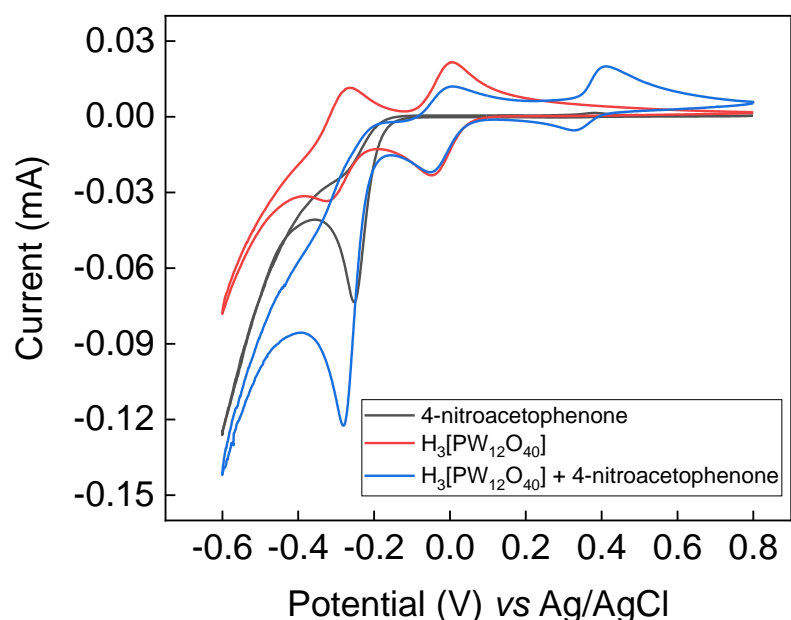


Figure 4.12: Cyclic voltammogram of the starting material 4-nitroacetophenone in 1 M aqueous H_3PO_4 , using 9.74×10^{-5} mol of both the nitroarene and the redox mediator. A glassy carbon working electrode (surface area = 0.071 cm^2), a Pt wire counter electrode and a Ag/AgCl reference electrode were used. Scan rate 10 mV/s.

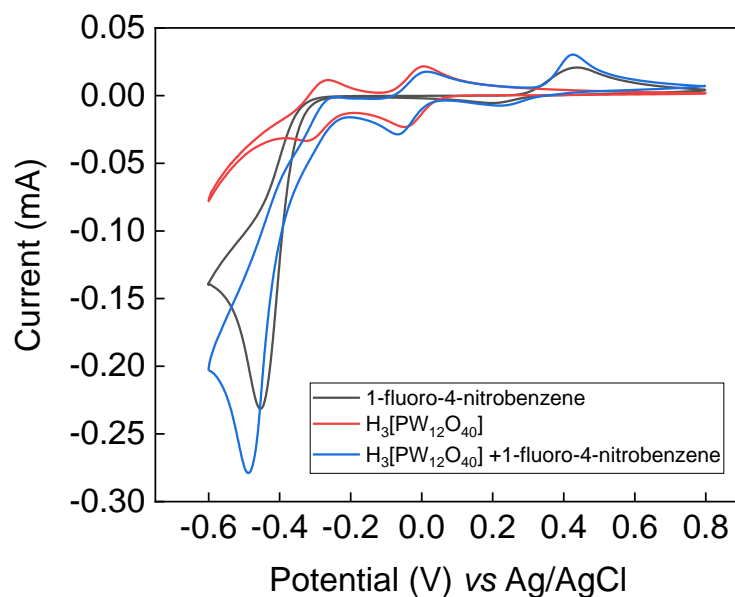


Figure 4.13: Cyclic voltammogram of the starting material 1-fluoro-4-nitrobenzene in 1 M aqueous H_3PO_4 , using 1.95×10^{-4} mol of starting material and 9.74×10^{-5} mol of the redox mediator. A glassy carbon working electrode (surface area = 0.071 cm^2), a Pt wire counter electrode and a Ag/AgCl reference electrode were used. Scan rate 10 mV/s.

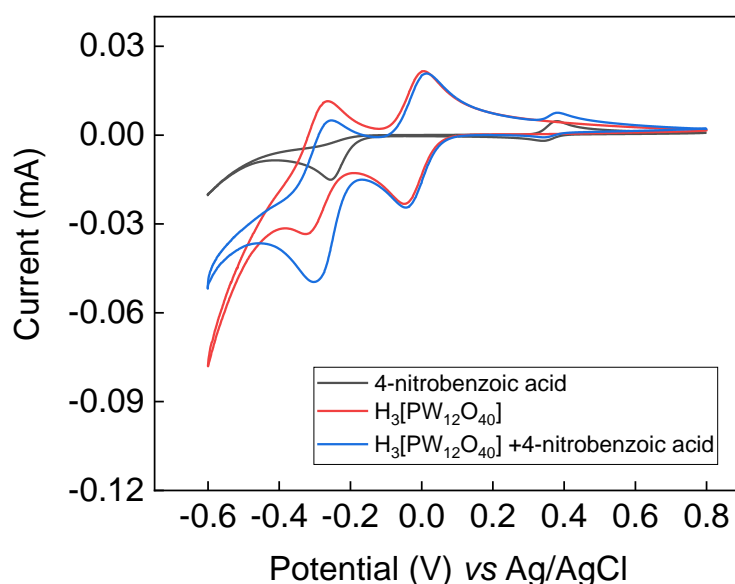


Figure 4.14: Cyclic voltammogram of the starting material 4-nitrobenzoic acid in 1 M aqueous H_3PO_4 , using 1.95×10^{-4} mol of starting material and 9.74×10^{-5} mol of the redox mediator. A glassy carbon working electrode (surface area = 0.071 cm^2), a Pt wire counter electrode and a Ag/AgCl reference electrode were used. Scan rate 10 mV/s.

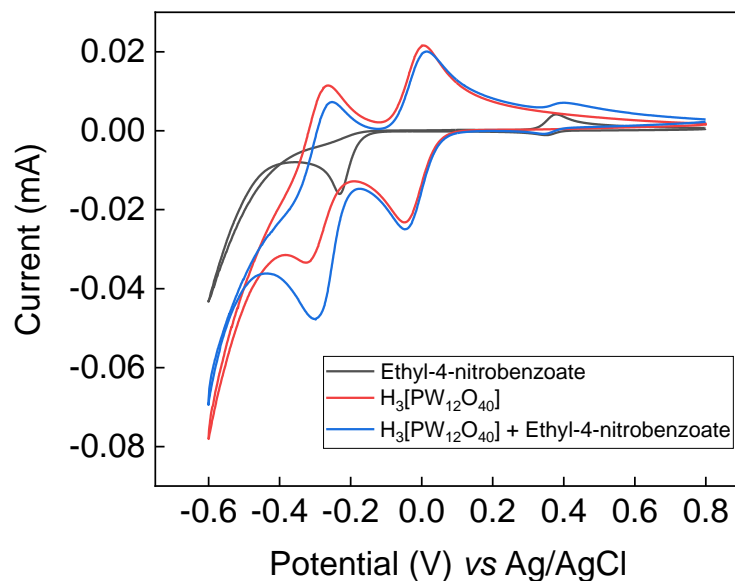


Figure 4.15: Cyclic voltammogram of the starting material ethyl-4-nitrobenzoate in 1 M aqueous H_3PO_4 , using 9.74×10^{-5} mol of both the nitroarene and the redox mediator. A glassy carbon working electrode (surface area = 0.071 cm^2), a Pt wire counter electrode and a Ag/AgCl reference electrode were used. Scan rate 10 mV/s.

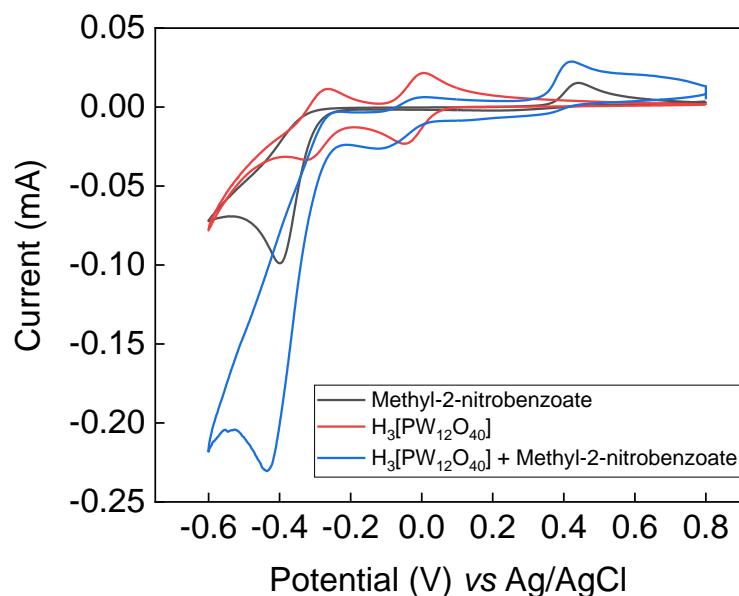


Figure 4.16: Cyclic voltammogram of the starting material methyl-2-nitrobenzoate in 1 M aqueous H_3PO_4 , using 1.95×10^{-4} mol of starting material and 9.74×10^{-5} mol the redox mediator. A glassy carbon working electrode (surface area = 0.071 cm^2), a Pt wire counter electrode and a Ag/AgCl reference electrode were used. Scan rate 10 mV/s.

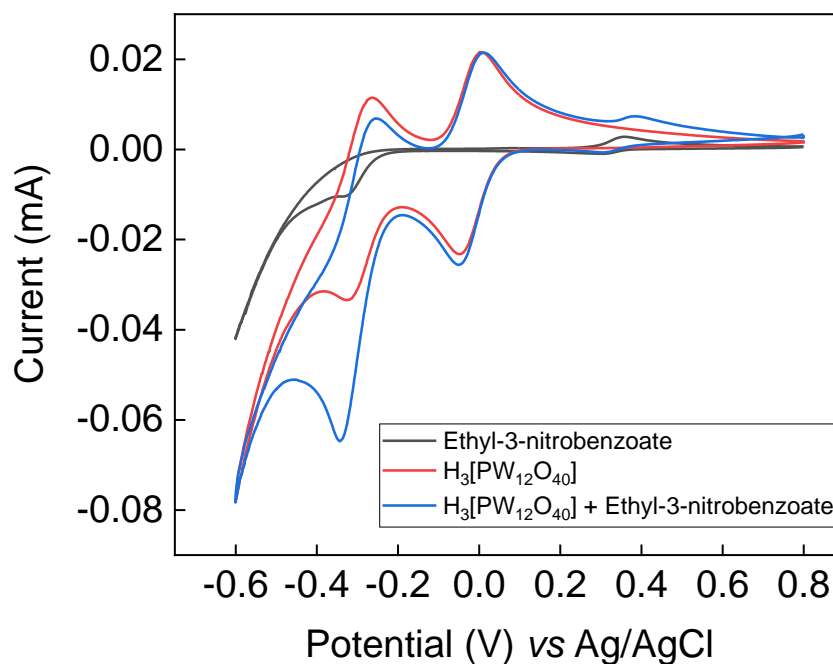


Figure 4.17: Cyclic voltammogram of the starting material ethyl-3-nitrobenzoate in 1 M aqueous H₃PO₄, using 9.74×10^{-5} mol of both the nitroarene and the redox mediator. A glassy carbon working electrode (surface area = 0.071 cm²), a Pt wire counter electrode and a Ag/AgCl reference electrode were used. Scan rate 10 mV/s.

4.5.2 NMR Analysis of Obtained Products

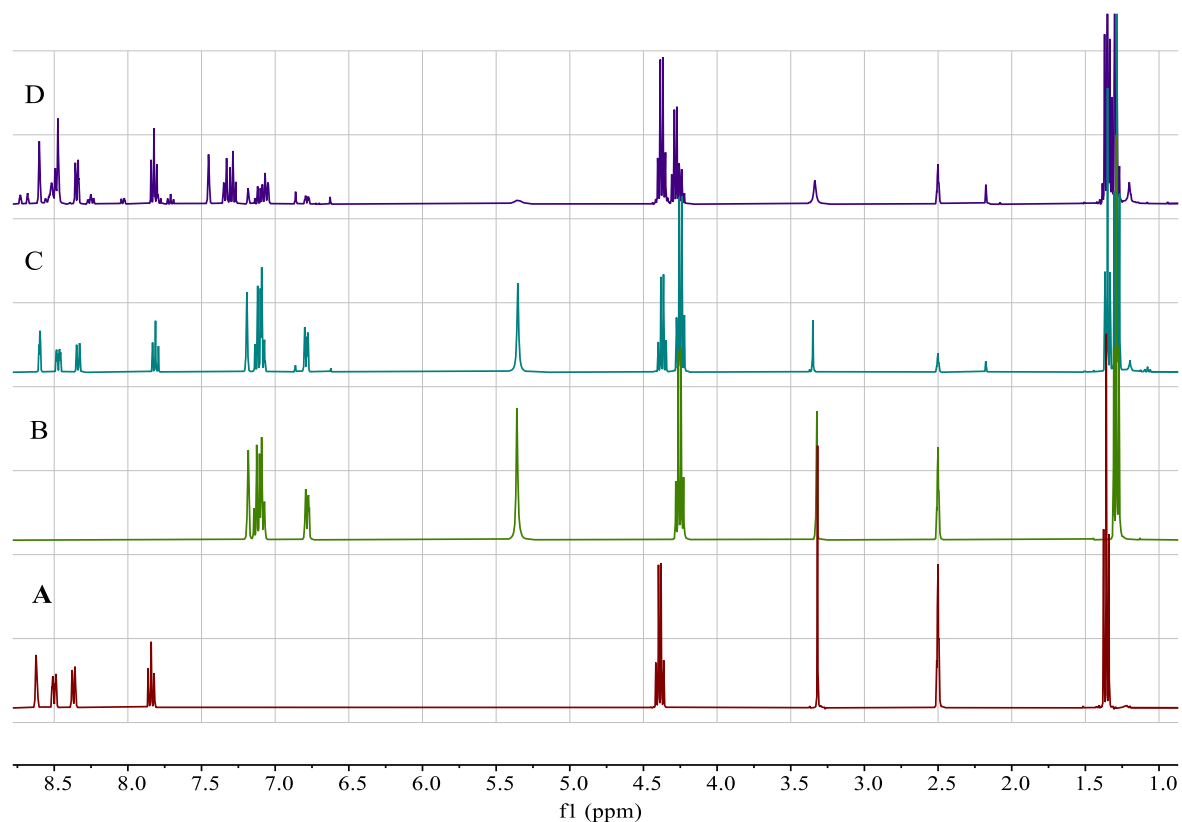


Figure 4.18: Reduction of ethyl-3-nitrobenzoate. ¹H NMR spectra of the ethyl-3-nitrobenzoate starting material (A), a sample of pure ethyl-3-aminobenzoate (B), the spectrum of the electrocatalytic reaction medium after extraction and concentration (C) and the spectrum of the extracted and concentrated reaction medium from a direct (*i.e.* non-mediated) electrochemical reduction of ethyl-3-nitrobenzoate (D). All spectra were obtained in DMSO-d₆.

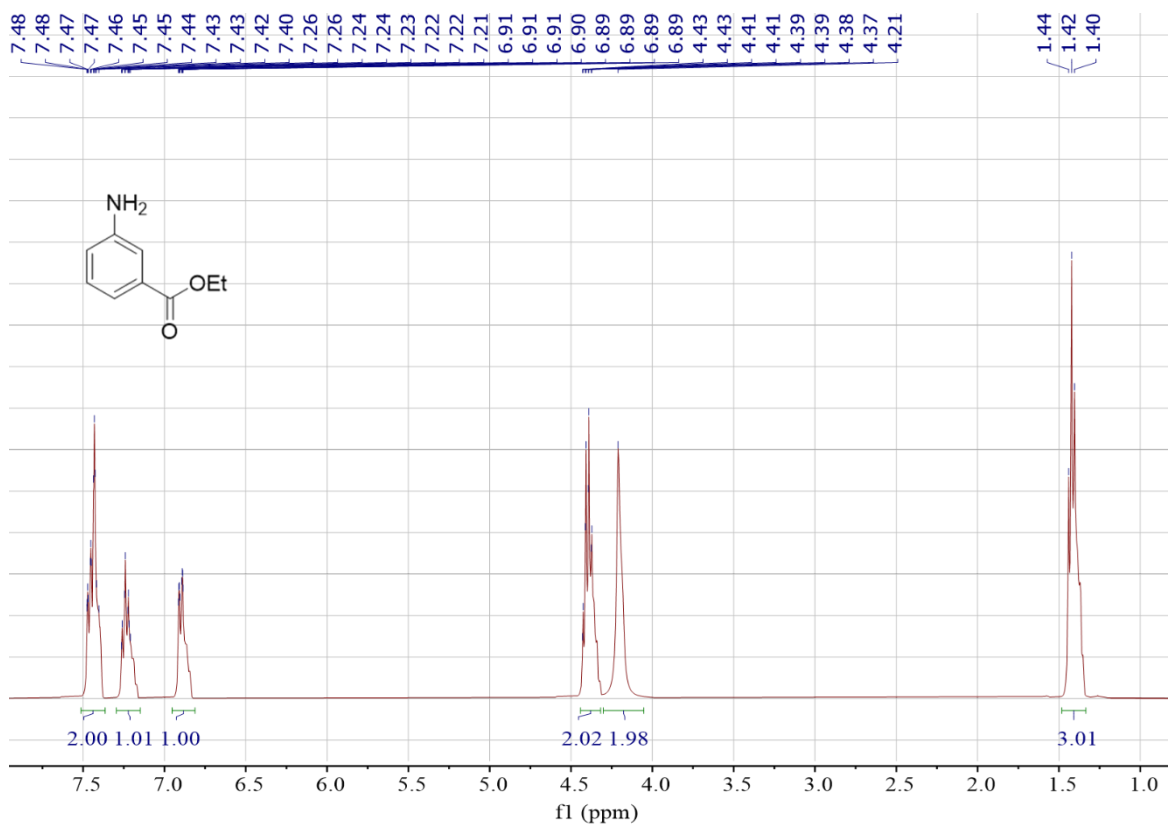


Figure 4.19: ¹H NMR (400 MHz, 298 K) spectrum of ethyl-3-aminobenzoate (Table 1, entry 12) from the electrocatalytic reaction medium after extraction, concentration, and purification. Spectrum was obtained in CDCl₃.

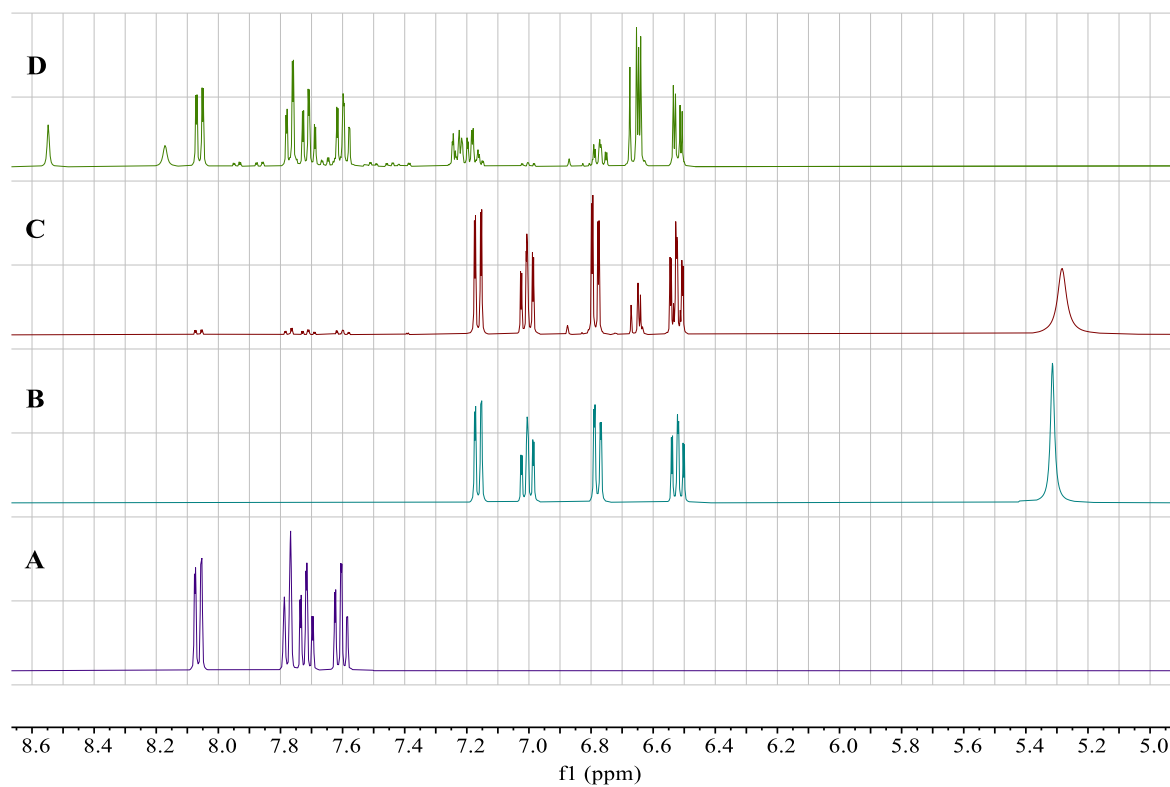


Figure 4.20: Reduction of 1-chloro-2-nitrobenzene. ^1H NMR spectra of the 1-chloro-2-nitrobenzene starting material (A), a sample of pure 2-chloroaniline (B), the spectrum of the electrocatalytic reaction medium after extraction and concentration (C) and the spectrum of the extracted and concentrated reaction medium from a direct (*i.e.* non-mediated) electrochemical reduction of 1-chloro-2-nitrobenzene (D). All spectra were obtained in DMSO-d_6 .

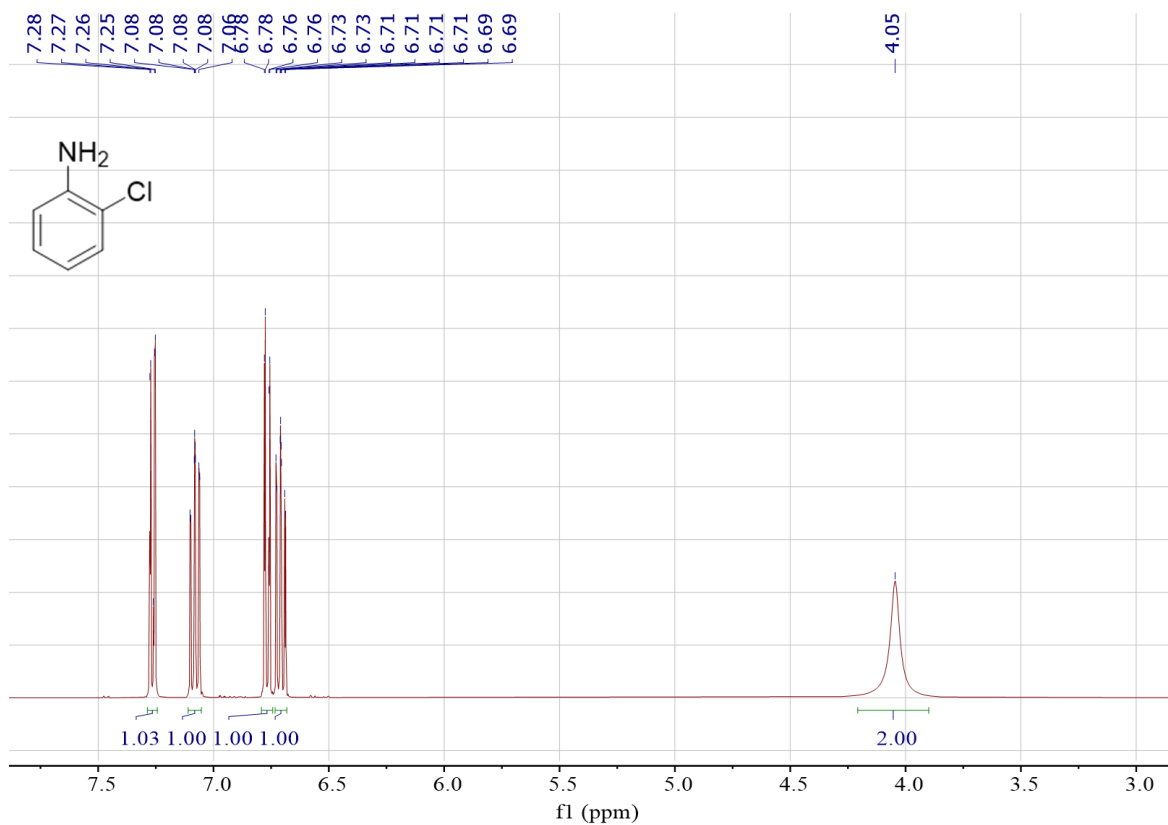


Figure 4.21: ^1H NMR (400 MHz, 298 K) spectrum of 2-chloroaniline (Table 1, entry 6) from the electrocatalytic reaction medium after extraction, concentration, and purification. Spectrum was obtained in CDCl_3 .

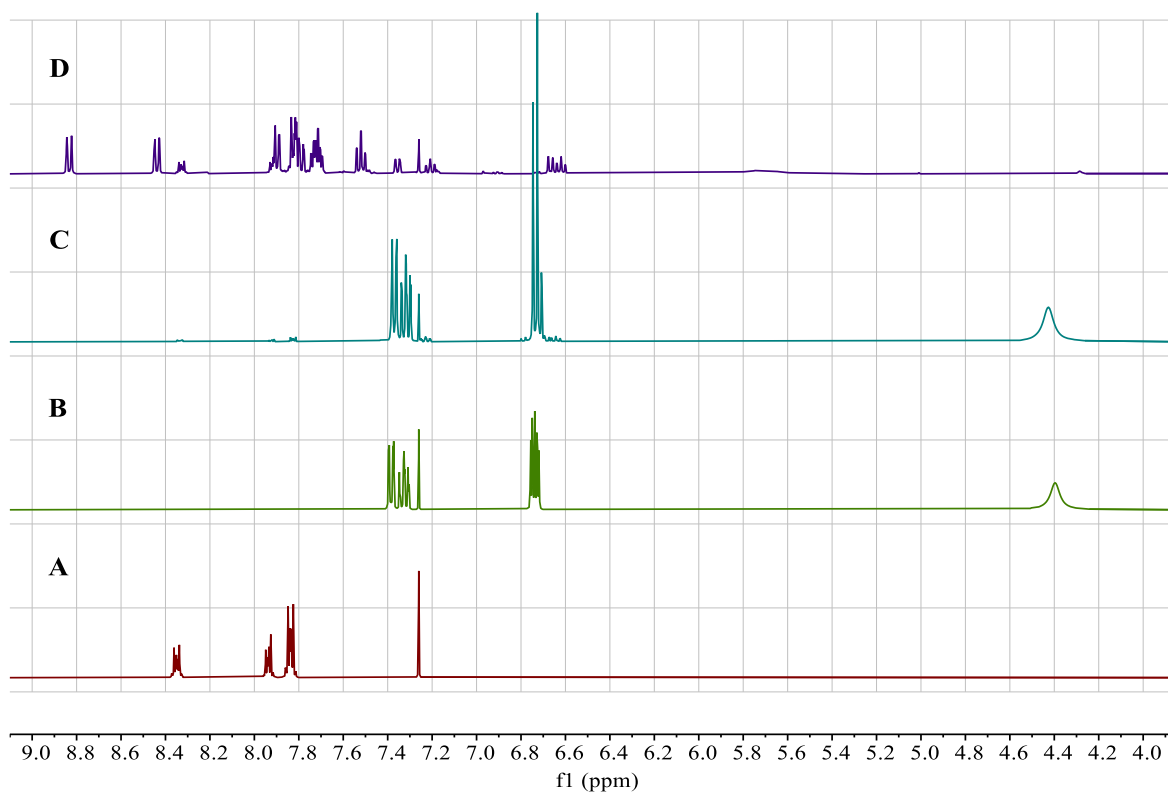


Figure 4.22: Reduction of 2-nitrobenzonitrile. ¹H NMR spectra of the 2-nitrobenzonitrile starting material (A), a sample of 2-aminobenzonitrile (B), the spectrum of the electrocatalytic reaction medium after extraction and concentration (C) and the spectrum of the extracted and concentrated reaction medium from a direct (*i.e.* non-mediated) electrochemical reduction of 2-nitrobenzonitrile (D). All spectra were obtained in CDCl₃.

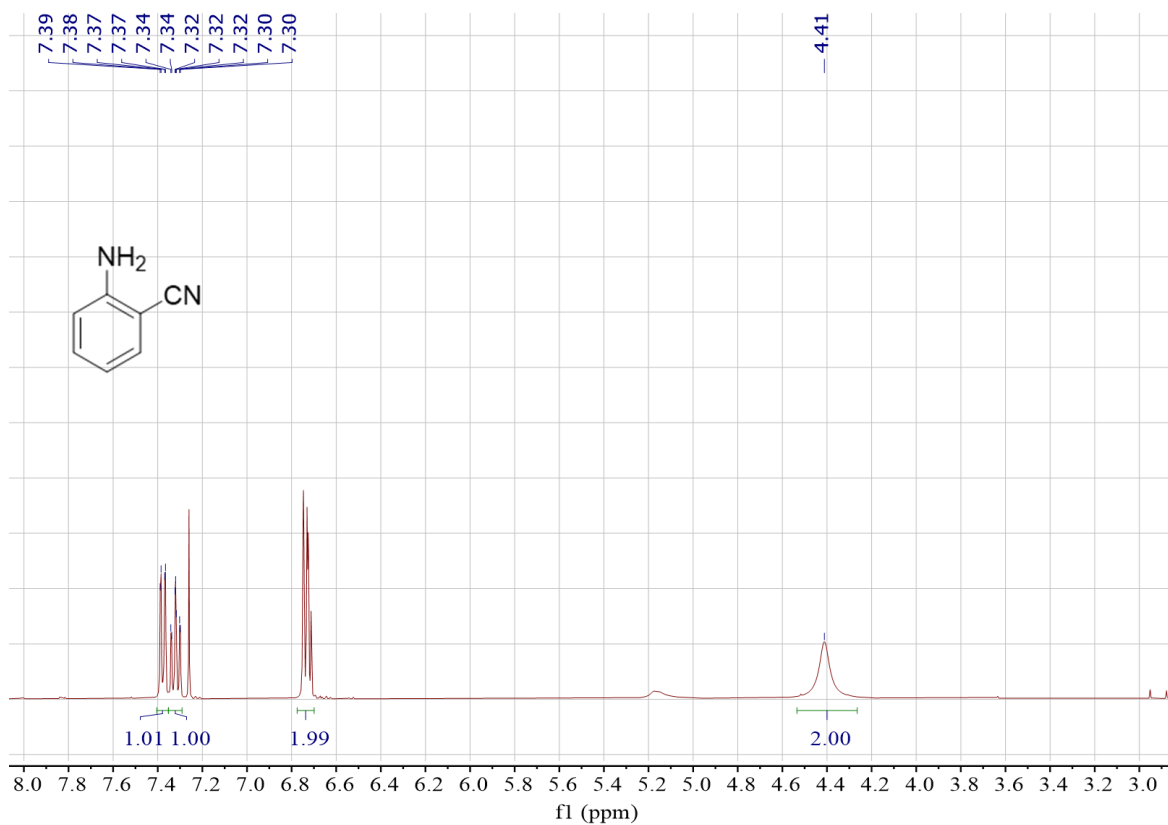


Figure 4.23: ^1H NMR (400 MHz, 298 K) spectrum of 2-aminobenzonitrile (Table 1, entry 4) from the electrocatalytic reaction medium after extraction, concentration, and purification. Spectrum was obtained in CDCl_3 .

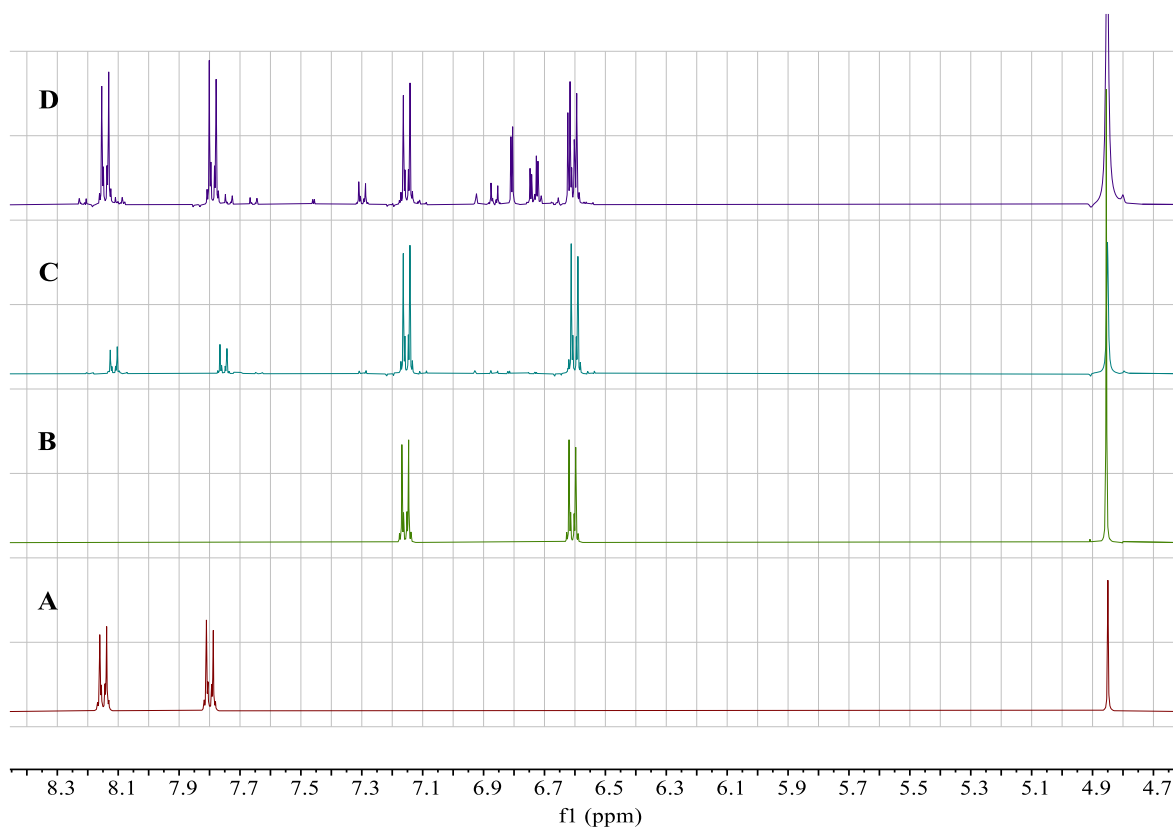


Figure 4.24: Reduction of 1-bromo-4-nitrobenzene. ¹H NMR spectra of the 1-bromo-4-nitrobenzene starting material (A), a sample of 4-bromoaniline (B), the spectrum of the electrocatalytic reaction medium after extraction and concentration (C) and the spectrum of the extracted and concentrated reaction medium from a direct (*i.e.* non-mediated) electrochemical reduction of 1-bromo-4-nitrobenzene (D). All spectra were obtained in MeOD.

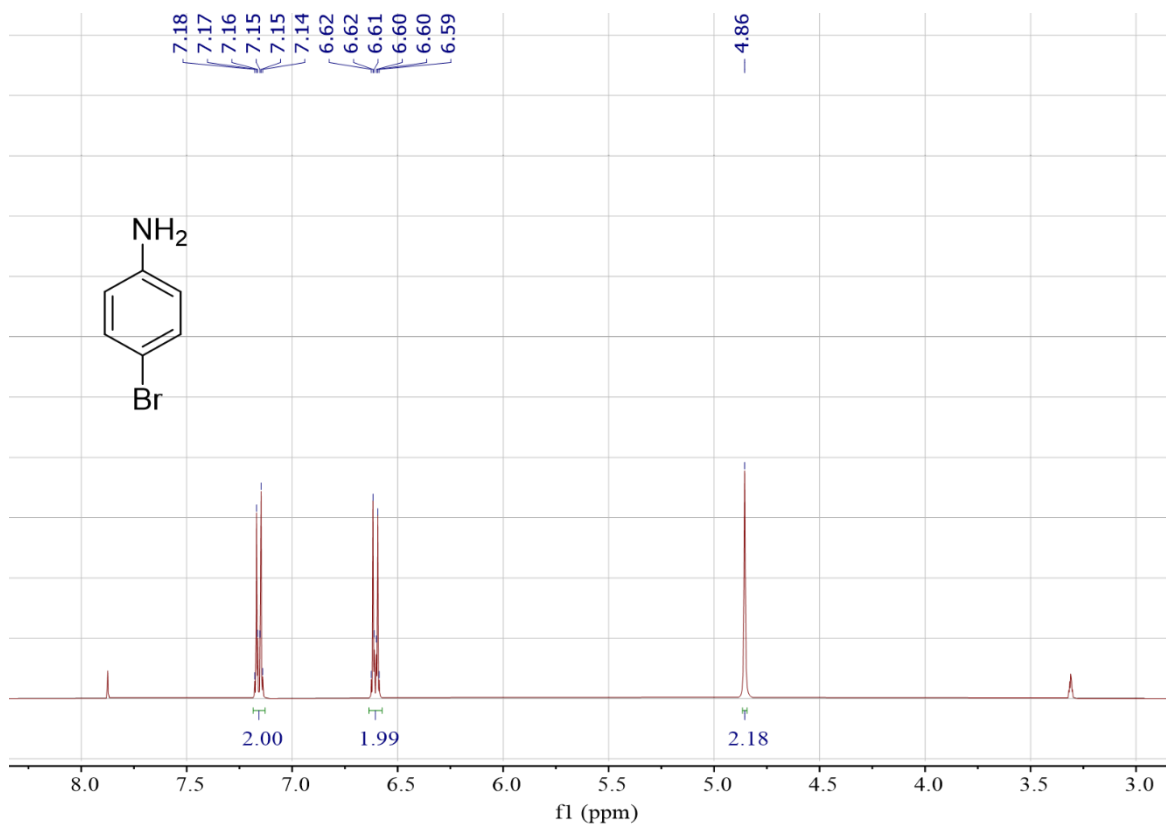


Figure 4.25: ^1H NMR (400 MHz, 298 K) spectrum of 4-bromo-aniline (Table 1, entry 2) from the electrocatalytic reaction medium after extraction, concentration, and purification. Spectrum was obtained in CDCl_3

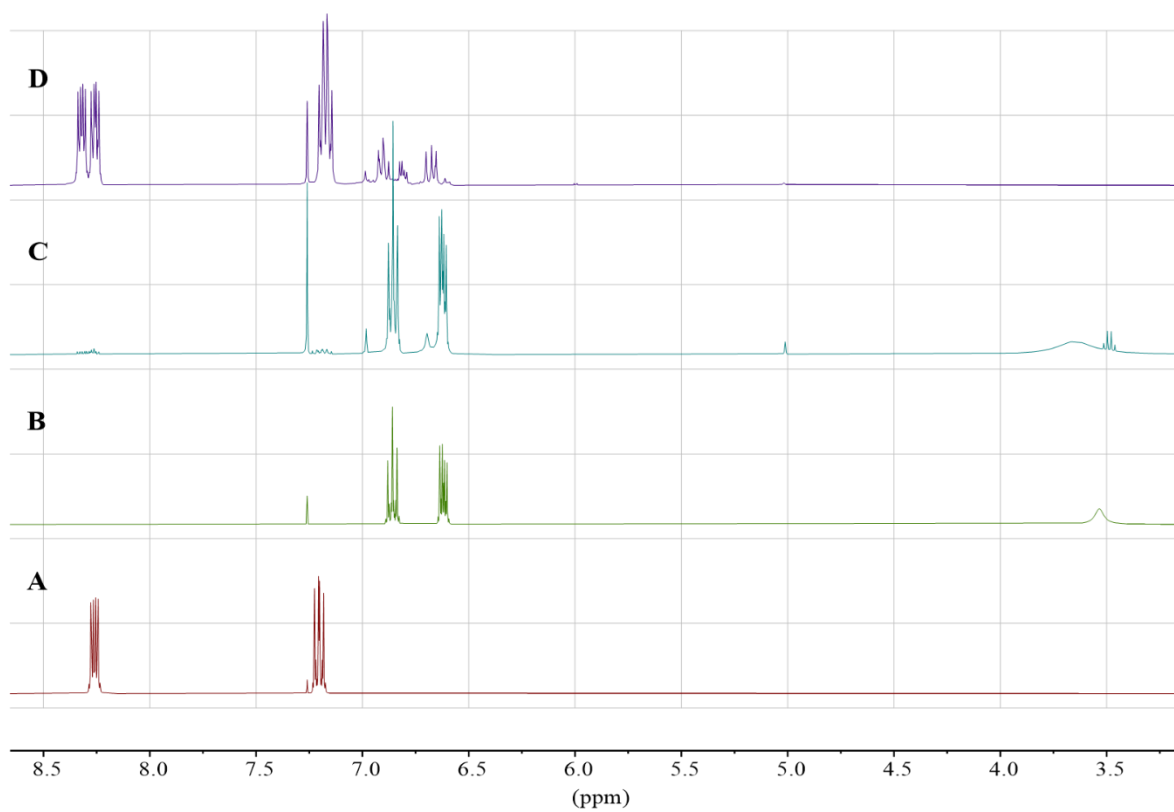


Figure 4.26: Reduction of 1-fluoro-4-nitrobenzene. ¹H NMR spectra of the 1-fluoro-4-nitrobenzene starting material (A), a sample of 4-fluoroaniline (B), the spectrum of the electrocatalytic reaction medium after extraction and concentration (C) and the spectrum of the extracted and concentrated reaction medium from a direct (*i.e.* non-mediated) electrochemical reduction of 1-fluoro-4-nitrobenzene (D). All spectra were obtained in CDCl₃.

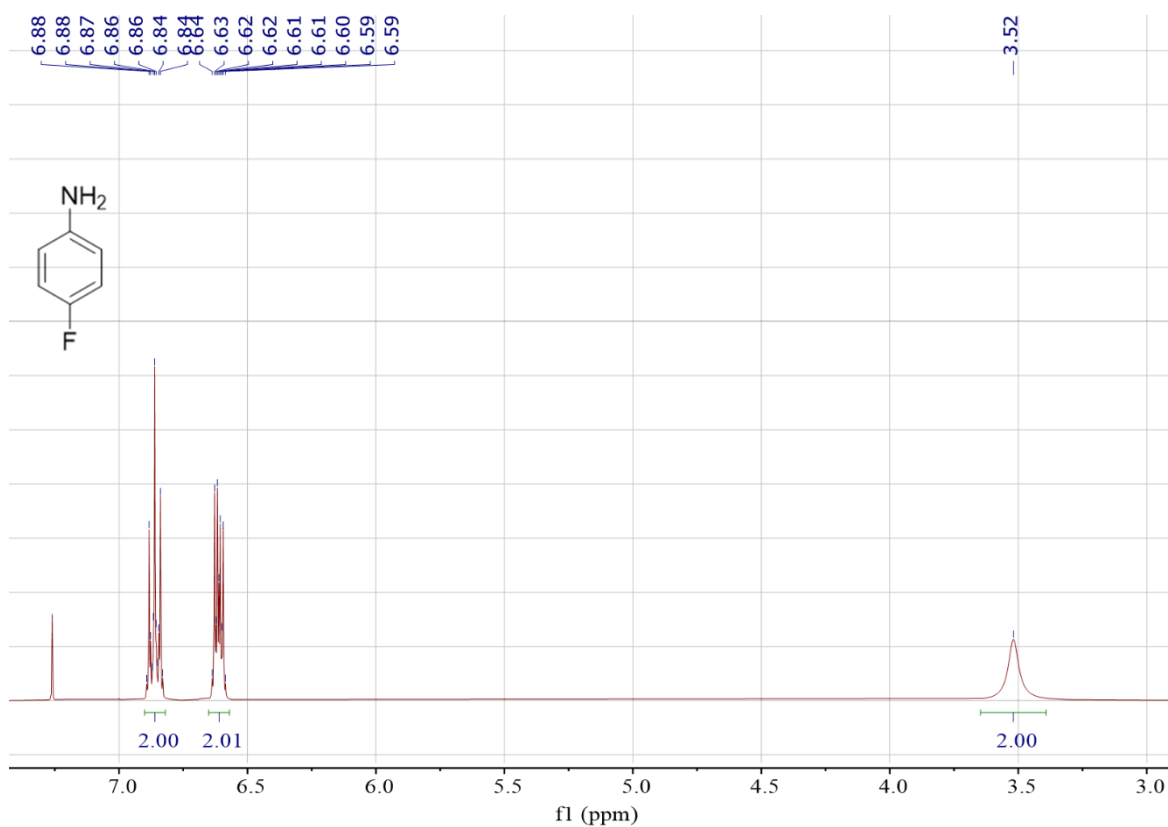


Figure 4.27: ¹H NMR (400 MHz, 298 K) spectrum of 4-fluoroaniline (Table 1, entry 9) from the electrocatalytic reaction medium after extraction, concentration, and purification. Spectrum was obtained in CDCl₃.

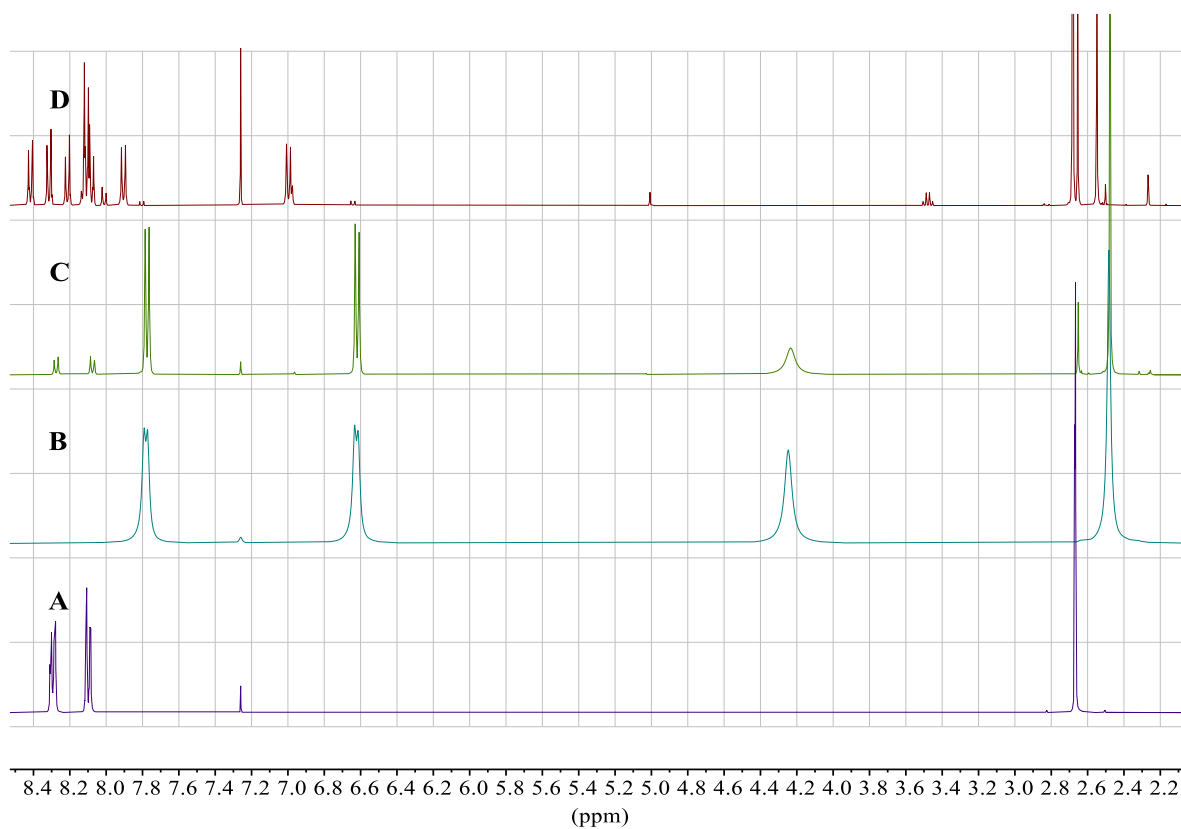


Figure 4.28: Reduction of 4-nitroacetophenone. ¹H NMR spectra of the 4-nitroacetophenone starting material (A), a sample of 4-aminoacetophenone (B), the spectrum of the electrocatalytic reaction medium after extraction and concentration (C) and the spectrum of the extracted and concentrated reaction medium from a direct (*i.e.* non-mediated) electrochemical reduction of 4-nitroacetophenone (D). All spectra were obtained in CDCl₃.

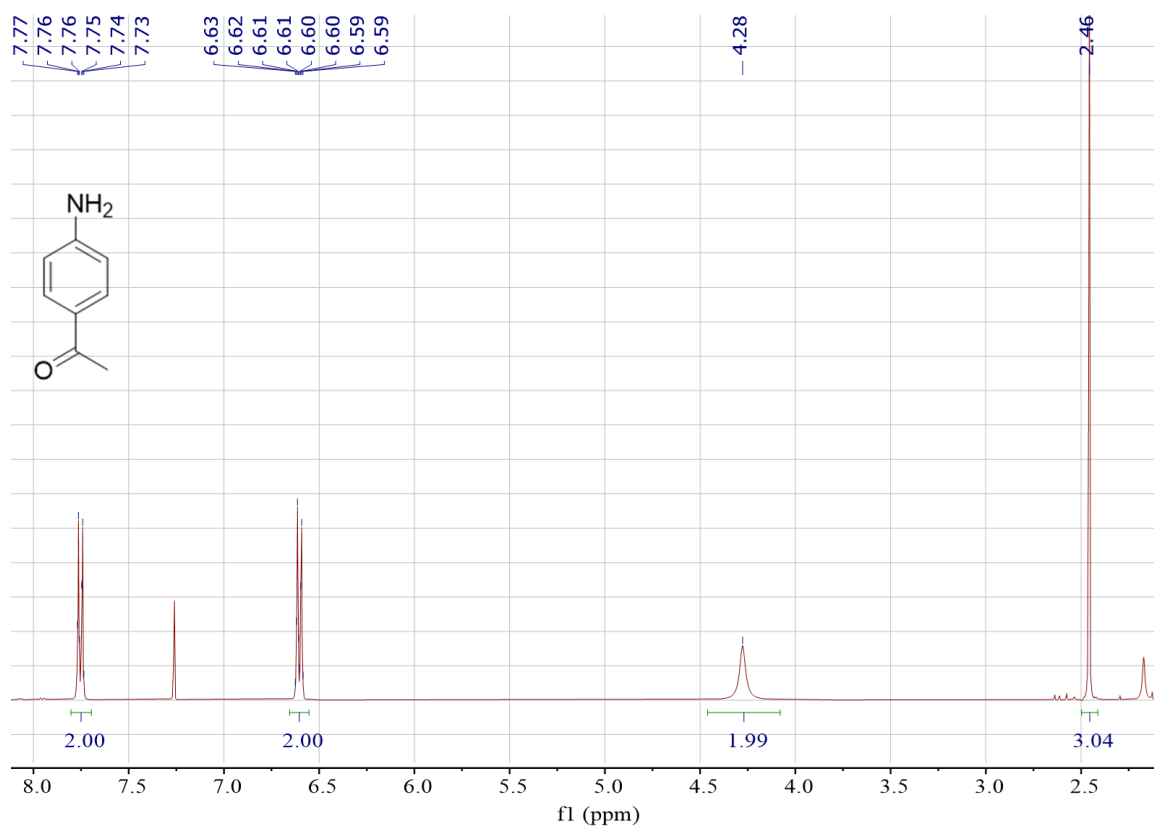


Figure 4.29: ¹H NMR (400 MHz, 298 K) spectrum of 4-aminoacetophenone (Table 1, entry 10) from the electrocatalytic reaction medium after extraction, concentration, and purification. Spectrum was obtained in CDCl₃.

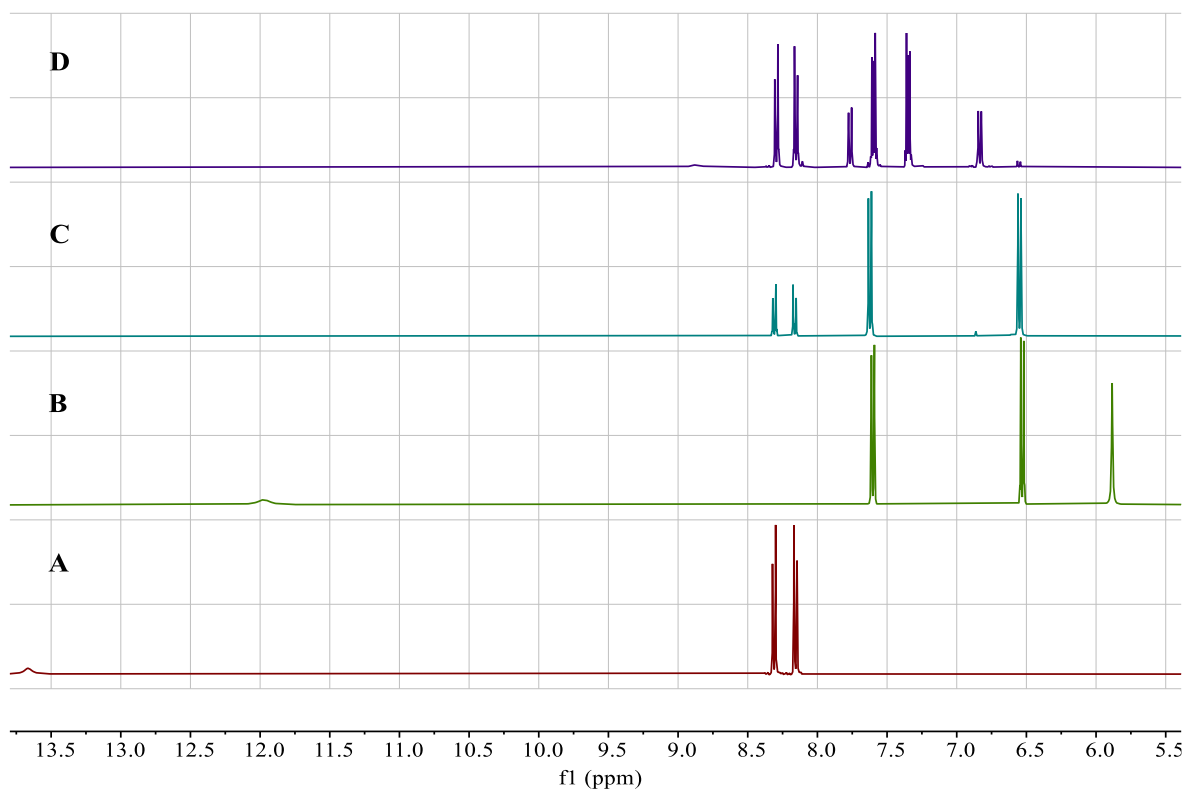


Figure 4.30: Reduction of 4-nitrobenzoic acid. ¹H NMR spectra of the 4-nitrobenzoic acid starting material (A), a sample of 4-aminobenzoic acid (B), the spectrum of the electrocatalytic reaction medium after extraction and concentration (C) and the spectrum of the extracted and concentrated reaction medium from a direct (*i.e.* non-mediated) electrochemical reduction of 4-nitrobenzoic acid (D). All spectra were obtained in DMSO-d₆.

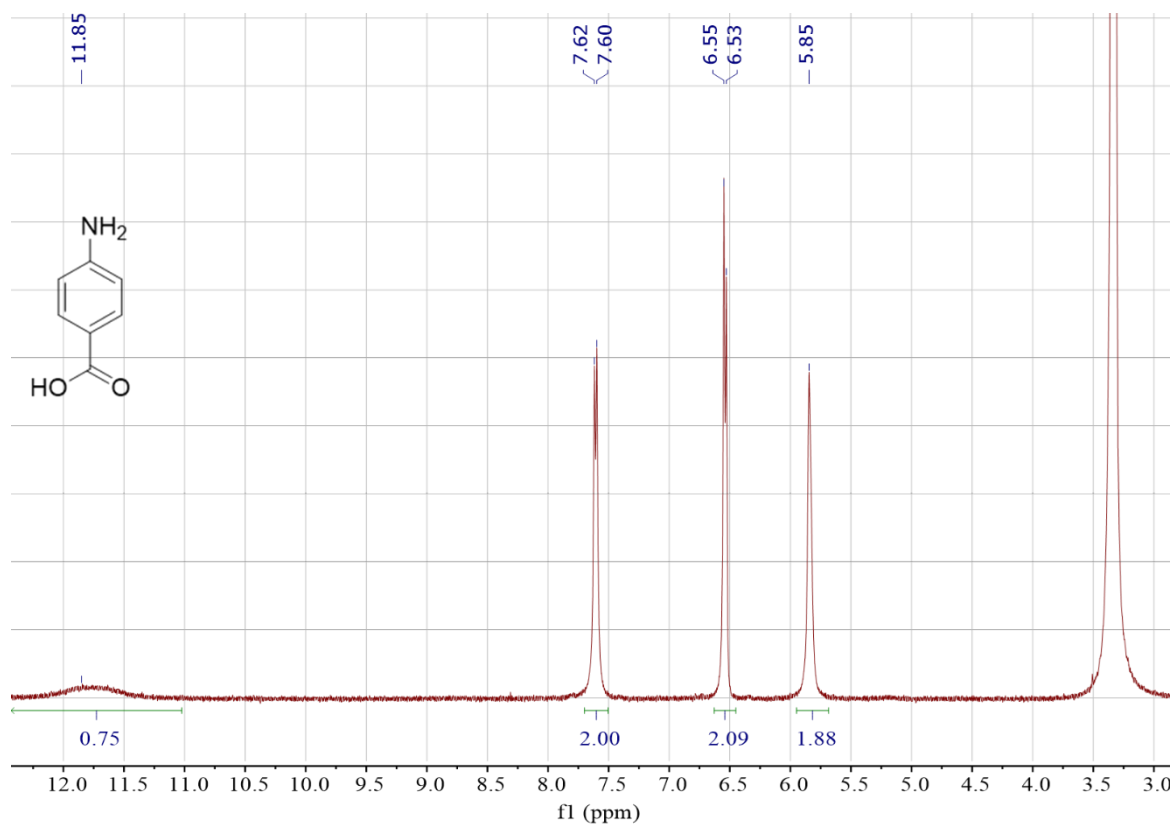


Figure 4.31: ¹H NMR (400 MHz, 298 K) spectrum of 4-aminobenzoic acid (Table 1, entry 8) from the electrocatalytic reaction medium after extraction, concentration, and purification. Spectrum was obtained in d₆-DMSO.

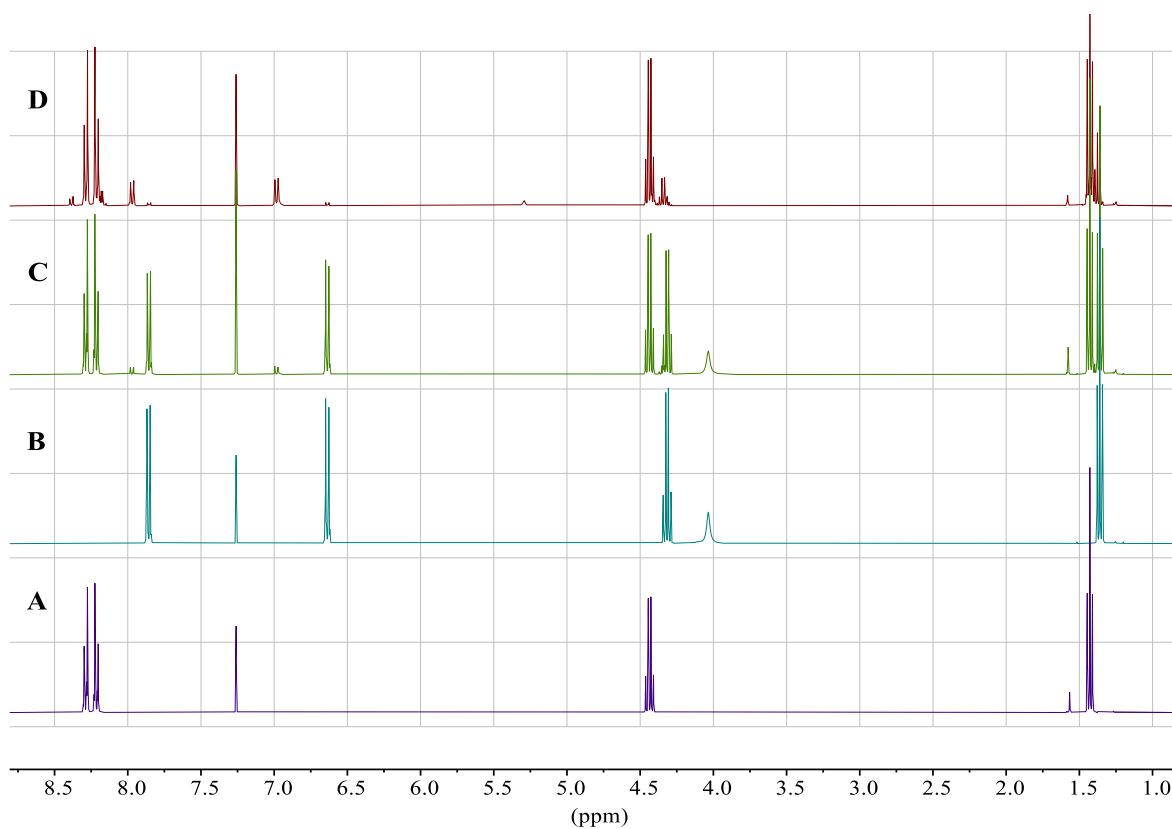


Figure 4.32: Reduction of ethyl-4-nitrobenzoate. ¹H NMR spectra of the ethyl-4-nitrobenzoate starting material (A), a sample of ethyl-4-aminobenzoate (B), the spectrum of the electrocatalytic reaction medium after extraction and concentration (C) and the spectrum of the extracted and concentrated reaction medium from a direct (*i.e.* non-mediated) electrochemical reduction of ethyl-4-nitrobenzoate (D). All spectra were obtained in CDCl₃.

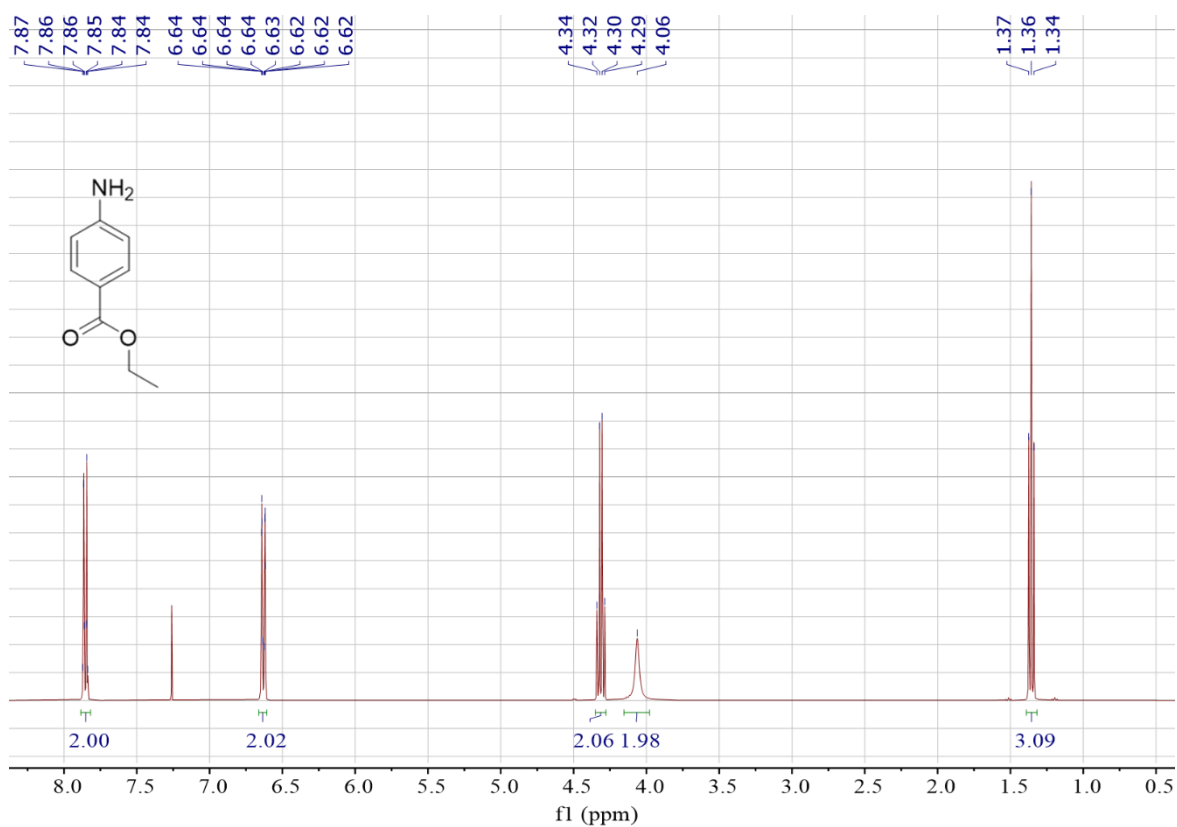


Figure 4.33: ¹H NMR (400 MHz, 298 K) spectrum of ethyl-4-aminobenzoate (Table 1, entry 7) from the electrocatalytic reaction medium after extraction, concentration, and purification. Spectrum was obtained in CDCl₃.

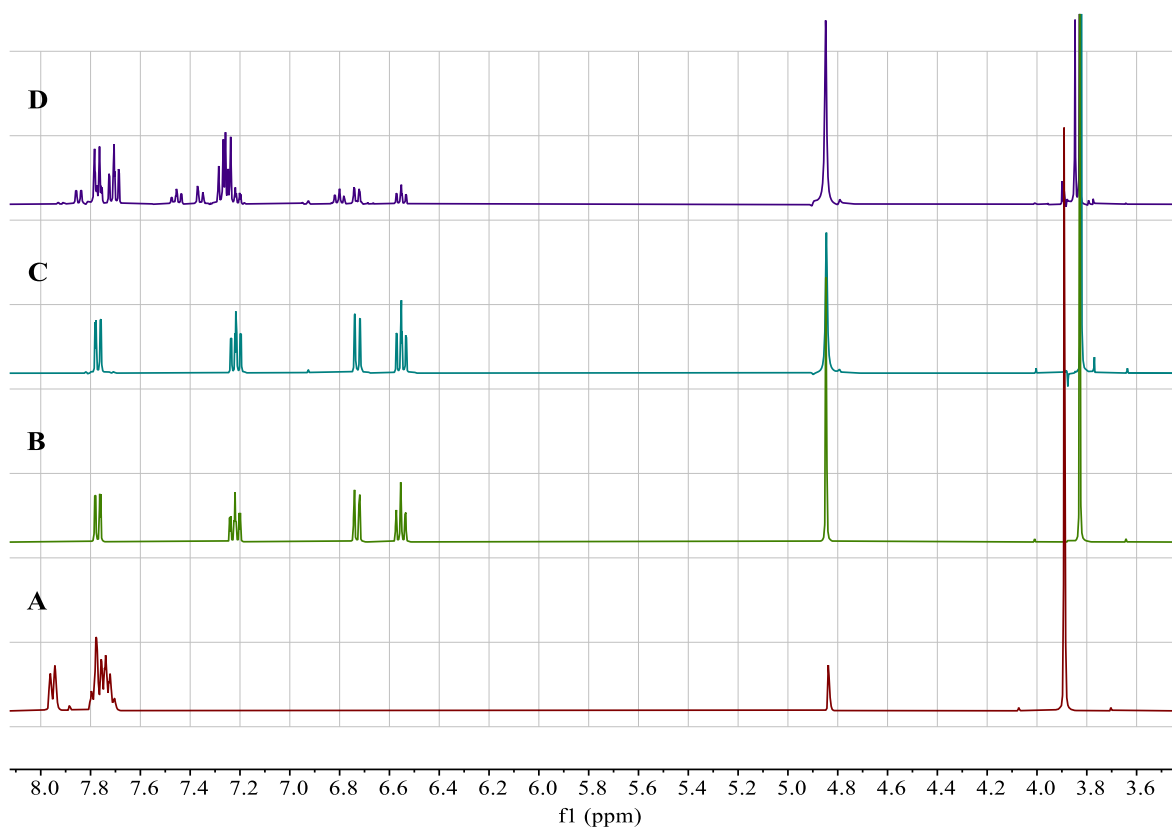


Figure 4.34: Reduction of methyl-2-nitrobenzoate. ¹H NMR spectra of the methyl-2-nitrobenzoate starting material (A), a sample of methyl-2-aminobenzoate (B), the spectrum of the electrocatalytic reaction medium after extraction and concentration (C) and the spectrum of the extracted and concentrated reaction medium from a direct (*i.e.* non-mediated) electrochemical reduction of methyl-2-nitrobenzoate (D). All spectra were obtained in MeOD.

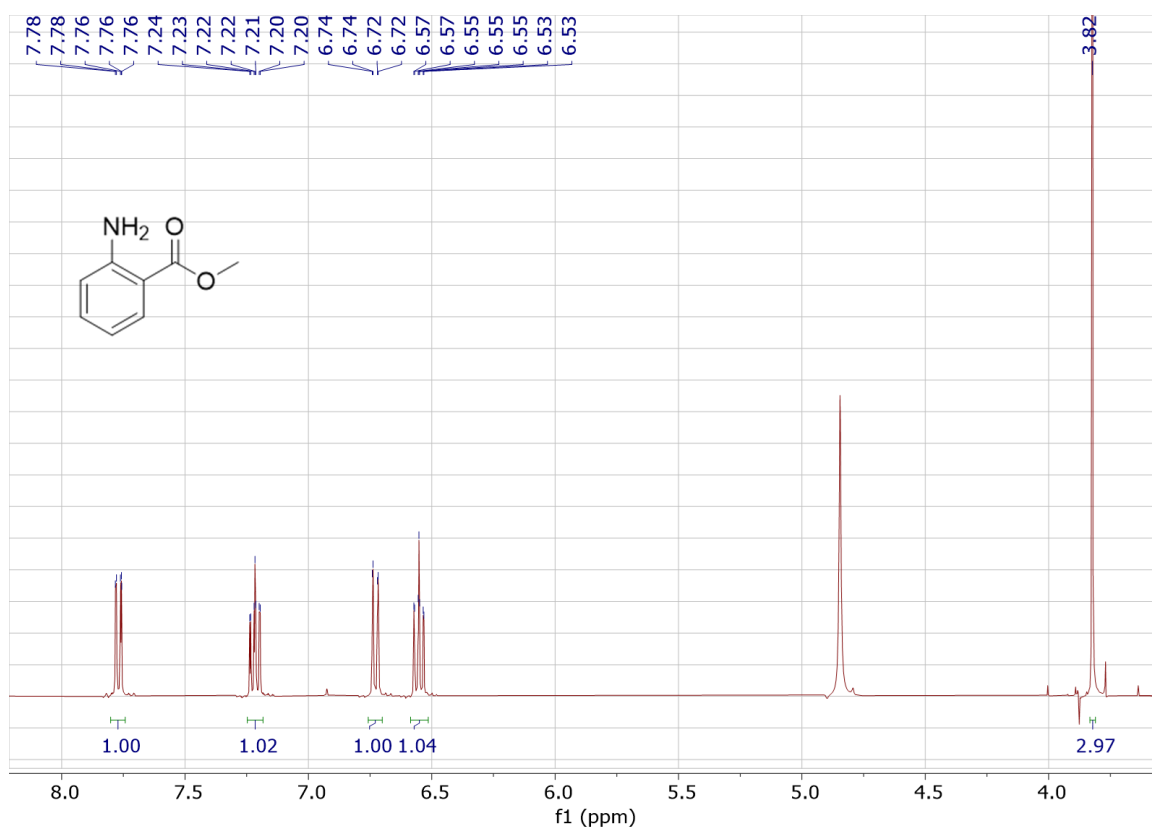


Figure 4.35: ¹H NMR (400 MHz, 298 K) spectrum of methyl-2-aminobenzoate (Table 1, entry 5) from the electrocatalytic reaction medium after extraction and concentration. The spectrum was obtained in MeOD. The peak at 4.8 ppm is due to water in the NMR solvent.

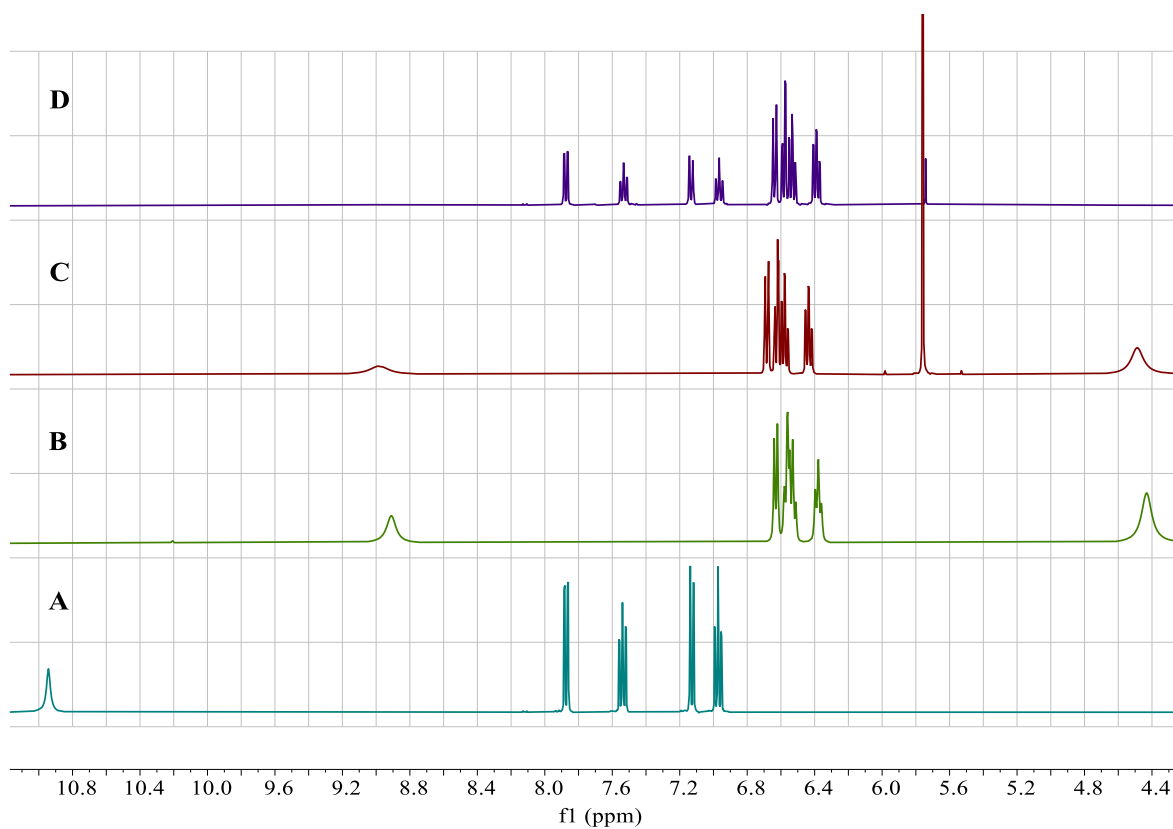


Figure 4.36: Reduction of 2-nitrophenol. ¹H NMR spectra of the 2-nitrophenol starting material (A), a sample of 2-aminophenol (B), the spectrum of the electrocatalytic reaction medium after extraction and concentration (C) and the spectrum of the extracted and concentrated reaction medium from a direct (*i.e.* non-mediated) electrochemical reduction of 2-nitrophenol (D). All spectra were obtained in DMSO-d₆.

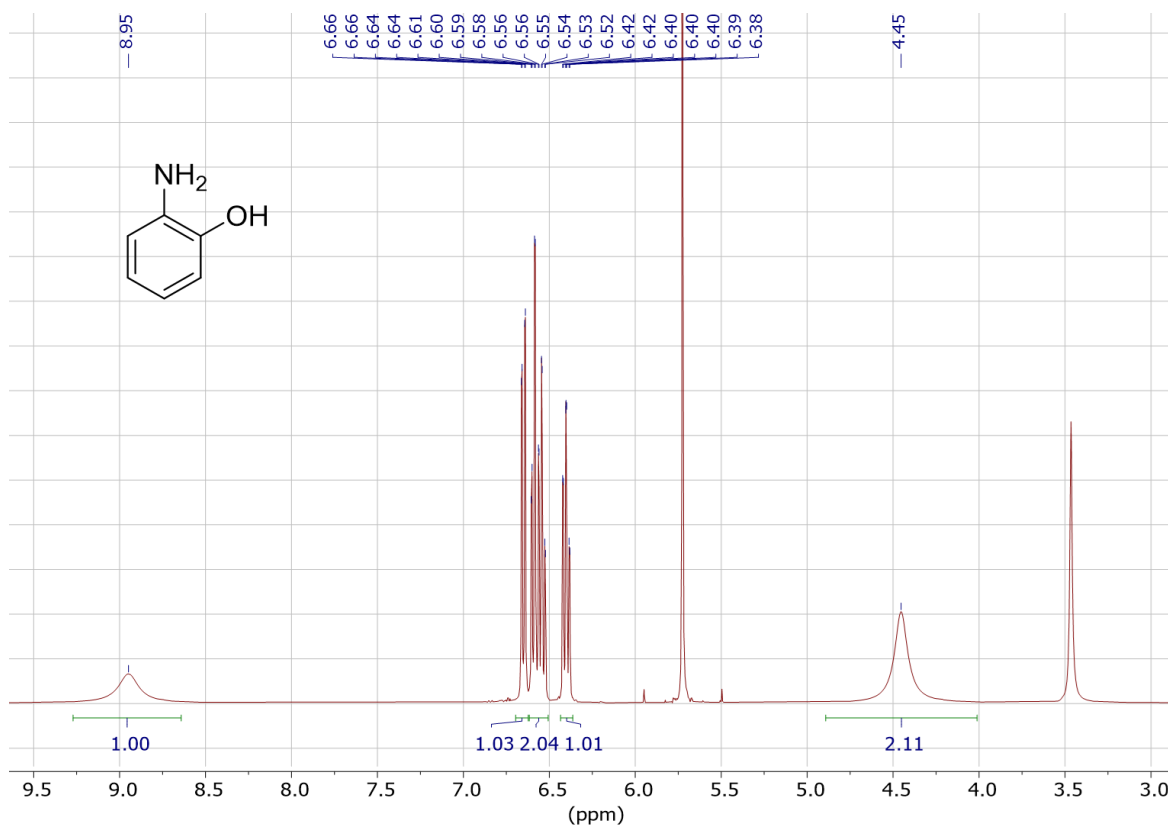


Figure 4.37: ^1H NMR (400 MHz, 298 K) spectrum of 2-aminophenol (Table 1, entry 1) from the electrocatalytic reaction medium after extraction and concentration. The spectrum was obtained in d_6 -DMSO. The peak at 3.5 ppm is water and the peak at 5.6 ppm is dichloromethane (from the extraction).

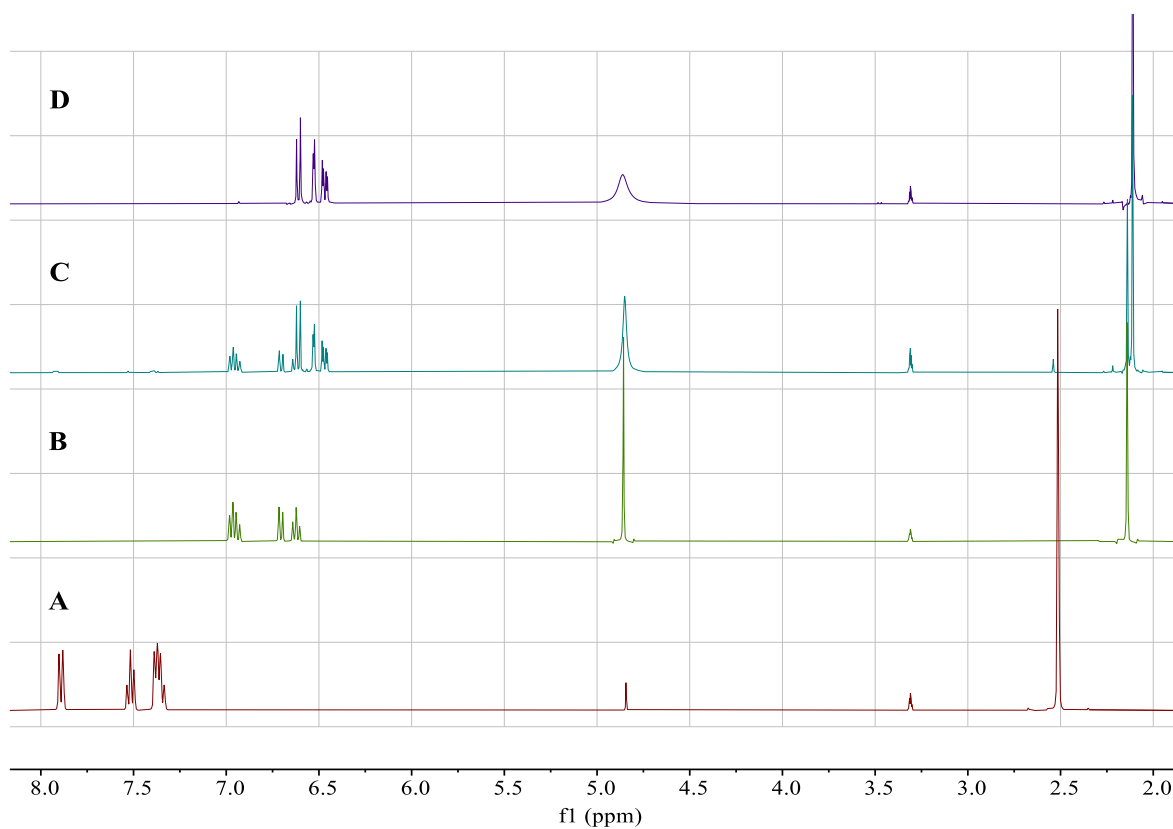


Figure 4.38: Reduction of 2-nitrotoluene. ¹H NMR spectra of the 2-nitrotoluene starting material (A), a sample of 2-aminotoluene (B), the spectrum of the electrocatalytic reaction medium after extraction and concentration (C) and the spectrum of the extracted and concentrated reaction medium from a direct (*i.e.* non-mediated) electrochemical reduction of 2-nitrotoluene (D). All spectra were obtained in MeOD.

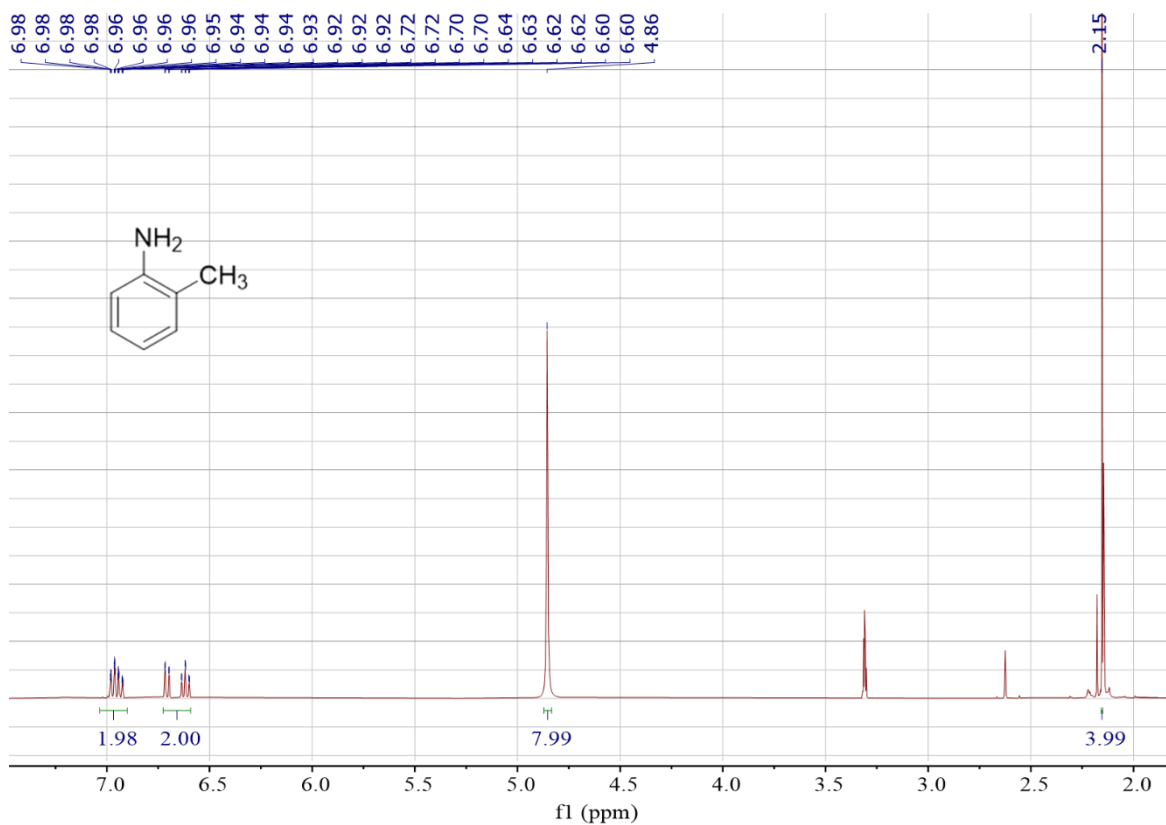


Figure 4.39: ^1H NMR (400 MHz, 298 K) spectrum of 2-methylaniline (Table 1, entry 3) from the electrocatalytic reaction medium after extraction, concentration, and purification. Spectrum was obtained in MeOD. The water peak at 4.8 ppm overlays the amine N-H peak.

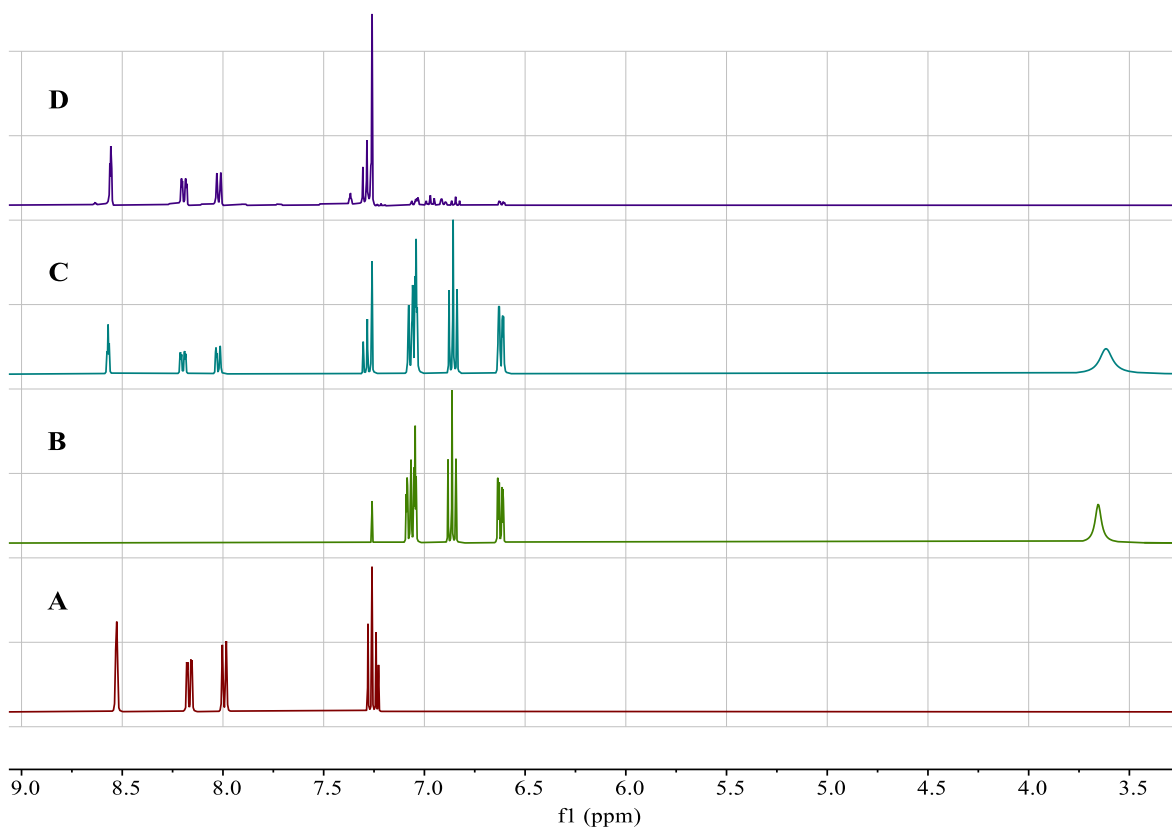


Figure 4.40: Reduction of 1-iodo-3-nitrobenzene. ¹H NMR spectra of the 1-iodo-3-nitrobenzene starting material (A), a sample of 3-iodoaniline (B), the spectrum of the electrocatalytic reaction medium after extraction and concentration (C) and the spectrum of the extracted and concentrated reaction medium from a direct (*i.e.* non-mediated) electrochemical reduction of 1-iodo-3-nitrobenzene (D). All spectra were obtained in MeOD.

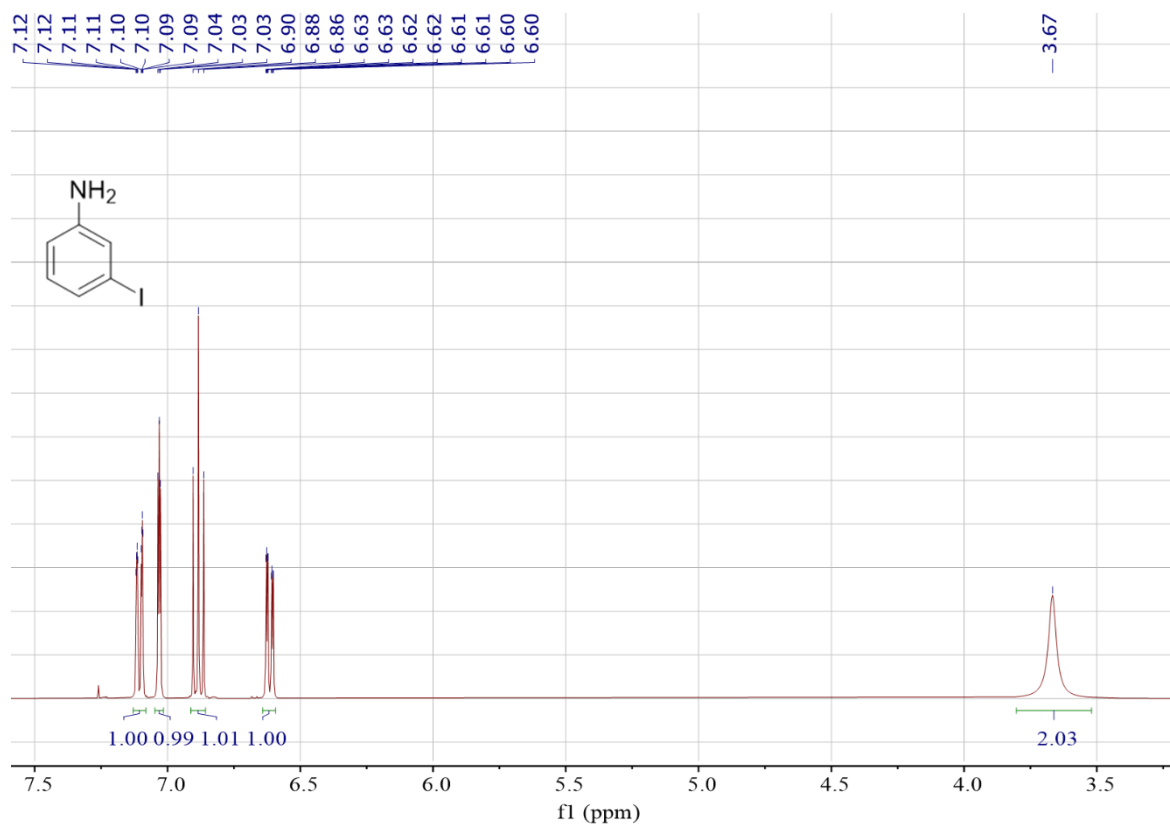


Figure 4.41: ^1H NMR (400 MHz, 298 K) spectrum of 3-iodoaniline (Table 1, entry 11) from the electrocatalytic reaction medium after extraction, concentration, and purification. Spectrum was obtained in CDCl_3 .

4.6 References

- 1 P. F. Vogt, J. J. Gerulis, *Ullmann's Encyclopedia of Industrial Chemistry*, Wiley-VCH Verlag GmbH & Co. KGaA., 2002.
- 2 H. K. Kadam, S. G. Tilve, *RSC Adv.*, 2015, 5, 83391-83407.
- 3 F. Ellis, Paracetamol: a curriculum resource, *Royal Society of Chemistry*, Cambridge, 2002, pp. 1-24.
- 4 A. S. Travis, *PATAI'S Chemistry of Functional Groups*, John Wiley & Sons, Chinchester, UK, 2009.
- 5 D. Formenti, F. Ferretti, F. K. Scharnagl, M. Beller, *Chem. Rev.*, 2019, 119, 2611-2680.
- 6 V. Pandarus, R. Ciriminna, F. Béland, M. Pagliaro, *Adv. Synth. & Catal.*, 2011, 353, 1306-1316.
- 7 M. Pietrowski, *Curr. Org. Synth.*, 2012, 9, 470-487.
- 8 P. Baumeister, H. U. Blaser, W. Scherrer, *Stud. in Surf. Sci. and Catal.*, 1991, 59, 321-328.
- 9 M. Sebek, H. Atia, N. Steinfeldt, *J. Flow Chem.*, 2021, 11, 333-344.
- 10 S. Gladiali, E. Alberico, *Chem. Soc. Rev.*, 2006, 35, 226-236.
- 11 E. Garcia-Verdugo, Z. Liu, E. Ramirez, J. Garcia-Serna, J. Fraga-Dubreuil, J. R. Hyde, P. A. Hamley, M. Poliakoff, *Green Chem.*, 2006, 8, 359-364.
- 12 M. V. Joshi, D. Mukesh, *J. Catal.*, 1997, 168, 273-277.
- 13 J. Marquez, D. Pletcher, *J. Appl. Electrochem.*, 1980, 10, 567-573.
- 14 W. H. Harwood, R. M. Hurd, W. H. Jordan, *Ind. Eng. Chem. Process. Des. Dev.*, 1963, 2, 72-77.
- 15 X. Chong, C. Liu, Y. Huang, C. Huang, B. Zhang, *Natl. Sci. Rev.*, 2019, 7, 285-295.
- 16 Y. Zhao, C. Liu, C. Wang, X. Chong, B. Zhang, *CCS Chem.*, 2021, 3, 507-515.
- 17 N. Daems, F. Risplendi, K. Baert, A. Hubin, I. F. J. Vankelecom, G. Cicero, P. P. Pescarmona, *J. Mater. Chem. A*, 2018, 6, 13397-13411.

- 18 X. Sheng, B. Wouters, T. Breugelmans, A. Hubin, I. F. J. Vankelecom, P. P. Pescarmona, *Appl. Catal. B: Environ.*, 2014, 147, 330-339.
- 19 Y.-P. Li, H.-B. Cao, C.-M. Liu, Y. Zhang, *J. Hazard. Mater.*, 2007, 148, 158-163.
- 20 X. Sheng, B. Wouters, T. Breugelmans, A. Hubin, I. F. J. Vankelecom, P. P. Pescarmona, *ChemElectroChem*, 2014, 1, 1198-1210.
- 21 C. Ravichandran, M. Noel and P. N. Anantharaman, *J. Appl. Electrochem.*, 1994, 24, 1256-1261.
- 22 N. Daems, J. Wouters, C. Van Goethem, K. Baert, C. Poleunis, A. Delcorte, A. Hubin, I. F. J. Vankelecom, P. P. Pescarmona, *Appl. Catal. B: Environ.*, 2018, 226, 509-522.
- 23 B. Wouters, X. Sheng, A. Boschini, T. Breugelmans, E. Ahlberg, I. F. J. Vankelecom, P. P. Pescarmona, A. Hubin, *Electrochim. Acta*, 2013, 111, 405-410.
- 24 Q. Zhang, Y. Liu, S. Chen, X. Quan, H. Yu, *J. Hazard. Mater.*, 2014, 265, 185-190.
- 25 A. D. Stergiou, M. D. Symes, *Cell Rep. Phys. Sci.*, 2022, 3, 100914.
- 26 E. B. Makovos, C. C. Liu, *Bioelectrochem. Bioenerg.*, 1986, 15, 157-165

Investigating the Electrochemical Reduction of Nitrite using Iron- Porphyrin Complexes

Acknowledgements and Declarations

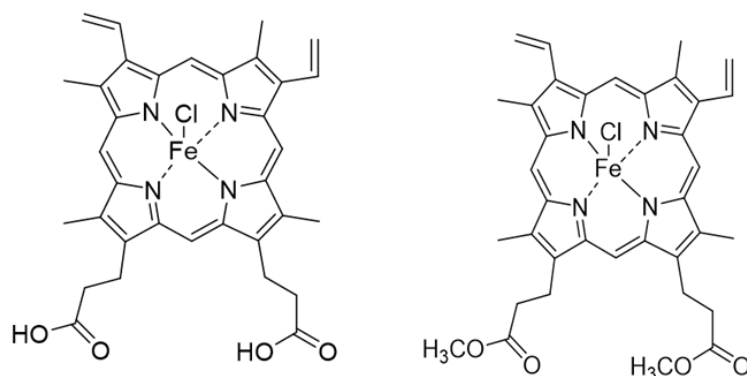
Athanasios Stergiou performed all experimental work for this chapter, except for the elemental analysis and the mass spectrometry experiments (performed by Dr Claire Wilson and Mr Gangi Reddy Ubbara respectively). Mark Symes conceived the idea and supervised the work.

Synopsis

NO_2^- , holds a central role in the nitrogen cycle and its reactions are of tremendous interest as they lead to commonly used compounds such as NH_3 . Symes group has previously examined the $1e^-$ reduction of nitrite to NO as well as the role of the proton-coupled-electron transfer (PCET) mechanism in the transformation. However, multi-electron NO_2^- transformations and the role of PCET in this system is yet to be examined. Designing a sustainable system to produce NH_3 would be of particular interest since ammonia is a widely used chemical especially in agriculture, and its current production using the Haber-Bosch process proceeds under harsh reaction conditions while fossil fuels are consumed to provide the H_2 gas required for the reaction.

In nature, these multi-electron transformations are mediated by enzymes containing haem-type units in their active sites. Therefore, complexes based on iron-porphyrin assemblies constitute a good starting point for the development of an artificial enzyme-mimicking system targeting the selective multi-electron reduction of NO_2^- to NH_3 and/or N_2 . The efficient reduction of these compounds will have an impact on the environment, through the purification of water by removal of $\text{NO}_2^-/\text{NO}_3^-$ which are particularly toxic for human life, as well as the utilisation of these pollutants to synthesise useful products.

In this chapter, we aim to design a catalytic system to selectively produce NH_3 and/or N_2 through the investigation the role of PCET. This will be achieved by comparing the catalytic efficiency of Fe-based porphyrins containing different types of units close to the active site of the catalyst. For this purpose, the electrocatalytic activity of hemin (left) and its methylated analogue dimethyl-hemin (right) will be examined.



By incorporating these units, we aim to tune the selectivity of our platform while obtaining insights into the reaction mechanism.

5.1 Introduction

5.1.1 Nitrogen Cycle

Nitrogen is the most abundant element in nature as it constitutes 78% of the atmosphere, even though one of the first names given to this element, azote, originates from the Greek word “αζωτικός” which means “without life”. Moreover, it constitutes the fourth most abundant element in living organisms behind only hydrogen, oxygen, and carbon making it essential for life.¹ In biology, nitrogen undergoes a great variety of oxidations and reductions that lead to important compounds in various oxidation states (from +5 in nitrate to -3 in ammonia).² N_2 itself is an inert molecule on account of its strong triple bond and therefore needs to be transformed to a more reactive form prior to its incorporation into larger molecules. This process is called nitrogen fixation with the most widespread route to be *via* its conversion to ammonia.^{1, 3} The constant alteration of nitrogen from the one oxidation state to the other, mediated by different natural systems is called the nitrogen cycle.² A schematic representation of the nitrogen cycle is depicted below (Figure 5.1), naming the main processes by which the organisms chemically convert nitrogen species from one form to another.¹ A closer inspection of the nitrogen cycle reveals the key role of the nitrogen oxides and their inter-conversions. Ammonia is particularly useful for organisms as it constitutes one of the starting building blocks for the synthesis of vital biological compounds such as amino acids and nucleotides.⁴

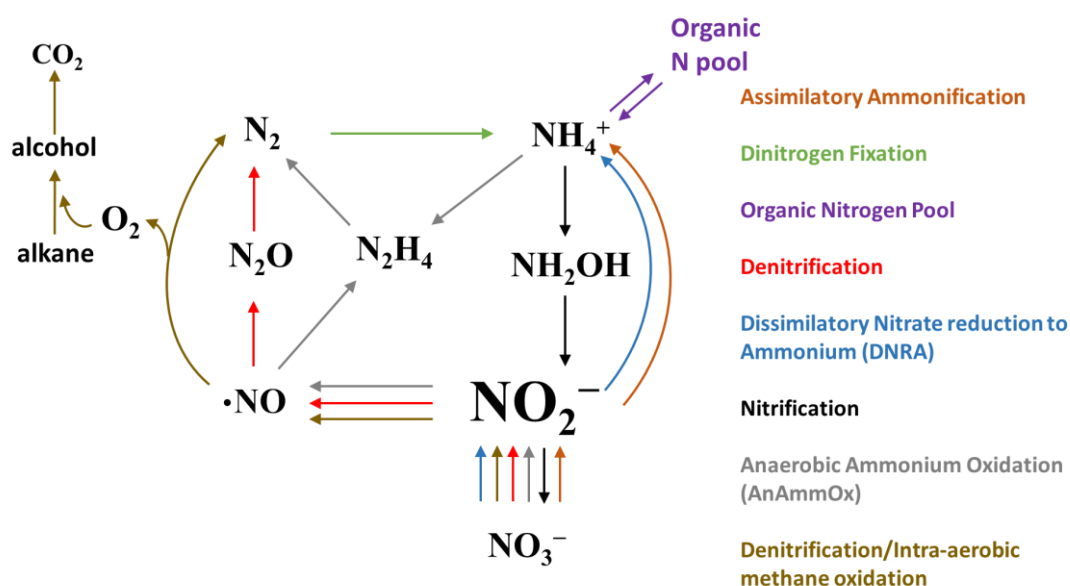
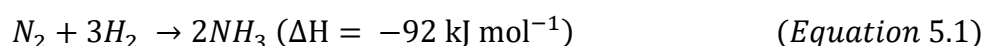


Figure 5.1: Schematic of the biochemical cycle of nitrogen. Redrawn from *Chem. Rev.*, **2014**, 114 (10), 5273.

In human life, nitrogen compounds, such as ammonia and hydroxylamine are of great economic value while they are produced in large amounts in industry. Moreover, ammonium nitrate is widely used in agriculture as a nitrogen-rich fertiliser,⁴ while other nitrogen compounds are present in major pharmacological drug classes including the antibiotics.⁵

Going back to nitrogen cycle, it is notable that nitrogen does not enter the cycle only through the fixation of N_2 to NH_3 but also in the form of nitrate.⁴ This is one of the main reasons why the nitrogen cycle has recently attracted increasing attention in the scientific world. The potential reuse of the polluting nitrate and nitrite, inserted into the biosystem through agricultural use, after the appropriate conversions would be of great environmental importance.⁶ In terms of pollution, a high concentration of nitrate in groundwater implies a serious threat to human health, and so its removal has become an emerging environmental concern.⁷ A report published by the environmental agency in 2005 highlights the importance of the reduction of nitrate (and nitrite) in the United Kingdom's groundwaters, as in some cases its concentration approaches the maximum limits set by the European Union.⁸

From the beginning of the last century, the increasing demand for nitrogen-containing products and especially ammonia, led to the development of industrial processes capable of large-scale synthesis of these compounds. The most significant of them is the Haber-Bosch process in which atmospheric dinitrogen (N_2) reacts with hydrogen (H_2) in the presence of an iron-based catalyst at high temperatures (400 – 450 °C) and pressures (200 atm) leading to the synthesis of ammonia (Equation 5.1).^{9, 10}



This discovery boosted the production of ammonia to the extent that nowadays half of global food production relies on synthetic fertilizers. Although Haber-Bosch is a very energy intensive process as energy demand during the process is at least 30 GJ/tonne of ammonia produced which is equal to about 1% of the global primary energy supply, it is still the primary method of ammonia production in industry. Moreover, 2.16 tonne CO_2 per tonne NH_3 (1.2% of the total anthropogenic CO_2 emissions) are emitted during the process having a significant contribution to global greenhouse gas emissions together with the extensive use of fossil fuels as the source of hydrogen.¹⁰⁻¹² Based on the above, the development of environmentally friendly processes or the utilization of renewable energy for the current process is of tremendous interest.

5.1.2 Role of Nitrite in Nitrogen Cycle

In the nitrogen cycle (Figure 5.1), the central role of nitrite as one of the key intermediates leading to the synthesis of many nitrogen products, is highlighted.¹ Despite the fact that it is one of the most reactive species in the nitrogen cycle, it shows a significant toxicity for the human beings as, for example, it appears to be the main cause of blue baby syndrome.⁴ In natural systems, enzymes are involved to access these inter-conversion reactions. Figure 5.2 provides an overview of the processes mediated by enzymes where nitrite is converted to other nitrogen-containing products.^{1,3}

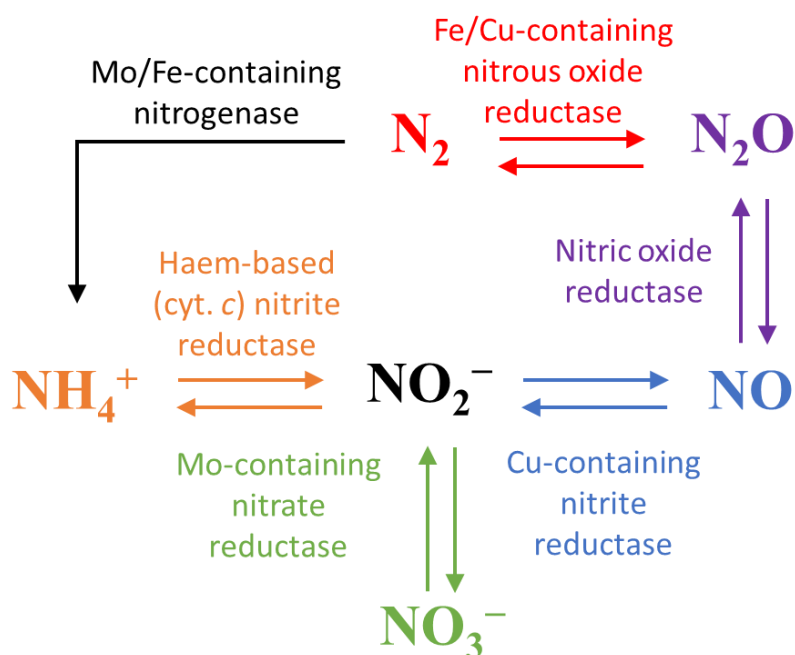


Figure 5.2: Schematic highlighting the central role of nitrite among the different products in the nitrogen cycle. Redrawn from *Chem. Soc. Rev.*, **2015**, 44, 6708.

Most of the reactions of nitrite catalysed by enzymes are multi-electron reduction processes as we can see in the following table, which also contains details about the specific enzymes catalysing each process as well as their standard redox potential vs NHE (Table 5.1). Thermodynamically, the preferable conversion is the reduction of nitrite (NO_2^-) to dinitrogen (N_2).^{1,4}

Well noted is the fact that these conversions rely on the coupled movement of protons and electrons to/from nitrogen species bound in a well-defined ligand environment as it has been stated in previous studies.¹³⁻¹⁶ Despite its importance, studies of the mechanism(s) of proton-

coupled-electron transfer (PCET)¹⁷ on the multi-electron transformations are to the best of our knowledge lacking, limiting the optimisation of artificial enzyme-mimicking systems.

Table 5.1: Biological nitrite conversions and the class of enzyme responsible.

Reaction	Enzyme, Metal on the active site	E° red/ox vs. NHE
$\text{NO}_2^- + 6e^- + 8\text{H}^+ \rightleftharpoons \text{NH}_4^+ + \text{H}_2\text{O}$	Cyt. <i>c</i> nitrate reductase, Fe	+0.897 V
$\text{NO}_2^- + 1e^- + 2\text{H}^+ \rightleftharpoons \text{NO} + \text{H}_2\text{O}$	Cu nitrite reductase, Cu	+1.202 V
$2\text{NO}_2^- + 6e^- + 8\text{H}^+ \rightleftharpoons \text{N}_2 + 4\text{H}_2\text{O}$	Cyt. cd1 nitrite reductase, Fe	+1.52 V
$\text{NO}_3^- + 2e^- + 2\text{H}^+ \rightleftharpoons \text{NO}_2^- + \text{H}_2\text{O}$	Nitrate reductase, Mo	+0.84 V

5.1.3 Proton Coupled Electron Transfer (PCET)

As the study of the effects of proton-coupled-electron transfer mechanisms is one of the key concepts in the ongoing research, it is important to highlight the main characteristics of this process. In nature, PCET has an important role in various key enzymatic pathways like photosynthesis, respiration and DNA repair.¹⁷ Moreover, as we mentioned earlier, it is found that PCET has its principles applied in other enzymatic pathways such as the catalytic reduction of nitrite and nitrate by nitrite and nitrate reductases respectively.¹⁷ On these grounds, PCET has attracted a lot of scientific interest in the recent years.

Before examining the development of a catalytic system mimicking the enzymatic process for the reduction of nitrite, the three different pathways of a reaction involving proton and electron transfer should be mentioned.¹⁸ A summary of these processes is presented in Figure 5.3.

- **Electron-Proton Transfer (EPT)** where electron transfer (ET) precedes the proton transfer (PT).
- **Proton-Electron Transfer (PET)** where proton transfer (PT) precedes the electron transfer (ET).
- **Concerted Proton-Electron Transfer (CPET)** where proton and electron transfer are concerted.

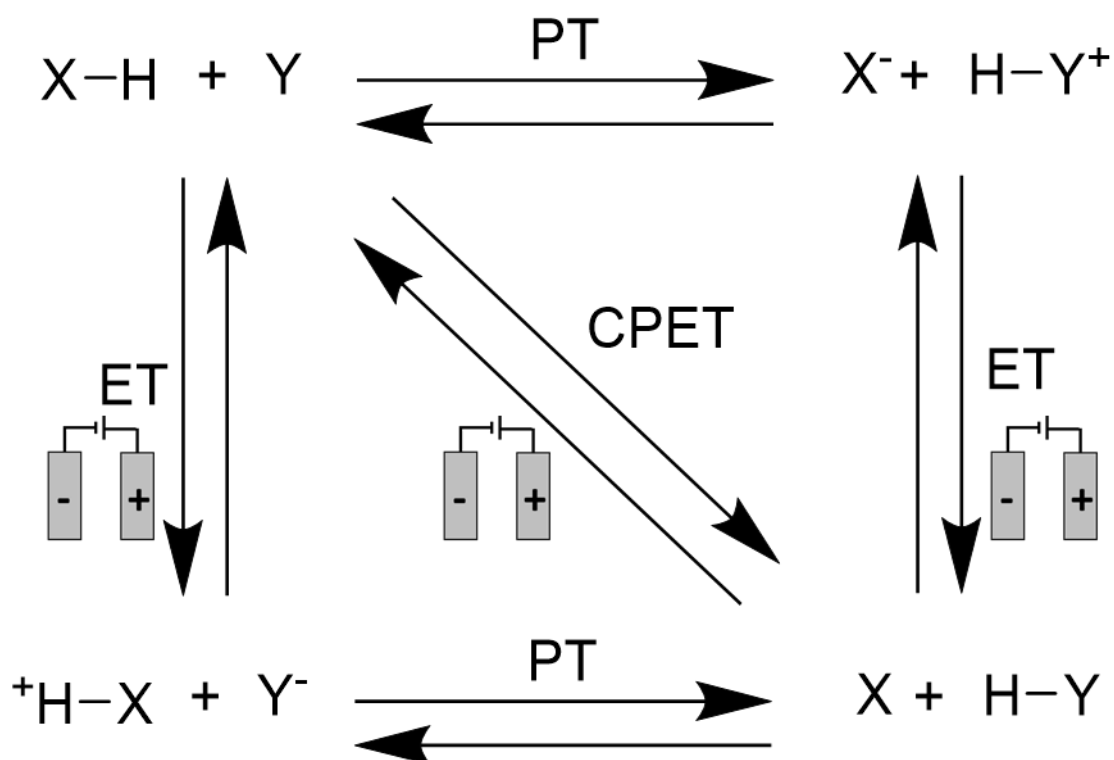


Figure 5.3: Schematic illustration of the different pathways of the electron and proton transfer in electrochemical systems. Electron transfer (ET), proton transfer (PT), concerted proton-electron transfer (CPET). The electrochemical steps are stated with the electrochemical cell. Redraw from *Acc. Chem. Res.*, **2010**, 43(7), 1019.

Although the exact mechanism(s) of PCET in these enzymatic processes is still under investigation from the research community, it is definite that CPET principles are applied to these enzymatic processes to avoid the formation of high-energy intermediates and to enable enzyme turnover.¹⁷

Electrochemical PCETs are attracting increasing attention because changing the electrode potential in an electrochemical system is an easy way to vary the driving force of the reaction while measuring the current through the electrodes is a direct measurement of the reaction's rate (including the diffusion of various species to or from the electrode). Using techniques such as cyclic voltammetry, we can get an activation-driving force relationship for the reaction. Properties at zero driving force are therefore a natural outcome of the electrochemical approach.^{18, 19} The effect of the pH on the redox potential in aqueous solutions during a proton-electron transfer has also been exploited.¹⁸ These studies provide information about the region in which the redox processes are influenced by the pH of the electrolyte as well as the conditions at which the CPET operates.

Metal complexes have been electrochemically studied to examine the effect that different functional groups have on PCET mechanisms in particular reactions such as O-O bond activation,²⁰ H₂ generation from weak acids²¹ and NO₂⁻ reduction to NO.²² In the two latter cases, the implementation of a proton-related moiety in close proximity to the metal centre of the complexes has shown tremendous improvement of the catalytic process compared with the complexes that lack such functionality, highlighting the key role of PCET and particularly CPET in the activation of the molecules under study.^{21, 22}

Despite its importance, no systematic studies of PCET in analogues of the enzymes containing iron in their active sites for nitrite conversion have to the best of our knowledge yet been performed. This lack of understanding prevents the development of artificial platforms mimicking the enzymatic processes, able to perform such multi-electron transformation in a more environmentally friendly and energy efficient way.

5.1.4 Iron Porphyrins for the Electrochemical Reduction of Nitrite

In nature, the dominant class of enzymes responsible for the multi-electron reduction of nitrite to NH₃ or N₂ (6 e⁻ processes in both cases, see table 5.1) contains a haem (iron porphyrin) unit as its functional core. The enzymes that catalyse the reduction of nitrite into these products in the nitrogen cycle are the cytochrome *c* (CcNiR) and cytochrome cd₁ (cd1NiR) nitrite reductase, respectively. Cytochrome cd₁ contains two haems per subunit,²³ while cytochrome *c* contains five covalently attached *c*-type haems per subunit.²⁴ Cytochrome *c*, which is the best characterised haem based system, can efficiently catalyse the six-electron reduction of nitrite to ammonia without the release of any detectable reaction intermediate, such as NO.^{3, 24} Neese and co-workers proposed a mechanism in which cytochrome *c* nitrite reductase mediates this process, based on crystallographic studies of the intermediates as well as DFT calculations (Figure 5.4).²⁵ The mechanism involves two proton-coupled-electron transfer steps while at the end of the cycle, the product is released in the form of ammonium allowing the enzyme to enter the next catalytic cycle.²⁵ From the above information, a porphyrin complex containing iron as its metal centre can be a good starting point for the development of a catalytic system which can effectively bind and then reduce nitrite to NH₃, N₂ or even NO under mild experimental conditions and a cost-effective manner.

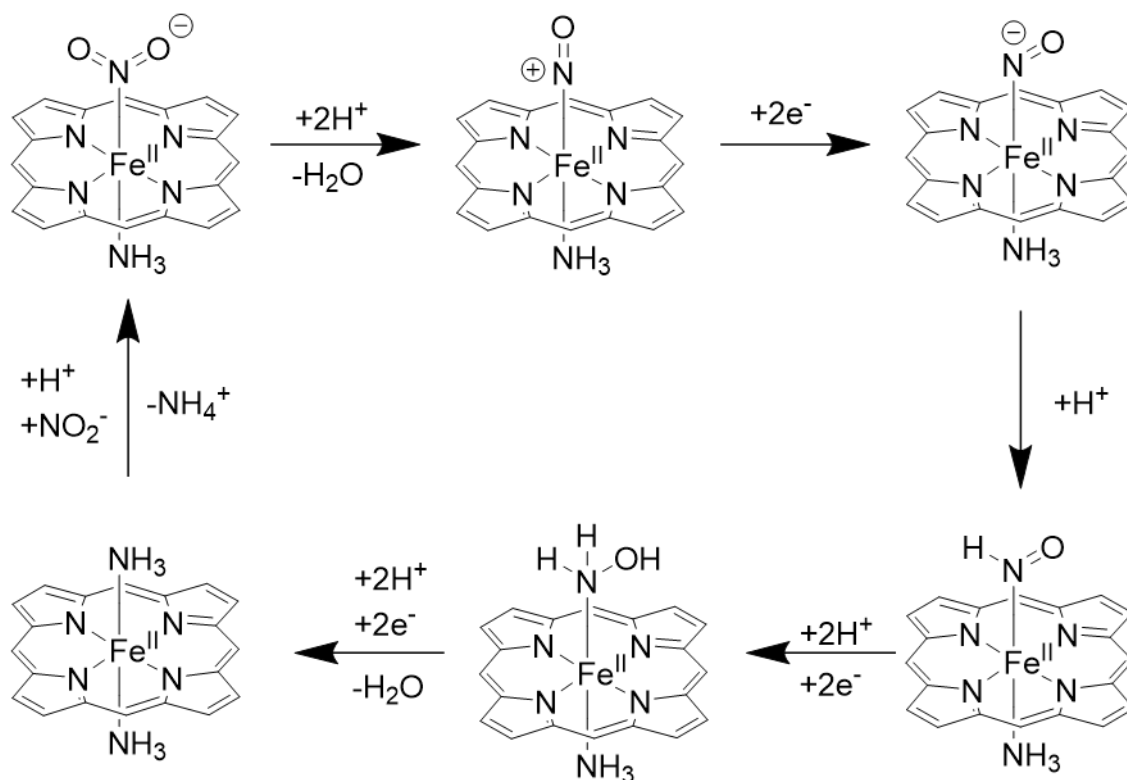


Figure 5.4: Mechanism of nitrite reduction by cytochrome *c* nitrite reductase (CcNiR) according to Neese and co-workers. Reproduced from *Chem. Soc. Rev.*, **2015**, 44, 6708.

The development of synthetic strategies mimicking enzymatic processes have attracted a lot of interest in the past years, as an alternative to the current methods. In the concept of nitrite and/or nitrate reduction, utilizing the knowledge we have from the enzymatic processes into an artificial catalytic system, will positively affect two main sectors. At first, by providing an environmentally friendly and energy/cost efficient alternative to the Haber-Bosch process for the synthesis of ammonia. Second, the purification of groundwaters from nitrite/nitrate and their potential reuse in the form of other useful nitrogen products, will have a significant environmental and economic impact. Systems utilising the knowledge we have from nature have been developed in the past,^{14, 26-33} however they have certain limitations which will be briefly discussed below.

In the early days, Meyer and co-workers used a water-soluble iron porphyrin in mildly acidic aqueous conditions to electrochemically reduce nitrite to ammonia, with significant amounts of hydroxylamine and N₂O also present as reaction by-products.²⁶ More recently, the 1e⁻ electrochemical reduction of nitrite to NO was examined using iron-based porphyrins, providing significant mechanistic studies. However, no multi-electron mechanistic studies were performed.^{27, 28} In 2009, Koper et al., used a heme-modified pyrolytic graphite (PG)

electrode, in a range of aqueous solutions from acidic (pH 1.7) to neutral (pH 7), to investigate the reduction of nitrite. The reactivity of the catalytic system was found to be largely pH-dependent, with a decreasing activity of the system in neutral solution. However, the dominant product was the hydroxylamine with various other nitrogen products to be detected, yet no ratios were stated.²⁹

5.2 Aim of the Project

The effective $1e^-$ reduction of the nitrite anion (NO_2^-) to nitric oxide (NO) via the use of a Cu complex and the investigation of the PCET mechanism in that conversion has been previously studied by the Symes group.²² In the present work, we aim to move a step forward by the synthesis and interrogation of systems for the multi-electron reduction of nitrite to NH_3 and/or N_2 . Complexes based on iron-porphyrins are promising starting points for such catalysts for reasons that have been analysed before. As we mentioned earlier, previous studies have shown that iron-porphyrins can be effective catalysts for the reduction of nitrite^{14, 26-30, 32, 33}, however, studies of PCET in this system are to this day lacking. Moreover, in studies to date, product specificity was a major issue with the ratios of $\text{N}_2 : \text{NH}_3 : \text{N}_2\text{H}_4$ found to vary widely while the efficiency of the electrochemical process was quite poor.

By examining PCET mechanisms in this kind of system, we are aiming to tune the reactivity of our system towards the formation of a single reduction product. The selective generation of any of these species, coming from the multi-electron process, will constitute a great improvement to the current processes.

To perform these studies, we chose to use hemin, which is a readily available iron-porphyrin complex. The study of the PCET mechanism will involve the comparison of the electrocatalytic activity of this complex with that of its methylated form, the dimethyl-hemin. The structures of the two complexes are presented below (Figure 5.5).

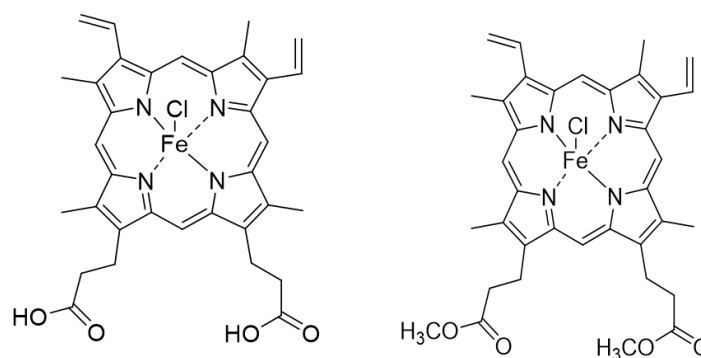


Figure 5.5: **Left:** Chemical structure of Hemin, **Right:** Chemical structure of Dimethyl-hemin.

As we can observe from the chemical structures of the two complexes, hemin has a carboxylic acid group in its secondary coordination sphere while dimethyl-hemin lacks such functionality. The presence of this proton-relaying unit was found to have a direct effect on the catalytic activity in the previously examined Cu complexes, as it was proven to switch on the catalysis.²² Herein, using the same principles, we aim to obtain insight into the role of PCET on the multi-electron reduction of nitrite.

5.3 Experimental Part

5.3.1 General Experimental Remarks

Tetrabutylammonium hexafluorophosphate (>98%) was purchased from both Tokyo Chemical Industry and Sigma Aldrich. Trimethyl orthoformate (99%), sulfuric acid (99.5%), sodium hydroxide (98%), tetrabutylammonium nitrite ($\geq 97\%$), phenol ($\geq 99\%$) and benzoic acid (99.5%) were purchased from Sigma Aldrich. Dichloromethane (99.5%) and magnesium sulfate was purchased from VWR. Ferrocene (99+%) was purchased from Thermo Scientific. Methanol was purchased from Fisher Scientific. Dimethyl sulfoxide ($\geq 99\%$) and hemin from porcine (97%) was purchased from Alfa Aesar. All chemical reagents were used as purchased.

The aqueous solutions were prepared with ultrapure deionised water (18.2 M Ω -cm resistivity), obtained from a Sartorius Arium Comfort combined water system. pH determinations were made with a Hanna HI 9025 waterproof pH meter. Experiments performed at “room temperature” were carried out at 25 °C.

5.3.2 General Electrochemical Methods

Electrochemical studies were performed in a three-electrode configuration using a CH Instruments CHI600D potentiostat. A glassy carbon button electrode (area = 0.071 cm²) was used as the working electrode, an Ag/AgNO₃ was used as pseudo-reference electrode and a graphite rod (>99.9995) purchased from Alfa Aesar, was used as the counter electrode. Glassy carbon working electrodes were polished using polishing powder and then washed with acetone and deionized water prior to use. Graphite rod counter electrodes were polished with polishing paper and then sonicated for about 5 min with water and acetone respectively.

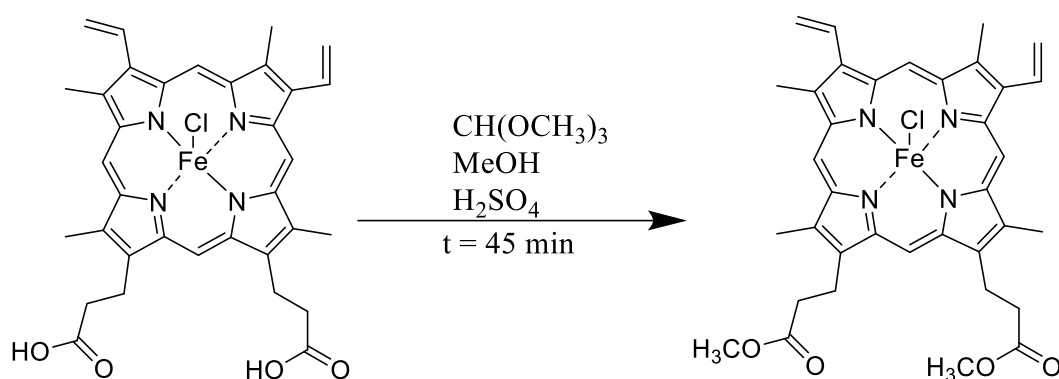
5.3.3 Cyclic Voltammetry

Cyclic voltammograms were collected in single chamber cells using a typical three-electrode set-up at room temperature and a scan rate of 100 mV/s in 0.1 M TBAPF₆ DMSO electrolyte. The solvent (10 mL) was thoroughly degassed with N₂ prior to the experiments and kept under inert atmosphere throughout the process. The electrochemical cell was sealed with parafilm to maintain the oxygen-free atmosphere. To this electrolyte, 2×10^{-5} moles of the relevant complex was added (concentration = 2 mM) and subsequently the stated equivalents in moles of the nitrite source (1-50 equivalents) and benzoic acid or phenol (1-20 equivalents) were added. The cyclic voltammograms are calibrated vs Fc⁺/Fc redox couple since a pseudo-reference electrode was used. Measurements were conducted without stirring and with *iR* compensation enabled.

5.4 Results and Discussion

5.4.1 Synthesis of Dimethyl Hemin

The synthesis of dimethyl hemin was performed following the method described by Byrne and Ward.³⁴ In this one-step process, 200 mg of hemin were added in a 50 mL round-bottom flask containing 10 mL of trimethyl orthoformate and 10 mL methanol, while 2 mL of concentrated sulfuric acid were added in drops with cooling to room temperature. The reaction mixture was stirred in room temperature for 1 h. After the reaction was completed, the mixture was diluted with an equal amount of H₂O (20 mL) and the pH was adjusted at 4.5 using 1 M aqueous NaOH. The mixture was then extracted with DCM (3 × 50 mL) and the organic extracts were washed with H₂O (3 × 50 mL). Magnesium sulfate was added to remove any traces of water from the organic extracts and subsequently the solvent (DCM) was evaporated under reduced pressure. The product was left overnight under high vacuum until it was completely dry. The reaction scheme is depicted below (Scheme 5.1).



Scheme 5.1: One step transformation of hemin to obtain the desired methylated substitute, dimethyl-hemin, at room temperature.

The isolated yield of the process was calculated to be $87\pm 2\%$ (187 mg obtained mass). The successful synthesis of dimethyl-hemin was confirmed by mass spectrometry (MS) and elemental (CHN) analysis. Mass spectrum: ESI-QTOF (acetonitrile/water 70/30% with 0.1% formic acid): $m/z = 644$ $[M]^+$ (calcd. for $C_{36}H_{36}FeN_4O_4$; 644.21). Moreover, the fragment at $m/z = 571$ corresponds to the loss of $CH_2CO_2CH_3$.³⁵ Anal. Calcd for $C_{36}H_{36}ClFeN_4O_4$: C, 63.59; H, 5.34; N, 8.24. Found: C, 64.02; H, 5.44; N, 7.86. The purity of the synthesized product was also tested with thin-layer chromatography (TLC) using a solvent system of Hexane : Chloroform : Methanol (1:1:0.3) where a single spot was obtained. The R_f values for hemin and dimethyl-hemin are 0.29 and 0.76, respectively.

5.4.2 Electrochemical Investigation of the Two Complexes

As it has already been stated, the electrochemical experiments were performed in a DMSO electrolyte, since this was the only solvent able to dissolve both complexes and at the same time provide useful electrochemical data. According to the literature, upon addition of the Fe complex in the electrolyte solution, DMSO coordinates in an axial orientation to the metal centre displacing the chloride ligand.³⁶ Moreover, the inert atmosphere should be maintained throughout the experiments since molecular oxygen can effectively displace a DMSO molecule to form a hemin-oxygen adduct. The coordinated oxygen can then be reduced to superoxide, its one-electron reduction product, making the cyclic voltammogram more complex, while it also consumes the electron from the Fe^{III}/Fe^{II} redox couple.³⁶ These findings

were also confirmed by our experiments, therefore a well-sealed electrochemical cell was necessary.

The cyclic voltammograms of hemin and its methyl-substituted complex are depicted in Figures 5.6 and 5.7, respectively.

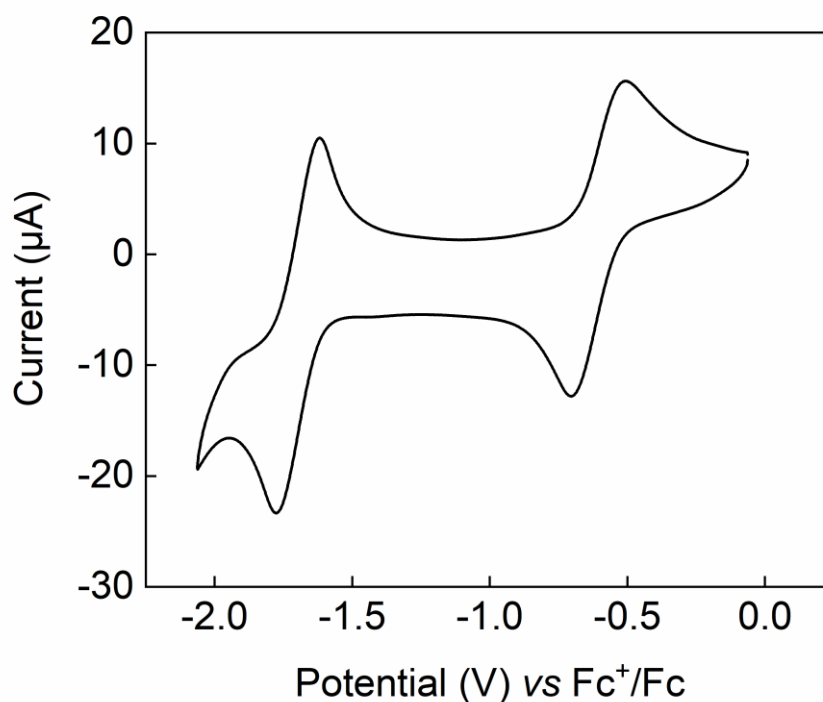


Figure 5.6: Cyclic voltammogram of Hemin (concentration = 2 mM) obtained in 1 M TBAPF₆ DMSO electrolyte, using a glassy carbon working electrode, a Ag/AgNO₃ reference electrode and a graphite rod counter electrode. Scan rate 100 mV/sec.

The first reversible wave occurring at the half potential $E_{1/2} = -0.605$ V vs Fc⁺/Fc can be attributed to the one-electron redox couple Fe^{III}/Fe^{II} while the second reversible wave occurring at $E_{1/2} = -1.7$ V vs Fc⁺/Fc can be attributed to the one-electron redox couple Fe^{II}/Fe^I.³⁰

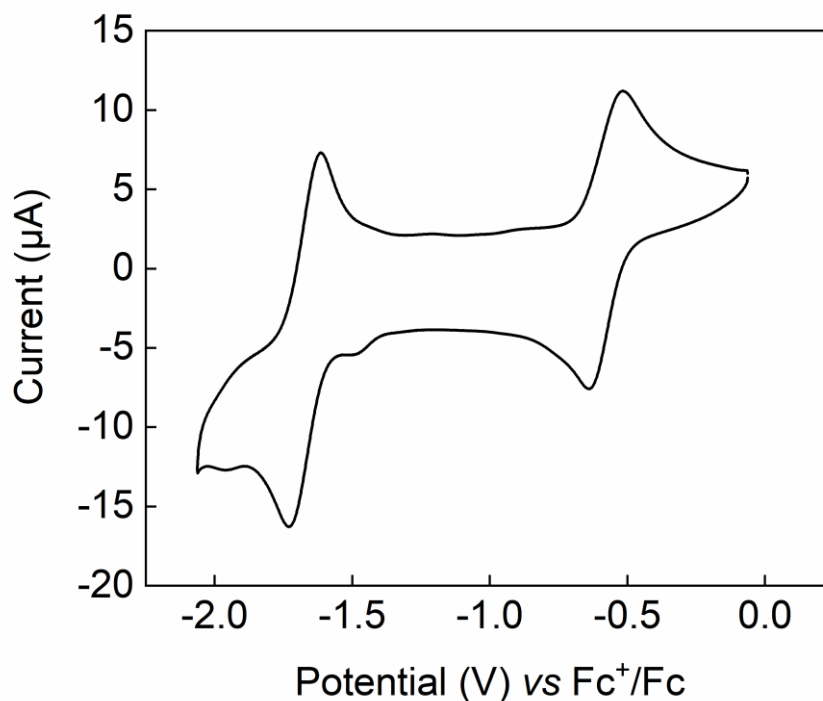


Figure 5.7: Cyclic voltammogram of Dimethyl-hemin (2 mM) obtained in 1 M TBAPF₆ DMSO electrolyte, using a glassy carbon working electrode, a Ag/AgNO₃ reference electrode and a graphite rod counter electrode. Scan rate 100 mV/sec.

Similar to what we have seen in the hemin complex, the reversible redox waves at half potential $E_{1/2} = -0.575$ V vs Fc⁺/Fc and $E_{1/2} = -1.665$ V vs Fc⁺/Fc, can be attributed to the Fe^{III}/Fe^{II} and Fe^{II}/Fe^I couples respectively. From Figures 5.6 and 5.7 a small shift in the redox waves to less negative potentials is noticeable upon the esterification of the carboxylic acid group, which might be attributed to the difference in the electron-withdrawing effect of the two groups; however, the difference of 30 mV for the first redox couple and 35 mV of the second redox couple is within the margin of error of a cyclic voltammogram that is up to 40 mV.

5.4.3 Addition of the Nitrite source

The coordination of nitrite to the iron centre of the complex was tested in the hemin complex using mass spectrometry, where the dominant peak found at $m/z = 646.20$ can be attributed to the hemin-NO complex. MS: ESI (negative polarity)-QTOF (acetonitrile/water 70/30% with 0.1% formic acid), $m/z = 646.20$ (calcd. for C₃₄H₃₂FeN₅O₅; 646.18). As we have discussed before, for catalysis to occur by these species, the coordination of nitrite at the

metal center is necessary. Moreover, validation of the coordination of nitrite in the iron center of the hemin complex in the solution phase through mass spectrometry, can support our hypothesis that the obvious difference in the cyclic voltammetry of the two complexes (Figure 5.10) is related to the structural difference of the two complexes. Finally, as we explain below, it does also supports the findings of the cyclic voltammograms that the small shift in the reduction potential of the two complexes is the result of nitrite coordination at the metal center.

Following the successful coordination of nitrite to the iron centre of the complex, cyclic voltammograms were collected in the presence of various mole equivalents of the nitrite source. The findings are presented in Figures 5.8 and 5.9 for the hemin and the dimethyl-hemin complex respectively.

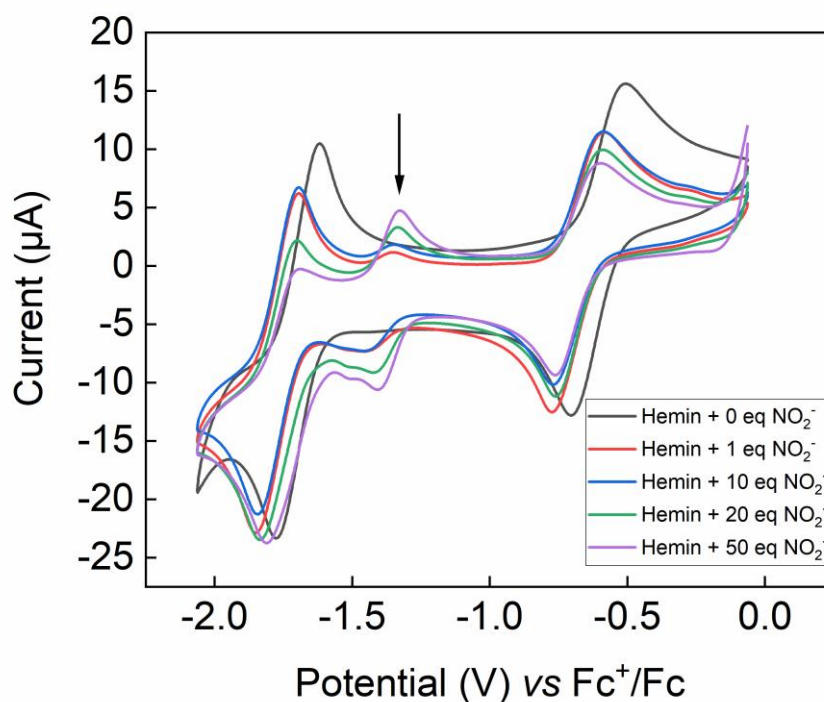


Figure 5.8: Cyclic voltammogram of hemin (2 mM) with addition of increasing equivalent moles of TBANO₂ salt, obtained in 1 M TBAPF₆ DMSO electrolyte, using a glassy carbon working electrode, a Ag/AgNO₃ reference electrode and a graphite rod counter electrode. Scan rate 100 mV/sec. The formation of a new redox wave is highlighted with the arrow.

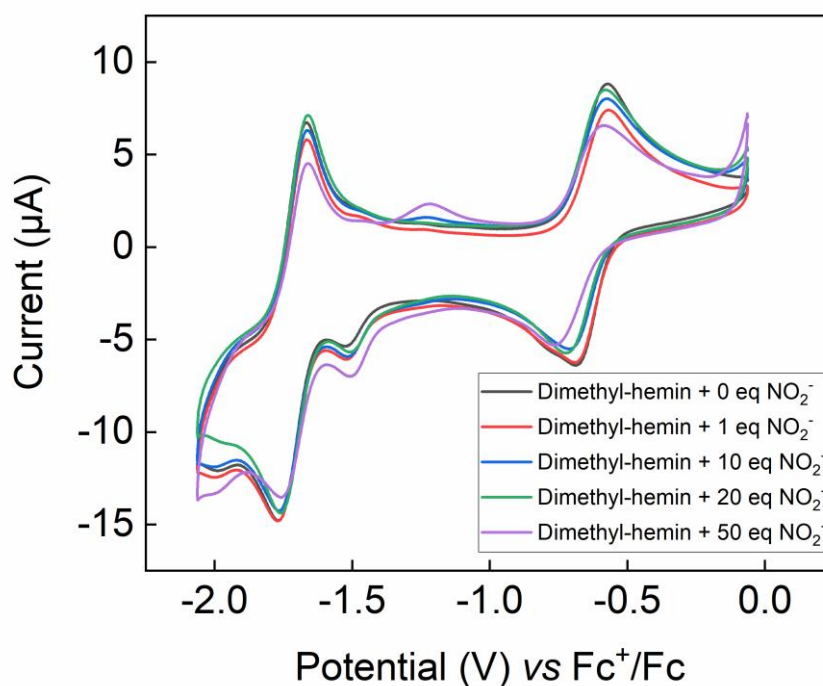


Figure 5.9: Cyclic voltammogram of dimethyl-hemin (2 mM) with addition of increasing equivalent moles of TBANO₂ salt, obtained in 1 M TBAPF₆ DMSO electrolyte, using a glassy carbon working electrode, a Ag/AgNO₃ reference electrode and a graphite rod counter electrode. Scan rate 100 mV/sec.

As we can observe from figures 5.8 and 5.9, the two complexes present a completely different behaviour after the addition of nitrite. In the case of the hemin complex, that has a carboxylate group in its secondary sphere, a third redox wave is formed at a half potential of $E_{1/2} = -1.365$ V vs Fc⁺/Fc (pointed out by the arrow in figure 5.8), while no such wave is observed in the case of the ester substituted hemin (dimethyl-hemin). However, a small oxidation peak is formed at around the same potential $E = -1.227$ V vs Fc⁺/Fc notable only upon the addition of 50 equivalents NO₂ (Figure 5.9). There is no evidence that this oxidation is related to nitrite addition, since it does not increase when more mole equivalents were added to the solution (data not shown). Note that the small reduction peak at -1.5 V in dimethyl-hemin is present in the cyclic voltammogram of the native complex (see Figure 5.7) and therefore there is no evidence of the formation of a reversible redox wave. It is possible that this reduction is related to the presence of some dissolved oxygen present during the experiment. The small oxidation peak at $E = 0$ V present in the cyclic voltammogram of both complexes can be attributed to the oxidation of free nitrite as it has been previously reported from the Symes group.³⁷

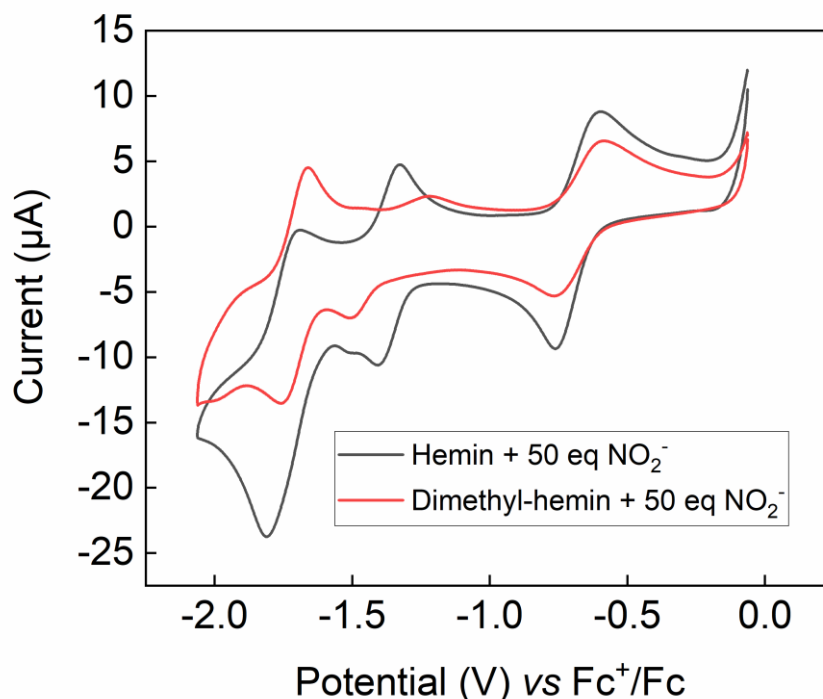


Figure 5.10: Direct comparison of hemin and dimethyl-hemin (2 mM) in the presence of 50 equivalents NO_2^- , obtained in 1 M TBAPF₆ DMSO electrolyte, using a glassy carbon working electrode, a Ag/AgNO₃ reference electrode and a graphite rod counter electrode. Scan rate 100 mV/sec.

There are two more things that we can extract from the comparison of the two complexes in the presence of nitrite. The cyclic voltammogram of the hemin complex has been slightly shifted to more negative potentials by about 60 mV for the first redox wave and 30 mV for the second redox wave. This is another indication that the nitrite is coordinated to the metal centre of the complex, since the replacement of a dimethyl sulfoxide ligand by the more electron rich NO_2^- ligand would be expected to make the reduction of the Fe centre more difficult. Moreover, the redox wave at -0.6 V becomes noticeably smaller upon the addition of increasing amounts of nitrite. At the same time, the new redox wave at -1.36 V becomes larger which indicates that the formation of the species responsible for the new redox wave are possibly related with the $\text{Fe}^{\text{III}}/\text{Fe}^{\text{II}}$ redox wave at -0.6 V. However, there is no supplementary data to support this hypothesis, at this stage. Furthermore, the redox wave at -1.7 V, the $\text{Fe}^{\text{II}}/\text{Fe}^{\text{I}}$ redox couple, shows signs of a catalytic activity after the addition of nitrite. We do not observe a profound catalytic peak but the change in the shape of the redox wave is an evidence of the initiation of a catalytic process. At the same time, we observe a small decrease of the first redox wave of the dimethyl-hemin complex, which is not

significant compared to the hemin complex. The same wave has also been shifted towards more negative potentials by 80 mV that constitutes an indication of the nitrite coordination to the iron centre, as explained before. The redox wave at -1.67 V of the ester complex becomes slightly smaller, but it does not lose its reversible nature. Figure 5.10, provides a direct comparison of the two complexes in the presence of 50 equivalents of nitrite.

5.4.4 Addition of Proton source

Moving forward, the addition of a proton source was the next step to test the catalytic activity of our system. The chosen acid was the benzoic acid which is a strong acid (pK_a 11 in DMSO)³⁸ and therefore a good proton donor. The obtained data for both hemin and dimethyl hemin upon the addition of excess acid are summarized in the figures below (Figure 5.11 and 5.12 respectively).

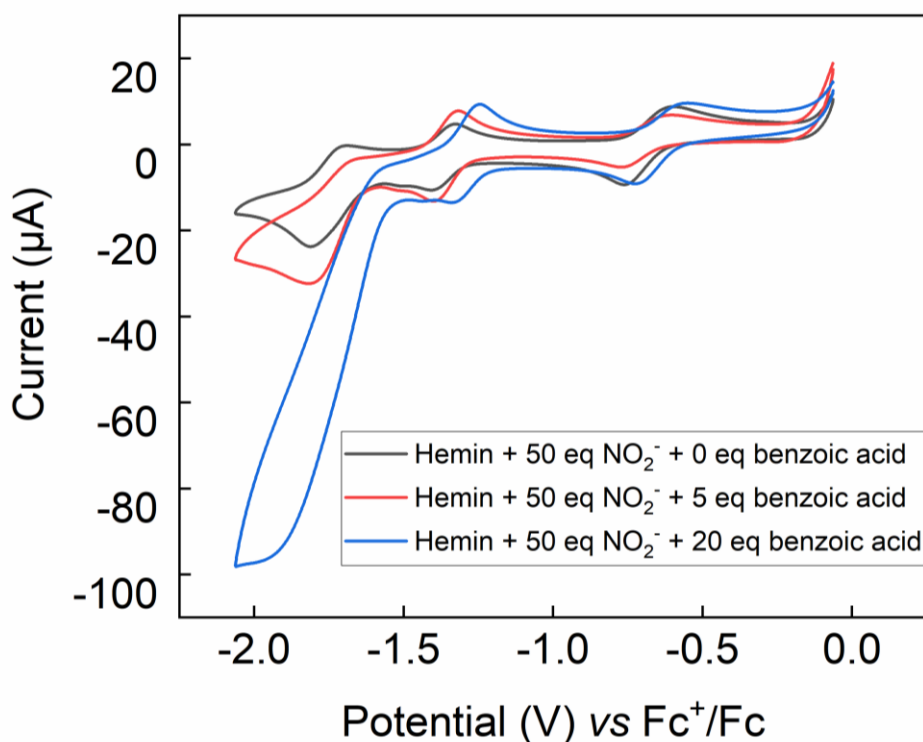


Figure 5.11: Cyclic voltammogram of hemin (2 mM) and 50 mole equivalents of nitrite with the addition of increasing equivalent moles of benzoic acid, obtained in 1 M TBAPF₆ DMSO electrolyte, using a glassy carbon working electrode, a Ag/AgNO₃ reference electrode and a graphite rod counter electrode. Scan rate 100 mV/sec.

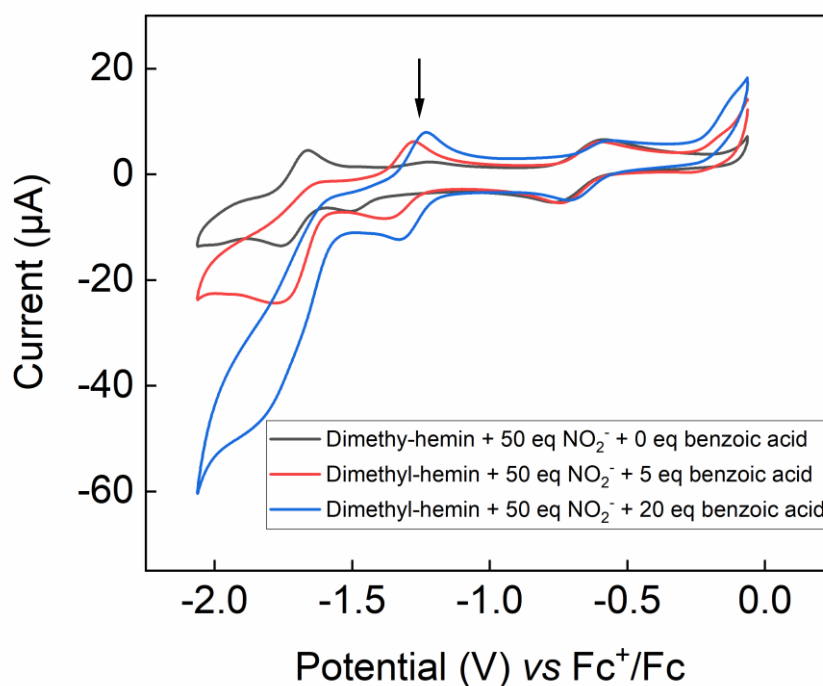


Figure 5.12: Cyclic voltammogram dimethyl-hemin (2 mM) and 50 mole equivalents of nitrite with the addition of increasing equivalent moles of benzoic acid, obtained in 1 M TBAPF₆ DMSO electrolyte, using a glassy carbon working electrode, a Ag/AgNO₃ reference electrode and a graphite rod counter electrode. Scan rate 100 mV/sec.

In both complexes, we notice that after the addition of the proton source the reversible wave attributed to the Fe^{II}/Fe^I (≈ -1.7 V) redox couple turns gradually into a well-defined catalytic wave. Hemin provides a more negative and profound catalytic wave with a current response of 96 μ A while in the case of the dimethyl-hemin complex, the catalytic wave provides a current response of 48 μ A. A key observation needs to be highlighted for the dimethyl-hemin complex. After the addition of the proton source, the reversible wave at -1.4 V that is present in the hemin complex upon the addition of nitrite does indeed form (Figure 5.12 pointed with the arrow). The increasing addition of benzoic acid seems to affect the formation of this new wave as it gets larger. In both cases, there is a small shift of about 60 mV on the reversible wave at about -1.4 V to more positive potentials. A direct comparison of the two complexes including a so-called control experiment is provided in Figure 5.13. For the control experiment, the maximum amount of nitrite (50 equivalents) and benzoic acid (20 equivalents) were dissolved in the electrolyte, without any complex being present, to prove that the catalysis indeed occurs in the metal centre of the complexes and not in solution from the proton source.

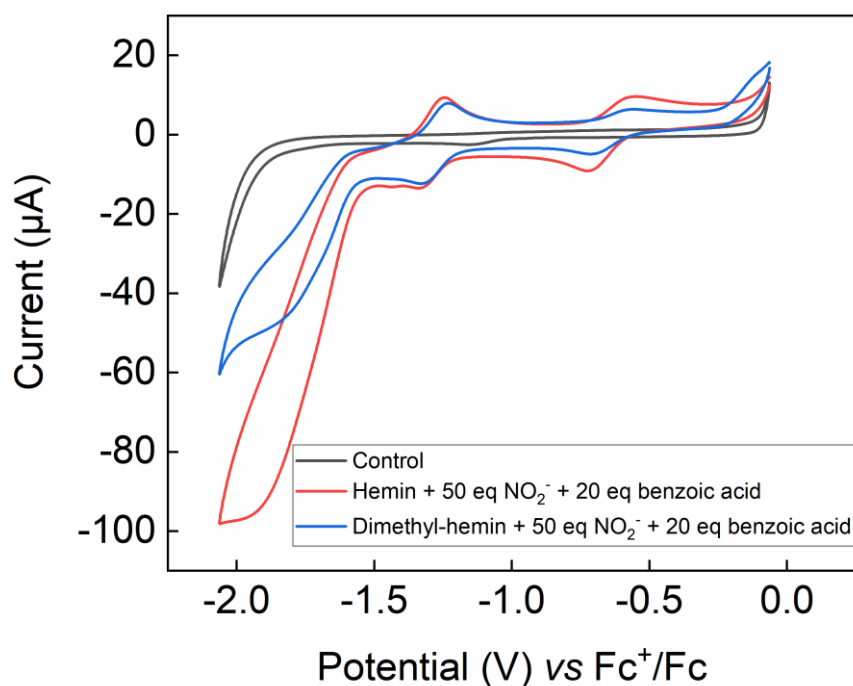


Figure 5.13: Direct comparison of the catalytic activity of 2 mM hemin (red line) and 2 mM dimethyl-hemin (blue line) in the presence of nitrite (50 mole equivalents) and benzoic acid (20 mole equivalents), obtained in 1 M TBAPF₆ DMSO electrolyte, using a glassy carbon working electrode, a Ag/AgNO₃ reference electrode and a graphite rod counter electrode. Scan rate 100 mV/sec.

The investigation of the effect of benzoic acid in the dimethyl hemin complex has also been studied to eliminate the possibility that the acid, and not the NO₂⁻, is responsible for the formation of the new reversible wave. As we can see from Figure 5.14, the addition of 20 equivalents in the solution in the presence of only the complex and absence of nitrite has no effect in the complex, apart from a negligible increase on the Fe^{III}/Fe^{II} redox wave. Therefore, the formation of this wave is related to the reduction of nitrite.

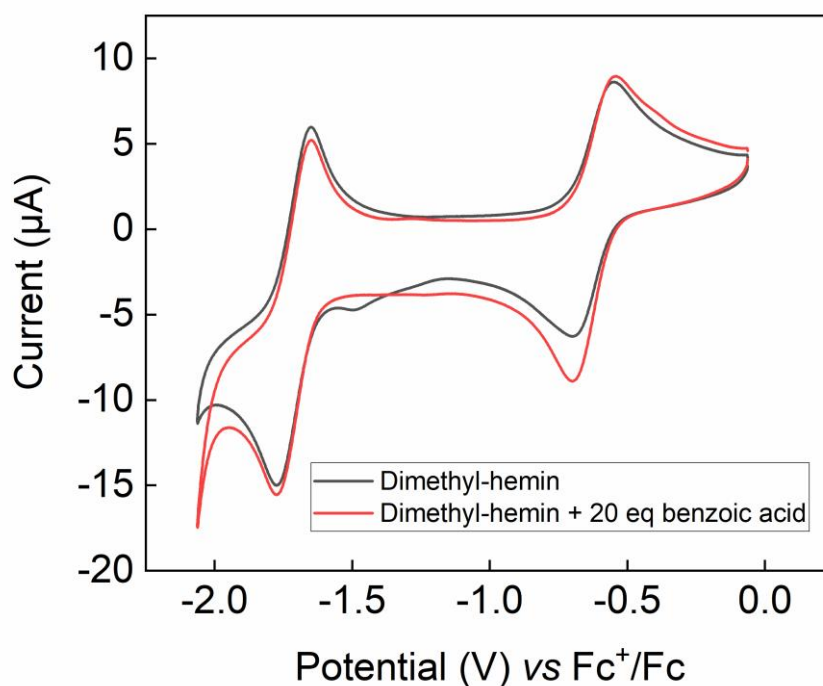


Figure 5.14: Cyclic voltammogram of dimethyl-hemin (2 mM) before and after the addition of benzoic acid (20 mole equivalents), obtained in 1 M TBAPF₆ DMSO electrolyte, using a glassy carbon working electrode, a Ag/AgNO₃ reference electrode and a graphite rod counter electrode. Scan rate 100 mV/sec.

Based on the above observations we can make the hypothesis that the difference in structure of the two catalysts, *e.g.*, the presence of the carboxylic acid group in the outer sphere of hemin, has a significant effect in the electrocatalytic behaviour of our system. Based on our findings, that are summarised in Figure 5.10, we hypothesize that in the absence of a proton source, the carboxylic acid labile proton of hemin can initiate the reduction of nitrite. We support this hypothesis with the formation of the new reversible wave at about $E_{1/2} = -1.36$ V and the change in the redox wave's shape at -1.7 V, to a more catalytic aspect, compared to the reversible wave attributed to the Fe^{II}/Fe^I redox couple. The dimethyl-hemin that lacks such functionality requires the presence of the proton source to provide similar activity. Even then, hemin is twice as electroactive as the dimethyl-hemin in terms of the current response of the catalytic wave. However, to fully support this hypothesis, more studies need to be performed (see Section 5.7).

5.4.5 Addition of a Weaker Proton Source

With benzoic acid being a relatively strong acid, we examined the possibility of using a weaker proton donor to provide a potentially milder environment for our complexes. A motivation for this was the hypothesis that benzoic acid could be cleaving some of the methyl groups from the dimethyl hemin, and thus giving some activity by converting this partly into demethylated hemin. In order to obtain more insight into whether this was actually the case or not, we chose phenol (which has a pK_a value of 18 in DMSO)³⁸ as a less acidic source of protons. The behaviour of the two complexes upon addition of phenol, in terms of the formation of the middle redox wave, is similar to that described before. The new wave appears after the addition of nitrite to the hemin complex while the addition of the proton source is necessary to form this wave in the case of the dimethyl hemin (Figure 5.16). However, in this case, the new wave was significantly smaller for dimethyl-hemin than in hemin. The Fe^{II}/Fe^I redox couple does not provide a well-defined catalytic wave in the hemin complex although it loses its reversible nature. At the same time, it does not change at all in the dimethyl-hemin (Figure 5.16). These findings support the hypothesis made in previous section that the presence of readily available protons in the structure of the complex enhances its electrocatalytic activity. Moreover, these results indicate that the ester complex is not hydrolysed in the presence of benzoic acid as the electrochemical behaviour of the two complexes looks to follow a similar pattern. The comparison of the two complexes in the presence of phenol can be found in Figure 5.15.

The effect of phenol on the electrocatalytic process is highlighted in Figure 5.16. In both cases, it seems that there is some small, but not obvious, catalytic effect upon the addition of 50 equivalents of phenol. Therefore, we can conclude that since the dimethyl hemin complex is not hydrolysed by the strong acid, using benzoic acid as the proton source is the optimal choice to investigate the electrocatalytic activity of our complexes, and especially the Fe^{II}/Fe^I redox couple.

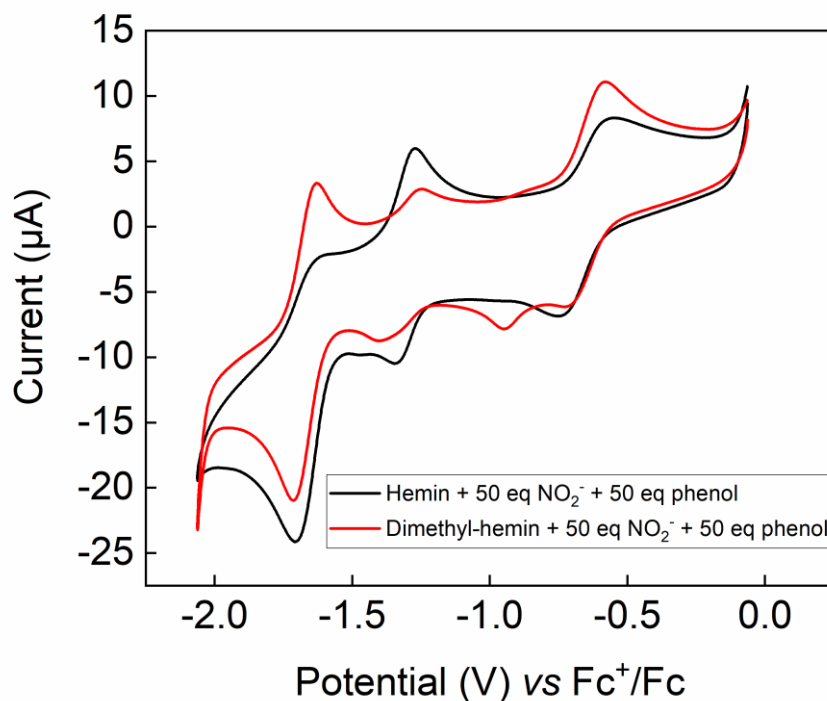


Figure 5.15: Direct comparison of the catalytic activity of 2 mM hemin (red line) and 2 mM dimethyl-hemin (black line) in the presence of nitrite (50 mole equivalents) and phenol (50 mole equivalents), obtained in 1 M TBAPF₆ DMSO electrolyte, using a glassy carbon working electrode, a Ag/AgNO₃ reference electrode and a graphite rod counter electrode. Scan rate 100 mV/sec.

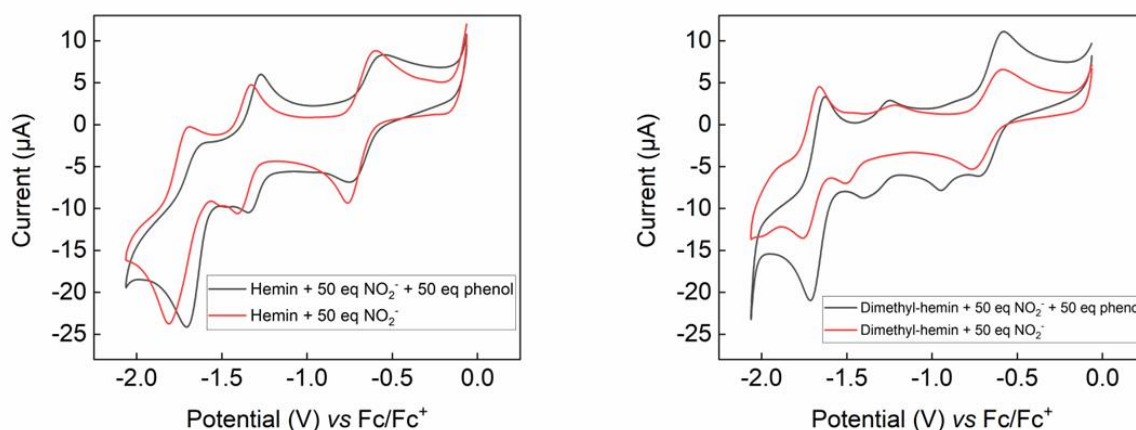


Figure 5.16: **Left**, electrocatalytic effect upon the addition of phenol (50 equivalents) in the hemin-nitrite solution. **Right**, electrocatalytic effect upon the addition of phenol (50 equivalents) in the dimethyl hemin-nitrite solution. Both graphs were obtained in 1 M TBAPF₆ DMSO electrolyte, using a glassy carbon working electrode, a Ag/AgNO₃ reference electrode and a graphite rod counter electrode. Scan rate 100 mV/sec.

5.5 Conclusion

In the present work, we attempted to gain insight into the reaction mechanism of the multi-electron electrochemical reduction of nitrite using an iron protoporphyrin catalyst. To prove that the mechanism involves PCET step(s), we tested and compared the electrochemical activity of two catalysts, hemin and its methylated counterpart, dimethyl-hemin. The esterification of the hemin complex was performed in a single-step synthesis, and the obtained product was fully characterized as the dimethyl-hemin. The two complexes behave very different in both the absence and presence of a proton source, which supports our theory that PCET is involved in the nitrite reduction process. In the absence of a proton source, hemin was the only catalyst that provided evidence of the initiation of a catalytic process while dimethyl-hemin required the addition of proton source to provide such activity. Even in the presence of a proton source, hemin was twice as electroactive as the dimethyl-hemin catalyst. This difference can be attributed to the labile proton of the carboxylic acid group in the secondary coordination sphere of the hemin complex, that is able to initiate the catalysis at first and following, to enhance its activity upon the addition of a proton source. However, to be able to provide stronger evidence, more studies need to be performed, as summarised in Section 5.7.

5.6 Future Work

As stated before, the most important part of the future work would be the identification of the species responsible for the formation of the new reversible wave which appeared in between the two redox couples (at about -1.4 V *vs* Fc⁺/Fc) attributed to the Fe centre. The formation of this wave constitutes a major difference in the activity of the two catalysts and its identification would provide a better insight into the mechanism of reaction. Taking as fact that both complexes are paramagnetic (Fe^{III} centre), this identification might be aided via electron paramagnetic resonance (EPR) analysis after completing a bulk electrolysis at a potential of about -1.45 V *vs* Fc⁺/Fc. If this reversible wave is formulated from a nitrite reduction product, the analysis of the electrolyte after the completion of bulk electrolysis will possibly provide evidence of its nature.

Moreover, the determination of the catalytic product(s) and the calculation of their yield(s) and ratio(s) will provide evidence of the suitability of our catalyst to perform multi-electron reduction of nitrite. This will be achieved by the application of different analytical techniques depending on the product(s) that we synthesize. Bulk electrolysis, using a large

surface working electrode (possible carbon plate or carbon felt) should be performed at -2 V vs Fc^+/Fc to allow the formation of the reaction products. Upon the electrolysis, the electrochemical cell's headspace and the electrolyte should be analysed for potential products. For example, gas chromatography will be used for the determination of N_2 and colorimetry or the indophenol blue (IPB) spectroscopic method, based on Berthelot reaction,³⁹ for NH_3 . Calorimetry can also be used for the detection of NO in a similar way to what has previously been reported.²² As we mentioned earlier, the selective formation of any of the above species will constitute a major step in the electrochemical reduction of nitrite. Furthermore, the comparison between the obtained current density and product formation of the two complexes will confirm (or not) our hypothesis, made from the cyclic voltammograms, that the labile proton at the outer sphere of hemin enhances the electrochemical activity of the catalyst.

Finally, kinetic studies of the catalytic process by cyclic voltammetry is something interesting to be examined. The electrocatalytic reduction of nitrite can be measured as a function of nitrite concentration in the presence of a large excess of proton donor. This study will allow us to understand the maximum rate of nitrite reduction in our electrocatalytic system.

5.7 References

1. L. B. Maia and J. J. G. Moura, *Chem. Rev.*, 2014, **114**, 5273-5357.
2. H. Bothe, S. J. Ferguson and W. E. Newton, *Biology of the Nitrogen Cycle*, Elsevier Science, Elsevier, 2006.
3. A. J. Timmons and M. D. Symes, *Chem. Soc. Rev.*, 2015, **44**, 6708-6722.
4. V. Rosca, M. Duca, M. T. de Groot and M. T. M. Koper, *Chem. Rev.*, 2009, **109**, 2209-2244.
5. N. Kerru, L. Gummidi, S. Maddila, K. K. Gangu and S. B. Jonnalagadda, *Molecules (Basel, Switzerland)*, 2020, **25**, 1909.
6. T. Hiratsu, S. Suzuki and K. Yamaguchi, *Chem. Comm.*, 2005, 4534-4535.
7. L. W. Canter, *Nitrates in Groundwater*, Taylor and Francis, CRC Press, 1996.
8. S. R. Buss, M. O. Rivett, P. Morgan and C. D. Bemment, *Attenuation of nitrate in the sub-surface environment*, Report SC030155/SR2, Environment Agency, 2005.
9. J. R. Jennings, *Catalytic ammonia synthesis: fundamentals and practice*, Springer Science & Business Media, 1991.
10. J. W. Erisman, M. A. Sutton, J. Galloway, Z. Klimont and W. Winiwarter, *Nat. Geosci.*, 2008, **1**, 636-639.
11. S. Ghavam, M. Vahdati, I. A. G. Wilson and P. Styring, *Front. Energy Res.*, 2021, **9**, 1-19.
12. C. Smith, A. K. Hill and L. Torrente-Murciano, *Energy Environ. Sci.*, 2020, **13**, 331-344.
13. H. Nagao, N. Komeda, M. Mukaida, M. Suzuki and K. Tanaka, *Inorg. Chem.*, 1996, **35**, 6809-6815.
14. J. N. Younathan, K. S. Wood and T. J. Meyer, *Inorg. Chem.* 1992, **31**, 3280-3285.
15. M. G. Almeida, C. M. Silveira, B. Guigliarelli, P. Bertrand, J. J. Moura, I. Moura and C. Léger, *FEBS Lett.*, 2007, **581**, 284-288.
16. S. Brenner, D. J. Heyes, S. Hay, M. A. Hough, R. R. Eady, S. S. Hasnain and N. S. Scrutton, *J. Biol. Chem.*, 2009, **284**, 25973-25983.

17. D. R. Weinberg, C. J. Gagliardi, J. F. Hull, C. F. Murphy, C. A. Kent, B. C. Westlake, A. Paul, D. H. Ess, D. G. McCafferty and T. J. Meyer, *Chem. Rev.*, 2012, **112**, 4016-4093.
18. C. Costentin, M. Robert and J.-M. Savéant, *Accounts of Chemical Research.*, 2010, **43**, 1019-1029.
19. C. Costentin, M. Robert, J.-M. Savéant and A.-L. Teillout, *Proceedings of the National Academy of Sciences*, 2009, **106**, 11829-11836.
20. J. Rosenthal and D. G. Nocera, *Acc. Chem. Res.*, 2007, **40**, 543-553.
21. C. H. Lee, D. K. Dogutan and D. G. Nocera, *J. Am. Chem. Soc.*, 2011, **133**, 8775-8777.
22. G. Cioncoloni, I. Roger, P. S. Wheatley, C. Wilson, R. E. Morris, S. Sproules and M. D. Symes, *ACS Catal.*, 2018, **8**, 5070-5084.
23. B. Ward, *Molecular Medical Microbiology (Second Edition)*, 2nd eds., Academic Press, Boston, 2015, pp. 201-233.
24. D. Bykov and F. Neese, *JBIC J. Biol. Inorg. Chem.*, 2011, **16**, 417-430.
25. O. Einsle, A. Messerschmidt, R. Huber, P. M. H. Kroneck and F. Neese, *J. Am. Chem. Soc.*, 2002, **124**, 11737-11745.
26. M. H. Barley and T. J. Meyer, *J. Am. Chem. Soc.*, 1986, **108**, 5876-5885.
27. J. L. Heinecke, C. Khin, J. C. M. Pereira, S. A. Suárez, A. V. Iretskii, F. Doctorovich and P. C. Ford, *J. Am. Chem. Soc.*, 2013, **135**, 4007-4017.
28. Y. Chi, J. Chen and K. Aoki, *Inorg. Chem.*, 2004, **43**, 8437-8446.
29. M. Duca, S. Khamseh, S. C. S. Lai and M. T. M. Koper, *Langmuir*, 2010, **26**, 12418-12424.
30. D. Mimica, J. H. Zagal and F. Bedioui, *J. Electroanal. Chem.*, 2001, **497**, 106-113.
31. B. C. Sanders, S. M. Hassan and T. C. Harrop, *J. Am. Chem. Soc.*, 2014, **136**, 10230-10233.
32. E. V. Kudrik, S. V. Makarov, A. Zahl and R. van Eldik, *Inorg. Chem.*, 2005, **44**, 6470-6475.
33. R. Lin, M. Bayachou, J. Greaves and P. J. Farmer, *J. Am. Chem. Soc.*, 1997, **119**, 12689-12690.

34. C. J. Byrne and A. D. Ward, *Tetrahedron Lett.*, 1988, **29**, 1421-1424.
35. R. T. Dean, L. J. DeFilippi and D. E. Hultquist, *Anal. Biochem.*, 1976, **76**, 1-8.
36. R. S. Tieman, L. A. Coury, J. R. Kirchhoff and W. R. Heineman, *J. Electroanal. Chem. Interfacial Electrochem.*, 1990, **281**, 133-145.
37. I. Roger, C. Wilson, H. M. Senn, S. Sproules and M. D. Symes, *R. Soc. Open Sci.*, 2017, **4**, 170593.
38. D. H. Ripin and D. A. Evans, Evans pKa table, http://ccc.chem.pitt.edu/wipf/MechOMs/evans_pKa_table.pdf, (accessed May 20 2022).
39. A. Aminot, D. S. Kirkwood and R. K erouel, *Mar. Chem.*, 1997, **56**, 59-75.

Final Conclusions and Future Work

In this thesis, we studied the use of suitable mediator/catalyst for the electrochemical reduction of organic nitrobenzenes and inorganic nitrite (NO_2^-).

In **Chapter 3** we describe the development of a novel catalytic electrochemical process for the reduction of nitroarenes to their corresponding anilines. Our process is a simple and potentially a more sustainable alternative to the traditional methods used in the industry due to the avoidance of the use of hydrogen gas, high temperatures, precious metal co-catalysts and sacrificial reagents. Our process is carried out in 1 M aqueous H_3PO_4 solution, at room temperature and pressure, with the electrons and protons required to reduce the nitrobenzenes originating from water. Using phosphotungstic acid as our redox mediator, and carefully controlling the applied potential in the electrochemical process, we were able to shut off the direct electrochemical reduction of the starting material at the working electrode surface that it is known to produce unwanted reaction intermediates. The overall process is highly selective towards the desired anilines and provides Faradaic efficiencies typically greater than 90%, even for catalyst loadings as low as 0.1% mol relative to the nitroarene starting material. Through various experiments and mechanistic studies, we were able to propose a reaction pathway that explains why this mediated process gives superior conversion and selectivity compared to direct electrochemical reduction of the starting material at the electrode surface. The ability of the phosphotungstic acid redox mediator to perform multiple rounds of nitrobenzene reduction was tested over the course of a week (*e.g.* four full cycles), providing >99% selectivity towards aniline with a 92% overall isolated yield for the reaction. Applying this method, we were also able to perform electrocatalytic reduction of sensitive nitrobenzene substrates such as *o*-iodides to their corresponding aniline derivatives in good yields. The successful gram-scale reduction of nitrobenzene using a two-electrode set-up was also reported, to provide some preliminary evidence for the use of the process in scaled-up reactions.

In **Chapter 4**, the process that we have developed in chapter 3 was used to significantly expand the scope of this approach to a variety of substituted nitroarenes, including potentially competing reducible groups and substrates that are difficult to reduce selectively by other means. Thus, it was shown that the polyoxometalate phosphotungstic acid is an effective redox mediator for the electrocatalytic reduction of halogenated, alkyl-, carbonyl-, ester-, hydroxyl-, cyano- and acid-substituted nitrobenzenes. In all cases, the effect of the

redox mediator was directly compared with the direct electrochemical reduction of the nitrobenzenes at the working electrode surface. In all cases, the phosphotungstic acid mediated process was superior to the direct electrochemical process in terms of selectivity towards the desired aniline substrate. The potential of this process to be developed under preparative conditions was also shown. In this case, a two-electrode electrochemical setup (no reference electrode was involved) and galvanostatic electrolysis conditions were applied in the reduction of the substrate methyl-2-nitrobenzoate. At the end of the reduction, 92% of the starting material had been converted to 2-aminobenzoic acid methyl ester (aniline product) with no formation of any reduction intermediates (>99% selectivity). Further optimisation of the scaled-up process can be attempted in the future mainly through a different electrochemical cell set-up where the distance between the working and counter electrode is smaller, leading to lower internal resistance. In this matter, a continuous-flow electrochemical system can provide a good alternative, whereby controlling the flow rate of the system we can potentially achieve similar results in terms of conversion and selectivity while reducing the required cell voltage. At the same time, we could also attempt to immobilise our redox mediator at the electrode surface. There are some studies in the literature where modified polyoxometalates are covalently attached to a glassy carbon electrode, this could potentially be good starting point.¹ Mediator immobilisation at the working electrode surface could provide enhanced efficiency in the flow cell system, compared to the dissolved mediator. The potential use of another electrocatalyst able to perform under similar standards to the polyoxometalate mediator, which is easier to attach at the electrode surface and potentially has a lower molecular weight than the polyoxometalate cannot be excluded.

Finally, in **Chapter 5**, the multi-electron electrochemical reduction of the inorganic nitrite (NO_2^-) was studied using iron porphyrin complexes as electro-catalysts. Our main focus was to obtain an insight into the reaction mechanism of the electrochemical reduction and mainly the involvement of PCET. For this reason, the reduction of NO_2^- was performed using two iron porphyrin complexes, hemin that contains a labile proton in the secondary coordination sphere and its methylated derivative, the dimethyl-hemin, that we successfully synthesised and lacks such functionality. Our studies thus far, have shown some evidence that PCET is indeed involved in the electrochemical reduction of nitrite using such complexes. In the absence of a proton source, there is evidence for the initiation of the catalytic process when the hemin catalyst was involved in the reaction, while no such evidence was observed in the

case of dimethyl-hemin. Moreover, in the presence of a proton source, hemin found to be twice as electroactive as the dimethyl-hemin. However, further work is required to provide stronger evidence for the efficiency of the two electro-catalysts. This future work mainly involves bulk electrolysis of the reaction solution both in the presence and absence of a proton source in various applied potentials and the identification and isolation of the reduction products. The formation of NO during bulk electrolysis can be quantified through calorimetric determination. Nitric oxide produced during bulk electrolysis, can be diffused into a Co-TPP (cobalt (II) *meso*-tetraphenylporphyrin) solution in dichloromethane. Co-TPP undergoes a highly characteristic shift in the position of its visible band upon NO binding. The electronic spectrum of the solution can then be recorded while observing the shift of the peak at $\lambda_{\max} \approx 530\text{nm}$. A calibration curve of the shift of the position of Co-TPP absorbance band *versus* the %NO generated relative to the moles of Co-TPP should then be constructed, to allow quantification of the generated nitric oxide. NO can also be detected using a chemiluminescence nitric oxide analyser, with the released NO from our bulk electrolysis cell being flushed to the analyser, where its concentration will be recorded.² As far as the N₂ determination, gas chromatography will be used by direct injection of the headspace of the bulk electrolysis, while the indophenol blue (IPB) spectroscopic method based on Berthelot reaction³ will be used for NH₃ determination.

References

1. C. Rinfray, G. Izzet, J. Pinson, S. G. Derouich, J. J. Ganem, C. Combellas, F. Kanoufi and A. Proust, *Chem. Eur. J.*, 2013, **19**, 13838-13846.
2. G. Cioncoloni, I. Roger, P. S. Wheatley, C. Wilson, R. E. Morris, S. Sproules and M. D. Symes, *ACS Catal.*, 2018, **8**, 5070-5084.
3. A. Aminot, D. S. Kirkwood and R. K erouel, *Mar. Chem.*, 1997, **56**, 59-75.